CYCLE CONTROL OF A REGENERATIVE MAGNETIC REFRIGERATOR OPERATING FROM 4.2 TO 15 K

by

FREDERICK J. COGSWELL

B.S.M.E., Cornell University
(1981)

S.M.M.E., Massachusetts Institute of Technology
(1985)

Submitted to the Department of Mechanical
Engineering in partial fulfillment of the
Requirements for the degree of

DOCTOR OF PHILOSOPHY

at the

MASSACHUSETTS INSTITUTE OF TECHNOLOGY

April 1989

Signature of Author_____
Department of Mechanical Engineering
April 1989

Certified by_____
Yukikazu Iwasa
Thesis Supervisor

Certified by_____
Joseph L. Smith, Jr.
Thesis Supervisor

Accepted by_____
Ain A. Sonin
Chairman, Mechanical Engineering Department Committee

CYCLE CONTROL OF A REGENERATIVE MAGNETIC REFRIGERATOR OPERATING FROM 4.2 TO 15 K

by
Frederick J. Cogswell

Submitted to the Department of Mechanical Engineering
on April 28, 1989 in partial fulfillment of the
requirements for the Doctor of Philosophy

ABSTRACT

This thesis presents both experimental data and analytical results which relate to regenerative magnetic refrigeration over the temperature range of 4.2 to 15 K. Our experimental device was designed to approximate a series of cascaded-Carnot cycles. It consists of a gadolinium gallium garnet (GGG) regenerative core and a solenoid capable of ramping from 0 to 4 tesla in 5 seconds. Heat was transported through the core by supercritical helium. The core was received from a previous project. Its design parameters include: the thermodynamic properties of the paramagnetic salt(s), the helium porosity, the helium pressure, and the active cross sectional area. Our magnet system consisted of a primary solenoid which produced a uniform magnetic field up to 4 tesla, and a perturbation solenoid which was later added to allow for greater field modification.

From the analysis a general understanding of the dynamics of active regeneration was gained. If the core and field profiles are not designed properly, then it is not possible to obtain Carnot-type cycles throughout the core. Some regions of the core will experience non-isothermal flow paths. When refrigeration is attempted at temperatures higher than the paramagnetic's Curie temperature, field-flow imbalances result in excess heat transport from the warm-end to the cold-end of the core, thus reducing or even eliminating refrigeration.

Although most of the system subcomponents worked well, steady-state refrigeration was not achieved with the experimental device. Full system test data indicated that the core did not work properly. Comparison of computer simulation analysis to this test data predicted that the helium porosity was too large, and that the core's axial conductivity was too high. Subsequent tests performed on the core, after it had been removed from the rest of the system, confirmed this result. With the test data correlated to analysis, the dynamics of active regeneration can now be explained. A potential design procedure for the next generation device is outlined.

Thesis Supervisor: Dr. Yukikazu Iwasa
Title: Senior Research Engineer, Francis Bitter National Magnet Laboratory

Thesis Supervisor: Prof. Joseph L. Smith
Title: Professor of Mechanical Engineering

ACKNOWLEDGEMENTS

I would like to thank my advisors Yuki Iwasa and Joseph Smith for their financial support and technical advise, and Prof. Mikić for his prompt reading and critique of the thesis drafts. Sangkwon, thank you for your help, and good luck continuing with this project.

My deepest thanks and love goes to my wife, Kathy, for her patience and her invaluable help as chief editor, organizer and illustrator.

Table of Contents

List of Symbols

This is a list of the standard symbols used in this thesis. Any other symbols are specified where they are used.

A: Cross-sectional Area of Core (cm^2)

C: Total Specific Heat of Core per Unit Length ($J\,cm^{-1}\,K^{-1}$)

c_H: GGG Specific Heat at Constant Field ($J\,g^{-1}\,K^{-1}$)

c_p: Helium Specific Heat at Constant Pressure ($J\,g^{-1}\,K^{-1}$)

h: Enthalpy per Mass ($J\,g^{-1}$)

h_{fg}: Heat of Vaporization per Mass (J/g)

$\mu_0 H$: Applied Magnetic Field multiplied by μ_0 (T)

H_g: Magnetic Enthalpy (J)

$\hbar$: Convective Heat Transfer Coefficient ($W\,cm^{-2}\,K^{-1}$)

K: Conductivity ($W\,cm^{-1}\,K^{-1}$)

m: Mass Flow of Helium Through the Core (g)

M_T: Total Shuttle Mass of Helium During Flow Process (g)

νM: Magnetization multiplied by Specific Volume ($A\,m^2\,g^{-1}$)

μ: Viscosity ($g\,cm^{-1}\,s^{-1}$)

P: Pressure of the Helium ($N\,m^{-2}$ or Atm)

por: Porosity: percent helium void by volume of GGG and helium

Q_c: Refrigeration (J)

Q_w: Heat of Rejection (J)

ρ: Density ($g\,cm^{-3}$)

S: Specific Entropy ($J\,g^{-1}\,K^{-1}$)

T: Temperature (K)

t: Time (s)

U, u: Specific Internal Energy ($J\,g^{-1}$)

v: Convection Wave Velocity ($cm\,s^{-1}$)

V: Volume (cm^3)

W: Work interaction (J)

x: Distance along the Core (cm)

The subscript ($_g$) refers to GGG, the subscript ($_{he}$) to helium, and the subscript ($_r$) to silicon rubber.

List of Figures

I. INTRODUCTION

The ultimate goal of this project is to design a regenerative magnetic refrigerator system operating between liquid helium (4.2 K) and liquid hydrogen (~15 K) reservoirs. This chapter reviews magnetic refrigeration, gives a brief background of various magnetic refrigerators, and describes the previous magnetic refrigerator project at the Cryogenic Engineering Laboratory at the Massachusetts Institute of Technology. The final section of this chapter presents an overview of the material contained in this thesis.

1.1 Magnetic Refrigeration

There are many scientific and engineering systems that require cryogenic environments. The compressor-expansion system is the conventional approach for cryogenic refrigeration, but because of its inherent limitations, this style of system is much less efficient than the ideal Carnot cycle. In a magnetic refrigerator, the working fluid is replaced by either paramagnetic or ferromagnetic salts, and property swings are accomplished by magnetization not by compression. In theory magnetic refrigerators can perform more closely to the Carnot machine than compressor-expansion systems. A few magnetic refrigerators have been built and tested.[1-8]

1.2 Basic Thermodynamic Relations

The paramagnetic salt used in our device is gadolinium gallium garnet (GGG). The equation of state of this material is shown in Figure 1, where the magnetization, M, is shown as a function of applied magnet field, $\mu_0 H$, and temperature, T. Note the strong coupling of temperature to magnetization over the temperature range shown. It is for this reason that GGG can be used as a "refrigerant" at low temperatures.

The appropriate reversible first law equation for a compressible fluid is:

$$dU = TdS - PdV$$

whereas the appropriate reversible first law equation for a magnetizable solid is

$$dU = TdS + \mu_0 \nu H dM$$

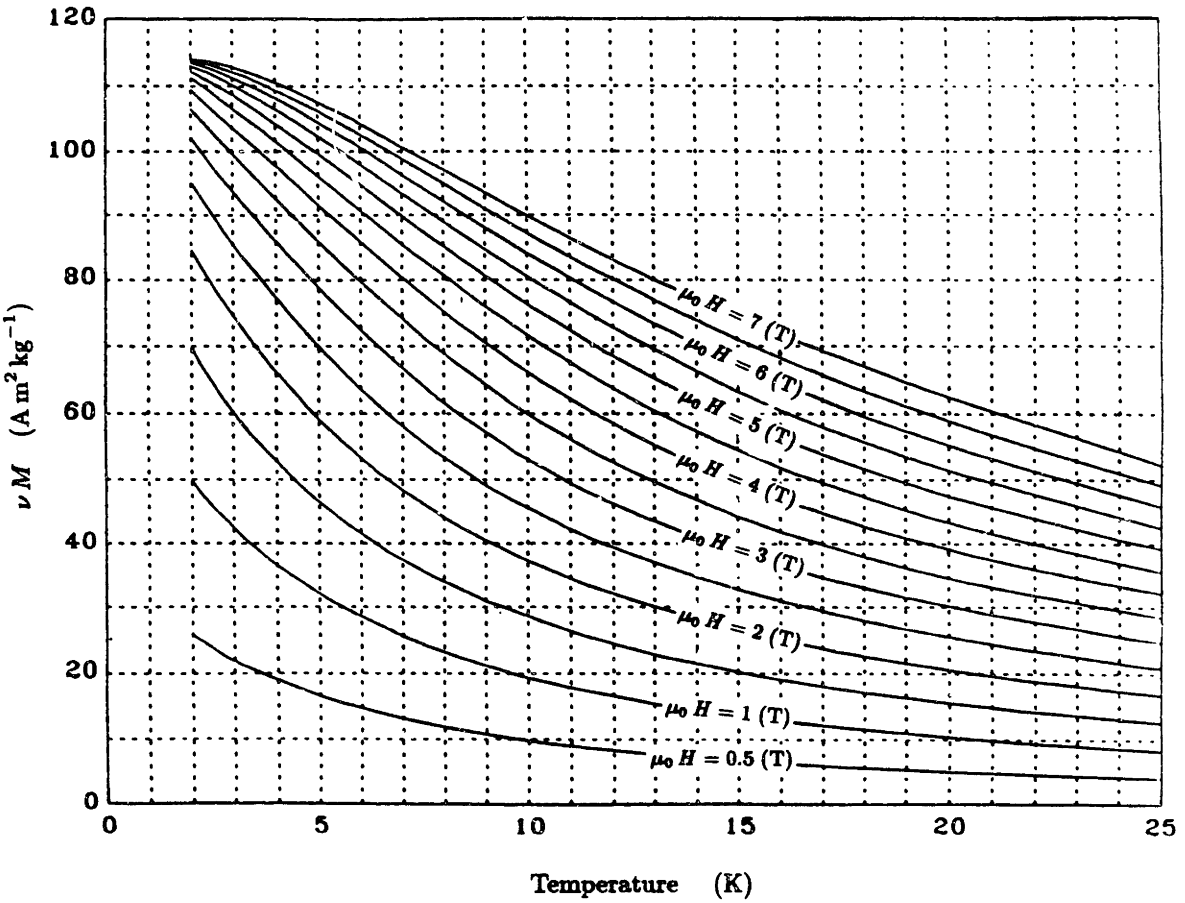

Fig. 1 GGG Equation of State, $M = f(T, \mu_0 H)$

Note that the work term is different in that pressure is replaced by applied field, and volume is replaced by magnetization. The similarity between these two equations can be seen by examining the specific heats. With a compressible fluid the specific heat at constant pressure is larger than the specific heat at constant volume because as heat is added to the system the volume must increase to prevent the pressure from increasing, and $-Pdv$ removes energy from the system. Figure 1 shows typical behavior of a paramagnetic salt above its Curie temperature. As the temperature of the salt is increased at constant field, the magnetization decreases. Since the work term, HdM, removes energy from the system, the specific heat at constant field is larger than at constant magnetization.

1.3 Some Magnetic Refrigeration Devices

1.3.1 Conduction Only

It is possible to design a magnetic refrigerator without using a heat transport medium such as helium within the paramagnetic material. Several such devices have been constructed.[5,6] In these devices heat travels through the GGG by conduction only. Thermal switches are used at the device boundaries to minimize heat flow in the wrong direction. Since the GGG need not contain helium, GGG-isentropic paths are obtainable.

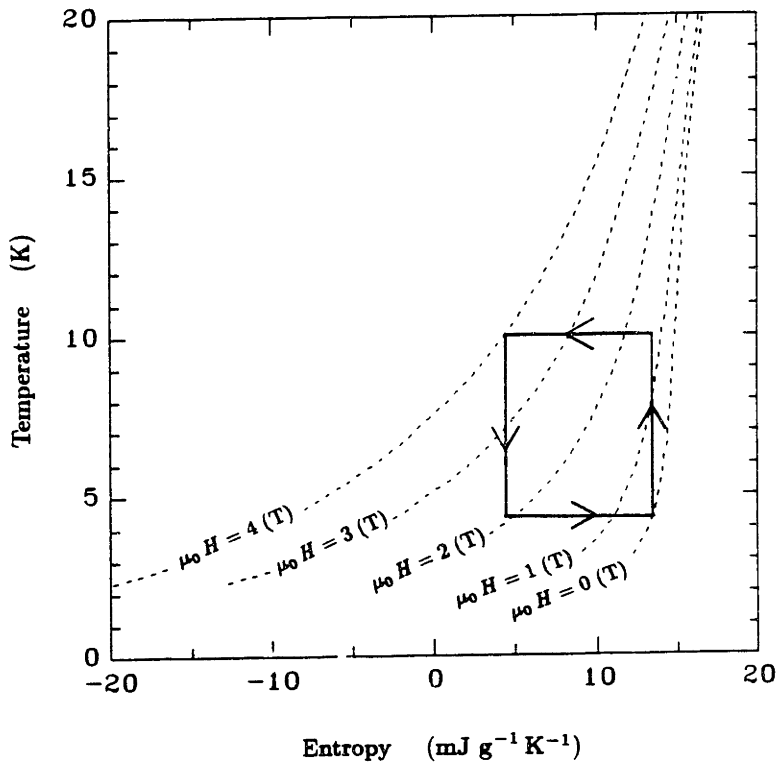

Fig. 2 A Carnot Cycle Plotted on a T-S Diagram of GGG

A Carnot-type cycle can be employed by these devices. Figure 2 shows an ideal Carnot cycle plotted on a GGG T-S diagram. The GGG begins in thermal equilibrium with the cold-reservoir at low field. Thermal contact is broken, and the GGG is magnetized adiabaticly until it reaches a temperature equal to the warm-reservoir's. At this point thermal contact is made with the warm-reservoir and magnetization

continues until the field reaches a maximum. Again the GGG is thermally isolated, and is demagnetized adiabaticly until it reaches a temperature equal to the cold-reservoir's. Thermal contact is now made with the cold-reservoir as demagnetization continues.

One problem with this device is that capacity is limited by the ability to transfer heat from the GGG through its thermal switch. Heat transport is relatively slow. Another problem with this device is that the maximum attainable temperature range must be less than the adiabatic temperature range of the paramagnetic material used. This method has been successfully employed for applications where the temperature range is relatively small.[6]

1.3.2 Wheel type devices

The next type of device employs the same Carnot-type cycle as described above, but now uses convective helium to transport the heat into and out of the GGG. Several wheel or carousel devices have been built and tested.[4,8] In a wheel type device, a wheel is constructed out of a paramagnetic material with internal slits to carry helium. A stationary magnetic field is applied to one side of the wheel. As the wheel is forced to rotate, it passes through regions of relatively high and relatively low magnetic field. The ideal cycle can be described as:

A. Adiabatic Magnetization: We begin at the cold-reservoir's temperature and at the minimum field. The wheel rotates, isolated from the helium reservoirs, into the higher field region. It increases in temperature to the warm-reservoir's temperature.

B. Isothermal Magnetization: The wheel continues to rotate into regions of increasing magnetic field while helium from the warm-reservoir is forced though the slits.

C. Adiabatic Demagnetization: Thermal contact with the helium in the warm-reservoir is broken. The wheel moves into regions of decreasing magnetic field. The temperature is decreased to the cold-reservoir's temperature.

D. Isothermal Demagnetization: The wheel rotates back to its original position while helium from the cold-reservoir is forced through its slits.

The problems with this device include frictional problems produced by the rotating wheel, and helium leakage through the device between the warm and cold-reservoirs.

It is difficult to block the helium slits during the adiabatic processes. To date this type of device has achieved only marginal success.

1.3.3 Thermally Active Regeneration

Thermally active regeneration has several advantages over other methods.[9] One advantage is that the active element remains stationary, and therefore the cold space need not contain any moving parts. Magnetization of the element is accomplished with a time-varying magnetic field. Because of recent advances in superconductor design, it is expected that time-varying-field-induced losses can be made acceptably small. Another advantage of active regeneration is that the regenerator core can be made to span a temperature range that is higher than that achievable with a single Carnot cycle. This is because individual segments in the core each cycle through a relatively small temperature range, while the total effect of all the segments is to cascade over a large temperature range. A simplified model can be used to describe the desired thermodynamic model. Figure 3a is a schematic of this model. The device is idealized as a system of "differential" Carnot refrigerators sitting side-by-side. Each differential Carnot refrigerator works between a different $T_c(x)$ and $T_h(x)$ depending on where it is located along the core. Figure 3b shows 6 cascaded Carnot cycles on a GGG T-S diagram. An ideal core would have an infinite number of overlapping cascaded Carnot cycles (too many to be shown on a single graph).

One potential disadvantage of a device based on active regeneration is that cycle control requires the proper balance between helium flow and magnetic field change at every location along the core. Proper initial design of the core and magnetic field profile is essential for the successful operation of a refrigerator based on thermally active regeneration.

1.4 System of Taussig

A schematic of the first test apparatus constructed and tested at MIT is shown in Figure 4.[10] The key components of this apparatus are the regenerator core, the heat exchangers and heaters, the displacers, and the superconducting solenoid. Supercritical helium at 3 atmospheres of pressure was used as the heat transport fluid. The apparatus was designed for the primary purpose of testing and optimizing the regenerative core.

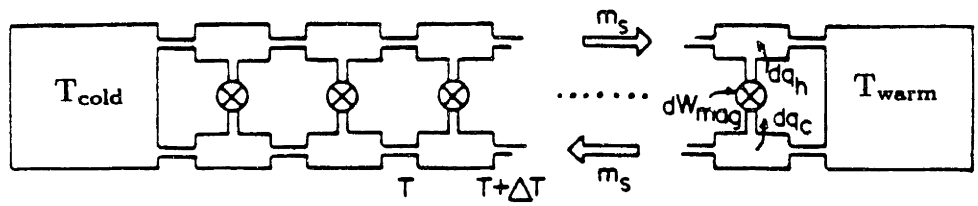

Fig. 3a Simplified Model of a Regenerative Refrigerator

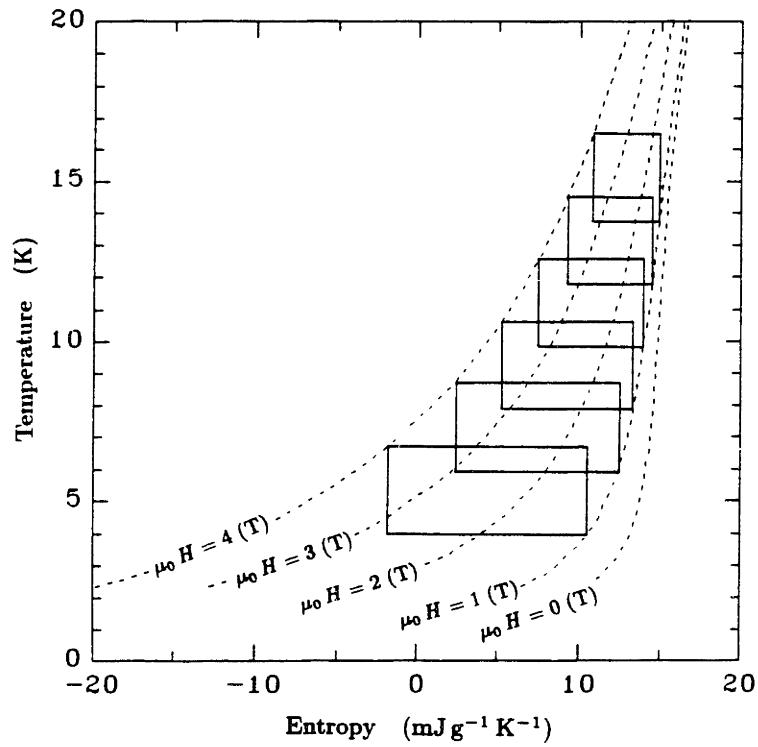

Fig. 3b Cascaded Carnot Cycles (6 shown)

The GGG core was designed to minimize the loss mechanisms of axial conduction, fluid friction, irreversible heat transfer, and helium entrainment. A heat exchanger and an electric heater are located at each end of the core. They were designed to control the temperature of the helium as it enters the core. The helium flow is controlled by two warm-sealed displacers. An external stepper motor drives the warm-side displacer. The cold-side displacer is free floating and acts as a compensator. The superconducting solenoid is cycled between 1 and 4 T by an external power supply. A microcomputer controls the field and the helium flow.

The thermodynamic cycle attempted is the cascaded-Carnot described in the previ-

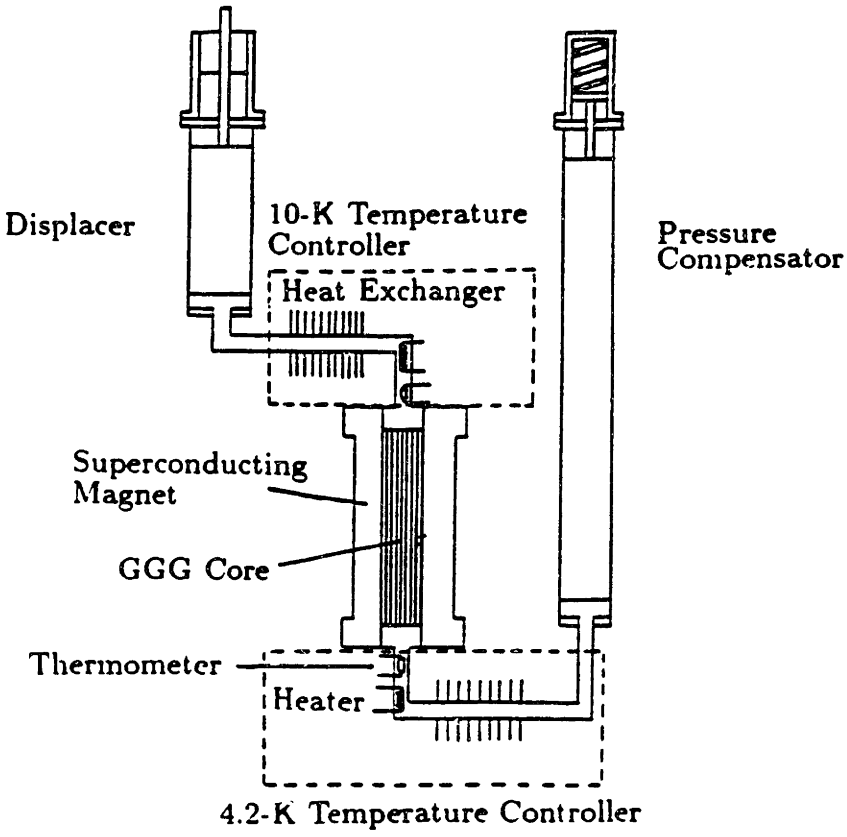

Fig. 4 Schematic of the Original Test Apparatus

ous section. It takes four paths to complete each Carnot cycle. First, the displacer initially at the top of its stroke moves down, forcing helium down through the regenerator core while the external field is lowered. Throughout this process the core assumes a prescribed temperature profile $T_c(x)$. With proper control, an isothermal process can be approached by each segment. In the second step, the displacer stops and the core is adiabaticly magnetized until the temperature assumes another prescribed profile $T_h(x)$. During the third step, the displacer moves back toward the top of its stroke drawing helium from the cold to the warm-reservoir while the core is isothermally magnetized. The final step completes the cycle by demagnetizing the core without helium flow until the temperature profile returns to $T_c(x)$. In the real device this cycle was not achieved.

1.5 Initial Tests, Analysis of Problems

The experimental setup, constructed by Carl Taussig, was tested altogether four times during 1986, twice by Taussig and twice by the author. The first two tests are described in Taussig's thesis.[10] Analysis of the data acquired during these test revealed several problems with the apparatus. In the Fall of 1986 the apparatus was tested twice more after several minor modifications to the both the drive system and the heater systems were made. From the results of these tests and the previous tests it was determined that, though the GGG core seemed to work well, the device could not be tested properly due to limitations in systems external to the core. Of the problems found, the most serious were the inability of the warm-end reservoir to properly control its temperature, and the uncertainty of the helium displacement system. We decided to make several major modifications to the test apparatus before continuing with any further experimentation.

1.6 Project Outline

This thesis is presented in three parts:

Part 1: Phase-One Experiment.

Part 2: Analysis.

Part 3: Phase-Two Experiment and Discussion.

Part 1 contains information relating to the initial design changes which were made to the system originally built by Taussig, and to the test results which relate to this phase.

Part 2 consists of six chapters; each containing a different type of analysis. It was found that although the computer simulation program could predict active regenerator behavior, it was a poor design tool. The most useful analysis in Part 2 explains the core's cycle response by examining certain aspects of the governing equation.

Part 3 contains the Phase Two system modification which was made to partially correct improper field-flow phasings in our device. The modifications were based on predictions from the analysis in Part 2. Part 3 also contains a discussion of all the test data, and a discussion of design concerns for the next generation core.

PART 1: PHASE-ONE EXPERIMENT

The information presented in Part One focuses on the modifications made to the original test apparatus. Chapter 2 discusses the modifications and the reasons for each. Chapter 3 examines experimental data from this phase of testing.

II. PHASE-ONE SYSTEM MODIFICATIONS

The initial test apparatus was received from Taussig.[10] As was mentioned in Chapter 1, there were several subsystems in this device which did not function properly. The redesigned and rebuilt subsystems that are discussed in this chapter are:

2.1) the heat exchangers and temperature control systems,

2.2) the fluid displacement system,

2.3) the external piping for helium and hydrogen, and

2.4) the electrical control logic for the heaters.

The regenerator core and superconducting solenoid were retained from Taussig's apparatus. Although the regenerator core was not redesigned in this phase, Section 2.5 presents information to be considered for possible future designs. A schematic of the new test apparatus is shown in Figure 5.

In addition to the major modifications, an agreement was reached on an overall design goal. This goal was to make the system operate as a refrigerator between a liquid helium bath and a liquid hydrogen bath.

2.1 Heat Exchangers and Temperature Control

In order for an active regenerator to work as a refrigerator, the helium inlet temperatures to the core must be properly controlled. A device cannot be properly tested if the reservoir temperature controllers do not work. The old device did not work. The primary reasons are 1) a convective lag between the heated helium and the temperature senor, 2) a time lag caused by thermal insulation on the heater, 3) trouble controlling the amount of cooling on the warm side, 4) helium dead space between the core and the heat exchangers.

The old temperature control systems were removed and replaced by a completely new system. The cold-end is to be kept at 4.2 K by thermal contact with the helium bath in the cryostat. The warm-end is to be stabilized by a hydrogen bath. The hydrogen bath is to be at ~15 K, a temperature slightly above its triple point and still within the practical working limit of GGG.

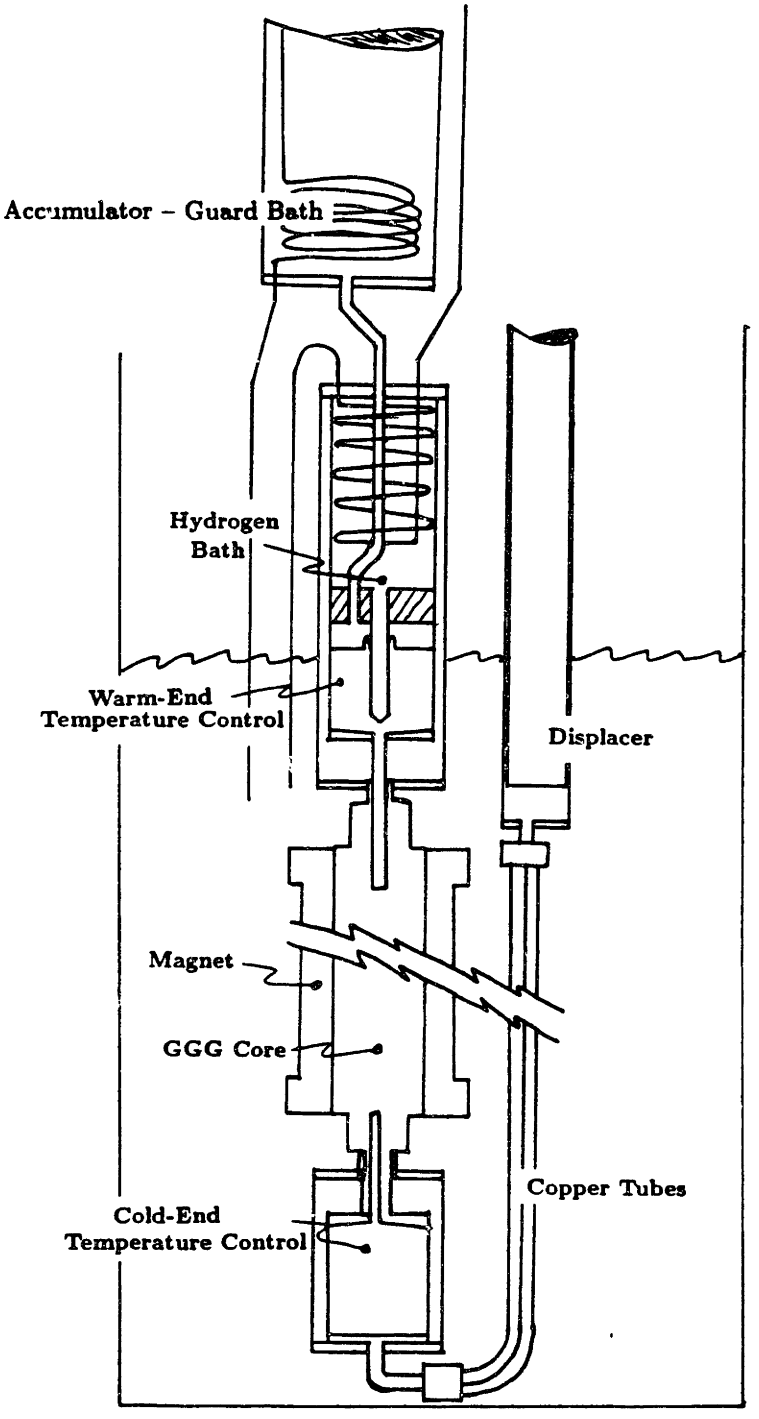

Fig. 5 Schematic of the Phase-One Modified Test Apparatus

There are three different temperature control modules. They are the cold-end control, the warm-end control, and the guard bath.

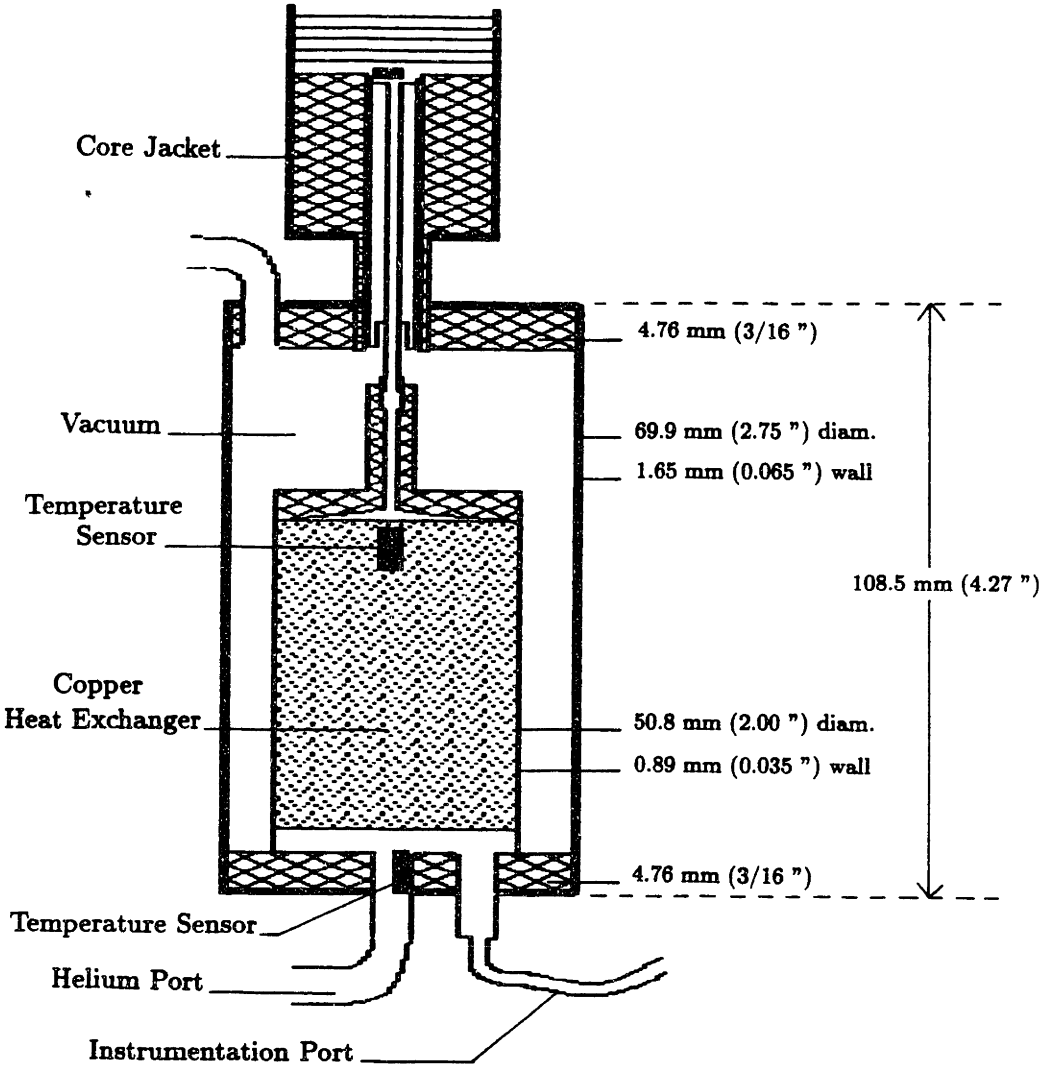

Fig. 6 Cold-End Temperature Control System

2.1.1 The Cold-End Control Module: (Figure 6) The cold-reservoir consists of a copper-block heat exchanger placed in a vacuum jacket. The ideal location for this heat exchanger (reservoir) would be inside the GGG core's jacket to minimize helium dead space. (Helium dead space is the helium which exists between the core and the reservoirs.) The heat exchanger is placed just outside of the core's jacket, with

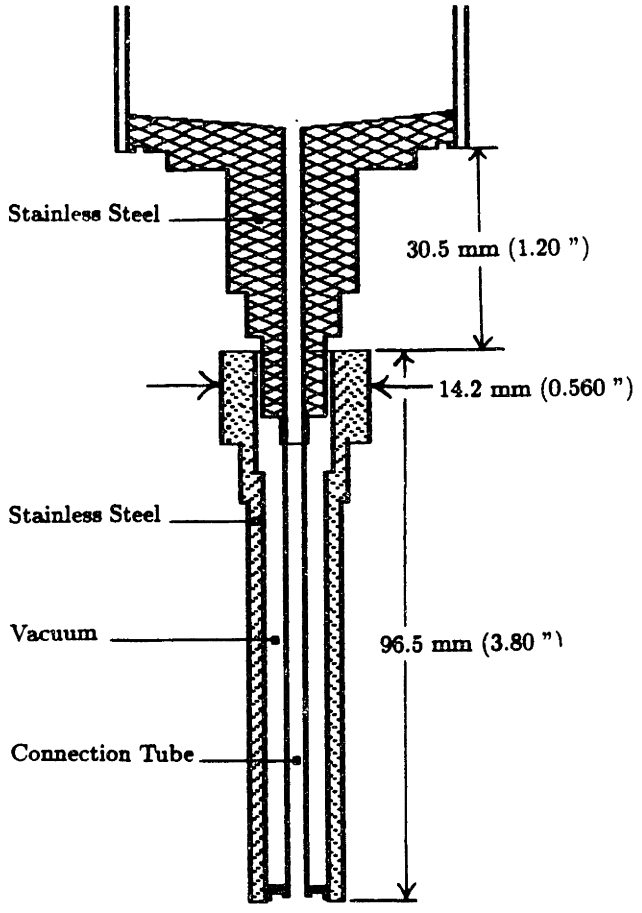

Fig. 7 Cold-End Connection Tube

an evacuated tube within a tube leading through the void area (Figure 7). The diameter of the inside tube was chosen as a compromise between helium dead space and pressure drop (Appendix B). The outside tube is shaped to fill up the void within the core jacket.

The copper block is a cylindrical plug with many small slits running in the radial direction. These slits were cut by EDM (Electrical Discharge Machining). Since the slits are radial, the magnetic flux passing through the copper will not induce large eddy currents (Appendix C). As the helium is forced through the slits on a down-flow, it is warmed back to 4.2 K by thermo-foil heaters embedded in some of the slits. The power provided by the heaters is equal to the refrigeration load. Appendix A describes the thermal design of the copper heat exchangers. Figure 8 is a drawing of the warm-end copper heat exchanger. The cold-end heat exchanger is identical to the warm-end, except that it contains neither the hole drilled into its center, nor the

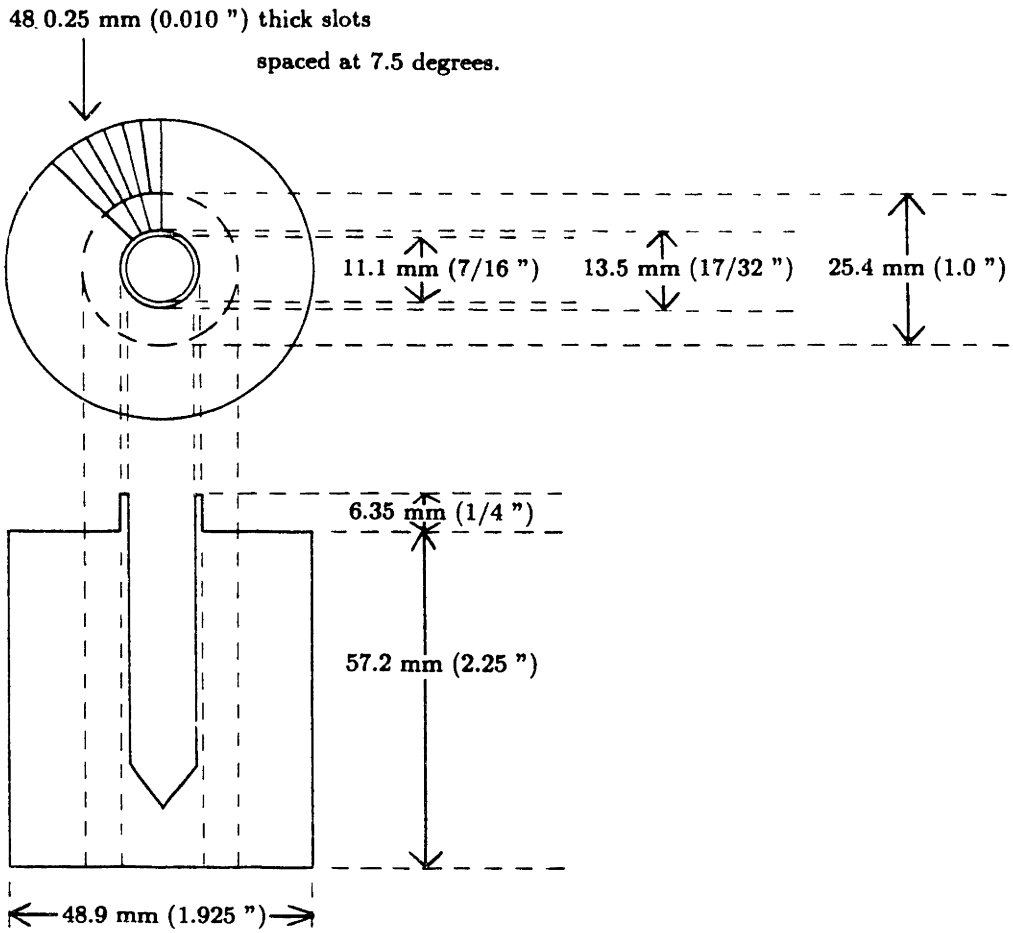

Fig. 8 Warm-End Copper Block Heat Exchanger

lip at the top of the hole.

On an up-flow the helium flows into the cold-end module from small copper tubes immersed in the liquid helium bath. Helium is thus provided to the cold-end at 4.2 K. This ensures accuracy of our load calculation.

2.1.2 The Warm-End Control Module: The warm-end reservoir (Fig. 9) has the same copper heat exchanger contained in the same vacuum jacket as does the cold-end, except that the warm-end receives cooling directly from the liquid hydrogen bath. The liquid hydrogen makes contact with the copper block through a hole that is drilled into its center (Figure 7). The hydrogen reservoir is contained in a chamber above the copper heat exchanger. It is a closed system. In order to maintain steady-state conditions within this chamber, hydrogen is condensed to replenish that

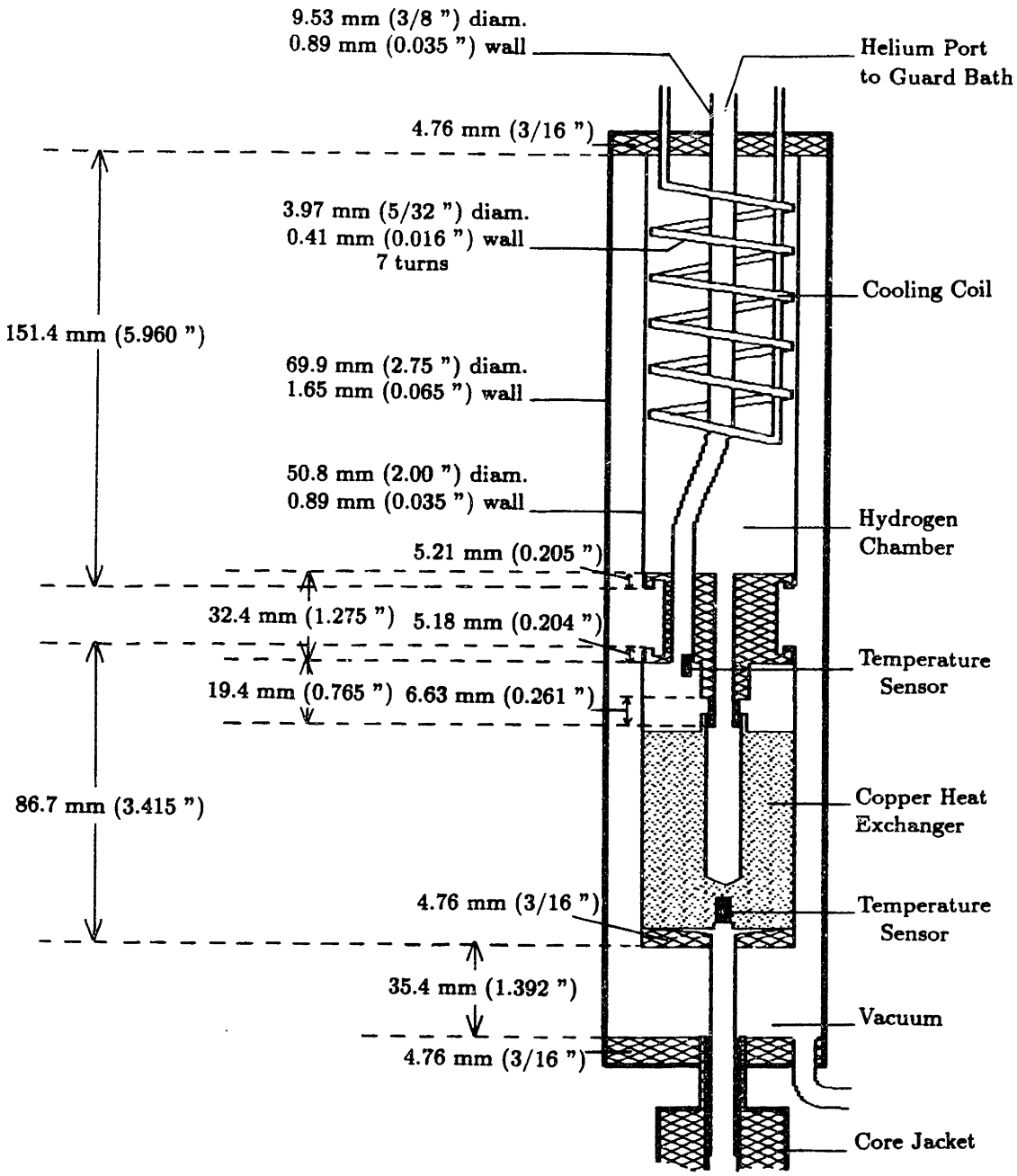

Fig. 9 Warm-End Temperature Control System

which boils away. A small stainless steel coil enters the hydrogen bath from the low pressure liquid helium bath in the cryostat. Liquid helium is forced through this tube to condense the hydrogen. It is possible that some hydrogen will freeze along portions of this tube. This should not hurt system performance. The helium will leave the tube at approximately the temperature of the hydrogen bath. By measuring the helium flow rate as it comes out of the cryostat, it is possible to calculate its cooling capacity, and therefore the time averaged heat of rejection.

A complete refrigeration system would use some other method for cooling the hydrogen. A space-based system, for example, could release hydrogen directly to space, thus using latent heat of vaporization to cool the bath. A cascaded refrigeration system would use the next stage to cool the hydrogen.

2.1.3 The Guard Bath: The guard bath sits at the bottom of the accumulator. It serves the same purpose as the immersed copper tubes do on the cold side; that is, it provides helium at the desired warm-end temperature to the warm-end heat exchanger. The guard bath thus ensures that the heat of rejection measured is accurate. Since it is difficult to predict the external heat load on the accumulator, the guard bath heat exchanger has the ability to both heat and cool. The temperature is kept uniform in the bottom of the accumulator by layers of copper screen. The screen also acts to diffuse the helium flow and keep it from mixing with warmer helium farther up the accumulator. The screen is soldered to a copper coil through which 4.2 K Helium flows to cool the bath. An insulated stainless steel wire wound through the copper screen is used as a heater.

2.1.4 Helium Dead Space

Helium dead space refers to the helium contained in the piping between the copper heat exchangers (reservoirs) and core. In our device the helium oscillates back and forth rather than continuing in a circular path. Dead space can diminish system performance. Cold helium which leaves the core on a down-flow but does not reach the heat exchanger is lost refrigeration. Warm helium which leaves the core on an up-flow but does not reach the warm-end heat exchanger cannot reject its heat. This heat is pulled back into the core when the flow reverses. For these reasons helium dead space must be minimized. Appendix B discusses the helium dead space design.

Chapter 11.6 discusses experimental and analytic results relating to dead space.

2.2 Fluid Displacement System

The old design chose to drive the helium with a piston-cylinder on the warm side of the core. A computer controlled stepper motor was to position the piston. The cold-end was equipped with a compensator which was to float with small changes in helium pressure. A leak on the warm-end prevented this system from working. We have since turned the warm side cylinder into an accumulator, and have moved the stepper motor over to the cold-end. There are two reasons for this action:

- The density of supercritical helium varies considerably with temperature. For this reason the warm-end displacer is designed to be much larger in area than the cold-end displacer. If the two displacer strokes are matched for one set of operating temperatures, then they will not be matched for other operating temperatures. Large pressure variations may result. Since a test rig needs the flexibility of being able to operate at any reasonable temperature range, an accumulator is desirable.
- Helium is far less compliant when it is below the critical temperature than when it is above. Flow can therefore be more accurately controlled from the cold-end.

The new drive system (Figure 10) hangs from the old drive support tower over the cold-end displacer. A cam-follower allows full displacement of the piston (5 cm), but stops travel before the bell diaphragm seal at the top of the cylinder is stressed. Limit switches tell the computer when the end of allowable travel is neared, and an LVDT is used to record the piston's position.

2.3 External Piping for Helium and Hydrogen:

The hydrogen system is completely new, and the helium system was modified. One new helium feature is the ability to pressurize the cryostat. This is necessary since operation of both the guard bath and the hydrogen bath require forced flow of liquid helium through their cooling tubes. Liquid helium is supplied from the bottom of the cryostat.

The working pressure and backing pressure lines were also redone because we had great difficulty controlling the working pressure during the previous experiments (probably due to a poor regulator and a leaking valve).

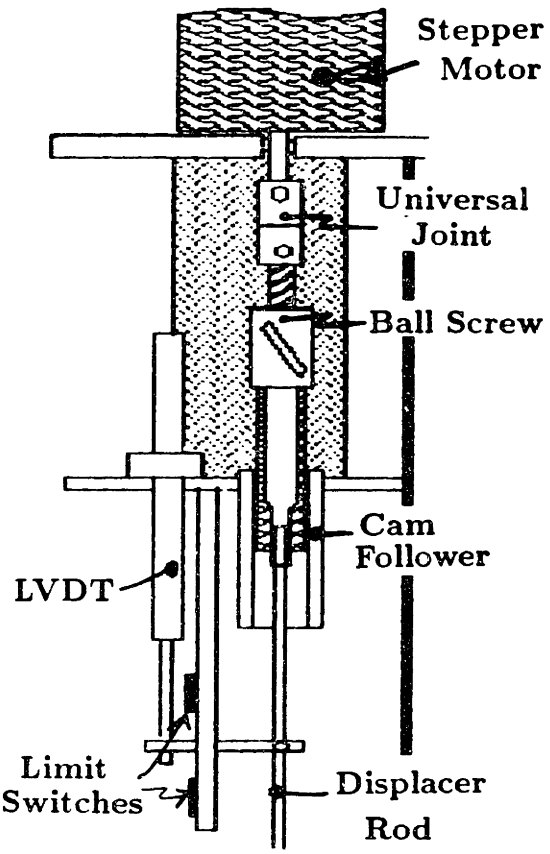

Fig. 10 Drive Mechanism for the Displacer

A schematic for the hydrogen system is shown in Figure 11. This system is contained within the control tower. The control tower stands next to the experiment and contains all of the electrical control circuits, and all of the helium and hydrogen control valves. The ports of the hydrogen system are labelled A through E. The system works as follows:

> The hydrogen chamber in the test apparatus is connected to port B. The entire system is evacuated through port E. Valve E is closed, and hydrogen is allowed to enter the system through port C. Hydrogen liquifies in the hydrogen chamber (Figure 8) whose temperature is kept cold with liquid helium. A vacuum gage is connected to the system via a toggle valve. Port A leads outdoors via a PVC plastic tube. A relief valve is set to relieve the hydrogen out port A if the system pressure ever exceeds 1.2 atm. A valve can also open port A.

The helium system is shown in Figure 12. This system is also contained within

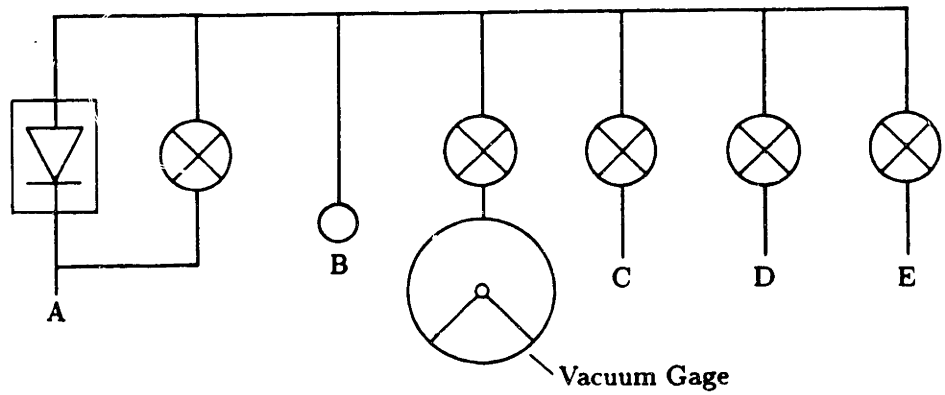

Fig. 11 Hydrogen Piping

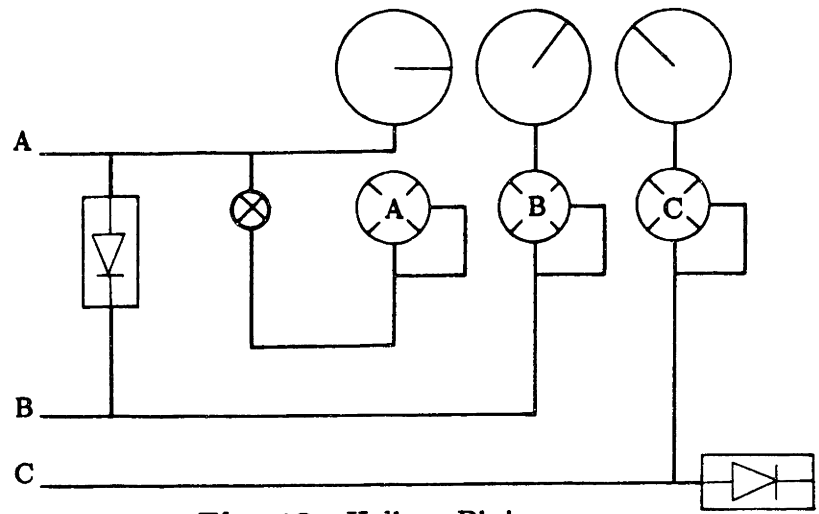

Fig. 12 Helium Piping

the control tower. There are three regulators, each is supplied with 14 atm helium gas. Regulator C controls the pressure of the cryostat. It can increase the cryostat pressure from 1 to 1.7 atm absolute. All the regulators are self-relieving, but for extra safety a relief valve is also included.

Regulator A supplies the working pressure. It maintains the helium transport fluid at a supercritical state. Regulator B supplies the backing pressure for the displacer. The backing pressure is applied to the "back" side of the displacer, opposite to the working pressure. It cancels most of the force which the displacer sees during operation and allows a moderately sized stepper motor to position the displacer. In order for the seal at the top of the displacer to function properly, the backing pressure should be maintained at approximately 1/4 atm below the working pressure. A relief valve between A and B prevents the working pressure from exceeding the backing pressure

by more than 2/3 atm.

A valve allows us to isolate regulator A from the system. This is necessary since we do not want helium to flow into and out of the top of the accumulator during testing, as the working pressure should fluctuate slightly as the system is cycled.

2.4 Electrical Control of the Heaters

A new control panel was designed to operate the heaters contained in each of the three temperature control modules. The heaters are powered by high gain Darlington transistors. A 3-position switch on the panel allows the heaters to be turned off, on, and put on automatic control. Automatic control compares an amplified voltage signal from the temperature sensor ($Vsens$) with a reference voltage ($Vref$). The reference voltages are easily adjusted. It is the nature of carbon resistor temperature sensors that the voltage signal increases with decreasing temperature. If $Vsens$ exceeds $Vref$, then the heater comes on. Since the thermal capacitance is large in the guard bath, the heater here is controlled by only on-off logic. Similarly the heater in the warm-end is controlled by on-off logic, but in this case the reason is different. This heater is only for maintaining the proper temperature for startup, and for defrosting the hydrogen should we lose control of the cycle. It is not for run-time temperature control.

The heater in the cold-end must match the refrigeration duty of the core, and it should not over heat the reservoir. A voltage is applied to this heater which is proportional to the difference between $Vsens$ and $Vref$. The proportionality constant is adjustable. (Figure 13)

All automatic control of the heaters must be enabled by a TTL signal. These signals can be used, for example, to enable power to the cold-end heater only when there is a down-flow in process. The signal can come from a 5-volt supply, or it can come from the computer. As the computer is controlling the refrigeration cycles, it will tell the control tower which direction the stepper is going, and whether the current generating the applied field is increasing or decreasing.

2.5 The Regenerator Core

The regenerator core (designed by Taussig and described in his Thesis) was designed

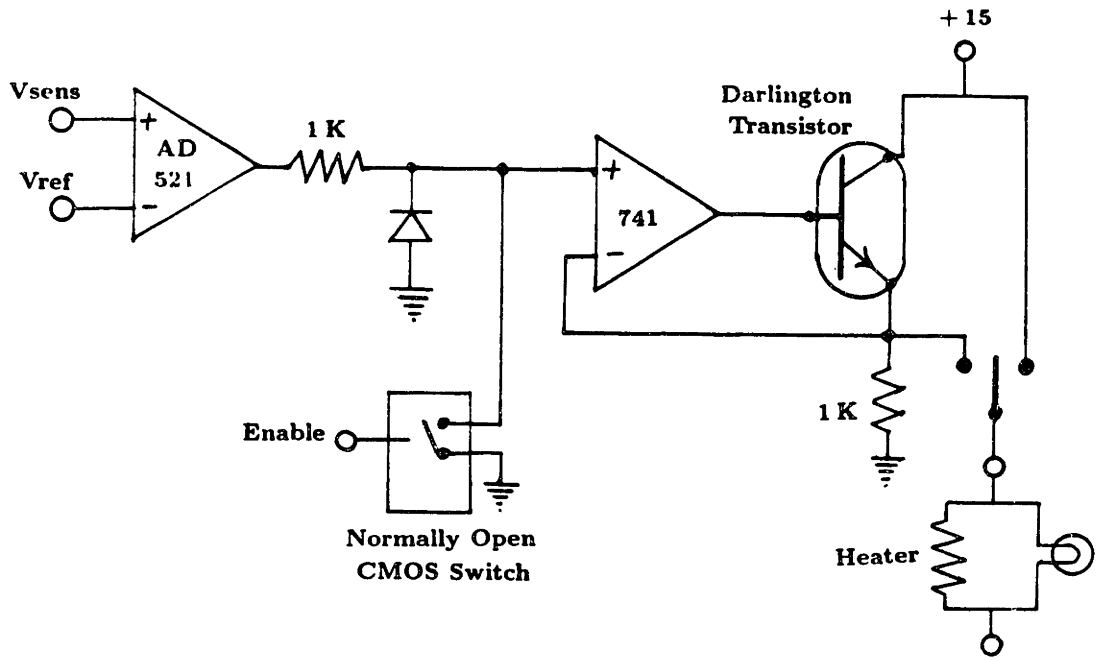

Fig. 13 Electric Circuit for the Cold-End Heater

to satisfy the basic requirements of: low axial heat conduction, low pressure drop, good heat transfer with the transport fluid, and minimum entrained helium.[10] Based on data obtained from the preliminary tests, the core appeared to meet these requirements. For this reason the core was not modified. A summary of some of the main considerations relating to the core design are presented below.

- Helium has an extremely low thermal conductivity and an extremely high specific heat compared with GGG at the temperature range of our interest. These properties require that the mass of helium in the flow passages through the GGG core be minimized. In general there is a trade off between irreversibility generated by pressure drop (increasing with smaller channels) and irreversibility generated by heat transfer (increasing with larger channels). In this case, however, machining and fabrication considerations determined the slot sizes to be $\sim 100\,\mu$m, which is greater than the optimum size. The main irreversibility is therefore due to heat transfer between the helium and the GGG core.

- Another problem shared by most magnetic refrigerators is helium entrainment. Our core was designed to have a helium void by volume of 4 to 5% with a working

pressure of 3 atm. Since helium has such a high specific heat, even this small void may add significantly to the effective zero field specific heat of the core. It is difficult to state the exact effect this has on the temperature swings available for a given field change, since changing the helium temperature induces flow which prevents the process from being adiabatic. The change in temperature of one segment therefore depends on the other segments in the core and on the flow boundary conditions imposed. A single isolated core segment starting a 5 K and magnetized from 0 to 4 T, for example, will experience a temperature change to 21 K with zero void, to 16 K with 5% void, and to 13 K with 10% void. Minimizing the helium void is an important design consideration; another option is to lower the working pressure.

III. PHASE ONE EXPERIMENTAL RESULTS

3.1 Introduction

After the Phase-One modifications were completed in the Fall of 1987, the experimental apparatus was tested five times. The first four tests were less than perfect due to various minor problems which were corrected before the final test was performed on January 29, 1988. All of the subsystems were operable at this time. Data from this test, and from previous tests, are analyzed in this chapter.

Section 3.2 examines the performance of the subsystems and provides experimental validation of the Phase One modifications. Section 3.3 provides a summary of the Phase One testing.

3.2 Experimental Validation of the Phase One Modifications:

This section examines the test data to determine if the subsystems performed properly after the Phase One modifications. The following subsystems are examined:

3.2.1 the Temperature Sensors,

3.2.2 the Copper Heat Exchangers,

3.2.3 the Reservoir Temperature Control,

3.2.4 and, the Displacer System.

3.2.1 Temperature Sensors:

The location of most of the carbon resistor temperature sensors is shown in Figure 14. The cold-end sensors, C-1 through C-5, are all nominal 47-ohm 1/4-W Allen Bradley resistors. They have been calibrated in the temperature range from 1.5 to 4.2 K. Readings much above 4.2 K are therefore out of the calibrated range and should be taken as approximate. The warm-end sensors, W-1 through W-5 are all nominal 220-ohm Allen Bradley resistors. These sensors have been calibrated over the larger temperature range of 4.2 to 20 K. Readings much above 20 K should be taken as approximate. Appendix D contains a detailed description of each temperature sensor.

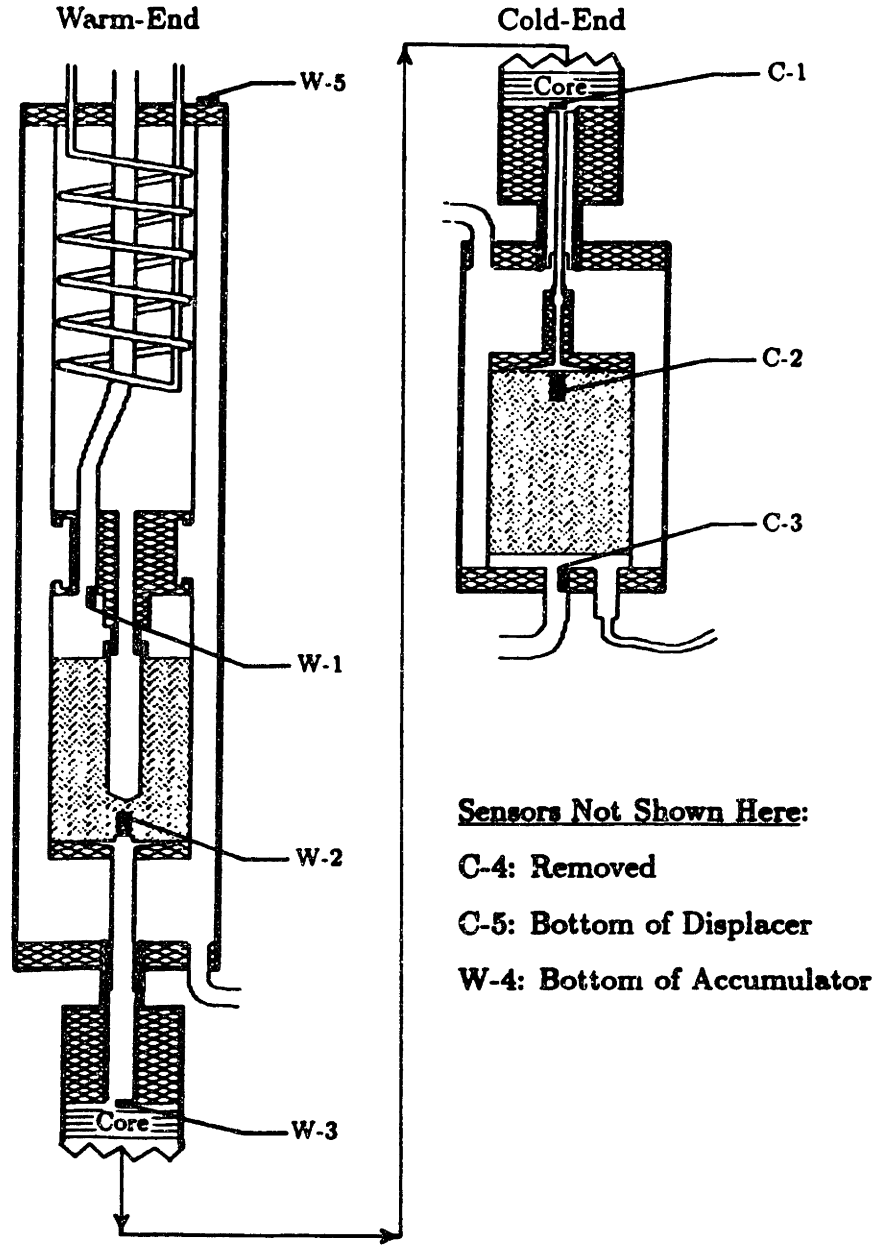

Fig. 14 Location of the Temperature Sensors

Response Rate and Accuracy of Sensors:

Two attributes of a good temperature sensor are that it accurately depicts the temperature of the medium of concern, and that it responds quickly to temperature changes. Our sensors do respond quickly. Figure 15a shows the sensor C-1 changing at a rate of 4.2 (K/s), and Figure 15b shows sensor W-3 changing at the rate of 12 (K/s). The sensor's response rate must therefore be at least this fast. (The period of the refrigeration cycle is 10 s.)

The accuracy of the temperature readings can be effected by the accuracy and repeatability of the calibrations, and the thermal contact of the sensor with the medium of concern. Our sensors seem to be very accurate and repeatable. Figure 16 shows sensors C-2 through C-4 just before commencement of a test run. Note that all sensors read 4.2 K ($\pm$ 0.03 K). The cold-end sensors where calibrated a few years ago. There seems to be no noticeable drift in calibration either with repeated use or with time.

Thermal Contact with Medium of Concern

The question of whether the sensors are in thermal contact with the medium of concern is more difficult to answer. In order to satisfy this requirement:

A. the temperature of the helium surrounding the sensor must equal the temperature that we wish to measure.

B. the support structure which holds the sensor in place must not influence the temperature of the sensor.

A.: In most test cases, we are interested in knowing both the temperature of the reservoirs and the temperature of the core. Sensors C-2 and W-2 are imbedded in the copper block heat exchangers, and they should reflect the temperature of their respective reservoir. Sensors W-3 and C-1, however, are not in direct contact with the core, but instead are located in the helium dead space between the core and the heat exchangers. The influence of the dead space varies depending on what type of thermodynamic cycle is being tested. For example, if the warm-end starts out cold, and then is heated by an up-flow from the core, then an unstable situation with respect to natural convection is created in the warm-end. The connection tube then

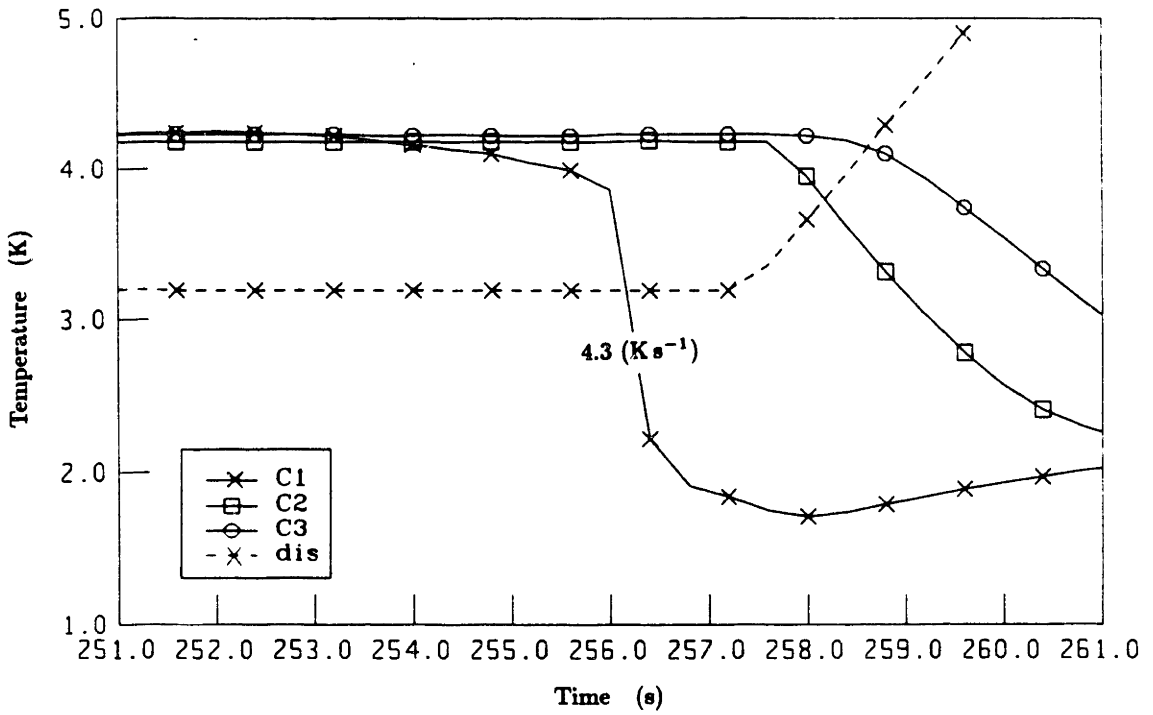

Fig. 15a Response Rate of Sensor C1

Code for the Figures in This Chapter

The graphs in this chapter present data recorded from the temperature sensors during testing. Also shown on some of the graphs are traces of the current in the primary solenoid, the displacer position, and the hydrogen pressure. For these traces:

Label	Description	Units
C1:	Temp. Just Below the Core	(K)
C2:	Temp. In Cold-End Copper Heat Exchanger	(K)
C3:	Temp. Below Copper Heat Exchanger	(K)
C5:	Temp. Just Below Displacer	(K)
W1:	Temp. Above Warm-End Copper Heat Exch.	(K)
W2:	Temp. In Warm-End Copper Heat Exch.	(K)
W3:	Temp. Just Above the Core	(K)
W4:	Temp. In the Guard Bath	(K)
cur:	Primary Current	(1 K = 10 A)
dis:	Displacer Position	(1 K $\simeq$ 1 g)
pres:	Hydrogen Pressure	(1 K $\simeq$ 0.5 atm)

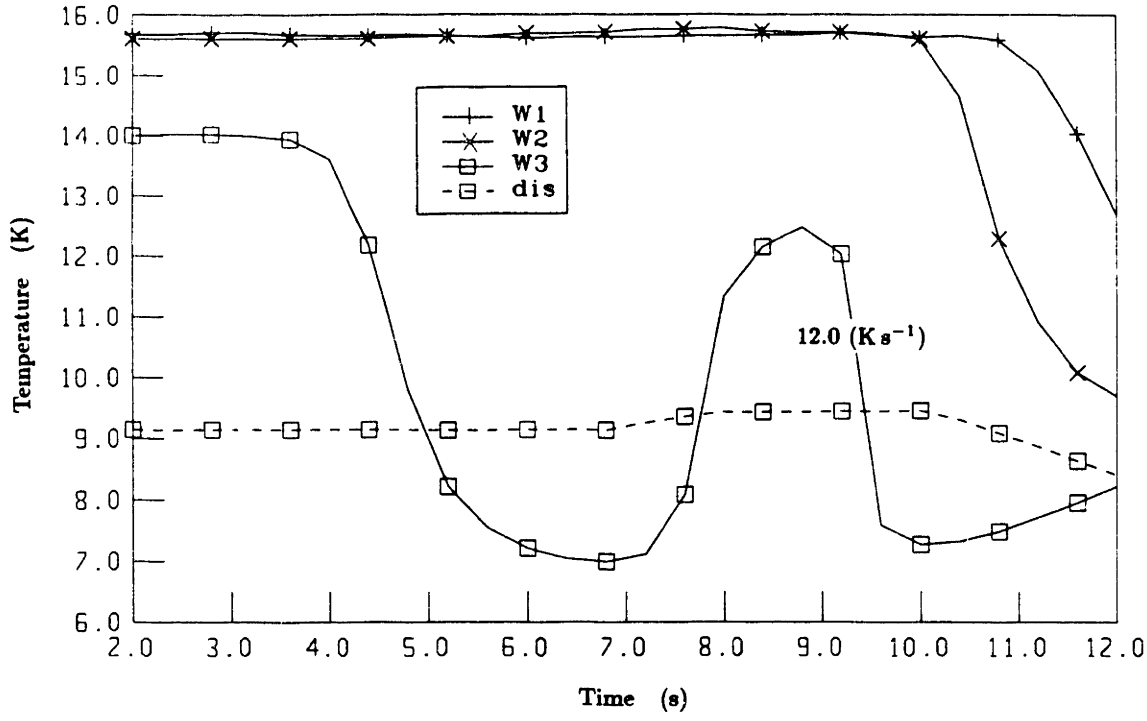

Fig. 15b Response Rate of Sensor W3

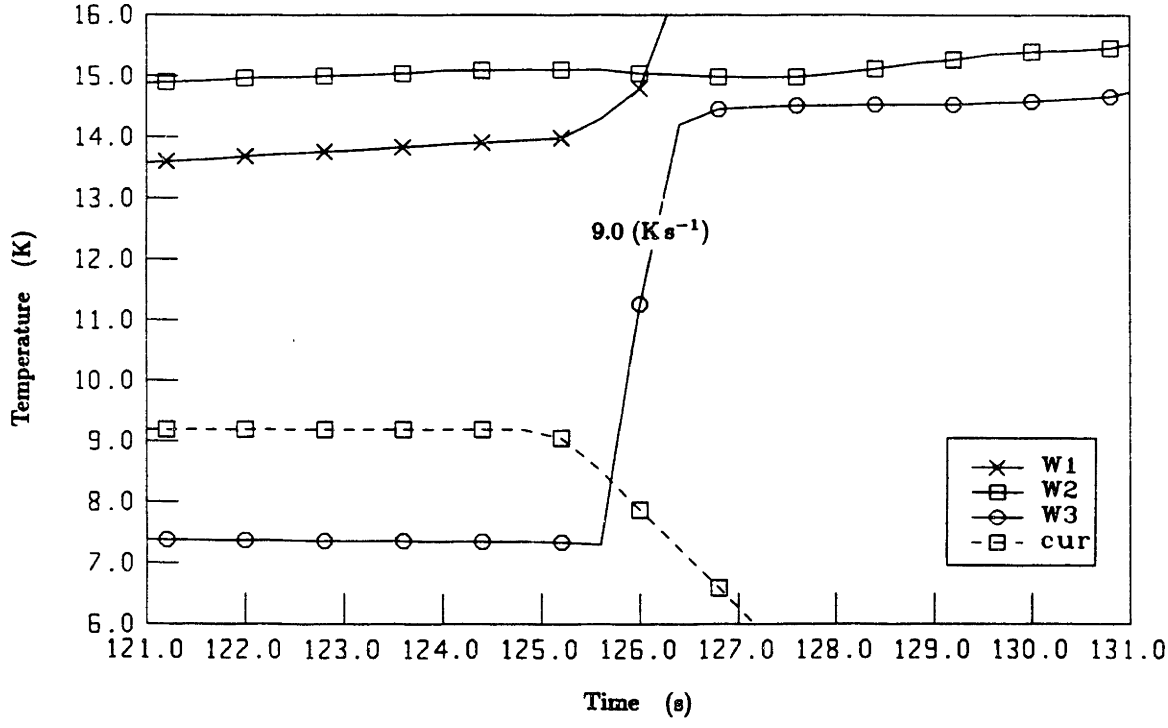

Fig. 15c Response Rate of Sensor W3

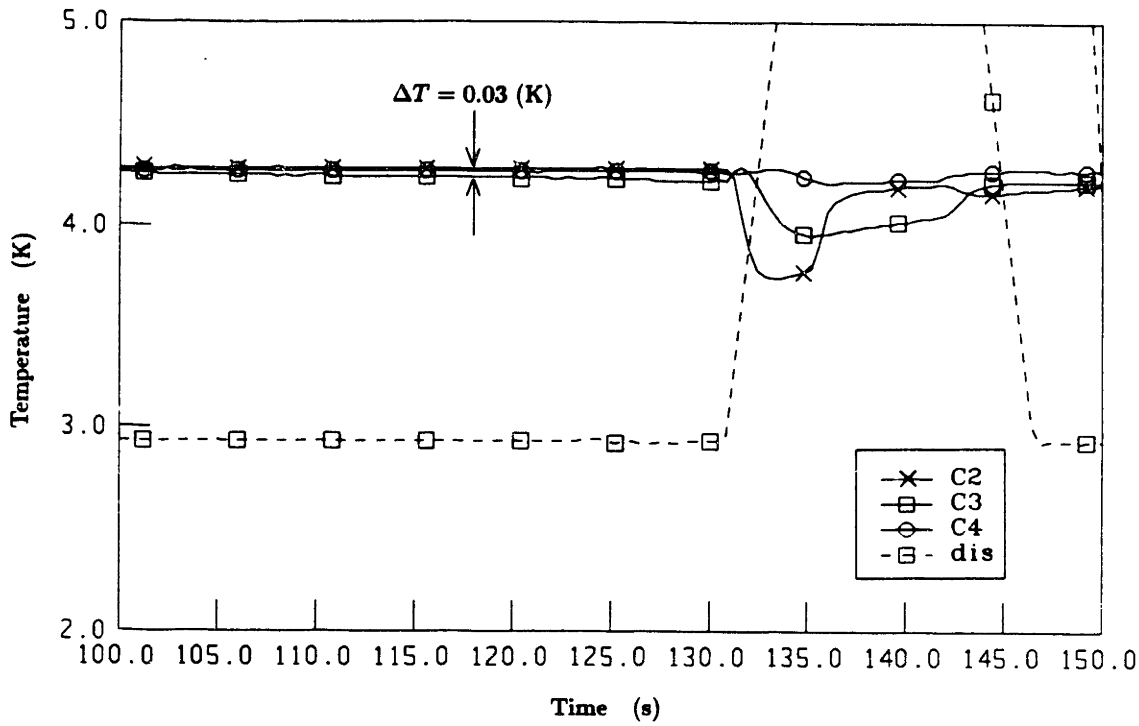

Fig. 16 Accuracy of Cold-End Sensors

acts as a well mixed reservoir which can only be heated uniformly. The temperature of the helium in the tube surrounding sensor W-3 trails the temperature of the helium leaving the core. The connecting tubes are designed (see Appendix B) so that the external helium void will be small under normal operation. Under normal steady-state operation, the warm-end connection tube should be at least as warm as the warm-end reservoir.

To examine how the temperature sensors respond during a test run, refer to Figure 17. This figure shows the response of sensors C-1, C-2 and C-3 during a down-flow process. Prior to the flow process, the cold-end of the core was cooled to ~2 K by an adiabatic demagnetization. During the flow process helium flows out from the core and passes by sensor C-1 before flowing down the connection tube to the copper heat exchanger where sensor C-2 is located. Helium is also flowing out of the heat exchanger into the helium void where sensor C-3 is located. The temperature at sensor C-1 is initially very cold, but then warms as the flow continues. The copper block heat exchanger should warm when the incoming helium is warmer than its

temperature, and should cool when the incoming helium is cooler than its temperature. Figure 17 shows that sensor C-2, is cooled while C-1 < C-2, and is heated while C-1 > C-2. When C-1 = C-2, C-2 reaches its minimum temperature. There is a negligible phase lag between the response of sensors C-1 and C-2. This indicates that the copper block is at a single temperature, and that the helium void between C-1 and C-2 is small. There is a phase lag between the response of sensors C-2 and C-3. This results from the relatively large helium void where sensor C-3 is located.

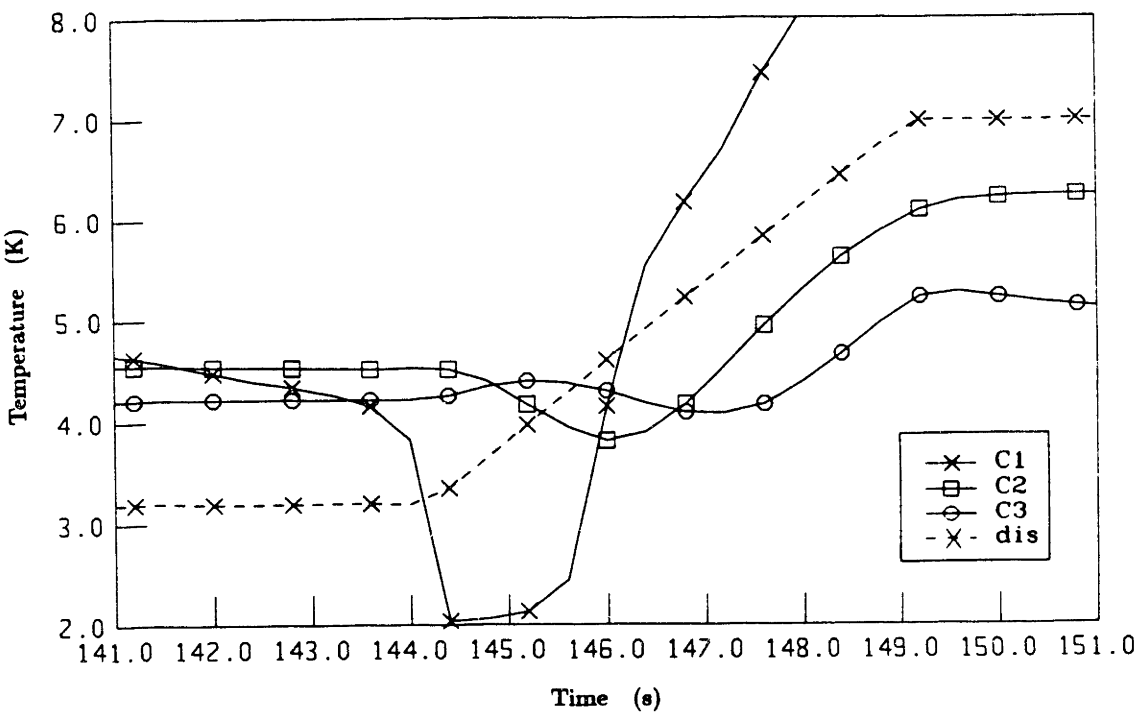

Fig. 17 Cold-End Sensor Response During a Flow Process

- Whenever temperature data are being analyzed, it is important to keep in mind how the thermal capacity of the helium volume surrounding the sensor is affecting the response.

B.: The other issue that may effect the accuracy of our temperature readings is that a sensor may reflect a temperature somewhere between the temperature of the helium in which it is submerged, and the temperature of the support structure which holds it in place. This, of course, can only make a difference if the support structure is at a significantly different temperature than the helium. Rough calculations show that

the support structure can only deviate appreciably in temperature at the warm-end. This is because the cold-end temperatures never deviate far from the helium bath temperature, and because the conductivity of the stainless at 4.2 is about 1/5 of that at 15 K.

Actually, the only sensor where this issue can become a problem is sensor W-3. This sensor is attached to the bottom of the evacuated stainless tube which connects the warm-end heat exchanger to the top of the core (see Chapter 2, Figure 7). The top of the outside section of this tube is in direct contact with the 4.2-K saturated liquid helium bath. The bottom of this tube is in contact with the 15-K supercritical helium. The thermal resistance of this tube has been estimated to be ~200 (K/W). The thermal resistance of the 15-K helium to the tube's bottom has been estimated to be ~37 (K/W). (This analysis is not shown.) The temperature of the tube is therefore roughly 13 K. From this analysis one can see that the tube wall will be slightly cooler than the helium, and that the temperature sensor may read low if it partially reflects the wall temperature.

Figure 18a and 18b show the response of sensors W-1, W-2 and W-3 during various test runs. During a down-flow, sensor W-3 is downstream of the copper block heat exchanger whose temperature is given by sensor W-2. Sensor W-3 should follow the response of sensor W-2, but it instead stays about 0.4 K colder. On an up-flow, if the copper block heat exchanger is heated (note that it can only be heated slightly due to liquid hydrogen stabilization), the helium passing sensor W-3 must be warmer than W-2. Many examples show the copper to be heating while sensor W-3 reads about 0.5 K below sensor W-2. This information indicates that sensor W-3 consistently reads about 0.5 K below the temperature of the helium stream.

3.2.2 Copper Block Heat Exchangers

The copper heat exchangers work well if they can control the temperature of the helium as it leaves them to enter the core. This requirement is satisfied if they have a large heat transfer area, good internal heat conductivity, and a method to stabilize there temperature. (See Appendix A for details of the heat exchanger design.)

On examination of data collected during the various runs, it can be seen that the copper blocks did have an acceptably large heat transfer area. Figures 18a and 18b

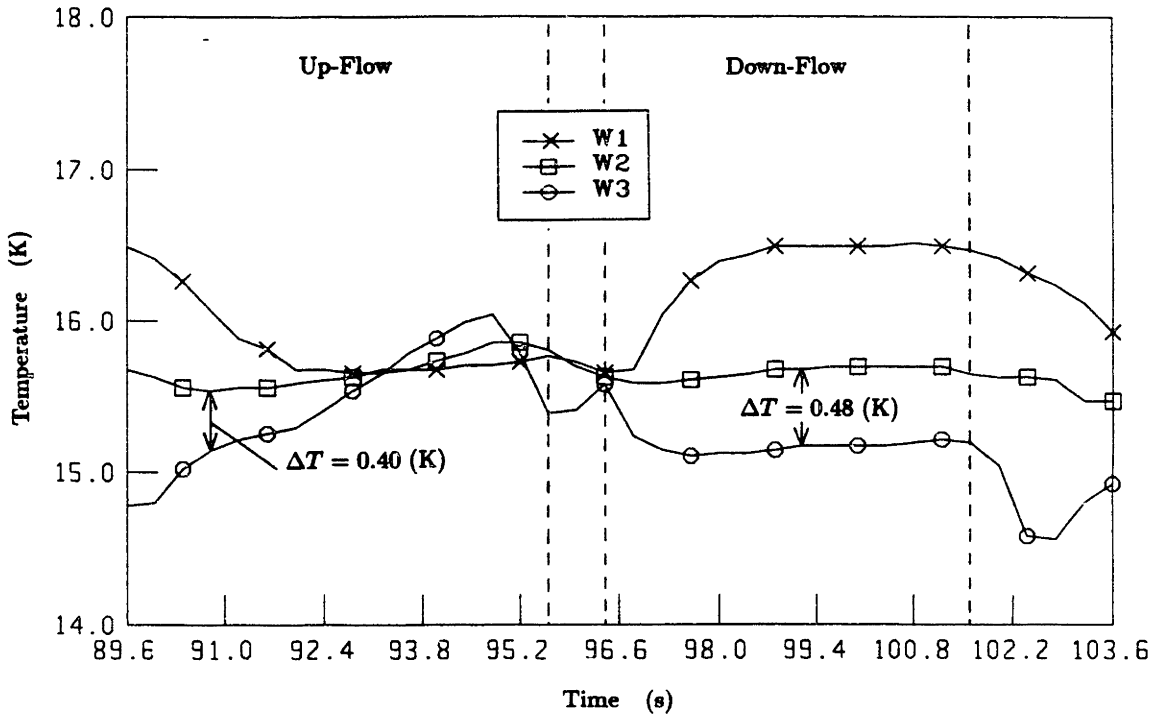

Fig. 18a Example of Sensor W3 Reading ~0.5 K too Low

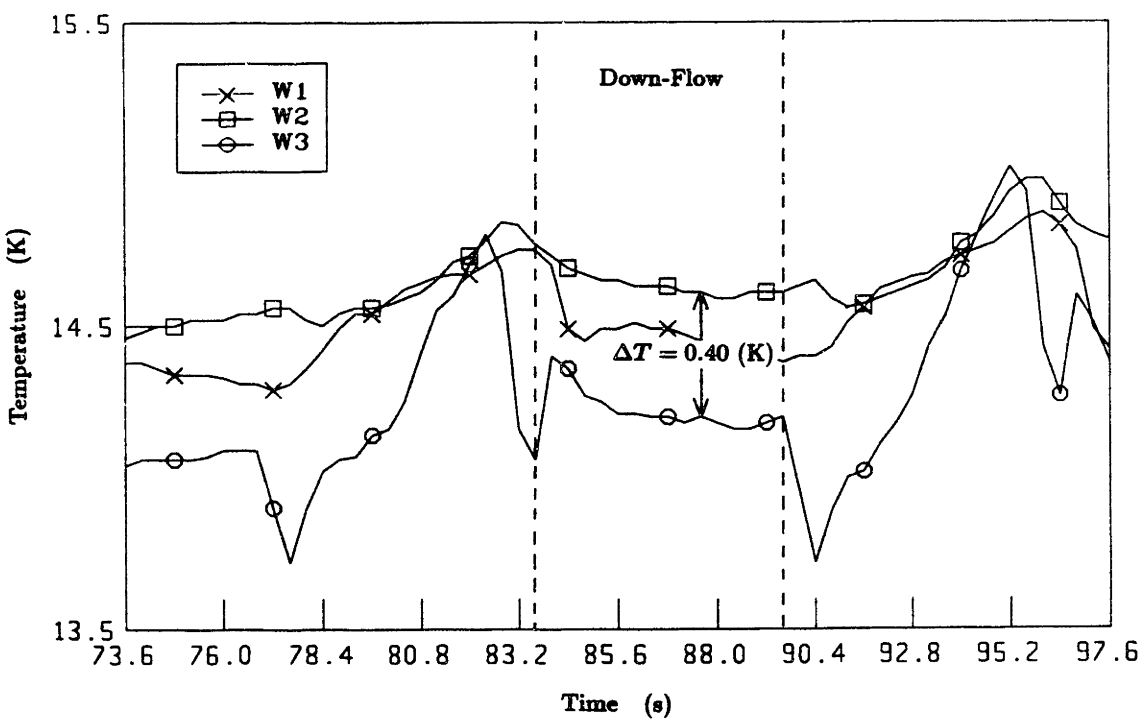

Fig. 18b Example of Sensor W3 Reading ~0.5 K too Low

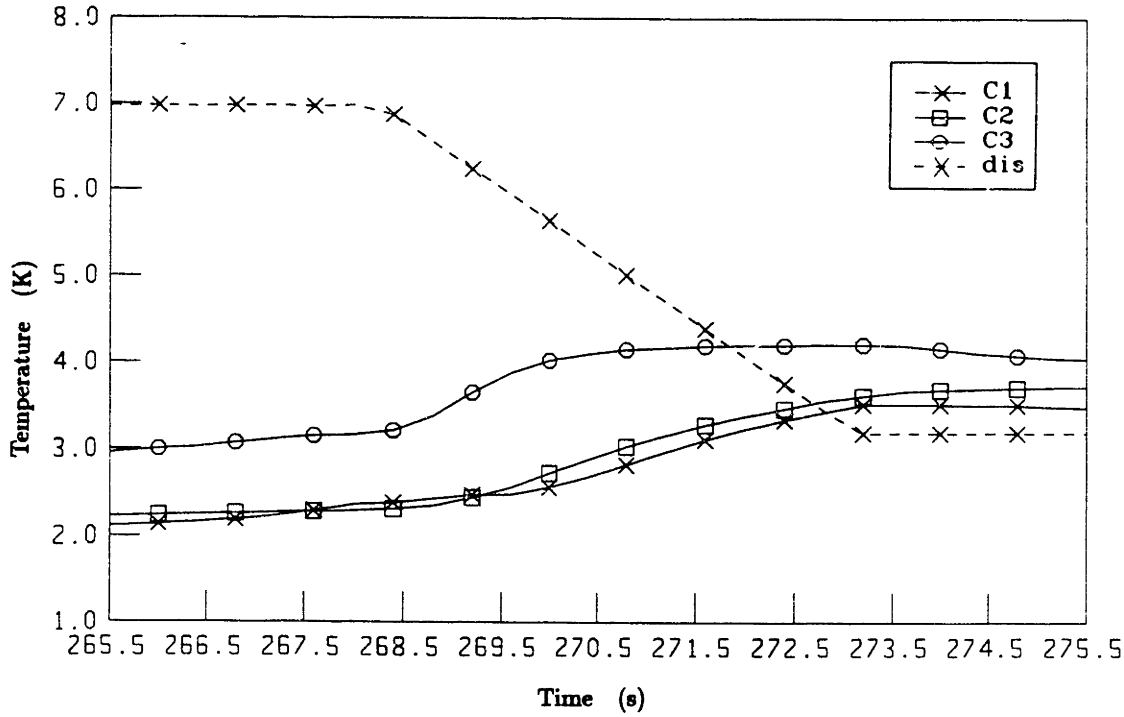

Fig. 19a Temperature Downstream of Copper Block

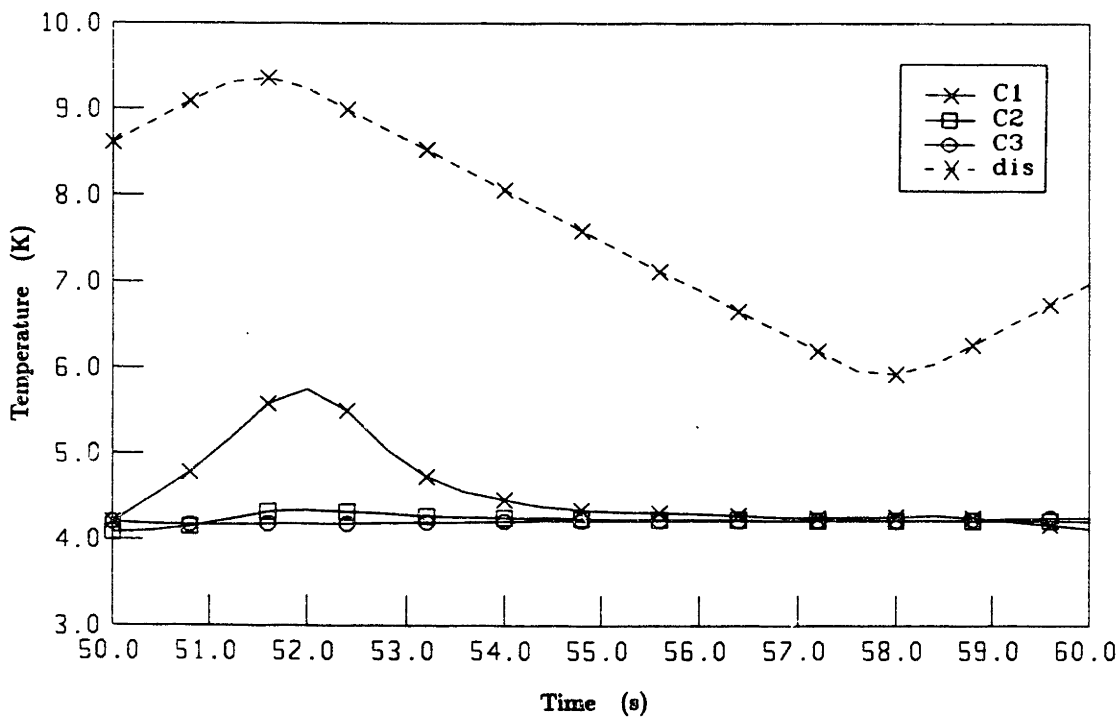

Fig. 19b Temperature Downstream of Copper Block

show how sensor W-3 follows the warm-end copper block temperature, W-2, when there is down-flow. Figures 19a and 19b show sensor C-1 following the cold-end copper block temperature, C-2, when there is up-flow. One can see that once helium contained in the connection tube dead volume has passed, the downstream sensor will follow the temperature of the copper block quite closely.

3.2.3 Reservoir Temperature Control

Control of the copper block's temperature, and therefore the helium temperature which enters the core, was done differently for the warm-end than for the cold-end. The warm-end was stabilized by boiling liquid hydrogen kept at constant pressure. In addition, the hydrogen (liquid or solid) adds a significant amount of specific heat to the warm-end reservoir. This extra specific heat can reduce the temperature swings experienced by the warm-end reservoir under cyclic operation. The warm-end reservoir was tested without hydrogen, with frozen hydrogen, and with liquid hydrogen. Figure 20a is a test which was performed with a vacuum in the hydrogen chamber. The warm-end temperatures fluctuate wildly. Figure 20b is a test where the hydrogen was frozen during this portion of the run. Though the copper temperature is more controlled, it still varies by almost 2 K during steady-state cycling. Figure 20c is a test where liquid hydrogen is maintained in the hydrogen chamber. The hydrogen saturation temperature during this run was close to its triple point, ~14 K. The temperature of the copper block at this time is about 14.5 K. The fluctuations are small, less than 0.4 K. It should be noted that different thermodynamic cycles reject different amounts of heat at the warm-end, and the fluctuations observed may differ.

3.2.4 Checking the Helium Flow Rate

We are using the position of the displacer to indicate the mass of helium flowing into the cold-end heat exchanger. It is possible to check some of our basic assumptions regarding both temperature sensor accuracy and helium flow measurement accuracy by observing the rate at which the heat exchangers change temperature.

The cold-end heat exchanger should experience the same flow rate as produced from the displacer motion, and as at the bottom of the core. The breathing effect in the core will result in a different flow rate through the warm-end heat exchanger than

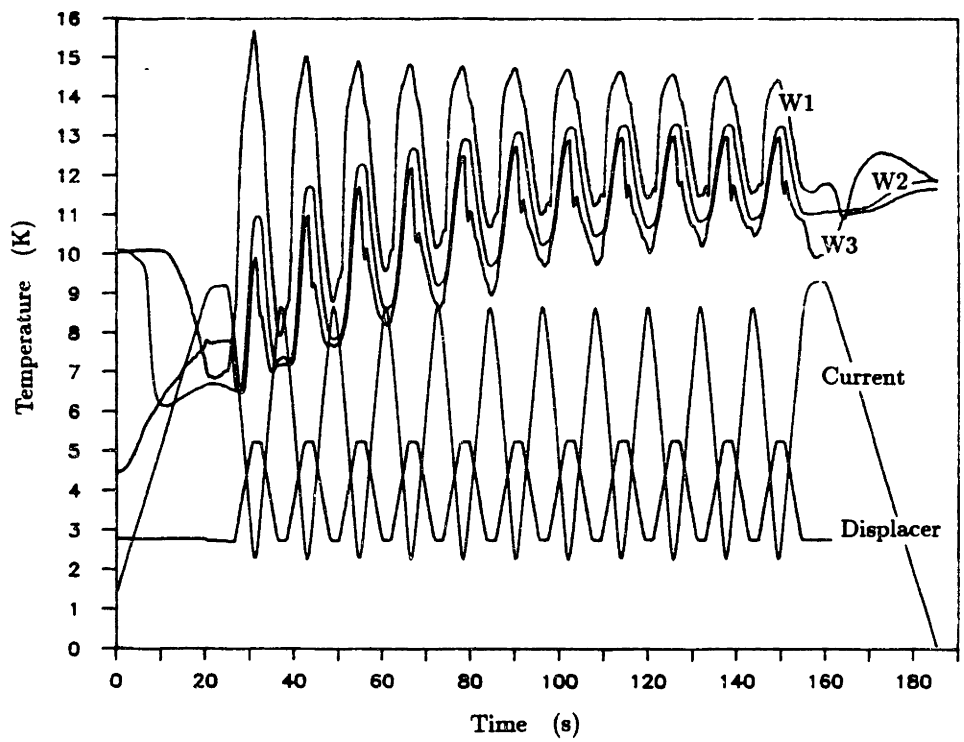

Fig. 20a Warm-End without Hydrogen

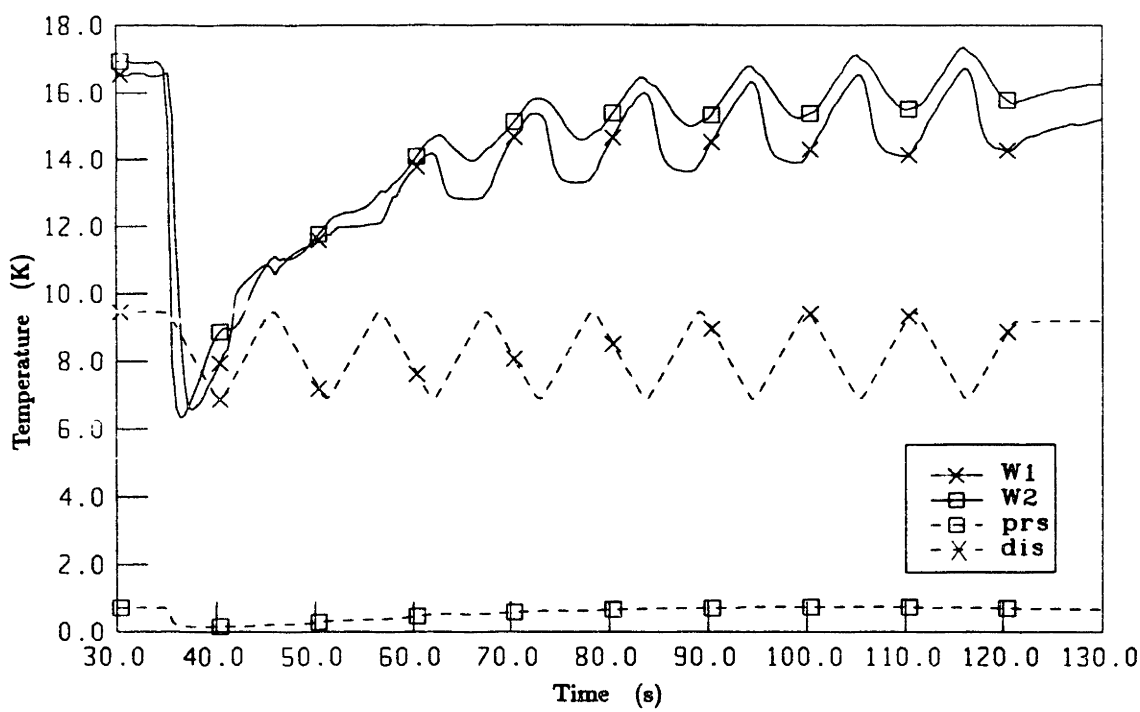

Fig. 20b Warm-end with Frozen Hydrogen

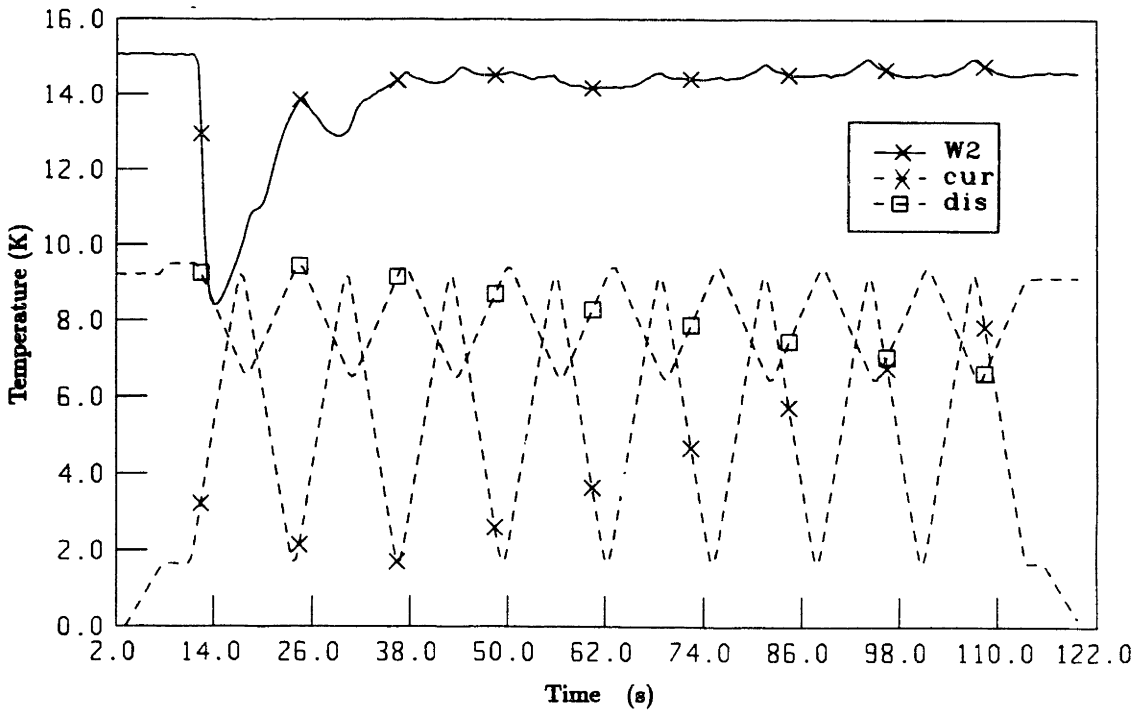

Fig. 20c Warm-End with Boiling Hydrogen

through the cold-end heat exchanger. For this reason the flow is checked only at the cold-end. The heat capacity of copper at 4.2 K is negligible so the only contribution to specific heat is by the helium entrained within the exchanger. From Appendix A we find that the helium void within each exchanger is ~12 cc. The void in the warm-end and cold-end connection tubes is 1.8 cc and 7.8 cc respectively. Assuming uniform helium properties in the heat exchanger a heat balance can be written:

$$d(\rho V u)_{he} = h_{in} dm_{in} - h_{out} dm_{out}$$

with mass continuity:

$$dm_{out} = dm_{in} - V_{he}\, d\rho$$

Assuming that the helium pressure is constant:

$$d(\rho u) = d(\rho h) = \rho\, dh + h\, d\rho$$

Since the temperature of the helium leaving the copper block is equal to the Copper's temperature, $h_{out} = h$. The heat balance can be rewritten as:

$$\rho V\, dh = dm_{in}(h_{in} - h)$$

With $dh \equiv c_p\, dT$ we find:

$$\dot{m}_{in} = \frac{(\rho V\, c_p)\frac{dT}{dt}}{h_{in} - h} \quad [\mathrm{g/s}] \tag{1}$$

Equation (1) gives the expected relationship for the rate of temperature change of the heat exchangers for a given enthalpy flux.

Test runs were performed at both 3 and 5 atm of pressure. Tables 1a and 1b show the specific heat of the heat exchanger components, and show values for the helium's enthalpy for use in Equation (1). Data are taken from several test runs, and the helium flow rate, $\dot{m}$, is calculated using Equation (1). This value is compared with the helium flow rate which is calculated from the displacer motion. The results are shown in Table 2. All errors are within 15 %. The scatter appears to be random.

3.3 Summary

The test data discussed in section 3.2 relate only to Phase One modified subsystem performance, and not to the performance of the core. Data relating to the performance of the core was not interpreted properly at this time. The conclusions from the Phase One Testing are:

- The data obtained from these tests could have been used to reveal the properties of the core, as will be discusssed in Chapter 11. (Unfortunately at the time this information was not properly analyzed.)
- All Phase One modifications of the subsystems performed satisfactorily.
- Steady-state refrigeration was not achieved during this phase.
- Analysis that was developed simultaneously to the testing predicted that steady-state refrigeration could not be achieved with the present experimental system. This analysis is presented in Part 2.

TABLE 1a Helium ($\rho V c_p$) at 3 Atm, (J/K)				
T (K)	Copper Heat Exch.	Warm Conn. Tube	Cold Conn. Tube	h_{he} (J/g)
2.2	4.8	3.1	0.7	−9.6
4.2	6.1	4.0	0.9	−4.5
10.0	1.1	0.7	–NA–	46.7
15.0	0.7	0.4	–NA–	74.9

TABLE 1b Helium ($\rho V c_p$) at 5 Atm, (J/K)				
T (K)	Copper Heat Exch.	Warm Conn. Tube	Cold Conn. Tube	h_{he} (J/g)
2.2	4.4	2.8	0.7	−8.4
4.2	5.7	3.7	0.9	−3.7
10.0	2.2	1.5	NA	43.2
15.0	1.2	0.8	NA	73.0

TABLE 2 Flow Check at Cold End			
Run #, (date)	$\dot{m}$ (g/s) From eq. (1)	$\dot{m}$ (g/s) from Displ.	% Deviation
8, (1-29-88)	0.95	0.99	−4%
12, (1-29-88)	0.67	0.76	−12%
12, (1-29-88)	0.83	0.76	+9%
4, (11-5-87)	1.06	1.07	−1%

PART 2: ANALYSIS

Part Two consists of six independent analyses, all using the real property data of helium and GGG. The material presented in these chapters is useful in providing an overall conceptual understanding to the dynamics of active regeneration. The computer simulation analysis presented in Chapter 5 should only be used as a design tool in conjunction with this overall understanding. A brief guide to the analyses contained in Part 2 is given on the following page.

Guide to the Analysis Presented in Part 2

Ch. 4: Ideal Carnot Analysis: This is a Second-Law approach. It begins by assuming that Carnot cycles are followed by every core segment, and then calculates the required field-flow phasing. It is useful in exploring some basic cycle parameters. Ideal refrigeration capacity is determined. In practice the field-flow phasing determined from this analysis cannot be achieved.

Ch. 5: Analysis by Computer Simulation: This is a First-Law approach. It has the same order of parameter dependence as the test device. It is useful in predicting core behavior for a given set of operating parameters. It is insufficient as an initial design tool.

Ch. 6: Closed Form Analysis: This is the mathematical background for the analysis in Chapters 7 and 8. A differential equation for an "ideal" core (containing helium porosity) is developed and analyzed in its limiting cases. Complete thermodynamic cycles are not discussed.

Ch. 7: Non-Carnot Active Regenerator Applications: Some non-Carnot applications are analyzed. These cycles are less complicated than the Carnot, yet they reveal important cyclic steady-state behavior of active regeneration.

Ch. 8: Explanation of Cycle Behavior: By using active convection wave logic, a qualitative understanding of the dynamics of active regeneration is developed. This is the first step in optimization and design.

Ch. 9: Irreversibility Analysis: This is a First-Order Analysis only. It looks at various sources of irreversibility which might affect a regenerator core of the design chosen for our system. Irreversibility can be included as a perturbation in the preceeding analyses.

IV ANALYSIS OF AN IDEAL CARNOT SYSTEM

The first stage of thermodynamic design is to analyze the system in its ideal limit, without system irreversibilities. An earlier analysis was simplified in that the helium properties were assumed constant, and in that there was no attempt to match the properties of the GGG to specific temperature-field requirements.[9] The purpose of this section is to determine the actual Ideal-Carnot limit for our device, and thus determine the maximum amount of refrigeration that is available for a given amount of GGG. The response of the device to changes in basic cycle parameters is determined by this analysis. The logic used to analyze the Ideal Carnot System is broken into three parts:

4.1 Determination of helium temperature profiles which allow for reversible Carnot Cycles throughout the core using only the second law.

4.2 Matching of these cycles to the GGG properties and plotting them on the T-S diagram of the GGG.

4.3 Iteratively modifying the helium temperature profiles in order to determine a set of cycles which use all of the available field swing, and determination of the required field profiles as functions of both percent of isothermal path, and position along the core.

The assumptions used in this analysis are:

1) Each segment experiences only Carnot Cycles; in this analysis the core, which consists of 120 wafers, is divided into 360 segments.

2) There are no irreversibilities other than helium mixing in the two heat sinks at the two ends of the core. Specifically this means that:

   - The heat transfer between the helium and GGG is sufficiently large so that the ΔT between the helium and GGG is negligibly small.
   - The GGG's conductivity is high enough to ensure uniform temperature within each segment.
   - The irreversibility due to the helium leaving one segment at that segment's

temperature and then entering the next segment at a different temperature approaches zero. It is shown in Chapter 9 that this approximation is very good for our core.

- Other heat transfer losses such as axial conduction, parasitic heat loads introduced by the specific heat of the spacers contained within the core, and conduction through the core's boundaries are negligible.

3) Accurate thermodynamic properties are used for both the helium and the GGG.

4) There is no helium entrainment within the core. This assumption also implies that there is no helium flow induced by the breathing effect.

4.1: Second-Law Determination of the Helium Temperature Profiles.

The first step of this analysis is to determine the helium temperature profiles which allow for reversible Carnot cycles throughout the core using only the Second Law. In order to have cyclic steady state, each segment must return to the same state after it undergoes a complete cycle. This means that there is no net change in entropy of the core. If there is no entropy generated within the segments (assumption 2) then the entropy into the segment on the down-flow must equal the entropy out of the segment on the up-flow, $dS_h = dS_c$. The helium carries the entropy into and out of the segments, and there are no other methods of heat transfer. $dS = mc_p d(\ln T)$ by definition of c_p. With the total flow of helium equal in both directions, then:

$$c_p(T_h)\, d(\ln T_h) = c_p(T_c)\, d(\ln T_c) \tag{2}$$

At this point we note that if the specific heat of the helium were constant, then we could cancel it out of Equation (2), and the equation will then reduce to $dT_h/T_h = dT_c/T_c$. The solution to this equation is $T_h/T_c = constant$. We can therefore see that if one of the temperature profiles is linear, then so is the other. This derives the results presented in earlier papers.[9]

To solve Equation (2) while keeping the specific heat as variable parameters, we first rearrange it to a numerical form suitable for computational analysis. The computer can use this equation to solve for one temperature profile given the other. We note

that there is freedom to choose one of the temperature profiles arbitrarily. A starting point on the other temperature profile must also be given.

For the first example we choose a linear profile on the down-flow. (This is the same as was used in the original design analysis.) Figure 21 shows the resulting up-flow profile which allows Carnot Cycles. Note the pinch which occurs around 5.6 K. This results from a peak in specific heat which occurs in the 3-atm supercritical helium as it nears the critical point. This peak causes the profiles to come together when approaching 5.6 K, and to disperse when leaving 5.6 K. A better choice for a starting point is to assume a down-flow profile which has equal changes of enthalpy per segment. This result is shown in Figure 22.

4.2 Matching Helium Properties to GGG Properties

The next step in the analysis is to use assumption 2. That is, the GGG temperature is equal to the helium temperature, and therefore the GGG has the same temperature profiles as does the helium. With these temperature profiles we know the isothermal temperature of each Carnot cycle of each GGG segment. What we still need to determine is the entropy of each adiabatic path.

One of these entropies is arbitrary and can be taken to occur at the starting field. For the purpose of this analysis all cycles are assumed to start at one tesla. All we need now is the ΔS_i of the i^{th} segment during the isothermal process, and we will be able to plot all the individual Carnot cycles.

To find ΔS_i we can use the fact that the area swept out by a refrigeration cycle on a T-S diagram is equal to the net work into the i^{th} segment during the cycle. For Carnot cycles:

$$(T_h - T_c)_i \, \Delta S_i = W_{net}\big|_i$$

Also, the work into the i^{th} segment is equal to the net enthalpy change of the helium passing through that segment:

$$dW_i = M_T [c_p(T_h)\, dT_h - c_p(T_c)\, dT_c]_i$$

where M_T is the total shuttle mass of helium, and the differential is introduced on the work term to show that each segment is essentially infinitesimally small. Putting

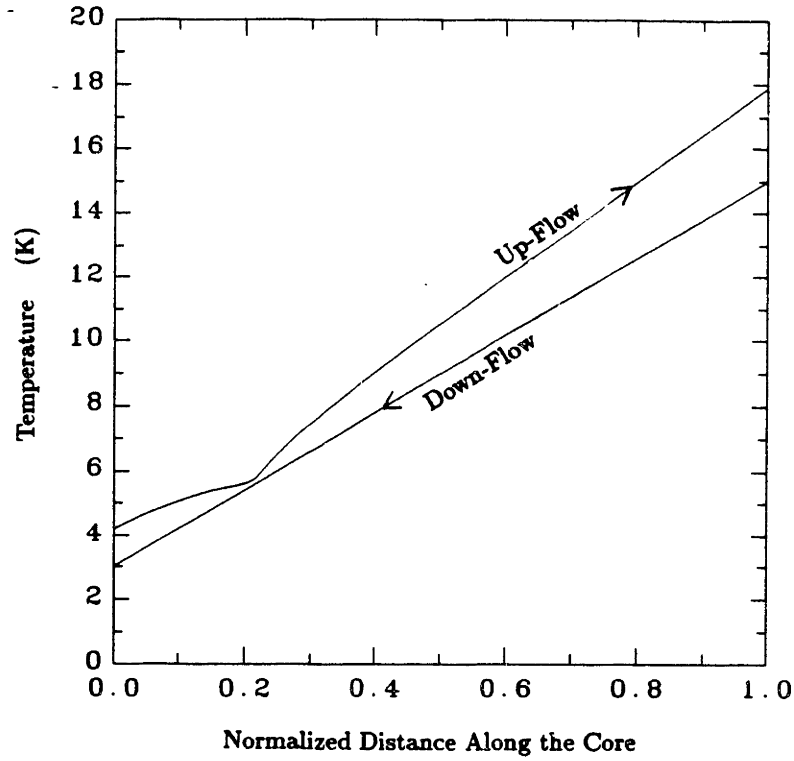

Fig. 21 Reversible Temperature Profiles with Linear Down-Flow

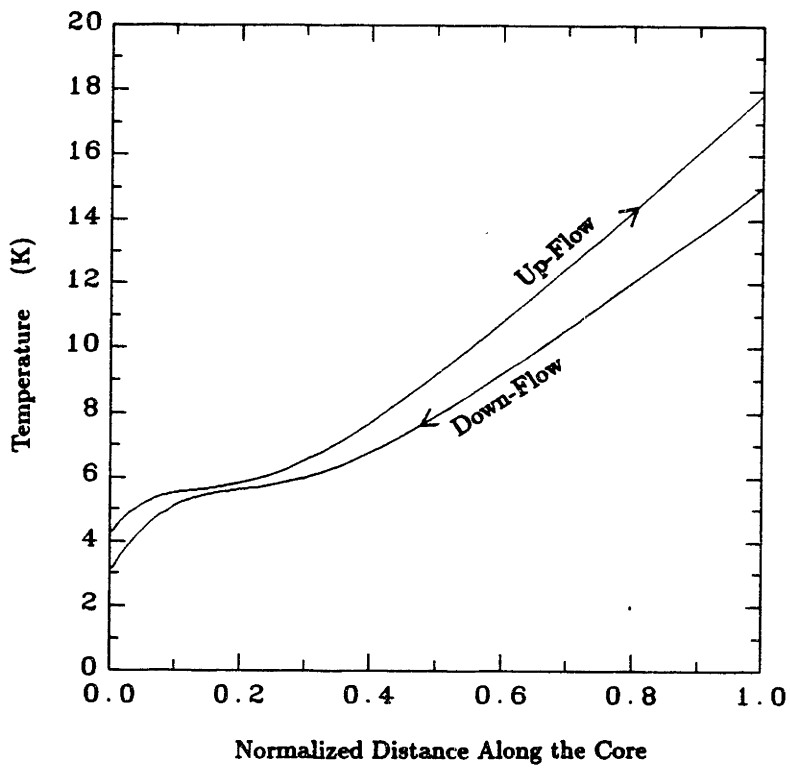

Fig. 22 Reversible Temperature Profiles with Uniform Δh down-flow

these together:

$$\Delta S_i = \frac{M_T[c_p(T_h)\,dT_h - c_p(T_c)\,dT_c]_i}{(T_h - T_c)_i} \tag{3}$$

We see that ΔS_i is proportional to the helium mass flow, and that all other values in Equation (3) are fixed by the proceeding analysis. We can increase the mass flow to increase the ΔS_i of all the segments together.

The maximum field induction that can be obtained by our magnet is 4 T. We expand all the Carnot cycles by increasing M_T until one of them reaches the maximum field. Figure 23 shows a T-S diagram of the GGG with five of the segment's cycles plotted. This is the result of using a linear down-flow temperature profile. Note that while one cycle spans the total field available, the others come up very short. Figure 24 shows the results obtained by starting with a down-flow which has equal changes of enthalpy per segment. The steepness of the down-flow temperature profile is adjusted so that the product of specific heat and ΔT_i remains constant. Note that this choice removes some of the mismatch caused by extremely variable helium properties, yet still most segments do not span the available field.

4.3 Determining the Field as a Function of Time and Space

It is possible for all the segments to go from 1 to 4 T if we can determine the proper set of temperature profiles. The computer proceeds to iterate, with new starting down-flow profiles, until every segment spans the entire field. Figure 25 shows the resulting temperature profiles and Carnot cycles which satisfy this requirement.

We have succeeded in finding a possible set of thermodynamic cycles which will allow, within the stated assumptions, our system to operate as a series of reversible Carnot Refrigerators, and we have plotted these cycles on a T-S diagram. We now need to determine how to operate these cycles; that is, for a given helium displacer position, what should the magnetic field be, spacial and temporal?

The relationship between the required magnetic field and displacer position comes from Equation (3). ΔS along the isothermal path is proportional to the net mass flow of helium through the segment. When the displacer has completed its stroke, all the helium has been forced through the core, and all the isothermal paths have reached their end point. At 50% stepper stroke, all isothermal paths are at 50% of

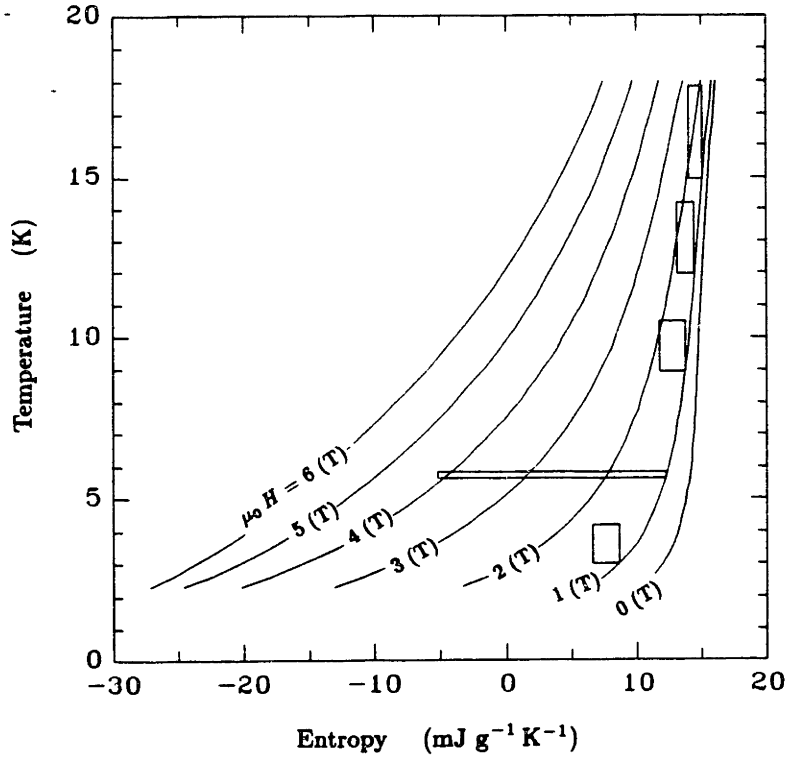

Fig. 23 *T-S* Diagram for a Linear Down-Flow Profile

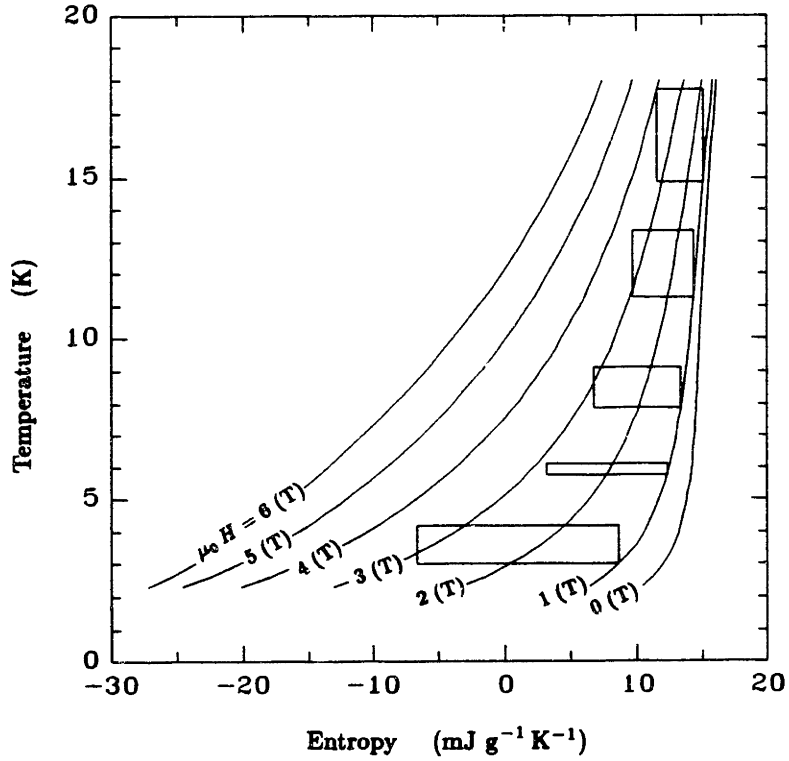

Fig. 24 *T-S* Diagram for a Uniform Δh Down-Flow

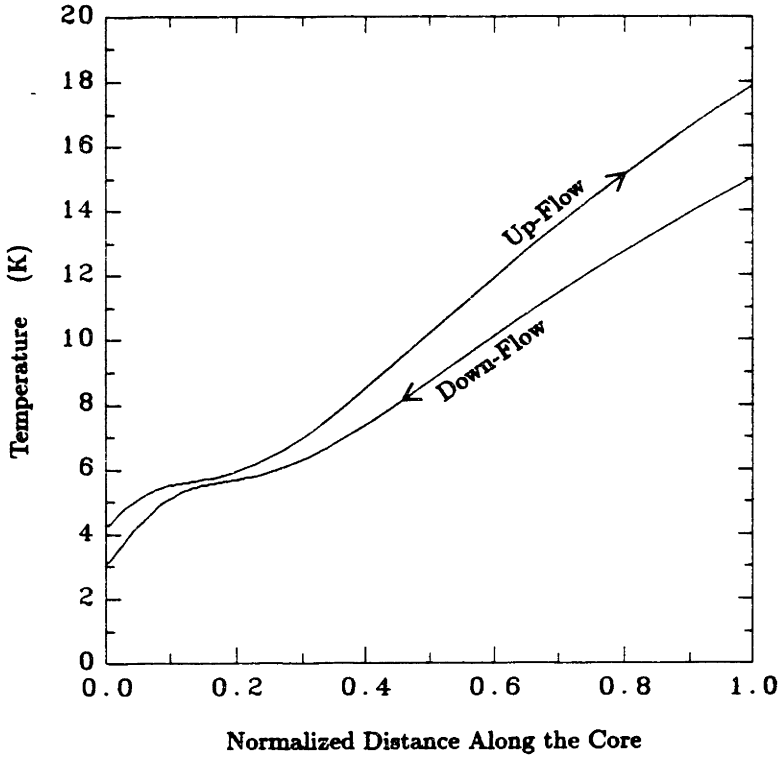

Fig. 25a Reversible Temperature Profiles Which Use All of the Available Field

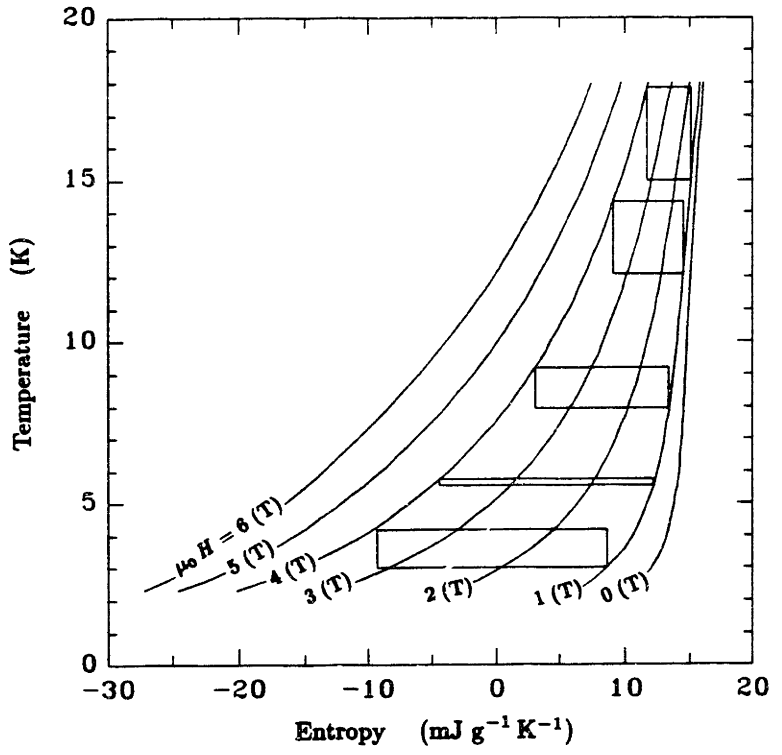

Fig. 25b *T-S* Diagram for above Temperature Profiles

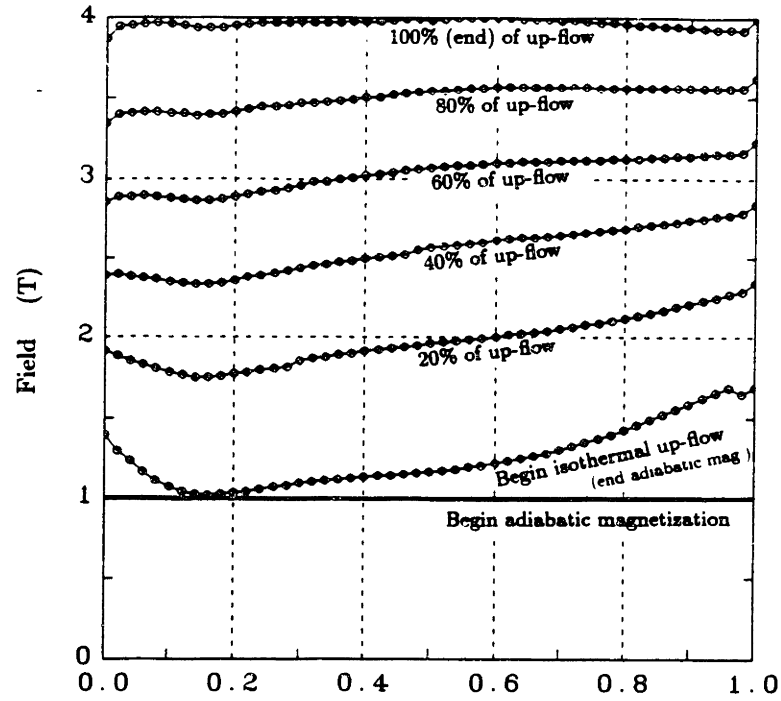

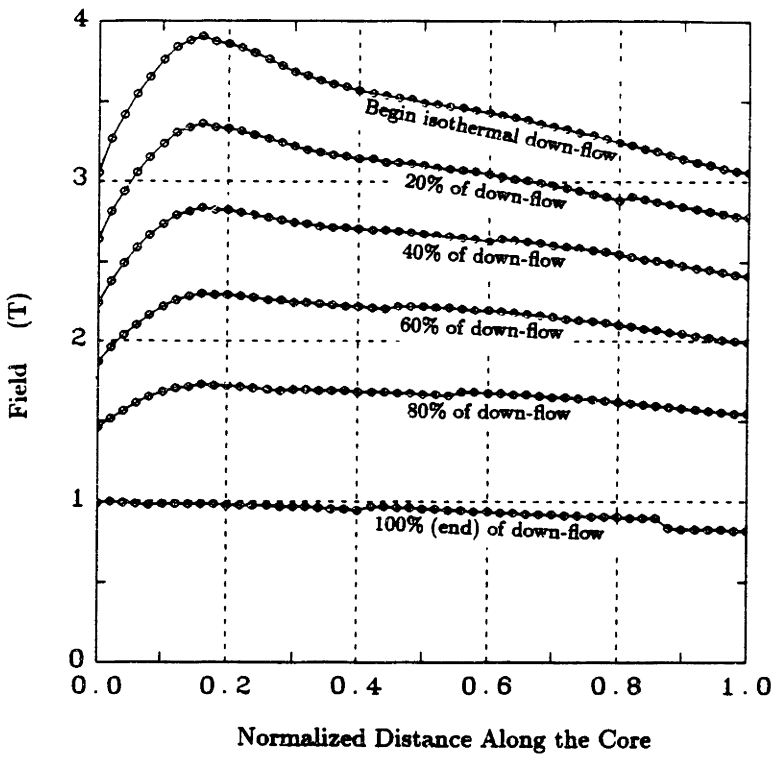

Fig. 26 Field Profiles Which result from the Temperature Profiles in Figure 25

their total ΔS_i. With this information we can plot the required magnetic field as a function of both position along the core and percent of isothermal path. Figure 26 shows the results for the cycles which span the entire magnetic field. This figure is an actual computer output. One can notice that the field profile at the end of the isothermal down-flow path deviates from the defined value of 1 T at the warm-end. This results from the GGG thermal properties. At 15 K and low applied fields, the derivative of S with respect to H at constant temperature is very small. Because of this, perturbations in S at constant temperature, due to the convergence accuracy of the numerical technique, may result in noticeable deviations in the calculated magnetic field in this region.

4.4 Results

The following general conclusions can be made from this analysis:

- The field must be a function of both time and position if Carnot cycles are to be achieved. This result is true even in the absence of all loss mechanisms and in the absence of breathing induced flow.
- The refrigeration per total shuttle mass of helium and the Carnot efficiency of the cycle are determined by the first and second laws, and are not functions of refrigeration optimization; they are functions only of the temperatures at the end of the core.
- The refrigeration per cycle per mass of GGG, and the required total helium flow per cycle per mass of GGG, are both determined by fitting the temperature profiles on the GGG properties.
- For a given set of reservoir temperatures, the independent parameter is the temperature difference between the reservoir and the temperature at which helium is rejected from the core into the reservoir. A larger temperature difference corresponds to using a greater percent of the available field swing for the adiabatic path.
- It is difficult to include in this analysis irreversibilities which are present in a real device. It is also difficult to account for the breathing effect.

Table 3 shows the performance of a regenerative core (with the assumptions previously stated), and with a total mass of GGG equal to 2.4 kg. T_{R_c} and T_{R_w} are the cold and warm-reservoir temperatures. T_{out_c} is the temperature of the helium leaving the cold-end of the core on a down-flow. M_T is the total helium shuttle mass per cycle, and $\dot{Q}_c$ and $\dot{Q}_w$ are the refrigeration and heat of rejection in watts, assuming a 10-second cycle time. The helium pressure is taken to be 5 atm. The important trends to note from this table are:

TABLE 3
Ideal Carnot System, Total mass of GGG = 2.4 kg

T_{R_c} (K)	T_{R_w} (K)	$T_{out_c}(K)$	M_T (g)	$\dot{Q}_c$ (w)	$\dot{Q}_w$ (w)
4.2	15.0	3.5	2.40	.53	2.18
4.2	15.0	3.0	2.15	.74	3.35
4.2	15.0	2.5	1.88	.83	4.22
10.0	15.0	9.5	6.18	1.85	2.93
10.0	15.0	9.0	5.09	3.07	5.16
10.0	15.0	8.0	3.10	3.86	7.38
4.2	10.0	3.8	4.05	.55	1.42
4.2	10.0	3.5	3.88	.86	2.37
4.2	10.0	3.0	3.59	1.24	3.74
4.2	10.0	2.5	3.29	1.46	4.90
4.2	10.0	2.2	3.00	1.52	5.56

- For a given set of reservoir temperatures, the total shuttle mass of helium decreases with decreasing T_{out_c}. There are two reasons for this. In order to obtain larger temperature differences at the ends of the core, a greater percentage of the total field swing must be used for the adiabatic part of the cycle. This leaves less magnetization available for the isothermal part. In addition, the isothermal temperature profiles must span a larger temperature range. This requires a steeper temperature profile which is obtained by decreasing $\dot{m}$ relative to $\dot{H}$.

- For a given set of reservoir temperatures, the refrigeration increases as T_{out_c} decreases. The refrigeration per shuttle mass of helium is determine directly from the three previously chosen end temperatures, and increases continuously with increasing difference between T_{out_c} and T_{R_c}, but since the allowable shuttle mass decreases, the refrigeration will eventually decrease also. The effect can be seen by looking at the T-S diagram for the GGG. If there is no adiabatic part to the cycle, the refrigeration goes to zero even though the shuttle mass is maximized. On the T-S diagram the Carnot cycles flatten out horizontally. If the temperature difference becomes too large, the isothermal part of the cycle goes to zero, which causes the shuttle mass to also go to zero. On the T-S diagram the Carnot cycles flatten out vertically. The maximum refrigeration is found at some intermediate cycle. All the cases shown in Table 3 happen to be on the more efficient side of this maximum, where the isothermal part of the cycle uses a greater percentage of the field swing than the adiabatic.

- As the reservoir temperature difference increases, M_T decreases as does Q_c.

4.5 Two-Stage Matching

In the later analysis it will be shown that it is not always possible to approximate Carnot cycles with our device when the temperature range is large. The reason for this is field-flow mismatches occur at various locations along the core. It is interesting to explore what would be involved in covering a large temperature range with two parts, a lower stage and an upper stage, each an independent Ideal Carnot device. With this two-stage system we will force:

a) The warm-reservoir for the lower stage is the cold-reservoir for the upper stage.

b) The net helium flow leaving the lower stage must equal the net helium flow entering the upper stage.

c) The net heat rejected from the lower stage must equal the net refrigeration of the upper stage.

The following discussion traces the steps involved in matching a lower stage which refrigerates at 4.2 K and rejects heat at 10 K, to an upper stage which refrigerates at 10 K and rejects heat at 15 K. The subscript l refers to the lower stage, and the

subscript u refers to the upper stage.

The first thing to remember is that all the values derived from the Ideal Carnot analysis are per mass of GGG; all the values presented in Table 3 have been multiplied by the the total mass of GGG contained in our test device. To use this mass as a total for the combined mass of a two-stage system, we proceed as follows where f is a fractional percent of the total mass of GGG assigned to the lower-stage core.

First, match the heat of rejection from the lower stage with the refrigeration of the upper stage:

$$f\,\dot{Q}_{w_l} = (1-f)\,\dot{Q}_{c_u}$$

And then match the shuttle mass:

$$f\,M_{T_l} = (1-f)\,M_{T_u}$$

Combining:

$$\frac{\dot{Q}_{w_l}}{M_{T_l}} = \frac{\dot{Q}_{c_u}}{M_{T_u}}$$

This criterion can easily be satisfied using information found in Table 3. One match is conveniently found between the second set of data in each group of 10 to 15 K and 4.2 to 10 K.

$$\frac{\dot{Q}_{w_l}}{M_{T_l}} = \frac{2.37}{3.88} = 0.61 \quad \text{(W/K)}$$

$$\frac{\dot{Q}_{c_u}}{M_{T_u}} = \frac{3.07}{5.09} = 0.60 \quad \text{(W/K)}$$

This is close enough. The refrigeration produced by this combination can be found by first determining the value of f from one of the above relations:

$$f\,(3.88) = (1-f)\,5.09$$

$$f = 0.57$$

and then by multiplying $\dot{Q}_{c_l}$ by this value:

$$\text{Refrigeration} = 0.57\,(.86) = 0.49 \quad \text{(W)}$$

For this example we find that a two-stage device could produce 0.49 W of refrigeration with $T_{out_c} = 3.5$ K. The one-stage system with the same T_{out_c} produced only slightly

higher refrigeration at 0.53 W. The heat rejected from the upper stage can be found by multiplying $\dot{Q}_{w_u}$ by $(1-f)$:

$$\text{Heat Rejected} = (5.16)\,0.43 = 2.22$$

The Carnot efficiency of the single-stage system is:

$$\frac{\frac{T_{R_w}}{T_{R_c}} - 1}{\frac{\dot{Q}_w}{\dot{Q}_c} - 1} = \frac{\frac{15}{4.2} - 1}{\frac{2.18}{0.53} - 1} = 0.83$$

and the Carnot efficiency of the two-stage system is:

$$\frac{\frac{15}{4.2} - 1}{\frac{2.22}{0.49} - 1} = 0.73$$

In this example the two-stage system produced slightly less refrigeration at ~10% less efficiency. The added irreversibility results from helium mixing between the two stages. Everything else being equal, it is preferable to use a single-stage system. Later chapters describe how cycle control can be difficult when the temperature range between the reservoirs is large. If proper thermodynamic cycles cannot be obtained over a large temperature range, one design option is to break the single stage into multiple stages.

V. ANALYSIS BY COMPUTER SIMULATION

The analysis of the Ideal Carnot System (Chapter 4) contained many simplifying assumptions. In order to more closely model our test device a computer simulation program was developed. There are several modeling differences between the simulation program and the model used in the previous chapter which studied the Ideal Carnot system. The important differences are as follows:

(1) The field is uniform along the core. Some simulation cases were tried with nonuniform fields, but only if they could be implemented by modifying our present device.

(2) There is a helium void of about 5% uniformly distributed throughout the core.

(3) Fewer elements are used in the simulation than there are segments in our actual device. This provides a numerical method of compensating for the real irreversibilities of axial conduction and nonzero heat transfer ΔT between the GGG and helium.

(4) The most important difference between computer simulation analysis and the Ideal Carnot analysis relates to which cycle parameters are independent and which are dependent. In the Ideal Carnot analysis we fixed the temperature at each end of the core for both the up-flow and down-flow processes, and the field functions were determined from the analysis. In a real device we choose the field functions, and the core's temperature profiles develop as they will. This is the same order of dependence as is used in the computer simulation program.

The first restriction prevents our core from ever achieving a isothermal process. This is because the heat of magnetization and the helium flow rate cannot be arbitrarily matched everywhere along the core. If a thermodynamic path is isothermal at one section of the core, it will not in general be isothermal elsewhere. For this reason it is impossible to run the core as a series of Carnot Refrigerators. It is important to determine: 1) if the core can be operated in such a way as to approximate a series

of Carnot refrigerators; 2) if deviations from Carnot paths deteriorate the overall system performance; and 3) if non-Carnot-type cycles can work as well.

Inclusion of helium in the core has many implications. Helium void has two major effects on system performance. First, it adds zero-field specific heat to the core reducing the available temperature swing for a given field change, and second it gives rise to what we call the breathing effect (defined in the Glossary of Terms).

The breathing effect makes an adiabatic process impossible since flow is induced from the core as the core's temperature is varied. An isothermal process would not produce any breathing effect; however, we have already seen that the first restriction listed above prevents isothermal processes.

In general, it is not possible to prescribe exactly what thermodynamic cycle each segment along the core will experience. As we vary the magnetic field and helium flow to control the temperature of one core region, we cannot control the other regions. Since our cycles cannot be preselected, it is necessary to develop a design tool which allows for non-Carnot, or even arbitrary, thermodynamic cycles.

5.1 The Computer Simulation Program

A computer simulation program has been developed to model our refrigerator system. This section describes that program. A listing of the program (SIMULATE.FOR) is contained in Appendix H.

5.1.1 The analytical basis of the program

The equation which models an active regenerator core is derived in this section. The core is broken into segments. A control volume for one segment is shown in Figure 27. The first two assumptions used are:

1. No axial conductivity,
2. No peripheral heat loss.

With these assumptions a First-Law heat balance can be written as:

$$\rho_g V_g \, dU_g + d(\rho V \, u)_{he} = [h_{in} \, dm_{in} - h_{out} \, dm_{out}]_{he} + V_g \mu_0 H \, dM$$

The next two assumptions used are:

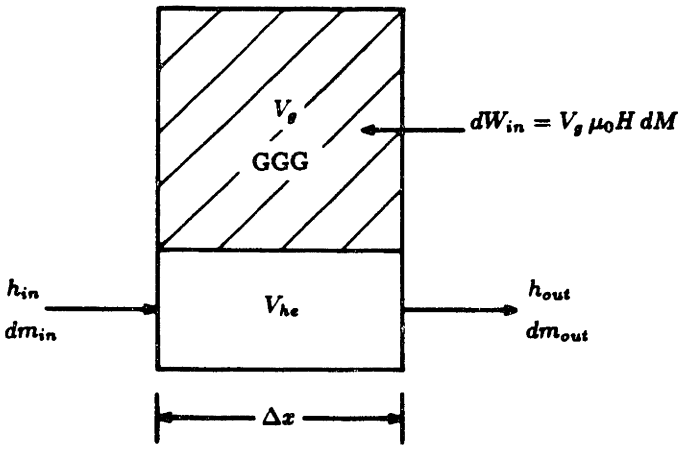

Fig. 27 Control Diagram for Equation (4)

3. Uniform GGG temperature within a segment, T
4. The GGG is internally reversible; that is, its thermal conductivity is infinite, and there are neither losses due to magnetic hysteresis nor eddie current generation.

With these assumptions a reversible First-Law equation can be written for just the GGG:

$$dU_g - \frac{\mu_0}{\rho_g} H dM = T\, dS_g$$

The GGG property data are expressed as a function of temperature and applied field. The entropy differential can be expanded as:

$$dS_g = \left.\frac{\partial S_g}{\partial T}\right|_H dT + \left.\frac{\partial S_g}{\partial H}\right|_T dH$$

Inserting this into the heat balance:

$$\rho_g V_g T \left[\left.\frac{\partial S_g}{\partial T}\right|_H dT + \left.\frac{\partial S_g}{\partial H}\right|_T dH\right] + d(\rho V u)_{he} = [h_{in}\, dm_{in} - h_{out}\, dm_{out}]_{he} \qquad (4)$$

Mass continuity can be written for the helium as:

$$dm_{out} = dm_{in} - V_{he}\, d\rho \qquad (5)$$

Equations 4 and 5 are solved numerically by the computer simulation program for each segment. Helium may enter a segment from a neighboring segment. Helium leaves a segment at that segment's temperature. The amount of helium leaving a segment will not be equal to the amount entering if the segment's temperature is changing during the process. This allows for the breathing effect.

5.1.2 Parameters: Fixed and Variable

There are many possible refrigeration cycles that can be attempted either by the computer simulation program, or by the test device. Some parameters are fixed by our particular test apparatus, and some remain variable.

The Fixed Parameters are:

1. The net forced helium flow on a up-flow must equal the net forced helium flow on a down-flow.
2. The helium porosity is fixed, and for the simulation program, it is taken to be 5 percent of the core volume.
3. The maximum field applied to the core is 4 T, and it is uniform along the core.
4. The cold-reservoir temperature is fixed at 4.2 K.

The Variable Parameters are:

1. Although the system operates at a given constant helium pressure, the program permits the operating pressure to be varied from a minimum of 2.5 atm (only slightly above the critical point) to a maximum of ~10 atm. Our present experimental system is limited to 5 atm, but could be modified to accommodate higher pressures.
2. The minimum field can go down to zero. In practice it is found that 1 T is a suitable minimum because the magnetic effect is very small between 0 and 1 T.
3. The warm-reservoir temperature is designed to be fixed by a bath filled with saturated hydrogen. Saturated hydrogen varies in temperature from about 20 K at 1 atm down to about 14 K at its triple point. This means that the warm end temperature should be set at somewhere above 14 K.
4. Any combination of field change and forced helium flow which meets the above requirements is permissible.

5.1.3 Using the Program as a Design Tool:

There are actually two programs used to analyze one set of operating conditions. The first is used to find the cyclic steady state, and the second is used to record and plot information about the cyclic steady state.

To run the first program, the user must enter the reservoir temperatures and the

field-flow phasing. The field-flow phasing is entered by specifying the helium flow for each increment in magnetic field. Often a total helium shuttle mass is entered for a group of field increments, and divided equally. The only other user-supplied input required for the first program has to do with numerical information such as the number of segments to be used and the number of time steps for each part of the cycle.

After a cyclic steady state has been reached, the program stops and records the final temperature profile. From here the second program is run which cycles the process one more time while recording information to be printed and/or plotted. Some of the graphs produced by this program include:

(1.) Temperature profiles at any pre-selected field increment. Often approximately 20 profiles will be plotted on four different graphs for one complete cycle.

(2.) Selected segments will be plotted on a T-S diagram of the GGG.

(3.) The net enthalpy flux along the core over a complete cycle, calculated at the each segment boundary, is plotted as a function of position along the core. Enthalpy flow is taken to be positive if the mass flow is from the cold-end to the warm-end, and is negative if from the warm-end to the cold-end. The derivative of this graph is the net work into the corresponding segment. The value at the cold-end (left) is the refrigeration, and the value at the warm-end (right) is the heat of rejection.

(4.) The net entropy flux along the core over a complete cycle is also plotted. It is defined in the same way as the enthalpy flux in item 3. The derivative of this graph is the net irreversibility generated by the corresponding segment. Steep sections in this curve represent inefficient regions in the core. In a good overall cycle, this curve will not increase much compared with its absolute value.

(5.) The net entropy flux at several selected segment boundaries, recorded at each time step of the cycle, is plotted against the corresponding temperature of the upstream segment. This curve shows in detail what went into making the graphs described in item 4. It also helps show why a segment is inefficient.

5.1.4 Using the Computer Program to Compare with Test Data:

The second program can be used by itself in order to examine non-steady state behavior of the system. This is useful when examining actual test data. It is important to correlate the program results with test data if it is to be used with confidence as a design tool. This aspect of the computer simulation program is discussed in Chapter 11 where test data are also presented.

5.2 Results from Computer Simulation Program

The analysis presented in this section was only aimed at producing cyclic steady state refrigeration with our present system. Many cycles were tested. The results are summarized in Tables 4,5 and 6 (found at the end of the chapter). T_c and T_w are the cold and warm-reservoir temperatures, ΔH_{ad} is the magnetic field swing in tesla which is used for the adiabatic path. In some cases a different field swing was used for the adiabatic magnetization and adiabatic demagnetization paths. For these cases two numbers appear in the table; the left number is for magnetization and the right number is for demagnetization. The total field swing is always between 1 and 4 T. M_T, the total helium shuttle mass, is a variable parameter; the helium pressure is 5 atm. The period for a complete cycle is 10 seconds. The methodology for performing two stage matching is given back in Chapter 4.5.

5.2.1 Uniform field, Various runs within the range of 4.2 to 15 K:

The important things to note from Table 4 are:

A. 4.2 to 15 K:

1. There is never any net refrigeration; $\dot{Q}_c$ is negative.
2. The heat flow at the cold-end, $\dot{Q}_c$, is insensitive to variations in the cycle parameters of M_T and field phasing.
3. The heat flow at the warm-end, $\dot{Q}_w$, responds to variations in these same cycle parameters.

B. 10 to 15 K & 4.2 to 10 K:

1. For a given adiabatic percent, there is a range of M_T where $\dot{Q}_c$ is fairly constant.
2. Below this constant range, $\dot{Q}_c$ decreases as M_T decreases.
3. There is a maximum M_T above which $\dot{Q}_c$ drops rapidly.

4. Matching M_T and $\dot{Q}$ for a two-stage device requires different adiabatic percents; it cannot be done simply by varying the flow.

C. General Remarks:

1. The ** in Table 4 refers to variable flow during the up-flow and down-flow processes. The flow rate can be varied during a single flow process in oder to more closely approximate isothermal paths. It was found that variable flow had little effect on $\dot{Q}_c$, but did help to improve the efficiency.
2. $\dot{Q}_c$ first increases and then decreases with increasing adiabatic percent. This is the same as was found in the Ideal Carnot analysis.
3. The efficiency decreases with increasing adiabatic percent. Again, this is a result found in the Ideal Carnot analysis.

5.2.2 Two Independent Uniform Fields, 4.2 to 15 K:

Cycles from 4.2 to 15 K with two independent magnetic field variations were tested by the simulation program. The results of this analysis are shown in Table 5. The things to note from this table are:

1. Refrigeration was obtained.
2. The field was split at 50/50 percent of the core, and at 33/67 percent of the core; only a slight difference in performance was noticed.

5.2.3 Uniform Field, 10 to 20 K:

Table 6 shows results from the computer simulation program when it was run over the temperature range of ~10 to 20 K. Note that this temperature range is about the same as the 4.2 to 15 K range, but the temperature ratio is the same as the 4.2 to 10 K range. These cycles could produce refrigeration, but their efficiency was poor. Upon examination of the plots produced by the computer simulation program, it was found that the cycle behavior was more similar to the 4.2 to 15 K runs than to the 4.2 to 10 K, or the 10 to 15 K runs.

The results presented in Table 6 demonstrate that:

1. Cycle phasing problems develop as the temperature range, ΔT, increases.
2. The severity of phasing problems on the overall performance of the device increases as the temperature ratio, $\Delta T/T$, increases.

TABLE 4
Computer Simulation – Uniform Field
(10-second cycle time)

T_c (K)	T_w (K)	ΔH^*_{ad} (T)	M_T (g)	$\dot{Q}_c$ (w)	$\dot{Q}_w$ (w)
4.2	15.0	0.25	2.2	−0.19	.98
4.2	15.0	0.5	1.0	−0.19	.96
4.2	15.0	0.5	1.5	−0.12	1.42
4.2	15.0	0.5	2.1	−0.13	1.96
4.2	15.0	0.5	2.2	−0.07	2.09
4.2	15.0	0.5	2.3	−0.11	2.16
4.2	15.0	0.5	3.0	−0.05	2.79
4.2	15.0	1.0	1.5	−0.17	2.65
4.2	15.0	1.0	1.8	−0.17	3.35
4.2	15.0	0, .5	2.2	−0.29	.69
4.2	15.0	0, 1.	1.5	−0.29	1.08
4.2	15.0	0, 1.	2.3	−0.24	1.77
4.2	15.0	0, 1.	3.0	−0.29	2.15
4.2	15.0	0, 1.	**2.15	−0.19	1.78
4.2	15.0	0, 1.5	1.0	−0.58	2.42
10.0	15.0	0.5	3.0	1.98	4.09
10.0	15.0	0.5	3.8	2.60	5.05
10.0	15.0	0.5	**4.0	2.56	4.75
10.0	15.0	0.5	**4.5	2.69	4.95
10.0	15.0	0.75	3.5	3.29	6.54
10.0	15.0	1.0	3.0	3.65	7.33
10.0	15.0	1.0	3.5	4.01	8.24
10.0	15.0	1.5	2.5	3.05	7.54
4.2	10.0	0.5	2.5	0.63	3.04
4.2	10.0	0.5	3.5	0.87	3.78
4.2	10.0	0.5	3.8	0.92	3.97
4.2	10.0	0.5	4.0	0.96	4.08
4.2	10.0	0.5	5.0	0.86	4.20
4.2	10.0	0.5	6.0	−0.65	1.87
4.2	10.0	1.0	2.0	0.79	4.65
4.2	10.0	1.0	3.0	1.23	6.82
4.2	10.0	1.0	3.5	1.38	7.75

*When there are two numbers: (mag,demag)
**Best result of variable flow

TABLE 5
Computer Simulation, 2 Independent Fields
(10-second cycle time)

T_c (K)	T_w (K)	ΔH_{ad} (T) (cold, warm)	M_T (g)	$\dot{Q}_c$ (w)	$\dot{Q}_w$ (w)
4.2	15.	[1](0.5, 1)	2.0	0.35	3.58
4.2	15.	[1](0.5, 1)	2.5	0.31	3.83
4.2	15.	[1](0.5, 0.75)	2.0	0.19	2.72
4.2	15.	[2](0.5, 1)	2.0	0.31	3.82

[1]Field split at 50/50 percent of the core
[2]Field split at 33/67 percent of the core

TABLE 6
Computer Simulation – Uniform Field
(10-second cycle time)

T_c (K)	T_w (K)	ΔH^*_{ad} (T)	M_T (g)	$\dot{Q}_c$ (w)	$\dot{Q}_w$ (w)
9.2	20.	1.0	2.0	0.17	2.59
9.2	20.	1.0	2.5	0.46	3.53
9.2	20.	1.0	3.0	0.47	4.08
9.0	20.	.25	2.2	0.16	1.15
10.	20.	0.5	2.0	0.18	1.37
10.	20.	.25,.5	**2.2	0.40	1.15
10.	20.	.25,.5	2.3	0.03	1.04

*When there are two numbers: (mag,demag)
**Best result of variable flow

VI. CLOSED FORM ANALYSIS

This chapter develops the mathematical background which will be used in Chapters 7, 8, and 12. Complete thermodynamic cycles are not discussed in this chapter.

The differential equation to describe an active regenerative core is derived, and certain aspects of this equation are examined. The magnetic interaction terms are studied in detail, and the equation is solved in its limiting cases which include: isothermal, adiabatic, and step-wise constant convection wave solutions.

6.1 Derivation of the Differential Equation

In Chapter 5 an equation was developed for a single segment in an active regenerator. That equation is:

$$\rho_g V_g T \left[\frac{\partial S_g}{\partial T}\bigg|_H dT + \frac{\partial S_g}{\partial H}\bigg|_T dH \right] + d(\rho V u)_{he} = [h_{in}\, dm_{in} - h_{out}\, dm_{out}]_{he} \qquad (4)$$

with mass continuity:

$$dm_{out} = dm_{in} - V_{he}\, d\rho \qquad (5)$$

The assumptions used to arrive at this equation were:

1. No axial conductivity,
2. No peripheral heat loss,
3. Uniform GGG temperature within a segment,
4. GGG is internally reversible.

In this analysis we make the additional assumptions:

5. Infinite convective heat transfer between the GGG and helium,
6. Infinite number of segments: $\Delta x \rightarrow dx$,
7. Helium pressure is constant.

By definition the helium enthalpy is related to its internal energy as:

$$h = u + \frac{p}{\rho}$$

and since the helium pressure is constant:

$$d(\rho u)|_p = d(\rho h)|_p = (\rho\, dh + h\, d\rho)|_p$$

Since the convective heat transfer is infinite, the helium entrained within in a segment is at the GGG's temperature, and the helium leaving a segment is at the GGG's temperature. This assumption implies:

$$h_{out} = h$$

Equation (4) can be rewritten as:

$$\rho_g V_g T \left[\frac{\partial S_g}{\partial T}\Big|_H dT + \frac{\partial S_g}{\partial H}\Big|_T dH \right] + V_{he}\rho dh = h_{in}\, dm_{in} - h_{out}\,(dm_{out} + V\, d\rho)$$
$$= dm_{in}\,(h_{in} - h_{out})$$

The volume of the GGG and that of helium in a segment can be expressed as:

$$V_g = A\,(1 - por)\,dx$$
$$V_{he} = A\,por\,dx$$

where A is the cross-sectional area of the core and por is the helium porosity. The enthalpy difference across the infinitesimal segment can be expressed as:

$$h_{out} - h_{in} = \frac{dh}{dx}dx$$

Substituting the above expressions into the Equation (4) and using the definitions for specific heat:

$$dh \equiv c_p\, dT \quad \text{, and} \quad c_H \equiv T\frac{\partial S_g}{\partial T}\Big|_H$$

results in:

$$\rho_g A\,(1 - por)\left[T\frac{\partial S_g}{\partial H}\Big|_T dH + c_H dT \right] + \rho_{he} A(por) c_p\, dT = -dm\, c_p \frac{dT}{dx}$$

An overall core specific heat per unit length can be defined as:

$$C \equiv (por)\rho_{he} c_p A + (1 - por)\rho_g c_H A \quad (\mathrm{J\,cm^{-1}K^{-1}})$$

which yields:

$$C dT + dm\, c_p \frac{dT}{dx} = [(1 - por)A\rho_g]\left(-T\frac{\partial S_g}{\partial H}\Big|_T dH \right) \quad (\mathrm{J/cm})$$

Finally a derivative with respect to time results in:

$$C\frac{dT}{dt} + \dot{m}\, c_p \frac{dT}{dx} = [(1 - por)A\rho_g]\left(-T\frac{\partial S_g}{\partial H}\Big|_T \right) \dot{H} \quad (\mathrm{W/cm}) \qquad (6)$$

Equation (6) applies at each location along the core. It includes the breathing effect. One should remember, however, that $\dot{m}$ will be a function of x when the core is not isothermal. In practice $\dot{m}$ can only be determined exactly by integrating the process along the core. The computer simulation program does this. This chapter solves Equation (6) in various limits (where computer simulation is not necessary) in order to develop a first-order understanding of the processes involved in active regeneration.

6.2 Magnetic Interaction Term

There are actually two terms in Equation (6) which relate to magnetic interaction, but one of them is lumped into the core's overall specific heat, and need not be considered as a driving function. The other term, $-T\partial S_g/\partial H|_T$, is what we will refer to as the magnetic interaction. This magnetic interaction term is plotted in Figure 28 as a function of temperature for several different fields. There are several important factors to notice about this function.

- The magnetic interaction is a strong function of both temperature and field.
- For increasing field, the peak value in this function occurs at higher and higher temperatures.
- At the maximum allowable field for our test device, 4 T, the peak occurs at 10.5 K. There is plenty of magnetic interaction to produce refrigeration over the entire temperature range of 4.2 to 15 K.
- For temperatures above 7 K and in the field range of 1 to 4 T, the magnetic interaction increases with increasing field.
- For temperatures below 7 K and in the field range of 1 to 4 T, the magnetic interaction first increases but then decreases with increasing field.

It is also useful to look at the average value of $-T\partial S_g/\partial H|_T$ over a range of magnetic fields where a flow process is likely to occur. Table 7 shows values obtained by averaging the magnetic interaction term at a particular temperature, over the given field range. The important things to note from Table 7 are:

- Over most temperatures, the average magnetic interaction is lower at lower fields.

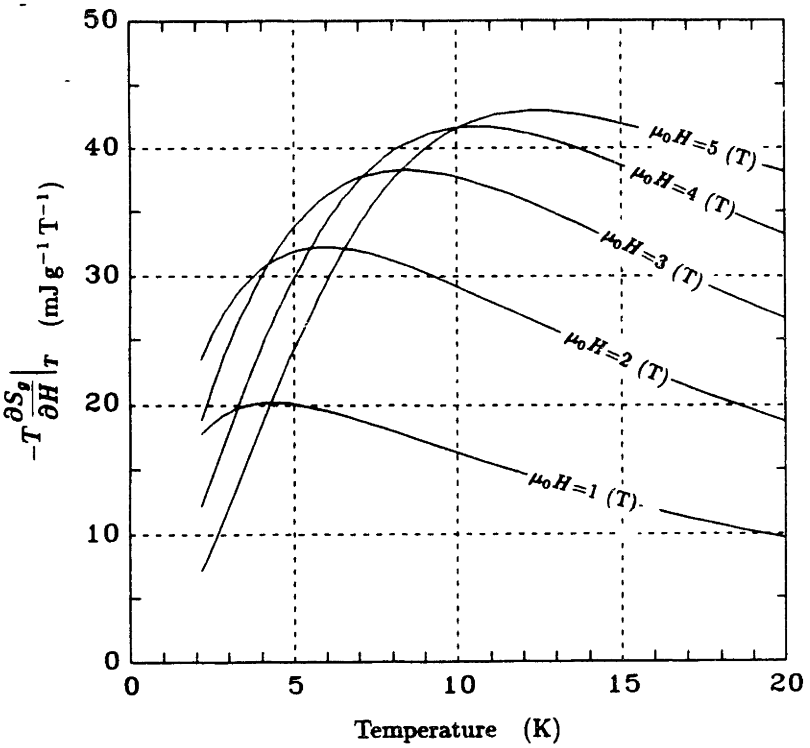

Fig. 28 GGG Isothermal Magnetic Interaction

TABLE 7
Average Magnetic Interaction (mJ g^{-1} T^{-1})

Temp. (K)	Field Range (T)				
	1 ↔ 3	1 ↔ 3.5	1 ↔ 4	1.5 ↔ 4	2 ↔ 4
4.0	28.0	28.2	27.8	28.9	29.0
6.0	30.0	31.2	31.8	33.6	34.8
8.0	29.5	31.3	32.7	35.0	36.8
10.0	28.0	30.2	32.0	34.5	36.8
15.0	22.5	24.7	26.7	29.1	31.3

- In general, the temperature profile in the core is not linear, and therefore the values listed in Table 7 will not be equally weighted over the core. However, for the thermodynamic cycles we are considering, the temperature profiles will be

uniform enough so that the magnetic interaction will be greater on the up-flow than on the down-flow.

6.3 The Isothermal Limit

In the isothermal limit dT/dt goes to zero and Equation (6) becomes:

$$\dot{m}\, c_p \frac{dT}{dx} = [(1 - por)\, A\rho_g] \left(-T \frac{\partial S_g}{\partial H}\Big|_T \dot{H} \right) \quad \text{(W/cm)}$$

The heat input from the magnet field interaction is balanced by the helium flow. Note that a given rate of magnetic interaction is balanced by a combination of $\dot{m}$ and dT/dx. The same magnetic interaction can be balanced by a low flow rate with a steep gradient, as well as by a high flow rate and a flat gradient.

It is not necessarily a requirement that our device be cycled in Carnot-type cycles, and for this reason isothermal paths need not be attempted. However, it will be shown that non-isothermal paths tend to lead to greater irreversibility and that the best compromise cycles are usually those which most closely resemble the Carnot. Another factor, discussed in Chapter 8.3, is that isothermal regions tend to develop downstream of the core's inlet during each flow process. For these two reasons it is useful to understand the behavior of the core in the isothermal limit.

The steady-state slope of the temperature profile is given by

$$\frac{dT}{dx} = \frac{(1 - por) A\rho_g}{c_p} \left(-T \frac{\partial S_g}{\partial H}\Big|_T \right) \frac{\dot{H}}{\dot{m}} \quad \text{(K/cm)} \tag{7}$$

Equation (7) is plotted as a function of temperature for different values of H in Figure 29 with the ratio $(\dot{H}/\dot{m})$ set to 1 (T/g). The only difference between the shape of this curve and the shape of the magnetic interaction curve shown in Figure 28 is that is has been divided by c_p, the helium specific heat.

There are several points to be made about the steady-state slope:

- If the steady-state slope were only a function of temperature and not of field, isothermal processes could be obtained in the core, where the steady-state profile would reflect the shape of this curve.
- If the steady-state slope were only a function of field, isothermal processes could

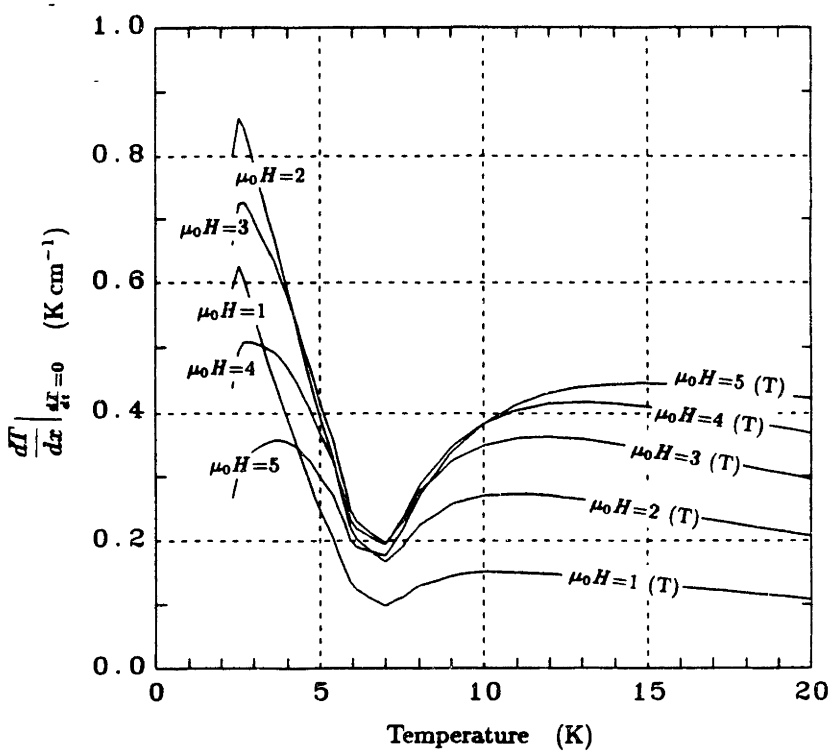

Fig. 29 Isothermal Slope for our Core, (p=5 atm), (por=0.05)

be obtained in the core, where the mass flow of helium is adjusted continuously to match the magnetic interaction.

- Since the steady-state slope is a function of both temperature and field, the only way to obtain isothermal paths is to vary the ratio ($\dot{H}/\dot{m}$) along the core. One way to do this is to have a magnetic field which can vary with position as well as with time.

- Larger temperature ranges imply steeper temperature gradients. For a given ΔH the larger the temperature range, the less the shuttle mass of helium.

- In practice one should not be concerned with a flow mismatch with the magnetic interaction, but instead with a flow/temperature-gradient mismatch with the magnetic interaction.

6.4 Isothermal Temperature Profiles

We can integrate Figure 29 to create temperature profiles which cover our desired

temperature range. The temperature at the inlet to the core (assuming large convective heat transfer) is fixed by the incoming helium. The ratio $(\dot{H}/\dot{m})$ can be varied to adjust the magnitude of the steady-state slope. If $(\dot{H}/\dot{m})$ is doubled, the steepness of the temperature profile is also doubled. Using this method we can fix a temperature at any other core location. Figure 30 shows some temperature profiles which were produced by this method. In Figure 30a helium enters the core's warm-end at 15 K, and the other fixed temperature, 3.5 K, is chosen at the core's cold-end.

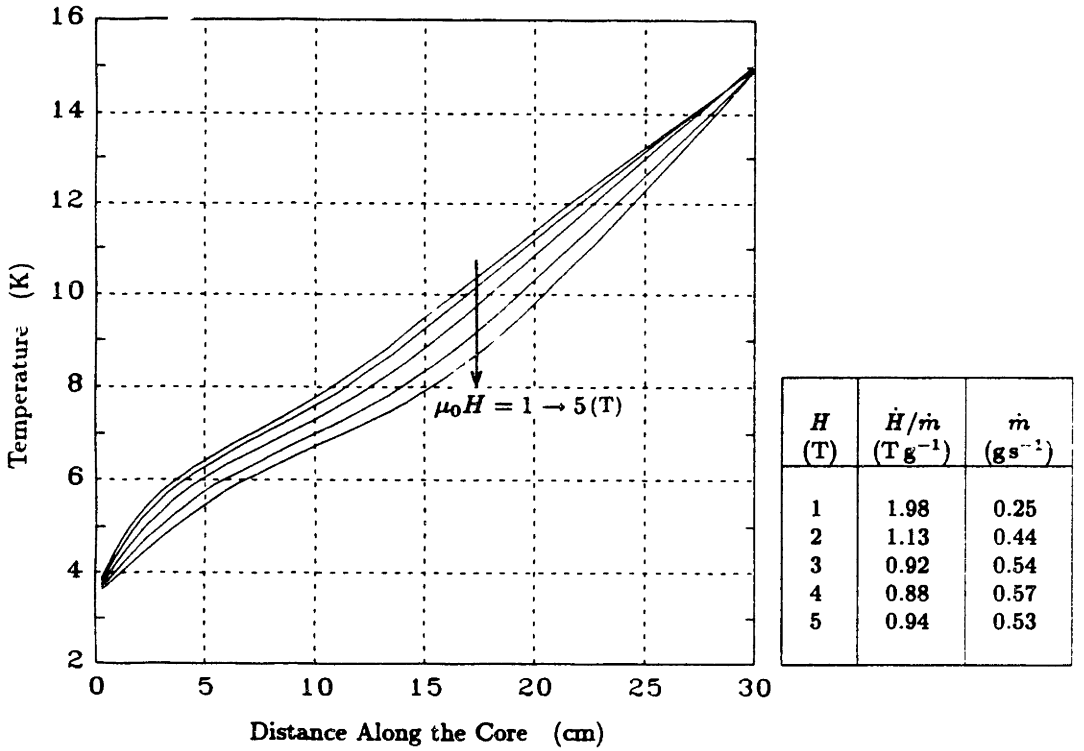

H (T)	$\dot{H}/\dot{m}$ (T g^{-1})	$\dot{m}$ (g s^{-1})
1	1.98	0.25
2	1.13	0.44
3	0.92	0.54
4	0.88	0.57
5	0.94	0.53

Fig. 30a Isothermal Temperature Profiles with End Points Fixed, (3.5→15 K)

In Figure 30b helium enters the core's cold-end at 4.2 K, and the other fixed temperature, 16.5 K, is chosen at the core's warm-end. A different profile is plotted for each field level from 1 to 5 T. The chart on the side of the graph shows the value of $(\dot{H}/\dot{m})$ which was used to obtain the given profile. The value of $\dot{m}$ is calculated by assuming $\dot{H} = 0.5$ (T/s). These graphs show temperature profiles which allow the core to be isothermal as the field passes a given value; that is, the derivative of T with respect to time in Equation (6) passes through zero at every location along the core. The graphs do not show how the temperature profiles will change with time

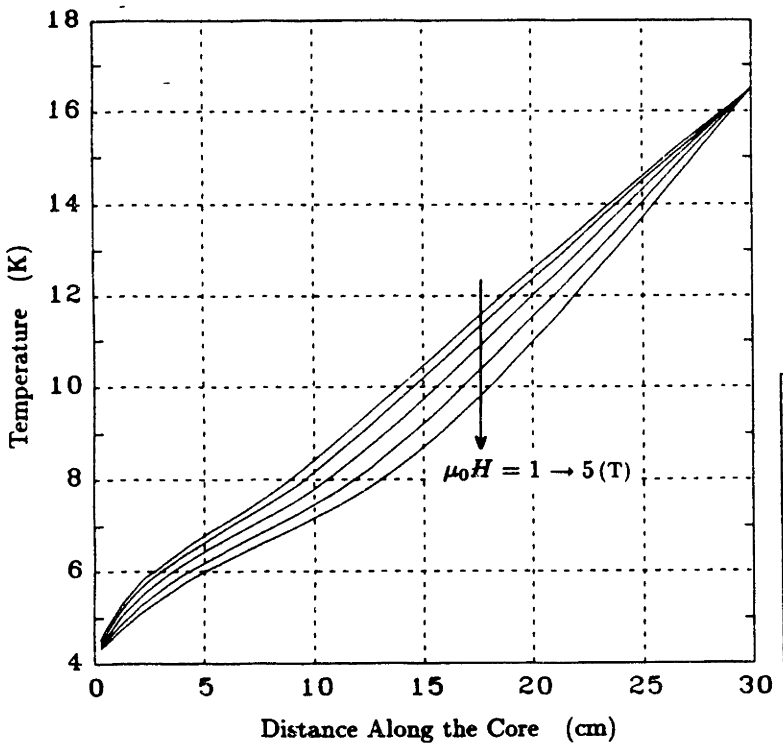

H (T)	$\dot{H}/\dot{m}$ (T g^{-1})	$\dot{m}$ (g s^{-1})
1	2.23	0.22
2	1.25	0.40
3	1.00	0.50
4	0.94	0.53
5	0.98	0.51

Fig. 30b Isothermal Temperature Profiles with End Points Fixed, (4.2→16.5 K) during a magnetization process.

- As the core's temperature profile deviates from the appropriate isothermal profile, isothermal imbalances become greater.
- When the isothermal profiles are different for different fields, it is impossible to have an isothermal situation in the core as the magnetization process continues.

Figure 31 shows the same type of graph as does Figure 30, only now the end temperatures are 10 and 16 K. Note that there is very little deviation in these profiles. Why is this? Mathematically we find that if the steady-state slope varies as a function of field times a function of temperature, then the ratio $(\dot{H}/\dot{m})$ can be adjusted to cancel the field dependence of the slope. (Chapter 12 discusses this in more detail.) This criterion can be expressed as:

$$\frac{dT}{dx} = f(T,H) \Rightarrow \text{Isothermal not possible}$$

$$\frac{dT}{dx} = f(T)g(H) \Rightarrow \text{Isothermal possible}$$

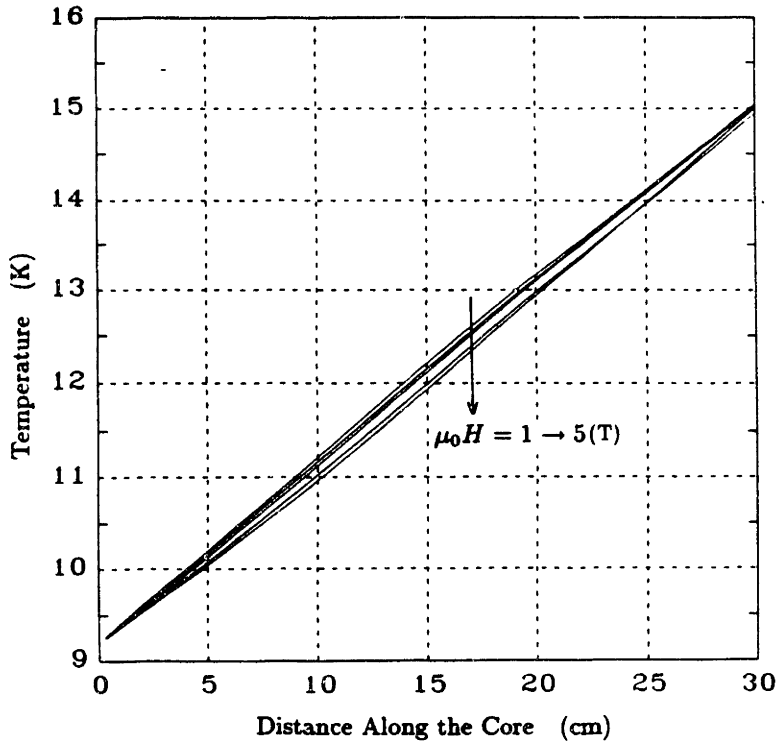

H (T)	$\dot{H}/\dot{m}$ (T g^{-1})	$\dot{m}$ (g s^{-1})
1	1.05	0.48
2	0.57	0.88
3	0.43	1.16
4	0.37	1.35
5	0.36	1.39

Fig. 31a Isothermal Temperature Profiles with End Points Fixed, (9.2→15 K)

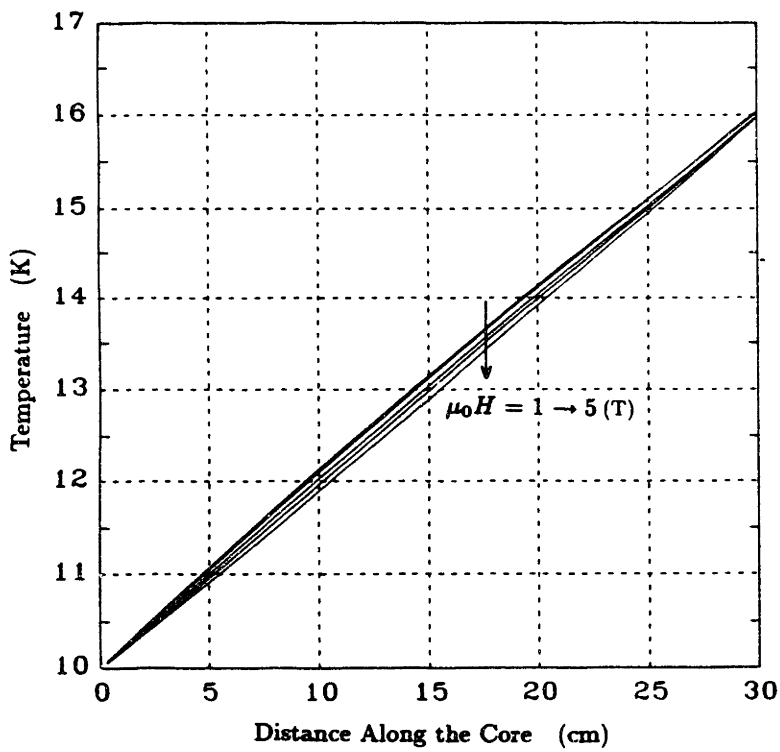

H (T)	$\dot{H}/\dot{m}$ (T g^{-1})	$\dot{m}$ (g s^{-1})
1	1.11	0.45
2	0.60	0.83
3	0.44	1.14
4	0.38	1.32
5	0.36	1.39

Fig. 31b Isothermal Temperature Profiles with End Points Fixed, (10→16 K)

Finally we show some other examples (Figure 32) where the temperature is fixed at various points inside the core. As the fixed point is moved back through the core closer to the inlet, the isothermal profiles become closer at the inlet end, and farther apart at the outlet end.

- It is possible to vary $(\dot{H}/\dot{m})$ to diminish the isothermal imbalances at one end of the core, but by so doing it is likely that the isothermal imbalances will be exaggerated at the other end.

6.5 The Adiabatic Limit

In the adiabatic limit $\dot{m}$ goes to zero, and Equation (6) can be written as:

$$\frac{dT}{dH} = \frac{(1-por)A\rho_g}{C}\left(-T\frac{\partial S_g}{\partial H}\Big|_T\right) \quad \text{(K/T)} \tag{8}$$

This function is shown in Figure 33. The function is created by dividing the magnetic interaction function shown in Figure 28 by the core specific heat which includes both GGG and entrained helium. Of course, the specific heat of the GGG is related to its magnetic interaction term.

It is interesting to note that in the absence of helium entrainment, $(por = 0)$, and:

$$\frac{dT}{dH} = -\left(\frac{T\frac{\partial S_g}{\partial H}|_T}{c_H}\right) = -\frac{\frac{\partial S_g}{\partial H}\Big|_T}{\frac{\partial S_g}{\partial T}\Big|_H} = \frac{\partial T}{\partial H}\Big|_{S_g},$$

which is simply stating that GGG constant-entropy paths will be followed in the absence of entrained helium. This curve is shown in Figure 34. Note that the entrained helium serves to lower the magnitude of dT/dH everywhere, especially where ρc_p of the helium is the greatest.

It has been shown previously that the breathing effect makes it is impossible to produce an adiabatic path over the length of the core. The breathing effect induces flow which influences the net effect of an adiabatic process. Figure 35 shows a computer simulation of an adiabatic magnetization starting with a linear temperature profile from 4 to 15 K which includes a 5% porosity in the core. If there were no flow, then one could conclude from Figure 33 that there would be a greater increase in core temperature at the warm-end than at the cold-end, but this does not happen. Flow is induced, flowing from the cold-end to the warm-end, which cools the warm-end.

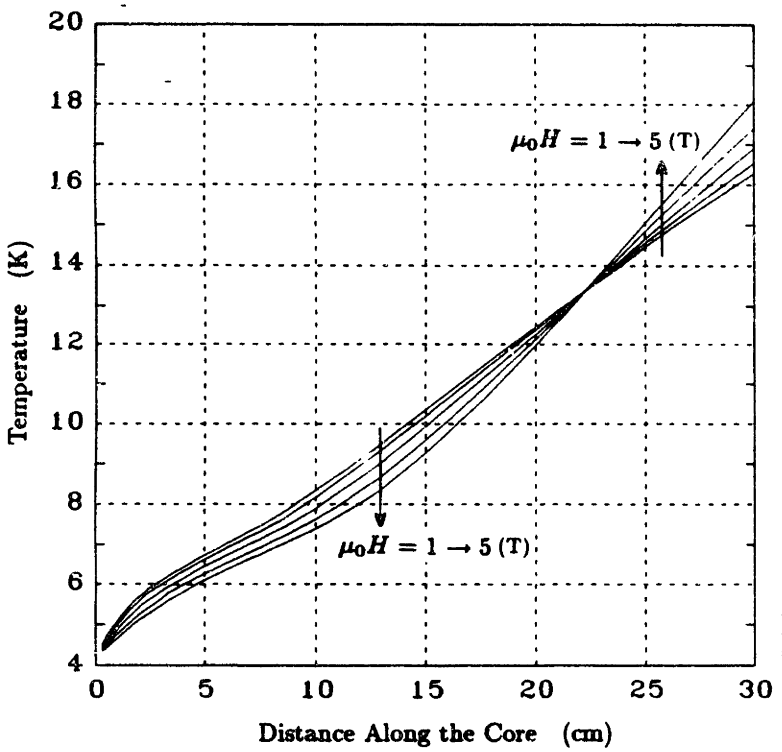

H (T)	$\dot{H}/\dot{m}$ (T g^{-1})	$\dot{m}$ (g s^{-1})
1	2.19	0.23
2	1.26	0.40
3	1.03	0.49
4	1.00	0.50
5	1.07	0.47

Fig. 32a Isothermal Temperature Profiles with Cold-End and Mid-Point Fixed

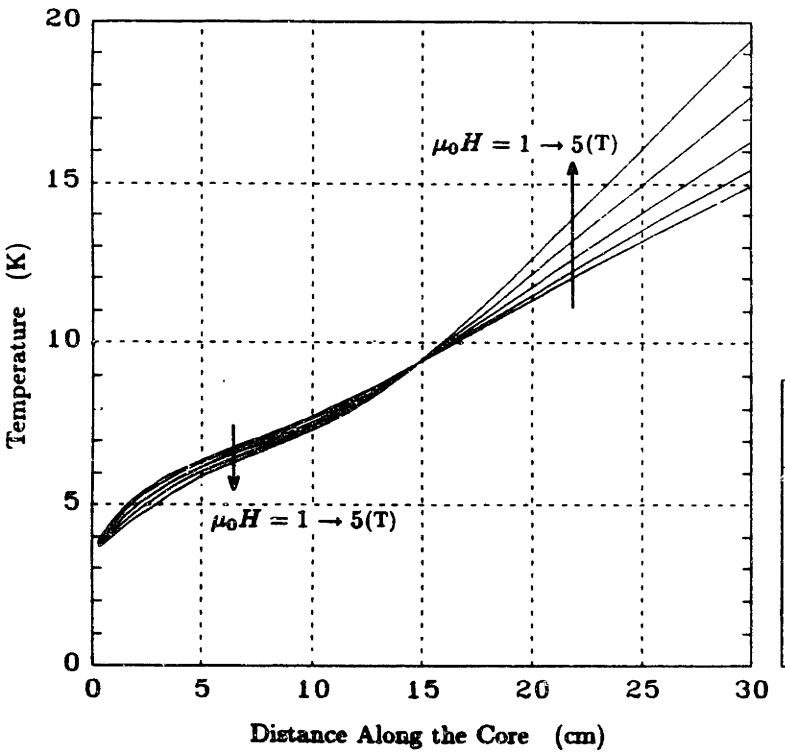

H (T)	$\dot{H}/\dot{m}$ (T g^{-1})	$\dot{m}$ (g s^{-1})
1	1.97	0.25
2	1.17	0.43
3	1.02	0.49
4	1.06	0.47
5	1.21	0.41

Fig. 32b Isothermal Temperature Profiles with Cold-End and Mid-Point Fixed

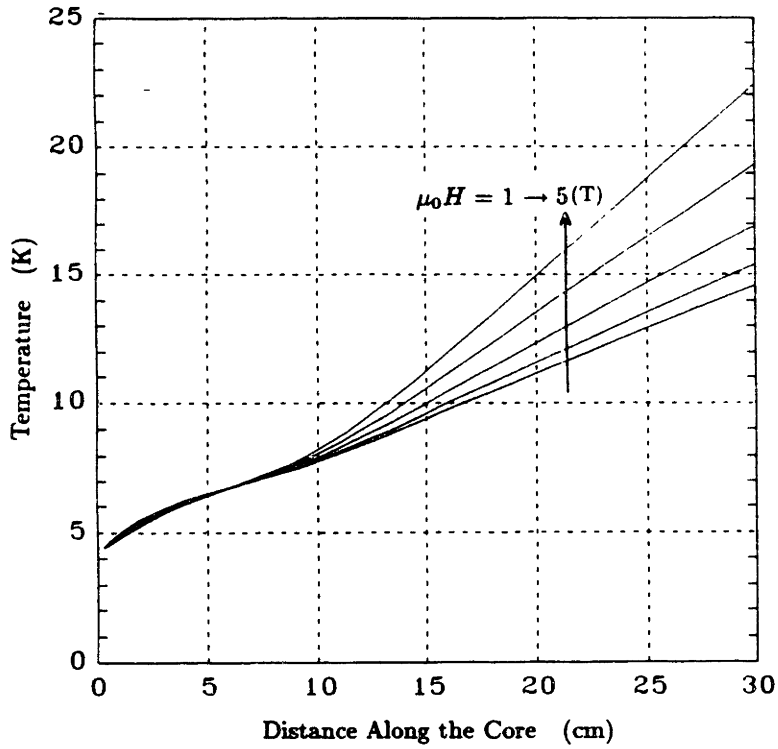

H (T)	$\dot{H}/\dot{m}$ (T g^{-1})	$\dot{m}$ (g s^{-1})
1	1.86	0.27
2	1.14	0.44
3	1.04	0.48
4	1.13	0.44
5	1.34	0.37

Fig. 32c Isothermal Temperature Profiles with Cold-End and Mid-Point Fixed

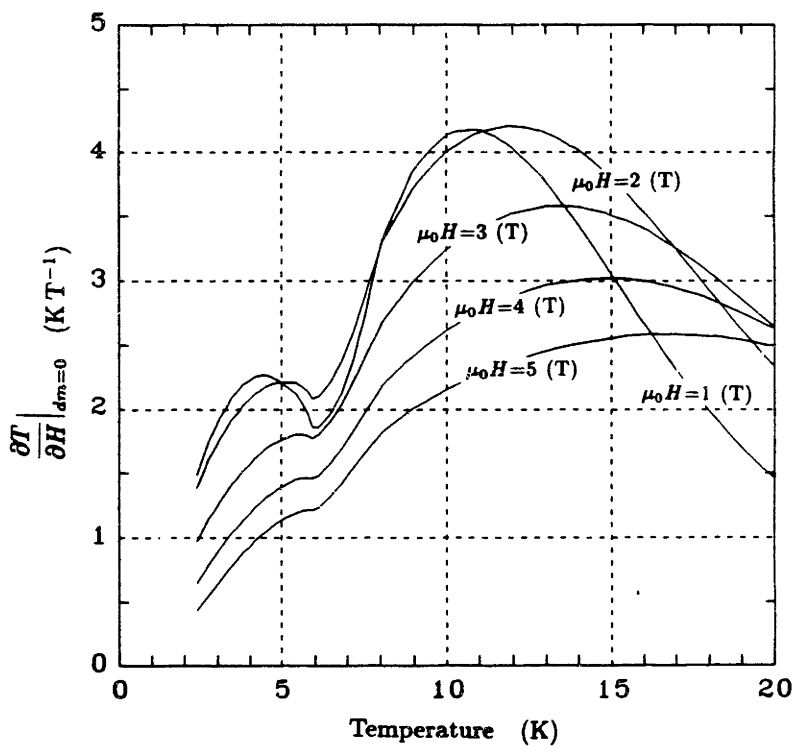

Fig. 33 Adiabatic Change in Temperature with Field, (p=5 atm), (por=0.05)

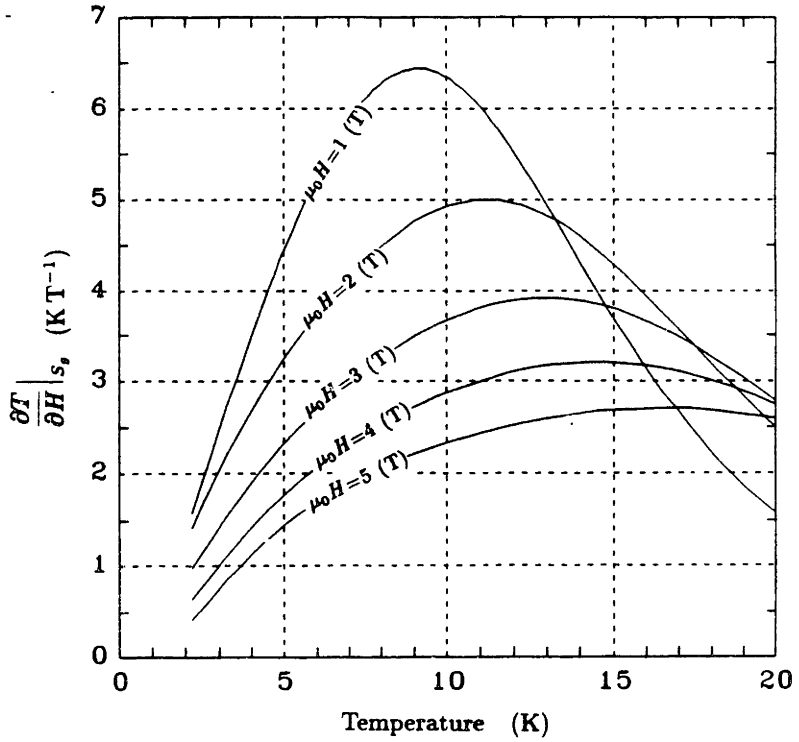

Fig. 34 GGG Isentropic Change in Temperature with Field

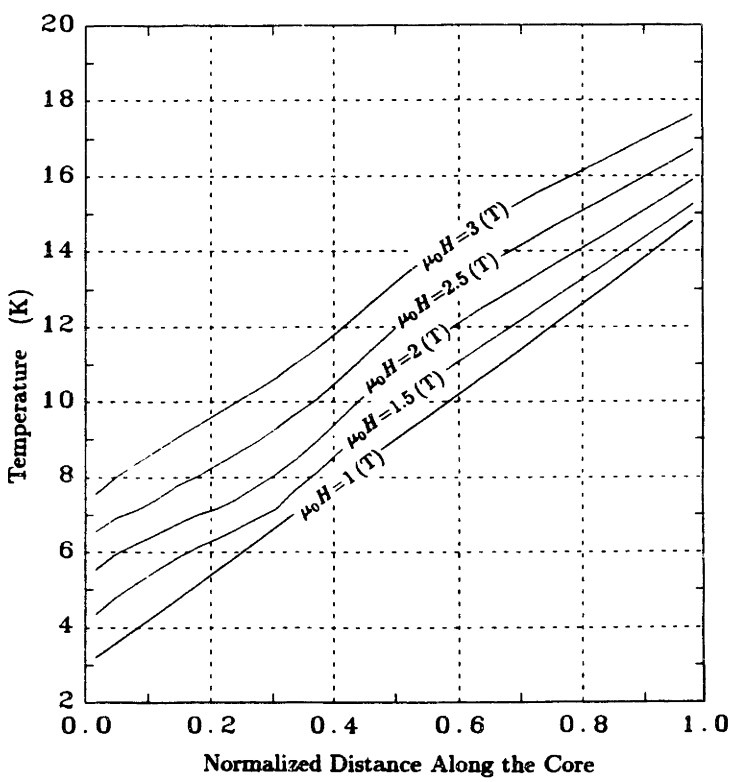

Fig. 35 "Adiabatic" Magnetization by Computer Simulation

- The net effect of an adiabatic magnetization, with uniform field and with 5% porosity, is to increase the temperature of the core fairly uniformly.

6.6 Active Convection Wave Solutions

If we take Equation (6) and divide through by the core's specific heat C, we can rewrite the equation as:

$$\frac{dT}{dt} + v\frac{dT}{dx} = q \quad \text{(K/s)} \tag{9}$$

Equation (9) is a wave equation where v is the velocity at which the convection wave propagates through the core and q is a perturbation of the wave equation which is due to the magnetic interaction between the paramagnetic salt and the applied magnetic field. The convection wave velocity is given by:

$$v = \frac{\dot{m}c_p}{C} \quad \text{(cm/s)}$$

The function q can be expressed as:

$$q = -\left(\frac{(1-por)A\,\rho_g}{C}\right) T\,\frac{dS}{dH}|_T\,\dot{H} \quad \text{(K/s)}$$

With $q = 0$, the solutions to the above equation are of the general form:

$$T = f(x - vt)$$

where f maintains its shape and moves along x at velocity v. The direction of propagation in this case is determined by the helium flow direction. The particular part of Equation (9) can be satisfied simply by adding a linear term in either space or time. Here it makes more sense to add it in time since without the convection term, the temperature will rise without bounds in time.

$$T = f(x - vt) + q\,t$$

In general Equation (9) is not easily solved in closed form since it is difficult to create via Fourier techniques an initial value solution which will maintain an arbitrary boundary condition at $x = 0$ for all time. Equation (9) is most easily analyzed by employing the method of characteristics. Solutions to the step-wise constant wave equation can provide valuable intuition into the behavior of our system.

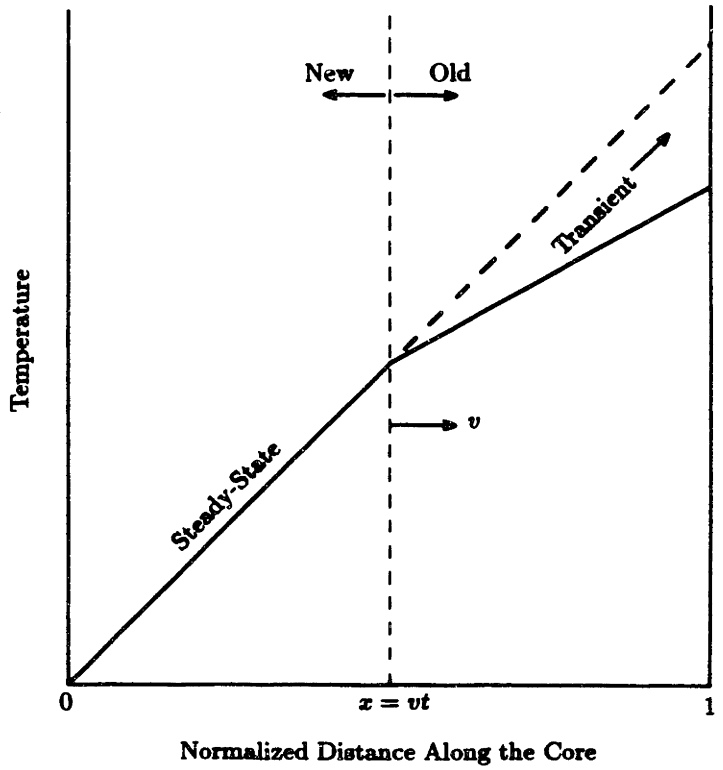

Fig. 36 Constant Parameter Active Convection Wave

A. Step-wise constant parameters

Appendix F shows many examples of the operation of an active core with step-wise constant parameters. Figure 36 shows one example where the convection wave has moved half way through the core. The results from this analysis can be summarized as:

- For any value of q and v, there is a steady-state solution; the slope is given by (q/v).
- For every process with q and v constant, a convection wave moves out from the inlet of the core at velocity v.
- Upstream of the wave front, the core has reached the appropriate steady-state temperature profile. As long as (q/v) remains the same, the steady-state profile remains isothermal.
- Downstream of the wave front, the temperature is moving towards its new steady-state profile, but as it does so, its gradient does not change. The temper-

ature gradient at any location downstream of the wave front, and at any time during the the flow process, is the same as the original gradient which existed before commencement of the process at the core location given by $x - v\,t$.

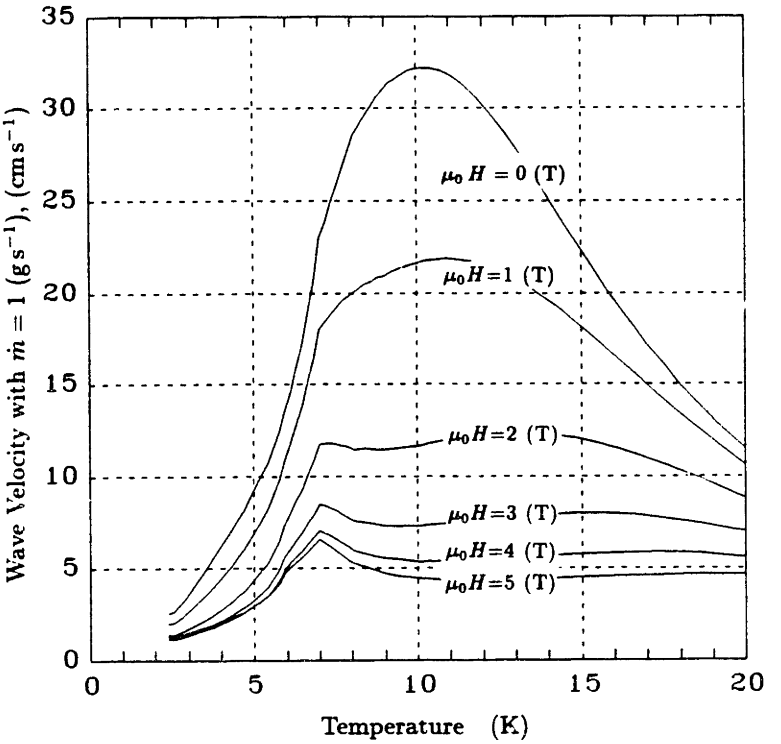

Fig. 37 Convection Wave Velocity, (p=5 atm), (por=0.05), ($\dot{m}$=1 g s^{-1})

B. The wave velocity, v

The convection wave velocity v is shown in Figure 37. This velocity varies considerably over the temperatures and magnetic fields of interest, (3 to 20 K); (0 to 5 T).

The time it takes for information to propagate from one end of the core to the other can be found by integrating the velocity with time. Unfortunately, $v = v(T, H)$, and it cannot be directly integrated. For a first-order analysis, we can integrate v by assuming a temperature profile and using numerical techniques. For this estimate the temperature profile derived from the steady-state analysis is used together with the flow rate which corresponds to that profile. With a computer program we follow the wave front as it moves through the core, changing the velocity as the temperature

and magnetic field change. We start with the wave front at the inlet of the core, and stop when either it reaches the outlet, or the magnetization process is over.

It was found that with a temperature range of 4.2 to 15 K, the wave front does not travel the entire core length (30 cm) during either an up-flow or a down-flow process. It comes up short by approximately 5 to 10 cm. This results because the path which the wave front happens to follow traces through low velocity regions in Figure 37 (also remember that the flow rate is less than 1 (g/s), the standard used in Figure 37). For a refrigeration process between 4.2 and 10 K, where the helium flow rate is almost doubled, the convection wave velocity is also doubled.

- For the parameters of our core, the convection wave does not travel from one end of the core to the other during a refrigeration process over the range of 4.2 to 15 K. However, it does for a refrigeration process over the range of 4.2 to 10 K.

VII NON-CARNOT ACTIVE REGENERATOR APPLICATIONS

Chapter 6 examined the mathematical basis of active regeneration, but did not apply that logic to a complete thermodynamic cycle. One of the goals of this thesis is to analyze the performance of an active regenerator core when it is used as a refrigerator. The proposed cycle design goal is the cascaded-Carnot cycle, where each element of the core experiences only Carnot cycles. Both the computer simulation program and the test data has indicated that Carnot-type cycles cannot be obtained with our device. One problem is that isothermal paths require proper field-flow phasing throughout the core, but this may not be achieved with the independent cycle parameters available to the cycle designer. The actual cycles experienced within the core are very complicated, and vary from one core location to another. Chapter 8 will use the logic presented in Chapters 6 and 7 to explain the behavior of an active regenerator when it is cycled as a refrigerator.

This chapter explores two non-Carnot applications of an active regenerator. These applications can be analyzed with relative ease (when compared to Carnot). It is hoped that the understanding of this chapter will help in the comprehension of Chapter 8, and will motivate the need for that chapter. Some of the concepts developed here apply to more complicated cycles. It should be noted that cycle behavior is a function of the type of magnetic material used. The principles discussed in this chapter apply to a regenerator core composed of GGG. Other paramagnetics materials may not exhibit the same behavior when cycled in the same way. Active regeneration with other magnetically active materials is discussed in Chapter 12.

7.1 The Adiabatic-Isofield Cycle

This section compares a single cycle device to an active regenerator device when both are cycled in non-Carnot type refrigeration cycles. It is a common misconception that these two devices respond in the same way to adiabatic-isofield cycles. This section shows how they differ.

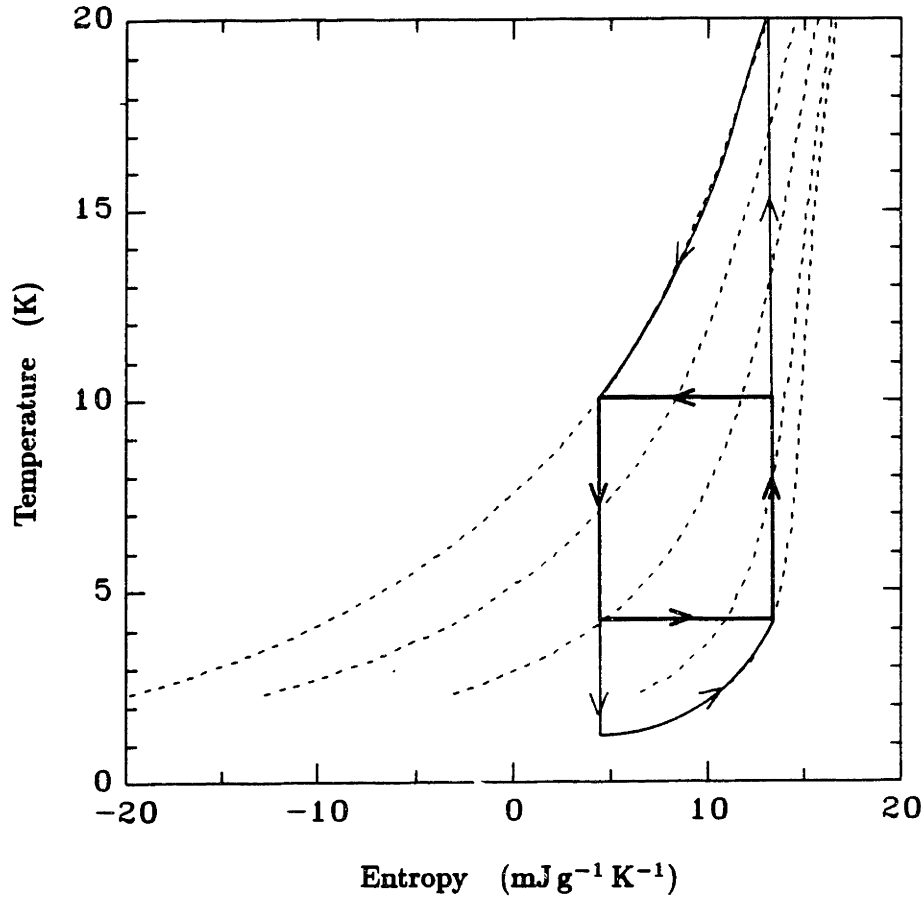

Fig. 38 Comparison of a Carnot Cycle to an Adiabatic-Isofield Cycle

7.1.1 A single cycle device:

The single cycle device was described in Chapter 1.3.1. In that chapter there is a description of how a Carnot refrigeration cycle can be implemented. It is also possible to run this type of device in non-Carnot type cycles. One possible cycle is the adiabatic-isofield. Figure 38 shows both the Carnot cycle and the adiabatic-isofield cycle on the same graph. The adiabatic-isofield cycle is implemented by the following paths:

1) Adiabatic Magnetization The magnetic field is raised from the minimum to the maximum value. There is no heat flow from the magnetic material.
2) Isofield Cooling Thermal contact is made to the warm-reservoir until their temperatures are equal.
3) Adiabatic Demagnetization The magnetic field is lowered from the maximum to the minimum. There is no heat flow to the magnetic material.

4) Isofield Warming Heat flows into the core from the cold-reservoir until their temperatures are equal.

In this way both cycles shown use the same total change in applied field, and reject and accept heat from the same thermal reservoirs.

It should be noted that the refrigeration (equal to $\int TdS$) on the isofield warming path is maximized by the Carnot cycle, and other cycles produce less refrigeration. It should also be noted that the efficiency is greatest for the Carnot cycle. In fact, the worse possible cycle under the conditions specified is the adiabatic-isofield. This cycle minimizes the amount of refrigeration and maximizes the amount of work into the process. It should therefore be the goal of the cycle designer to approach the Carnot cycle as closely as is possible.

In a real system irreversibilities will force the cycle to deviate from the Carnot. The flow processes will trace a path which lies somewhere between the two extreme cases shown in Figure 38. Yet even if the device is cycled in the worse case, the adiabatic-isofield cycle, refrigeration is still achieved. Any cycle from the Carnot to the adiabatic-isofield will work to produce some amount of refrigeration.

7.1.2 Active Regeneration

Now we will examine the behavior of an active regenerator core when it experiences an adiabatic-isofield cycle.

1) Adiabatic Magnetization The magnetic field is raised from the minimum to the maximum value. There is no helium flow to transport heat out of the core.
2) Isofield Cooling (Up-Flow) The field is held constant as helium flows from the cold-end to the warm-end. For the example shown there is enough helium flow so that the convection wave moves through one quarter of the core.
3) Adiabatic Demagnetization The magnetic field is lowered from the maximum to the minimum value. There is no helium flow.
4) Isofield Warming (Down-Flow) The field is held constant as helium flows from the warm-end to the cold-end. The shuttle mass of helium must be equal in each direction. The distance the convection wave travels for a given amount of helium flow is inversely proportional to the core's specific heat.

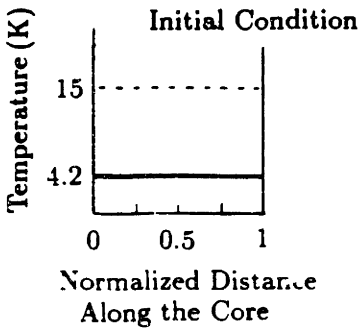

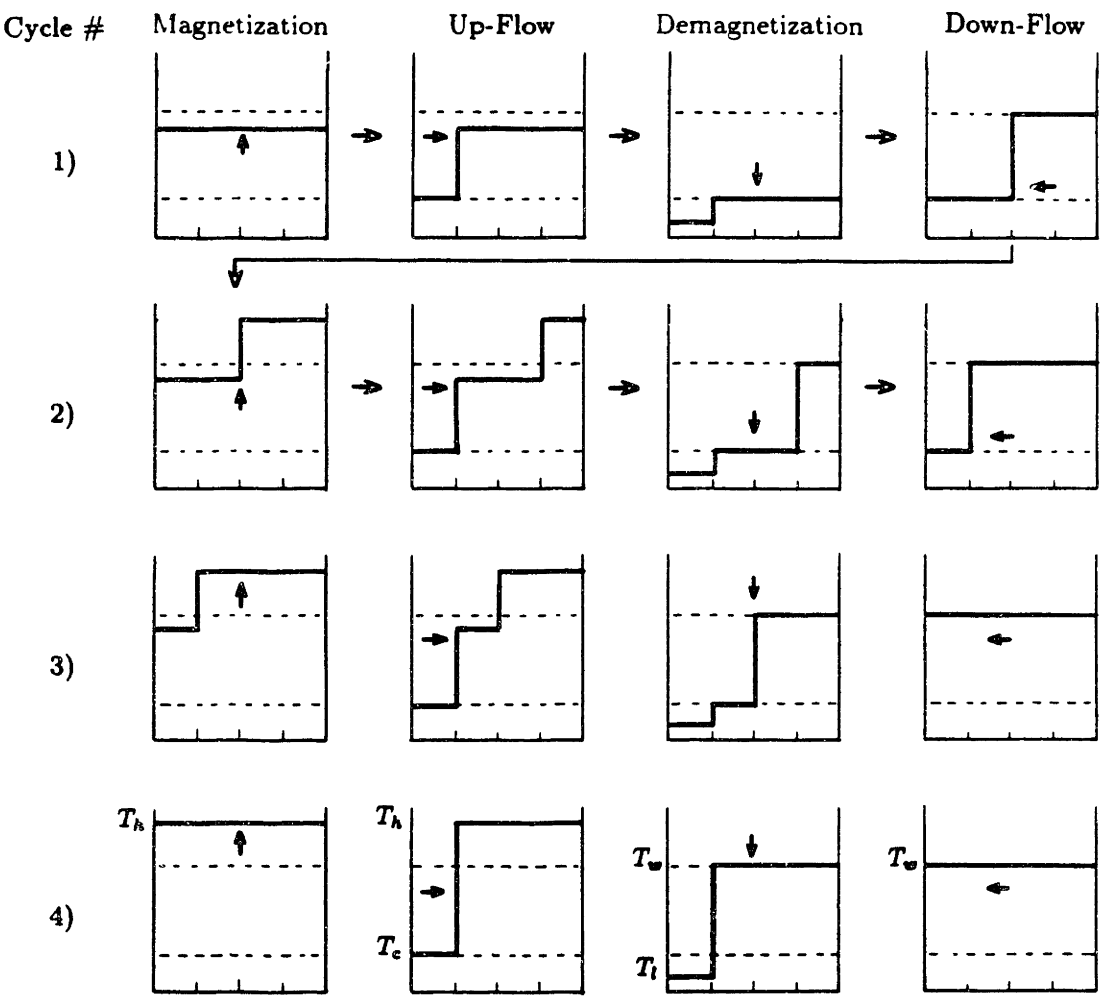

Fig. 39 The Adiabatic-Isofield Cycle in a Regenerative Device

Figure 39 shows a fictitious core where the specific heat (at constant field) is twice as large at the high field as at the low field. (In a real GGG core the specific heat ratio is actually much larger, and it is temperature dependent.) Convection waves are described in Chapter 6.6 and Appendix F. In this simplified example dispersion of the convection wave front is ignored. The isofield convection wave travels twice as far on the down-flow as on the up-flow. This demonstration shows how unmatched core specific heat can lead to the following results:

- Regardless of the initial temperature profile eventually the entire core ends up at the warm-reservoir temperature. In the example given it takes three complete cycles for the core to go from all cold to all warm.

- Subsequent cycles will repeat with excess warm helium flowing into the cold-reservoir at a temperature above the reservoir's temperature. This results in negative refrigeration.

The steady-state cyclic temperature at the core's warm-end and cold-end are shown in Figure 40. It can be seen that though the warm-end continuously rejects heat, the cold-end receives just as much helium at 15 K as it does at 1 K. In this example there is enough warm helium entering the cold-reservoir at the end of the down-flow to more than eliminate all the previously obtained refrigeration. Negative refrigeration results.

The example described above used fictitious properties in order to demonstrate the core's overall behavior under repeated adiabatic-isofield cycling, without introducing complications which result from actual core properties. It should be noted that even the adiabatic-isofield cycle can produce net refrigeration if the temperature range of refrigeration is small enough. When this happens the negative refrigeration which occurs at the end of the down-flow does not completely cancel the positive refrigeration which occurs at the beginning of the down-flow. In order to find the temperature range which results in no net refrigeration for a core composed of GGG, the above analysis is continued with the following assumptions:

1) The core contains GGG,
2) There is no entrained helium,
3) The helium specific heat is constant,

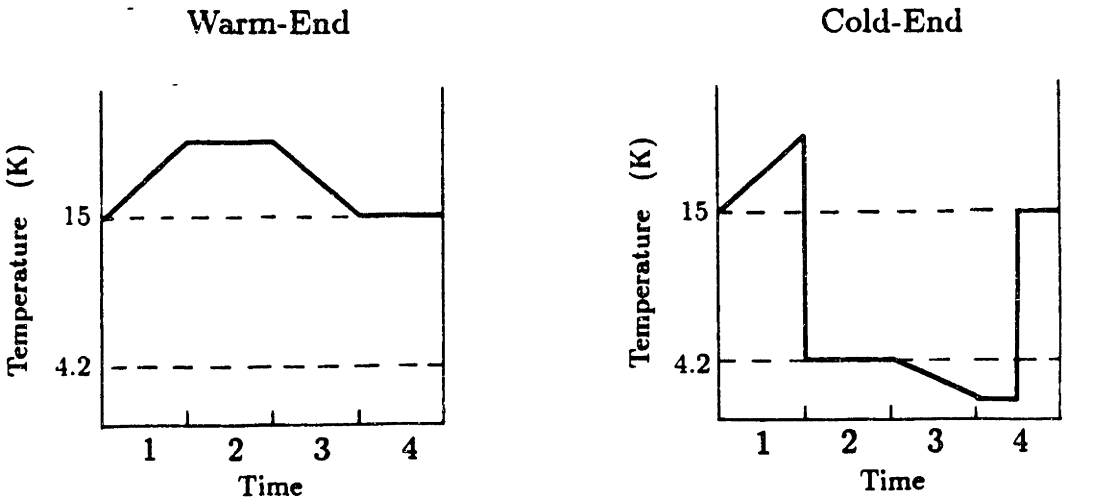

Fig. 40 Temperature vrs. Cycle Time

4) There is no loss-induced dispersion of the convection wave.

The last assumption implies all of the ideal core assumptions previously listed in Chapter 6.1.

For a isofield process the change in the core's magnetic enthalpy is equal to the net helium enthalpy into the core. This leads to the following two equations.

$$\text{Up} - \text{Flow} \quad \Rightarrow \quad x\, M_c \left[\mathrm{H}_g(T_h, H_h) - \mathrm{H}_g(T_c, H_h)\right] = \Delta m\, c_p\, (T_h - T_c)$$

$$\text{Down} - \text{Flow} \quad \Rightarrow \quad x\, M_c \left[\mathrm{H}_g(T_w, H_l) - \mathrm{H}_g(T_l, H_l)\right] = \Delta m'\, c_p\, (T_w - T_l)$$

Δm is the amount of helium pushed into the core on the up-flow (less than that which would cause the convection wave to push all the way through the core). It is also the total shuttle mass of helium for the cycle. x is the fractional distance the up-flow convection wave travels through the core. In Figure 39 this distance is 25% of the core. M_c is the total mass of GGG in the core. $\Delta m'$ is the amount of helium

flow on the down-flow which occurs before the warm-end temperature blows through to the cold-end. The total helium flow on the down-flow must equal the shuttle mass, Δm; $\Delta m'$ is always less than Δm. The other variables in these equations are:

T_c: The cold-reservoir temperature (in Figure 39 $T_c = 4.2$ K)

T_l: The coldest temperature, reached at the cold-end after demagnetization from T_c.

T_w: The warm-reservoir temperature (in Figure 39 $T_w = 15$ K)

T_h: The warmest temperature, reached after magnetization from T_w

H_h: The highest magnetic field

H_l: The lowest magnetic field

H_g: GGG magnetic enthalpy, a function of temperature and field

We can divide these two equations to find:

$$\frac{\Delta m'}{\Delta m} = \left[\frac{\mathrm{H}_g(T_w, H_l) - \mathrm{H}_g(T_l, H_l)}{\mathrm{H}_g(T_h, H_h) - \mathrm{H}_g(T_c, H_h)}\right]\left(\frac{T_h - T_c}{T_w - T_l}\right) = \frac{\bar{C}_{H_l}}{\bar{C}_{H_h}}$$

With the assumptions previously stated we find that the ratio of mass flow on the down and up-flow necessary to drive a convection wave through the core is equal to the ratio of the average core specific heats encountered during the respective isofield paths.

The net refrigeration is equal to the net enthalpy flux, Δh_c, carried by the helium through the core's cold-end over a complete cycle. On the up-flow the flux is positive, and enters the core from the cold-reservoir at T_c. On the down-flow the flux is negative. The first part of the down-flow has a mass flux of $\Delta m'$ at a temperature T_l, while the remainder of the down-flow has a mass flux of $\Delta m - \Delta m'$ at a temperature of T_w; this part is the blow-through from the warm-reservoir.

$$\Delta h_c = \Delta m\, c_p\, T_c - \Delta m'\, c_p\, T_l - (\Delta m - \Delta m')\, c_p\, T_w$$

This equation can be rewritten as:

$$\frac{\Delta h_c}{\Delta m\, c_p} = (T_c - T_w) + \frac{\Delta m'}{\Delta m}(T_w - T_l)$$

To determine T_h from T_w, and T_l from T_c, we can follow isentropic paths on the GGG T-S diagram (Appendix E, Figure E-1). With these temperatures, we can

use the magnetic enthalpy diagram (Appendix E, Figure E-2) to determine the average specific heat ratio, and therefore the mass flow ratio. The net refrigeration for the adiabatic-isofield cycle with an ideal core is then determined from the above equations. Table 8 shows the results of this analysis. When the normalized net refrigeration, $\Delta h_c/\dot{m}c_p$, is positive, refrigeration can be achieved by the adiabatic-isofield cycle. Note that even with a regenerator that has no helium entrainment and induces no losses, the adiabatic-isofield cycle results in complete loss of refrigeration when the temperature range is greater than $\sim$3 K.

Analysis in Chapter 8 will show that it is imperative for a refrigeration device based on active regeneration to be cycled in Carnot-type cycles. When device imperfections result in deviations from the Carnot cycle, the blow-through behavior exhibited in the adiabatic-isofield cycle will be seen superimposed on the proper cycle, and will result in a loss of potential refrigeration.

7.2 As a Stirling Cycle Regenerator:

Another potential application for an active regenerator is for use in a Stirling cycle refrigeration system. The Stirling cycle is not presently used in low temperature refrigeration even though in theory it could be more efficient than the Gifford-McMahon or other similar cycles presently used.[11] The reason is that the Stirling cycle efficiency is critically dependent on the performance of its regenerator, and to date there have been no suitable low-temperature regenerators available. The reason is that at low temperatures metals loose their specific heat. Paramagnetic salts at high magnetic fields can offer a large apparent specific heat.

There are two basic modes in which a GGG regenerator could potentially be used in a Stirling cycle: 1) constant field, and 2) constant temperature.

1) Constant Field

Constant Field is the easy approach. Raise the GGG core to a high magnetic field and maintain this field. The specific heat at constant field of GGG is shown in Appendix E, Figure E-4. Figure 41 shows a convection wave moving back and forth in the core. The amount of helium flow is chosen so that the convection wave travels about 3/4 of the distance of the core. After a while dispersion will cause the wave to spread out

TABLE 8
Net Refrigeration, Adiabatic-Isofield Cycle
No Helium Void, No Dispersion

T_c (K)	T_l (K)	T_w (K)	T_h (K)	$\frac{\Delta m'}{\Delta m}$	$\frac{\Delta h_c}{\Delta m\, c_p}$ (K)
Field from 0 to 3 Tesla					
4.2	0.8	15	22	0.36	-5.7
4.2	0.8	10	20.7	0.30	-3.0
4.2	0.8	8	20.0	0.50	-0.2
4.2	0.8	6	19.3	0.76	+2.2
7	1.3	15	22	0.28	-4.2
10	1.9	15	22	0.25	-1.7
12	2.2	15	22	0.23	0
Field from 0 to 4 Tesla					
4.2	0.5	15	24	0.32	-6.2
4.2	0.5	10	23	0.42	-1.8
4.2	0.5	8	22.5	0.50	0

as shown. There is no mismatch problem as described in the previous section since the field, and therefore the total heat capacity of the core, is the same for the up and down-flow.

2) Constant Temperature

It is not practical to design a core that is so large as to dominate the heat capacity of the helium; however, it may be possible to vary the applied magnetic field in such a way as to maintain an isothermal profile in the core. This in effect simulates an infinite core specific heat. If the isothermal profiles are not separated by adiabatic paths, then each segment of the core will traverse lines of constant temperature. This is neither a refrigeration nor a work cycle.

In reality the control of isothermal paths in this application introduces the same

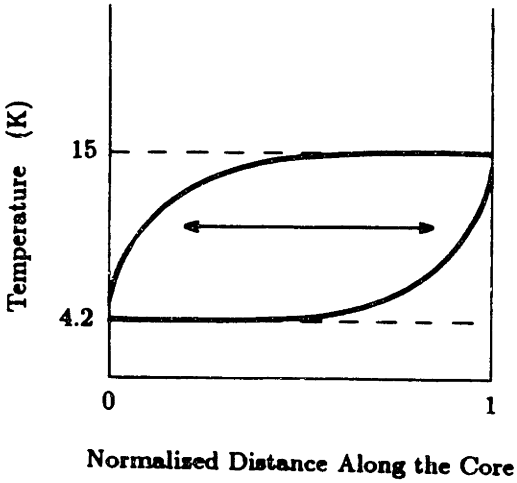

Fig. 41 An Isofield Regenerator

problems as are encountered when attempting Carnot cycles for refrigeration. The finite temperature difference generated between the GGG and the helium results in a required adiabatic path simply to overcome this hysteresis. This in turn results in the up-flow occurring at a higher field than the down-flow which produces a mismatch similar to that described in the adiabatic-isofield cycle.

7.3 Summary

The results of this chapter can be summarized as:

- The adiabatic-isofield cycle in a GGG core cannot produce refrigeration when the temperature range between the reservoirs exceeds $\sim$ 3 K.
- In order for an isofield up-flow to be "balanced" with an isofield down-flow, the specific heat of the core at constant field, averaged over the length of the active core, must be the same for each flow process.
- When using GGG (or any paramagnetic above its Curie temperature) as a refrigerant, any isofield process will result in excess warm-helium pushing through the cold-end of the core and polluting the cold-end reservoir.

VIII. EXPLANATION OF CYCLE BEHAVIOR

Chapter 5 presented the results of many computer simulation runs. The cycle behavior described there could not be easily explained. This chapter uses the analysis in Chapter 6 to explain the results of Chapter 5. From this analysis comes an understanding of the dynamics of active regeneration. Cycle optimization and design of more efficient refrigeration systems can be more easily accomplished with qualitative understanding than with computational trial and error.

8.1 Basic Requirements for Any Refrigeration Cycle:

Below is a list of the basic requirements for any steady-state refrigeration cycle that can be attempted with our type of device. Beyond these restrictions, there are many variations that could conceivably produce refrigeration. It is important to remember that the only way to transport heat through the core is by helium flow. The basic restrictions are:

1) Net Helium Flow = 0: This is a steady-state requirement. Over a complete cycle, the total helium flow on an up-flow must equal the total helium flow on a down-flow.
2) Net $\Delta H = 0$: This is another steady-state requirement. The magnetic field must return to its original value at the end of every cycle. The same amount of ΔH is available for magnetization and demagnetization.
3) $(\bar{T}_h - T_c > T_w - \bar{T}_l)$: This requirement follows from the most basic expressions of the second law. For any steady-state process:

$$\text{Second Law}: \qquad Q_w \geq \frac{T_w}{T_c} Q_c$$

where T_c and T_w are the cold and warm-reservoir temperatures respectively. Since helium is our only method of heat transport this translates to the difference between the average rejection temperature, and the reservoir temperature must be greater at the warm-end.

$$\bar{T}_h - T_w > T_c - \bar{T}_l$$

where $\bar{T}_h$ is the mass average helium temperature leaving the core's warm-end and entering the warm-reservoir during the up-flow process, and $\bar{T}_l$ is the mass average helium temperature leaving the core's cold-end and entering the cold-reservoir during the down-flow process. This requirement can in turn be translated to the average gradient on the up-flow must be greater than the average gradient on the down-flow.

4) An adiabatic path must proceed the flow path: In order to have a refrigeration cycle as opposed to a work cycle, it is necessary to have the up-flow temperature profile higher than the down-flow temperature profile. This is accomplished by having an "adiabatic" magnetization before the up-flow process, and by having an "adiabatic" demagnetization before the down-flow process.

A generic description of a refrigeration cycle can be expressed as:

Magnetization $\Rightarrow$ Adiabatic -then- up-flow

Demagnetization $\Rightarrow$ Adiabatic -then- down-flow

(In this description "Adiabatic" means no forced helium flow from the displacer. As was seen before, the breathing effect produces helium flow and prohibits actual adiabatic paths in our core.)

8.2 Basic Cycle Parameters

8.2.1 Parameters Which Can Be Used for Cycle Control

There are three major parameters which can be used to alter the basic cycle behavior of our device. They are listed below in order of importance, and then subsequently discussed in greater detail.

(1) Adiabatic Percent: percentage of the total field change used for the adiabatic process.

(2) Total shuttle mass: the total helium shuttle mass during the flow process, measured at the cold end, M_T. The value of $(\Delta H/M_T)$ is also determined since ΔH is fixed at 3 T (1$\leftrightarrow$4 T).

(3) Fine Phasing: The helium flow rate variation during a flow path; the value of $(\dot{H}/\dot{m})$ as it varies with time.

The general effect of varying the adiabatic percent is well described by the results presented in both Chapters 4.4 and 5.2. It should be noted that the maximum allowed flow decreases with increased adiabatic percent.

The total shuttle mass of helium can have a wide range of values. For the purpose of defining cycle type, we will use three limiting cases.

- Low-Flow-Rate is defined as when the heating (or cooling) due to magnetic interaction is greater than the cooling (or heating) due to helium convection. The limiting case here is the adiabatic process (Chapter 6.5).
- High-Flow-Rate is defined as when the heating (or cooling) due to helium convection is greater than the cooling (or heating) due to magnetic interaction. The limiting case here is the isofield process (Chapter 6.6).
- Balanced-Flow is defined as when the average temperature of the core does not vary during the flow process. An isothermal process may be approached in certain instances. The shuttle mass of helium which produces balanced-flow over a complete flow path is defined as M_b.

In general, different regions of the core may experience different types of flow at any given cycle time. It is often the case that the inlet end of the core will have developed the proper temperature gradient to allow for balanced-flow, while the downstream end of the core is still in either a high-flow-rate or a low-flow-rate transition. For the purpose of the above definitions we will use the average core temperature to define the type of flow process. For example, a process will be considered to be balanced if the average core temperature remains constant, even if the process is not isothermal.

8.2.2 A cycle parameter which is not independently controlled

There is one more cycle parameter which, unlike the previous parameters, cannot be independently controlled. It has been found that the convection wave velocity (v) can have a significant impact on the behavior of a refrigeration cycle. Perturbations from balanced-flow move through the core at the convection wave velocity.

- A high-shuttle-mass process has enough flow so that a convection wave can easily travel from one end of the core to the other during a flow process. All initial temperature information contained in the core before the flow process is pushed

out the end and lost.

- A low-shuttle-mass process doesn't have enough total helium flow during a flow process for the convection wave to travel the length of the core. Some of the temperature information initially in the core remains in the core at the outlet end.

Of course, the convection wave velocity is related to the amount of helium flow. We have an expression for the convection wave velocity derived in Chapter 6.6:

$$v = \frac{\dot{m} c_p}{C},$$

which was plotted in Figure 37 with a helium flow rate $\dot{m}$=1 (g/s). Everything else being constant, v is proportional to $\dot{m}$. For a given temperature range, there is an amount of helium flow which will allow the convection wave to travel the length of the core. We will define this shuttle mass of helium as M_e. M_e varies somewhat with the overall temperature range as the specific heat of the helium and core varies with temperature.

8.2.3 Comparison of M_b to M_e

Figure 42 shows the general dependency of both M_b, the helium shuttle mass which allows for balanced-flow, and M_e, the helium shuttle mass which allows for the convection wave to travel the length of the core, with overall temperature range. (On a zero-order, M_b goes as $1/\Delta T$, and M_e is not a function of ΔT.) Note that there is a temperature range at which $M_b = M_e$ This temperature range is defined as ΔT_c.

- If the temperature range is greater than ΔT_c, then $M_b < M_e$, and M_b is in the low-shuttle-mass range.
- If the temperature range is less than ΔT_c, then $M_b > M_e$, and M_b is in the high-shuttle-mass range.

8.3 Proper Adiabatic Paths

Section 8.1 states that it is necessary for the up-flow temperature gradient to be steeper than the down-flow temperature gradient. A proper adiabatic path, therefore, must not only raise (or lower) the temperature profile, but should also adjust the

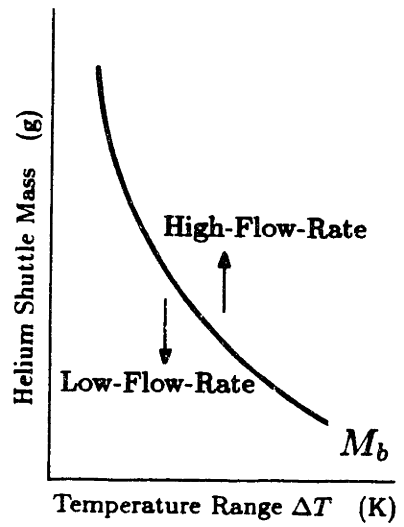

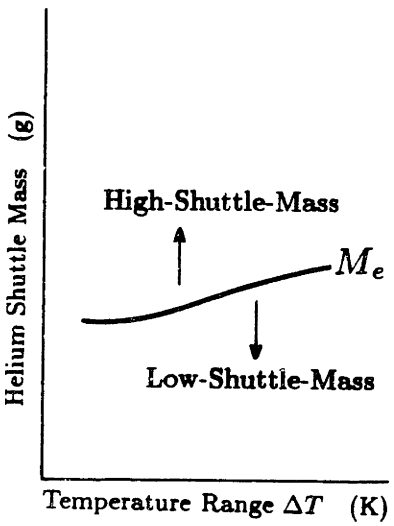

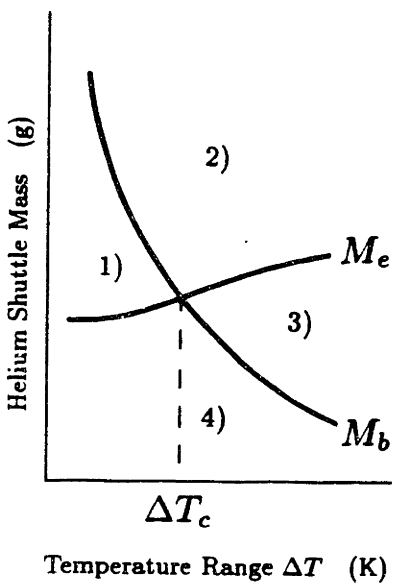

1) Low-Flow-Rate, High-Shuttle-Mass

2) High-Flow-Rate, High-Shuttle-Mass

3) High-Flow-Rate, Low-Shuttle-Mass

4) Low-Flow-Rate, Low-Shuttle-Mass

Fig. 42 Comparison of Shuttle Mass and Flow Rate

steepness of the gradient. An adiabatic magnetization should steepen the gradient from the down-flow profile to the up-flow profile. It would do so by raising the temperature of the warm-end more than the cold-end. As is shown in Chapter 6.5, the net effect of an adiabatic magnetization in the test device with uniform field is to raise the temperature profile fairly uniformly along the core.

Our device cannot begin its flow paths with the proper initial temperature profile. The improper adiabatic paths result in nonisothermal behavior during the flow paths. Whether the nonisothermal behavior significantly hurts the overall performance of our device depends on other cycle parameters.

8.4 Various Flow Examples to demonstrate Cycle Behavior

Figure 42 has four quadrants; each depicting a different type of flow path. Sections 8.4.1 through 8.4.4 discuss cycle behavior when the cycle's flow paths lie in these quadrants. It should be noted that the transition from one quadrant to another is fuzzy, and the descriptions that follow represent cases where the helium shuttle mass is not close to the M_b line. Cycles which have flow paths close to M_b are considered to be almost balanced, and are discussed in section 8.4.5. Carnot-type cycles fit this description.

8.4.1 Low-Flow-Rate, High-Shuttle-Mass:

A low temperature range application may be successful even if it is cycled with severe isothermal imbalances. The advantage to high-shuttle-mass can be seen in this case. The convection wave travels the length of the core during each flow path, all previous temperature information is pushed out the end of the core and lost. The advantage of this is that flow imbalances that exist at the beginning of the flow process need not return when the flow is reversed. Even if the shuttle mass is only marginally high the advantage gained from erasing previous temperature information is still available.

It was found from the computer simulation program that refrigeration cycles were easily controlled when the reservoirs were either 4.2 to 10 K, or 10 to 15 K. The reason for this is that both these ranges allow for high-shuttle-mass flow. As will be seen in later sections, GGG properties may be inappropriate for temperatures above 10 K, yet refrigeration is easily obtained over the 10 to 15 K range.

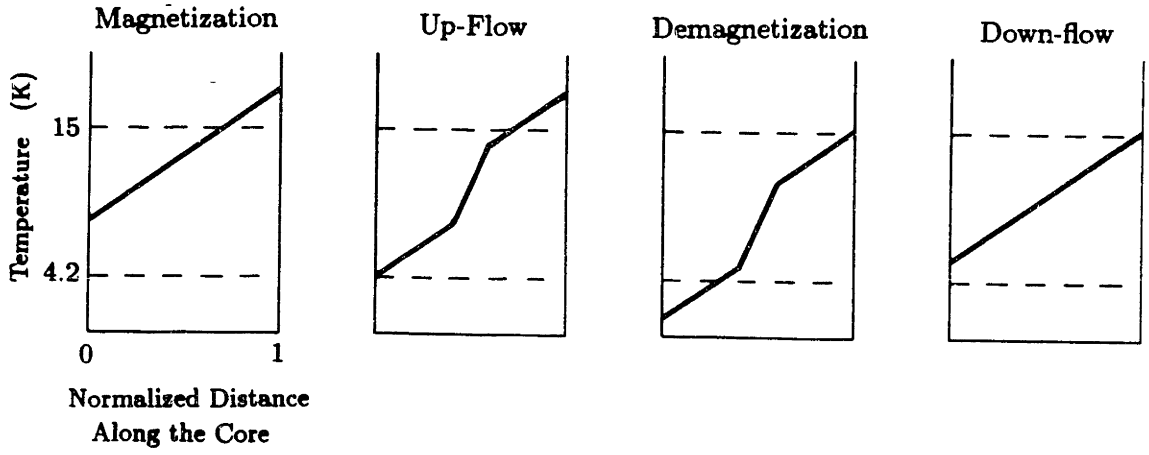

Fig. A

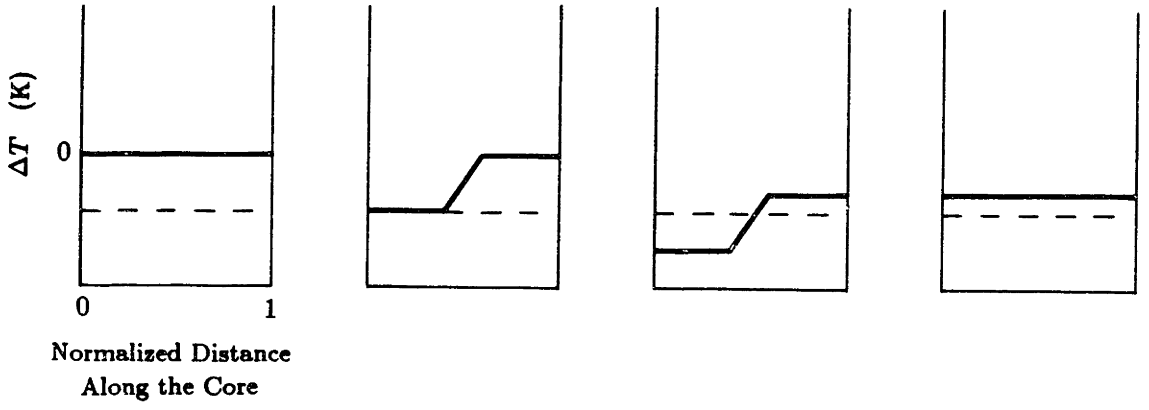

Fig. B

Fig. 43 High-Flow-Rate Example

8.4.2 High-Flow-Rate, Low-Shuttle-Mass:

Figure 43a shows a cycle which is high-flow-rate on both the up and down-flows. By the end of the down-flow, helium leaves the cold-end of the core at a temperature higher than the cold-reservoir temperature. Similarly, extrapolation of the up-flow profile to the warm-end reaches a temperature lower than the warm-reservoir temperature. Figure 43b is created by subtracting the up-flow isothermal profile from all the lines shown in Figure 43a. Note that the remaining temperature profiles behave in a way identical to adiabatic-isofield cycle described in Chapter 7.1. Any excess flow above that required for balanced-flow creates a convection wave which eventu-

ally carries heat from the warm-end to the cold-end. This thermal pollution of the cold-reservoir reduces refrigeration.

8.4.3 High-Flow-Rate, High-Shuttle-Mass:

In the case of high-flow-rate, the shuttle mass is irrelevant. The cycle behavior is the same as that described above. Excess flow is not desirable regardless of whether the cycle is high or low-shuttle-mass.

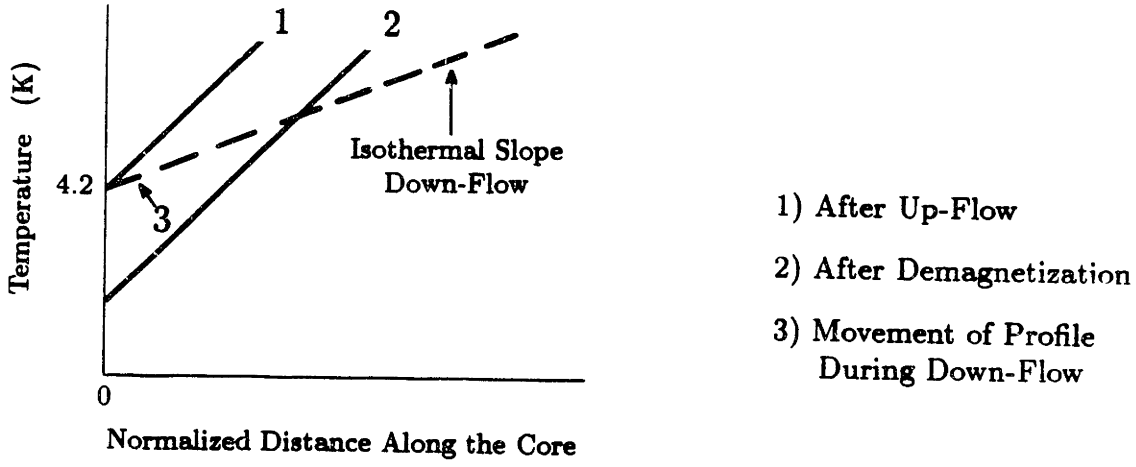

Fig. 44 Low-Flow-Rate Example, Cold-End

8.4.4 Low-Flow-Rate, Low-Shuttle-Mass:

Since a high-flow-rate cycle produces excess warm convection waves which result in thermal pollution of the cold-end, one might suspect that a low-flow-rate cycle would result in a cold convection wave which would not damage the cycle. Unfortunately this is not the case. The low-flow-rate cycle is difficult to describe in that it takes many cycles to reach a steady-state. Figures 44 and 45 are used to aid in the low-flow-rate cycle description. The cold-end of the core is here defined as the section of the core which is traversed by the up-flow convection wave front, the warm-end of the core is the region which is traversed by the down-flow convection wave front, and the middle of the core lies between these two regions.

First look at the cold-end of the core (Figure 44). The up-flow sets up an isothermal profile at the cold-end. Since the flow is low, the profile is steep. The core is then demagnetized. This steep profile is lowered, but its slope is more or less maintained.

As the flow is reversed for the down-flow, the same gradient passes back through the cold-end (plus a little more due to the difference in convection wave velocities). The cold-end receives the same average slope and the same total helium flow on the down-flow as on the up-flow. However, the isothermal gradient is greater on the up-flow, since the average magnetic interaction on the down-flow is less. The resulting isothermal imbalance results in the cold-end temperature rising during the down-flow. This is not necessarily bad since the cold-end temperature need not rise above the cold-reservoir temperature. Since the convection waves move farther on the down-flow, the cold-end will also receive some temperature information which comes from the middle region of the core. Whether this part of the flow will be warm or cold depends on the pre-down-flow temperature of this region.

Now let's look at the warm-end (Figure 45). The down-flow sets up an isothermal profile which is less steep than the up-flow isothermal profile. After adiabatic magnetization, the up-flow occurs with an isothermal imbalance which again causes the warm-end temperature to rise. When the up-flow is over, the warm-end is at its maximum temperature. After the adiabatic demagnetization, the warm-end temperature is greater than the warm-reservoir temperature. The down-flow begins with a warm convection wave superimposed on the down-flow isothermal profile. This warm convection wave is introduced on every cycle. The middle of the core is warmed by this action.

If you follow many cycles, you will find that the cold-end does not see the warm-end temperature, but instead sees a temperature which is several steps warmer. The lower the velocity of the convection wave the warmer the middle of the core becomes. The excess flow on the down-flow pollutes the cold-reservoir.

If you look at just the warm-end, then you find that the flow processes are low-flow-rate; the magnetic terms dominate the convection terms. However, if you look at the cold-end, you find that the temperature gradient becomes steep enough for the convection terms to dominate the magnetic terms. The paradox with a low-flow-rate process is that the cold-end becomes high-flow-rate in the cyclic steady-state.

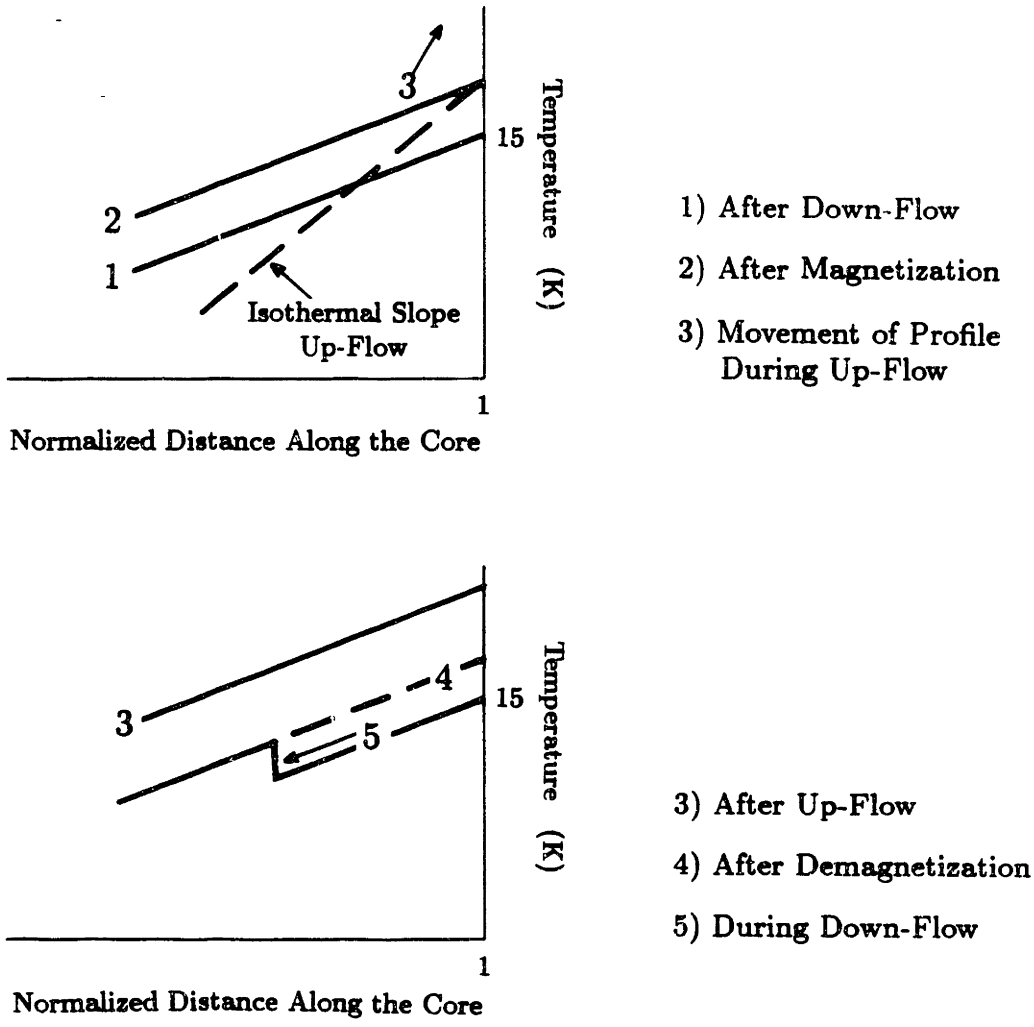

Fig. 45 Low-Flow-Rate Example, Warm-End

8.4.5 Almost Balanced-Flow

The almost balanced-flow cycles are Carnot-type cycles in that isothermal paths are attempted. When the shuttle mass is high, there is no problem in controlling this cycle, but when the shuttle mass is low the cycle becomes quite complicated.

Isothermal paths cannot be obtained by our device; the reasons for this have been presented throughout this thesis. A balanced-flow path will deviate from an isothermal path along (at least) part of the core. In order to describe a balanced-flow path it is useful to employ the convection wave logic presented in Chapter 6.6 and in Appendix F. Using the equations in Appendix F and assuming the inlet temperature of

the core is constant, we can write:

$$T_{new} = s\,x$$

$$T_{old} = s_0\,x + (s - s_0)\,v\,t$$

Where T_{new} is the section of the core upstream of the convection wave front, T_{old} is the section of the core downstream of the convection wave front, s is the isothermal slope for the present core interactions, and s_0 is the slope that existed prior to this set of core interactions. The amount that the downstream end of the core deviates from the final isothermal profile is:

$$T_{old} - T_{new} = (s_0 - s)\,[x - vt]$$

This is the equation of a convection wave moving through a nonactive core, with the size of the convection wave given by the difference of the initial profile, and the isothermal profile. The main points to be learned from this analysis are:

(1) On a first-order analysis, any flow process in the core can be treated as the sum of the isothermal solution plus an isothermal imbalance.

(2) The isothermal imbalance moves through the core in the same way as a convection wave moves though an isofield core.

(3) The distance a convection wave travels for a given amount of helium flow is inversely proportional to the cores specific heat; the convection wave therefore travels farther on the down-flow which occurs at lower fields than on the up-flow which occurs at higher fields.

In a low-shuttle-mass cycle, all isothermal imbalances which remain in the core at the end of the up-flow will eventually come out of the cold-end. Also, all isothermal imbalances which are in the core at the beginning of the up-flow will not make it out of the core, and will eventually come out of the cold-end.

One of the worse sources of isothermal imbalances comes from improper adiabatic paths. An improper adiabatic path causes an isothermal imbalance to form at the beginning of the flow path. Our experimental device is such that the gradient of the temperature profile cannot be adjusted during the adiabatic path. This results

in the profile being too flat for the up-flow and too steep for the down-flow. Both of these result in a rising temperature profile at the downstream end of the core. The net result of this behavior is described in section 8.4.4. A warm isothermal imbalance moves out from the warm-end and pollutes the cold-reservoir at the end of the down-flow.

In the Chapter 10 it is suggested that a perturbation field be added to the main field in our device. The primary purpose of this field is to modify the adiabatic paths so that a larger adiabatic field swing occurs at the warm-end than at the cold-end. By doing this we can set up the proper temperature profiles before the flow paths begin, and thus eliminate the main source of isofield imbalance. It is interesting to note that should the up-flow profile be made too steep, and the down-flow profile be made too flat, the isothermal imbalance will be "cold." A cold isothermal imbalance will travel to the cold-end of the core, but it will not pollute the cold-reservoir. There are some isothermal imbalances which cause no first-order damage to the cycle.

(Irreversibilities introduced into the process by a real core will always be "warm", and will therefore act as warm-perturbations introduced by improper field-flow phasing. Real system irreversibilities are discussed in Chapter 10.)

8.5 Summary

This chapter has explained the results of the computer simulation, and has shown why our device cannot be operated efficiently. We have found from this analysis that:

- It is always the goal to have balanced-flow (or Carnot) cycles. Other schemes using low or high-flow-rate never produce more refrigeration than can be produced by the Carnot-type cycle.
- Deviations from the Carnot cycle will result from improper field-flow phasing.
- The greater the temperature range of the cycle, the more critical it is to have proper field-flow phasing.
- Our device does not have sufficiently proper field-flow phasing, and will not work with a uniform magnetic field.

One way to prevent field-flow imbalances in a low-shuttle-mass cycle is to have greater control over the magnetic field as both a function of position along the core and time. The greater the control of the field, the closer an isothermal process can be approximated. In practice it is not necessary to have perfect field-flow phasing.

The largest isothermal imbalance is introduced to our cycle by improper adiabatic paths caused by the uniform magnetic field and the breathing effect. We have found with the computer simulation program that if two independent fields are used over the core, the warm-end can be given a larger adiabatic swing than the cold-end. This creates better initial temperature profiles for the flow paths. Under this condition the program predicts net refrigeration.

IX. IRREVERSIBILITY ANALYSIS

9.1 Introduction

Up to now this thesis has ignored standard regenerator design considerations. One reason for this is that the core was designed and constructed by Taussig, and his thesis contains this analysis.[10] This thesis has pursued an experimental track which assumed that the core would produce minimal irreversibilities when cycled in the proper way. Unfortunately, the test data have indicated that the core does not meet this requirement. Chapter 11, which discusses test data, shows how the core did not behave as a good regenerator in the conventional sense. In order to help understand the test data, this chapter contains a detailed analysis of standard regenerator design considerations.

The old core model used in the computer simulation program did not accurately depict our core, especially when used at temperatures above ~12 K. Section 9.2 describes a new core model which allows for more accurate correlation between the computer simulation program and some basic test runs.

Sections 9.3 through 9.6 present analyses of the following irreversibility sources:

10.3: Convective heat transfer and finite number of segments;
10.4: Maladjusted flow;
10.5: Axial conduction;
10.6: Partially insulated helium void.

(Pressure-drop-induced losses are not discussed because Taussig predicted these losses to be minimal.[10])

Section 9.7 analyzes how these irreversibility sources may effect our core, and compares their relative importance.

When is a First-Order Analysis Useful?

Throughout this chapter, first-order analysis is used to discuss irreversibilities present within the core. In a first-order analysis some parameters (such as specific heat and density) are assumed constant during the process being analyzed. A first-order anal-

ysis allows us to compute solutions directly without resorting to computer simulation. Often more insight to the dependence of various parameters is gained from first-order analysis than can be gained from computer simulation.

A first-order analysis is useful in determining the general behavior of the core's temperature profile over a single cycle, provided that we know the initial temperature profile. However, a first-order analysis is not useful in determining the cyclic steady-state solution for a given set of operating parameters. The reason for this is that the differences between the real solution and the first-order solution may accumulate over time. The initial temperature profile for the n^{th} cycle cannot be determined by a first-order analysis; steady-state refrigeration can only be computed by high order analysis such as by computer simulation.

9.2 A New Model For the Core

In all previous computer simulations it was assumed the the core could be modeled as containing 95% GGG and 5% helium void by volume.[12] Upon closer inspection it has been determined that the silicon rubber used as an encapsulant can add significantly to the core's zero-field specific heat. It is also suspected that helium voids may form between the rubber and the inside wall of the stainless steel tube which contains the core. The core model used in the computer simulation program was modified to include these two effects. Figure 46 shows the core's cross section with the helium gap and silicon rubber dimensions somewhat exaggerated. The internal diameter of the stainless tube which contains the core is 3.886 cm (1.530 inch). The total cross sectional area of the core is 11.86 cm^2. Within this area 71.4% is GGG. If there is no helium gap, g, on the outside edge of the core, then 3.3% of the core is helium and 25.3% is rubber. As the outside gap increases, the percent helium increases, and the percent rubber decreases. The helium porosity is defined as the percent helium divided by the percent of GGG and helium; this value is a minimum of 4.4%. With g expressed in cm:

$$x_{he} = 0.033 + \frac{\pi\,(3.866 - g/2)\,g}{11.86}$$

$$x_r = 0.253 - \frac{\pi\,(3.866 - g/2)\,g}{11.86}$$

$$x_g = 0.714$$

$$por = x_{he}/(x_g + x_{he})$$

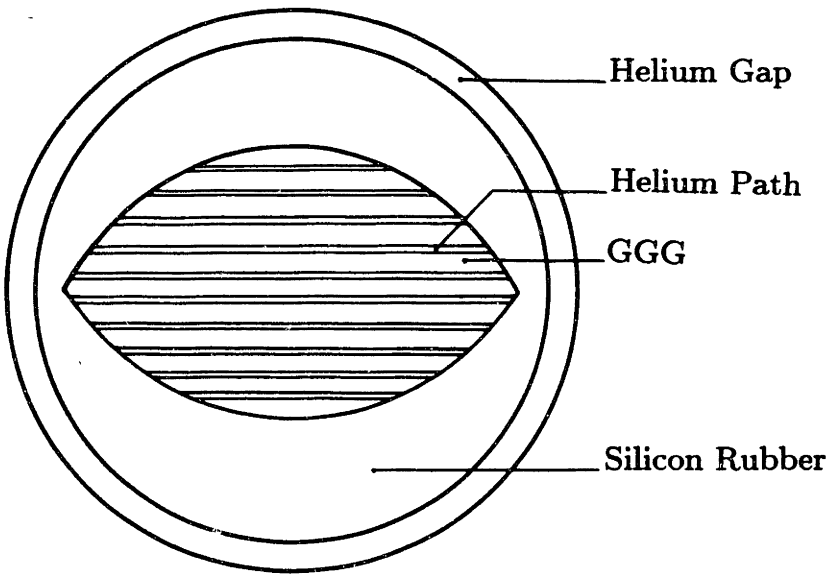

Fig. 46 Schematic of Core's Cross Section

For example, if there is a helium gap of 0.05 cm, then the helium fraction becomes:

$$x_{he} = 0.033 + \frac{\pi\,(3.886 - 0.025)\,0.05}{11.86} = 0.084$$

which translates to a helium porosity of:

$$por = 0.084/(0.714 + 0.084) = 10.5\%\,.$$

The specific heat per unit length of the core was defined in Chapter 6.1 . In this definition the specific heat of the rubber was not included. A more accurate expression of the specific heat is:

$$C = [x_{he}\rho_{he}\,c_p + x_g\rho_g\,c_H + x_r\rho_r\,c_r]\,A$$

The enthalpy for silicon rubber was found for several temperatures between 4.2 and 20 K.[13] It was found that a quadratic polynomial could fit this data satisfactorily. The equation used, with T in K, is:

$$H_r = 4.4\,T^2 - 62\,T + 250 \qquad \mathrm{mJ\,g^{-1}}$$

for $T > 7.0$ K, and $H_r \simeq 0$ for $T < 7.0$ K . The enthalpy of rubber is only significant when the temperature is greater than ~10 K. The density of the silicon rubber was

measured to be only slightly greater than that of water. A density of 1 ($g\,cm^{-3}$) is used.

9.3 Convective heat transfer ΔT and Finite Number of Segments

The convective heat transfer ΔT and finite number of segments must be discussed together since their effects on irreversibility are interrelated. As will be shown in the following analysis, the greater the convective heat transfer coefficient, the more segments it takes to have negligible loss due to a finite number of segments.

In order to study this problem we will analyze an isothermal process where the helium temperature entering and leaving the core is prescribed. Figure 47 is used to aid in the understanding of this analysis. The solid lines in Figure 47 represent a core that contains only one segment. Because of the high thermal conductivity of GGG that is comparable with that of copper, we can assume that the GGG is at a uniform temperature, T_g. The helium enters the core at T_{in} and leaves at T_{out}. One first-order assumption is that the helium has constant specific heat with temperature.

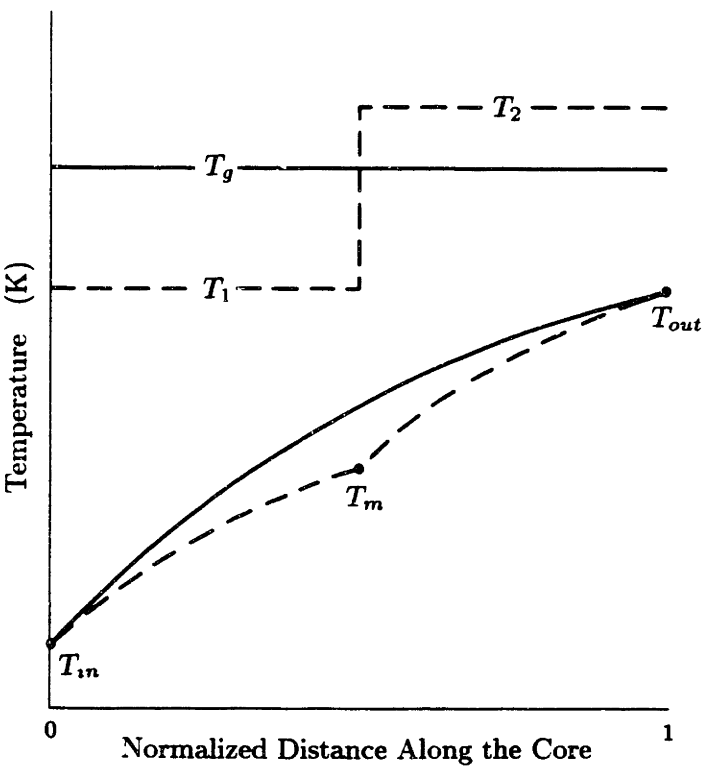

Fig. 47 Finite Number of Segments and Finite Convective Heat Transfer Model

A simple convective model is used to determine the heat transfer between the helium and GGG. This model leads to the following equation:

$$\dot{m}\, c_p \frac{dT}{dx} = \hbar P (T - T_g)$$

where $\hbar$ is the convective heat transfer coefficient, P the total perimeter of the flow channel, L the length of the segment, and $T(x)$ the temperature of the helium averaged over the segment cross section. One can solve this equation to find the helium outlet temperature as:

$$T_{out} = T_g - (T_g - T_{in})\, e^{-\beta L}$$

where

$$\beta \equiv \frac{\hbar\, P}{\dot{m}\, c_p}$$

Since we choose the inlet and outlet temperatures as our independent variables, we rewrite the above equation as:

$$T_g = \frac{T_{out} - T_{in}}{1 - e^{-\beta L}} + T_{in}$$

Defining $(T_g - T_{in})$ as T'_g, and $(T_{out} - T_{in})$ as T'_{out}, we can write:

$$T'_g = \frac{T'_{out}}{1 - e^{-\beta L}}$$

(In this analysis a prime means that the temperature is relative to T_{in}.)

The next step is to divide the single segment into two segments of equal length $L/2$, each with uniform GGG temperature. The helium inlet and outlet temperatures are to remain the same. The dashed lines in Figure 47 represent this case. Using the same convective heat transfer model we can write:

$$T_m = T_1 - (T_1 - T_{in})\, e^{-\beta L/2}$$

$$T_{out} = T_2 - (T_2 - T_m)\, e^{-\beta L/2}$$

where T_1 and T_2 are the GGG temperatures of the two segments. The above relations can be made relative to T_{in}:

$$(T_m - T_{in}) = (T_1 - T_{in}) - (T_1 - T_{in})\, e^{-\beta L/2}$$

$$T'_m = T'_1 (1 - e^{-\beta L/2})$$

$$(T_{out} - T_{in}) = (T_2 - T_{in}) - ((T_2 - T_{in}) - (T_m - T_{in}))\, e^{-\beta L/2}$$

$$T'_{out} = T'_2 - (T'_2 - T'_m)\, e^{-\beta L/2}$$

By going from one to two segments an additional unknown variable, T'_m, is introduced. This is the intermediate helium temperature between the two segments. Because of this, one more equation is needed in order to solve for unique solutions of T'_2 and T'_1. This equation should be chosen so as to represent the thermodynamic path that is being modeled. For this first-order analysis, the specific heat of the helium is assumed constant, and the magnetic interaction per change in field is assumed constant over the core (not a strong function of temperature). Since each segment should experience the same $\delta Q_g = T dS_g$, and the heat out of the GGG is equal to the heat into the helium, the helium should experience the same change in temperature for each segment it passes through. This condition can be stated mathematically in several ways. One expression is that T_m is the average of T_{in} and T_{out}.

$$T'_m = \frac{T'_{out}}{2}$$

With this additional equation, the GGG segment temperatures can be solved:

$$T'_1 = \frac{T'_{out}}{2} \frac{1}{1 - e^{-\beta L/2}}$$

$$T'_2 - T'_1 = \frac{T'_{out}}{2}$$

We can look at this analysis recursively and continue to divide the core into more and more segments. With proper book-keeping of the recursive substitutions, we find for N segments with i from 1 to N that:

$$T_i = T_{in} + \frac{T'_{out}}{N} \left[\frac{1}{1 - e^{-\beta L/N}} + (i - 1) \right]$$

In the limit where $N \to \infty$ we can solve for the linear profile temperature difference between the helium and GGG. Since

$$e^x = 1 + x + \frac{x^2}{2} + ...$$

then

$$N\left(1 - e^{-\beta L/N}\right) \simeq N\left(\beta L/N\right) = \beta L \qquad \text{(for large } N\text{)}$$

We find that

$$T'_1 = \frac{T'_{out}}{\beta L}$$

This is the same result as would have been found if we solved the linear temperature case with a continuous profile. Now that the temperature profile for the GGG is determined, we can calculate the entropy generated by the process. The entropy rate into the helium is simply:

$$\dot{S}_{he} = \dot{m}\, c_p \ln\left(\frac{T_{out}}{T_{in}}\right)$$

While the entropy out of each GGG segment is:

$$\dot{S}_i = \frac{\dot{m}\, c_p (T_{(i+1)} - T_i)}{T_i} = \frac{\dot{m}\, c_p \frac{T'_{out}}{N}}{T_i}$$

Substituting T_i from above we get:

$$\dot{S}_i = \frac{\dot{m}\, c_p \frac{T'_{out}}{N}}{T_{in} + \frac{T'_{out}}{N}\left[\frac{1}{1-e^{-\beta L/N}} + (i-1)\right]}$$

The entropy generated is the difference of the entropy into the helium, $\dot{S}_{he}$, and the sum of all $\dot{S}_i$.

$$\frac{\dot{S}_{gen}}{\dot{m}\, c_p} = \ln\left(\frac{T_{out}}{T_{in}}\right) - \frac{T'_{out}}{N}\sum_{n=1}^{N}\left[\frac{1}{T_{in} + \frac{T'_{out}}{N}\left[\frac{1}{1-e^{-\beta L/N}} + (i-1)\right]}\right]$$

One can see that this expression can be written in terms of the ratio of:

$$\frac{T'_{out}}{T_{in}} = \frac{T_{out}}{T_{in}} - 1 \equiv \Delta T_r$$

$$\frac{\dot{S}_{gen}}{\dot{m}\, c_p} = \ln(1+\Delta T_r) - \frac{\Delta T_r}{N}\sum_{i=1}^{N}\left[\frac{1}{1 + \frac{\Delta T_r}{N}\left[\frac{1}{1-e^{-\beta L/N}} + (i-1)\right]}\right] \tag{10}$$

In the limit where $N \to \infty$, the above summation can be translated to an integral and the equation becomes:

$$\begin{aligned}
\frac{\dot{S}_{gen}}{\dot{m}\, c_p} &= \ln(1+\Delta T_r) - \frac{\Delta T_r}{L}\int_0^L \left(1 + \frac{\Delta T_r}{\beta L} + \frac{\Delta T_r}{L}\, x\right)^{-1} dx \\
&= \ln(1+\Delta T_r) - \ln\left(1 + \frac{\Delta T_r}{\beta L} + \frac{\Delta T_r}{L}\, x\right)\Big|_0^L \\
&= \ln(1+\Delta T_r) + \ln\left(1 + \frac{\Delta T_r}{\beta L}\right) - \ln\left(1 + \Delta T_r + \frac{\Delta T_r}{\beta L}\right)
\end{aligned} \tag{11}$$

The irreversibility which results from the convective heat transfer ΔT is given by Equation (11). This equation is plotted in Figure 48 as a function of βL with the parameter ΔT_r varying from 0.4 to 2.0 . As βL increases, the losses decrease. As ΔT_r increases, the losses increase. The graph has been normalized by the flow quantity $\dot{m}\, c_p$.

Figure 49 shows the result of subtracting Equation (11) from Equation (10). The resulting equation is plotted as a function of the number of segments, with the parameter βL varying from 4 to 100, when $\Delta T_r = 2$. This graph represents the normalized irreversibility which results from having a finite number of segments. As βL increases, this loss also increases. The better the heat transfer, the more segments it takes to realize the benefit of the good heat transfer. All lines reach $\sim$0 by a segment number of $\sim$60. Our core has 120 segments.

9.4 Maladjusted Flow

Another possible source of flow-related loss is maladjusted flow. The helium passes passes the core through many parallel slits, each 0.1 mm wide. If we look at the relation for fully developed laminar flow in a slit,

$$\frac{Q}{w} = -\frac{5\,t^3}{12\,\mu}\left(\frac{dP}{dx}\right)$$

we find that for the same driving pressure gradient, the mass flow goes as the width of the slit, t, cubed. It is reasonable to assume that each slit in the core is not exactly the same thickness, and therefore does not pass the same amount of helium during a flow process. If we assume that the slits may vary by $\pm 10\%$ in thickness, we can expect the flow to differ up to a factor of $(1.1/.9)^3 \simeq 2$ among slits.

To analyze how maladjusted flow may effect the process, we first must consider the thermal resistances along the core's cross section. GGG has a thermal conductivity which varies from 1.4 $\mathrm{W\,cm^{-1}\,K^{-1}}$ at 4.2 K, to 6.9 $\mathrm{W\,cm^{-1}\,K^{-1}}$ at 15 K.[12,14] The helium's conductivity is only $\sim$ 0.2 mW $\mathrm{cm^{-1}\ K^{-1}}$. It can be seen from the core's geometry (Figure 46) that the GGG offers negligible resistance to heat flow in the core. All temperature gradients in the direction normal to the flow direction must be maintained across the helium gaps.

If there is maladjusted flow, then a temperature gradient will develop along the core's

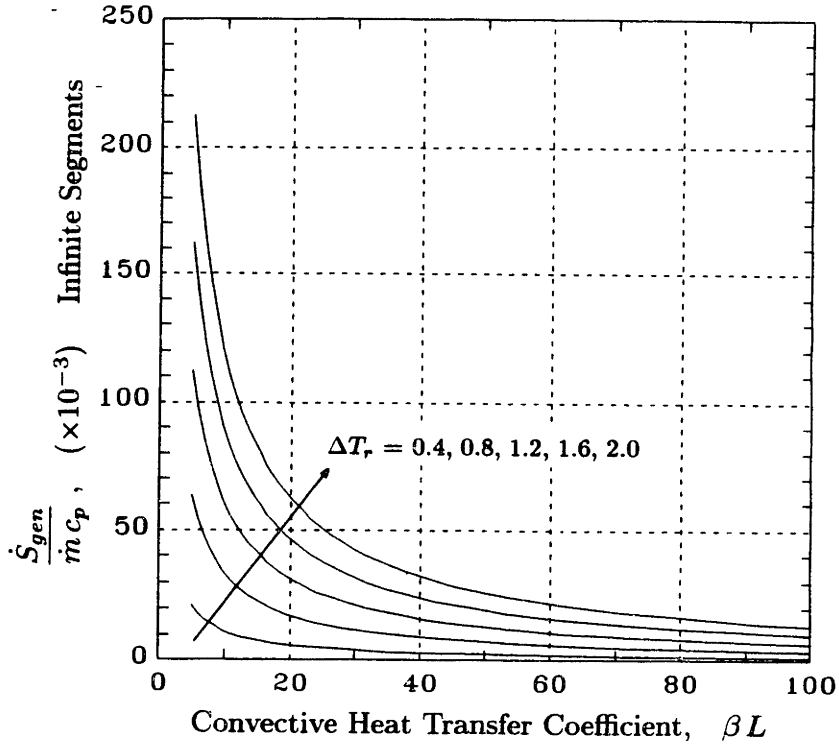

Fig. 48 Losses due to a Finite Convective Heat Transfer Coefficient

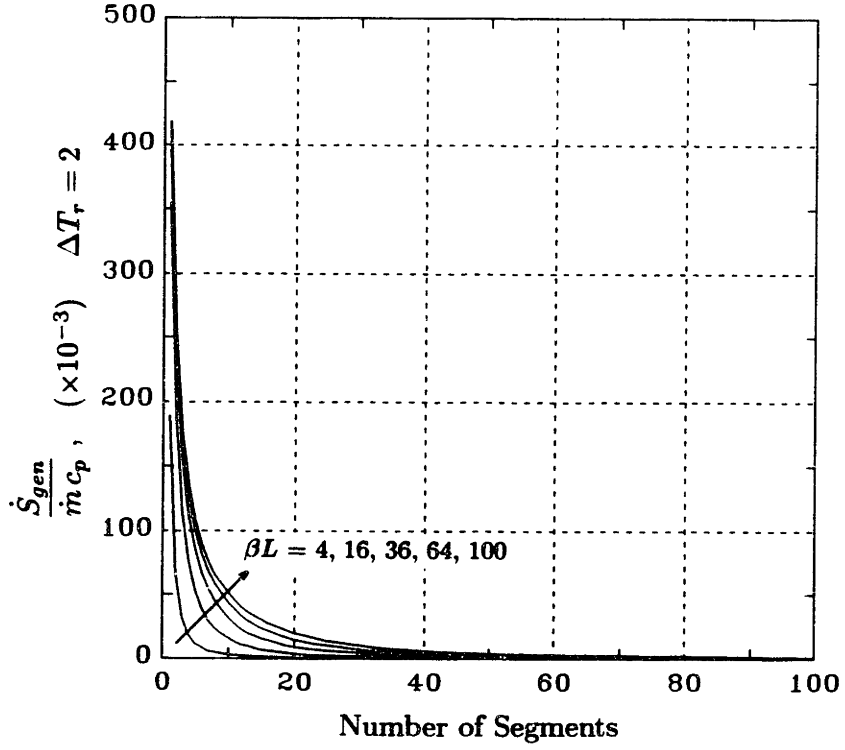

Fig. 49 Losses due to a Finite Number of Segments

cross section. The first step in this analysis is to determine if the heat conducted across the helium gaps is significant compared to the heat transported by convection down the core. For the convection term to dominate:

$$\dot{m}\, c_p \frac{\partial T}{\partial x}\, dx \gg K_y\, D \frac{\partial T}{\partial y}\, dx$$

K_y is the effective conductivity in the radial direction crossing the helium gaps, and is averaged from the step-wise properties of the core. Since the conductivity of the GGG is much larger than that of the helium:

$$K_y = \frac{t_g}{t_{he}} K_{he} = 25.4\, K_{he} \simeq 5 \quad (\mathrm{mW\,cm^{-1}\,K^{-1}})$$

On an order of magnitude basis $dx \rightarrow L$, and $dy \rightarrow D$ so:

$$\dot{m}\, c_p \frac{\Delta T}{L} \gg K_y\, D \frac{\Delta T}{D}$$

which yields:

$$\dot{m} \gg \frac{K_y\, L}{c_p} \sim \frac{(0.005)\, 7.5}{5.5} \sim 0.007 \quad (\mathrm{g\,s^{-1}})$$

The flow processes used in our device employs an $\dot{m}$ of $\sim$0.5 (g/s). Conduction across the helium gaps can be ignored for this analysis.

The model used to study the entropy generated by maladjusted flow assumes a fully developed temperature profile, and no conduction in the radial direction. In an isolated channel, the steady-state temperature profile is determined by the helium flow rate in the channel and the rate of magnetic interaction, $\dot{Q}$. Figure 50 is used to aid in the understanding of this analysis. Three steady-state temperature profiles are shown. The temperature at the end of each of these profiles is given by:

$$T_0 = \frac{\dot{Q}L}{\dot{m}_0 c_p} + T_{in}$$

$$T_1 = \frac{\dot{Q}L}{2\,\dot{m}_1 c_p} + T_{in}$$

$$T_2 = \frac{\dot{Q}L}{2\,\dot{m}_2 c_p} + T_{in}$$

In this example stream 0 uses the whole core with helium flow $\dot{m}_0$ uniformly distributed over the core's cross section, and stream 1 and 2 each use half the core with

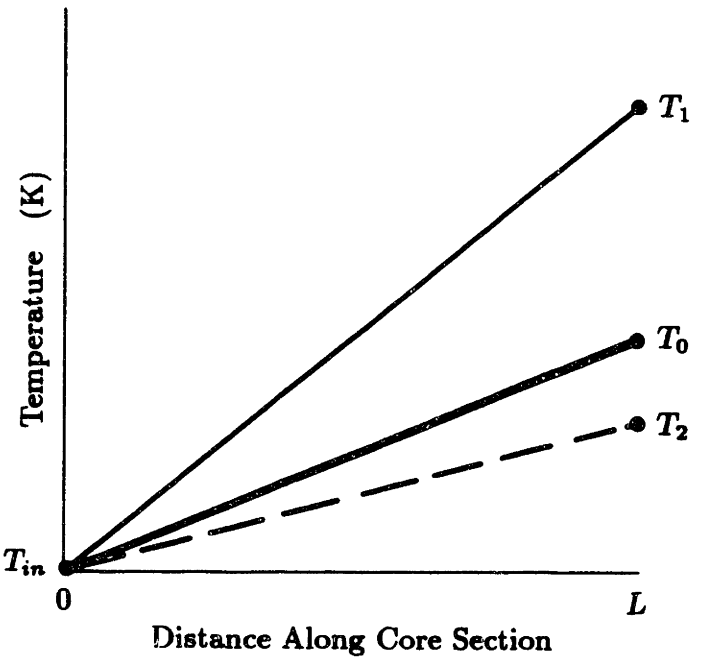

Fig. 50 Maladjusted Flow Model

helium flow of $\dot{m}_1$ and $\dot{m}_2$ uniformly distributed over their respective half core. $\dot{Q}L$ is the total heat into the core by magnetic interaction and is assumed constant for this first order analysis. We can define:

$$T_0 - T_{in} = \frac{\dot{Q}L}{\dot{m}_0 c_p} \equiv \Delta T_0$$

as the temperature range achieved by balanced flow, and

$$\dot{m}_1 = f\,\dot{m}_0$$
$$\dot{m}_2 = (1-f)\,\dot{m}_o$$

where f varies from 0 to 1. With $f = 1$, all the flow goes through channel 1 and none through channel 2, and with $f = 0$ the situation is reversed. When $f = 0.5$, $m_1 = m_2 = m_0/2$, and the flow is balanced. When the two streams reach the end of the core section, they mix. It turns out that the helium temperature range achieved by the balanced flow is the same as that achieved by the maladjusted flow after it has mixed. The reason for this is evident from First-Law considerations.

With these definitions the temperature expressions can be written as:

$$T_0 = \Delta T_0 + T_{in}$$
$$T_1 = \frac{\Delta T_0}{2f} + T_{in}$$
$$T_2 = \frac{\Delta T_0}{2(1-f)} + T_{in}$$

With these temperatures we can now calculate the entropy of mixing which occurs as a result of having maladjusted flow:

$$\dot{S}_{out} = \dot{m}_1 c_p \ln(T_1) + \dot{m}_2 c_p \ln(T_2)$$

$$\dot{S}_{mix} = \dot{m}_0 c_p \ln(T_0)$$

And after a little algebra:

$$\frac{\dot{S}_{gen}}{\dot{m}_0\, c_p} = \frac{\dot{S}_{mix} - \dot{S}_{out}}{\dot{m}_0\, c_p}$$
$$= \ln\left(\frac{\Delta T_0}{T_{in}} + 1\right) - f\,\ln\left(\frac{\Delta T_0}{2f\,T_{in}} + 1\right) - (1-f)\ln\left(\frac{\Delta T_0}{2(1-f)\,T_{in}} + 1\right)$$

As in the previous section we can define the ratio of $\Delta T_0/T_{in}$ as ΔT_r, and rewrite the above equation as:

$$\frac{\dot{S}_{gen}}{\dot{m}_0\, c_p} = \ln(\Delta T_r + 1) - f\,\ln\left(\frac{\Delta T_r}{(2f)} + 1\right) - (1-f)\ln\left(\frac{\Delta T_r}{(2-2f)} + 1\right) \qquad (12)$$

Equation (12) is plotted in Figure 51 as a function of f, with the parameter ΔT_r varying from 0.2 to 1.0. As ΔT_r increases, the losses increase. Our core has four sections, each experiencing a ~3 K temperature range.

The extra entropy generated by the maladjusted process does not appear in the helium stream, but instead remains in the GGG at the end of the process. As can be seen from Figure 50, the average temperature of the GGG is greater for the maladjusted case. This entropy difference can be calculated and has been shown to be of the same order of magnitude as the entropy of mixing from Equation (12). This method assumes that the GGG specific heat is constant with temperature. The method used to derive Equation (12) assumes that the magnetic interaction is

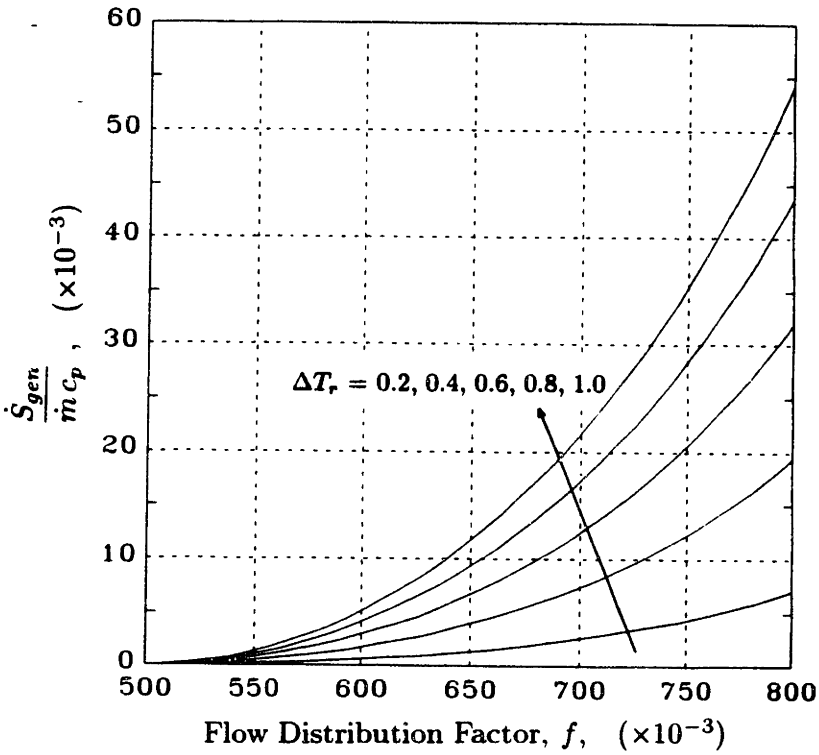

Fig. 51 Losses due to Maladjusted Flow

constant with temperature. The difference between these two methods is due to the basic thermodynamic first-order assumptions used in each. These assumptions are thermodynamically inconsistent.

9.5 Axial Conduction

The axial conduction in our device was calculated by Gallagher.[12] He predicted that 0.04 W would leak into the cold-end reservoir when the core is used over the temperature range of 4.2 to 10 K. When we decided to increase the warm-end reservoir's temperature to 15 K, we nearly doubled the temperature gradient, and more than doubled (conductivity increases with temperature) the amount of heat leak due to axial conduction. Extrapolating Gallagher's analysis, it is reasonable to expect a new value of ~0.1 W when the temperature range is from 4 to 15 K.

The entropy generated by axial conduction goes as $1/T$. If 0.1 W leaks to the 4.2 K reservoir, then $\dot{S}_{gen} = 0.1/4.2 = 24\ \mathrm{mW\,K^{-1}}$.

An isolated core section reaching thermal equilibrium.

It was determined from test data (Chapter 11) that our core has excessively high thermal conductivity. For this reason it is useful to explore a core which has larger than predicted axial conductivity between segments, but is still insulated between core sections by the helium mixing chambers. (Our core has 4 sections, each of 30 segments separated by a mixing chamber.) It is important to realize that increasing the conductivity between the GGG segments in just one of the core sections does not significantly change the amount of heat that conducts from the warm-end to the cold-end of the core. The main negative effect of axial conductivity is to reduce the effective number of segments in the core. A section with large axial conductivity acts as a single segment.

With no helium flow and no magnetic interaction (isofield), the heat equation can be written as:

$$K_x A \frac{\partial^2 T}{\partial x^2} = C\, A \frac{\partial T}{\partial t}$$

where K_x is the effective conductivity in the axial direction, and the specific heat C in this example is defined in Chapter 6.1 as the total core specific heat per unit length. This equation can be solved by separation of variables to yield:

$$T = \sum_n e^{-t/\alpha_n} \left[\; A_n \sin\left(\sqrt{\frac{C}{\alpha_n K_x}}\, x\right) + B_n \cos\left(\sqrt{\frac{C}{\alpha_n K_x}}\, x\right) \; \right]$$

There are three unknown constants in this equation. Two boundary conditions and one initial condition are required. Since the core section is isolated, there is heat flow at neither end. With x defined as zero at one end and L at the other end, the boundary conditions yield:

$$A_n = 0$$

and

$$\alpha_n = \frac{C\, L^2}{K_x\, n^2\, \pi^2}$$

The constants B_n can be determined via Fourier techniques applied to an initial condition. We are interested in how long it takes a linear profile to decay into a flat profile. Because of the $1/n^2$ dependence on α, only the $n = 1$ term in the Fourier series needs to be considered. The first term of a Fourier linear profile can be written

as:

$$B_1 = \frac{4}{\pi^2}\Delta T_0$$

As the profile decays:

$$\Delta T \simeq 2\, B_1\, e^{-t/\alpha_1} = \frac{8}{\pi^2}\, \Delta T_0\, e^{-t/\alpha_1}$$

or:

$$\frac{\Delta T}{\Delta T_0} \sim e^{-t/\alpha_1}$$

where

$$\alpha_1 = \frac{C\, L^2}{K\, \pi^2}$$

From the test data it is noticed that the temperature profile seems to flatten on the order of 1 second. This implies that $\alpha_1 \sim 1$ s s. Typical values for the specific heat C are 0.1 ($\mathrm{J\,cm^{-1}\,K^{-1}}$), and the length of one core section is $L = 7.5$ cm. The effective conductivity can be calculated to be $\sim$500 $\mathrm{mW\,cm^{-1}\,K^{-1}}$. If the core were working properly, K_x would be governed by the epoxy junctions, and would have a value of:

$$K_x = \frac{t_g}{t_{epoxy}}\, K_{epoxy} \sim 25 \quad (\mathrm{mW\,cm^{-1}\,K^{-1}})$$

This value of axial conductivity, determined approximately from full system test data, is $\sim$20 times higher than the expected value.

9.6 Partially insulated helium void

If the helium void is in full thermal contact with the GGG, then entropy need not be generated directly by heat transfer between the GGG and the helium in the void. (Although excess void will increase the zero field specific heat, and induce the breathing effect, both of which may prohibit successful operation of the device.) If the helium void is well insulated from the GGG, then the device could cycle without heat transfer to the void, and again entropy need not be generated. The worst void is one which is partially insulated from the GGG, as it results in nonequilibrium heat transfer. As will be discussed in Chapter 11.2, our core contains excess helium void, much of which may be partially insulated. (It is important to remember that helium void is only significant during non-isothermal paths. When a path is isothermal, the specific heat of the core is irrelevant, and helium flow is not induced by the breathing effect.)

The entropy generated by partially insulated helium void is path dependent. In order to estimate the magnitude of this loss in our core, we must first specify the non-isothermal path which we expect to encounter. The case modeled here is described by first magnetizing the GGG in thermal equilibrium with only that part of the helium which is entrained within the flow channels, and then allowing it to reach thermal equilibrium with the partially insulated helium void (in the gap) at constant field. Entropy is generated in the segment only during the constant field relaxation.

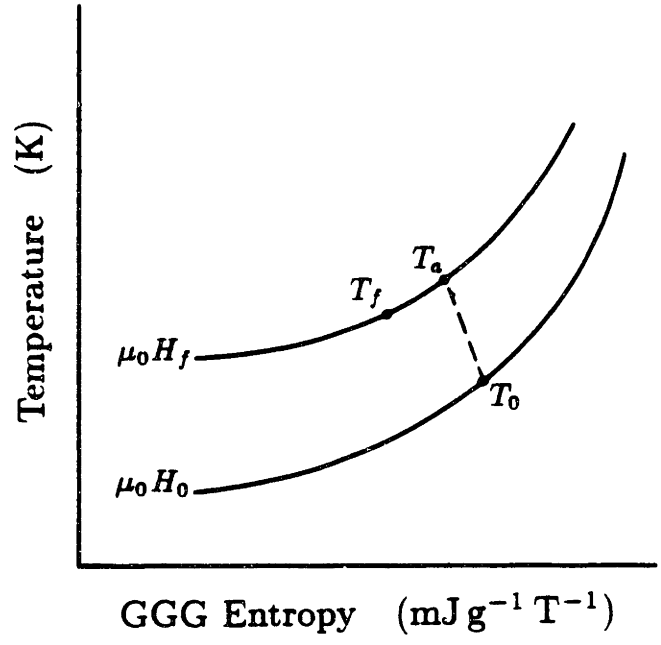

Fig. 52 Partially Insulated Void Model

Figure 52 is used to aid this analysis. Plotted are two isofield entropy curves for GGG. The initial magnetic field is H_0, and the final magnetic field after magnetization is H_f. T_0 is the initial temperature of the entire core section, T_a is the temperature of the GGG (and participating helium) after an "adiabatic" magnetization, and T_f is the temperature after thermal relaxation. T_a is determined by using the computer simulation program for an "adiabatic" magnetization path (graphs of "adiabatic" magnetizations are presented in Chapter 11.2.1), and T_f is determined by a First-Law heat balance of the segment. Unfortunately, the breathing effect complicates

this heat balance. As the partially insulated void is heated from T_0 to T_f, the entrained helium expands and part of it is expelled. As the helium entrained in the flow passages is cooled from T_a to T_f, it contracts and helium is pulled into the segment. The assumptions which relate to where the expelled helium goes, and from where the deficit helium comes, influence the heat balance equation. Figure 53 shows a schematic of the assumptions used to model the breathing effect for this analysis. All the helium leaving the gap, V_1 (volume 1), passes through the flow passages, V_2 (volume 2). It is assumed that:

1. dm_1 leaves volume V_1 at temperature T_1,
2. dm_2 leaves volume V_2 at temperature T_2,
3. and the helium pressure is constant.

With these assumptions the First-Law equation for helium volume V_1 can be written as:

$$\rho_1 V_1 \, d(h_1) = \delta Q$$

Similarly the First-Law equation for the GGG and helium volume V_2 is:

$$\rho_g V_g \, T_2 dS_g + \rho_2 V_2 d(h_2) = -\delta Q - (h_2 - h_1) \, dm_1$$

where

$$dm_1 = -V_1 d\rho_1$$

These equations are not valid if either dm_1 or dm_2 is negative. For this reason we will only examine magnetization process. During a magnetization process dm_1 is always positive with this model, and dm_2 is positive for most cases. These equations cannot be integrated directly, they are solved by step-wise computer simulation until $T_1 = T_2 = T_f$.

The entropy generated by this process can be calculated from the appropriate Second-Law equation:

$$\rho_g V_g \, dS_g + V_1 \, d(\rho_1 s_1) + V_2 \, d(\rho_2 s_2) = dS_{gen} - s_2 dm_2$$

where the control volume in this case is drawn around the entire segment including both V_1 and V_2. Integrating this equation and rearranging we get:

$$\Delta S_{gen} = \rho_g V_g \, \Delta S_g + V_1 \, \Delta(\rho_1 s_1) + V_2 \, \Delta(\rho_2 s_2) + \int s_2 \, dm_2$$

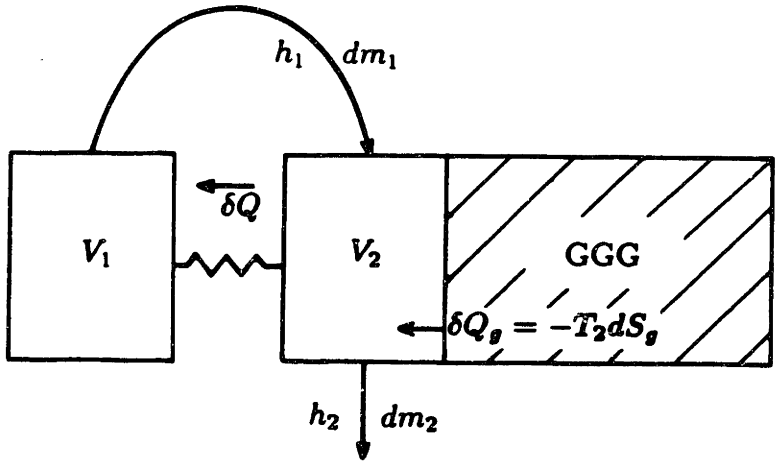

Fig. 53 Schematic of Partially Insulated Void Model

Again the breathing term requires that this equation be solved by step-wise computer simulation. The computer program which does this analysis, "VOID.FOR," is contained in Appendix H. S_{gen} has been calculated for several different cases which apply to the intended operating parameters of our device. Table 9 presents values of S_{gen} where $\mu_0 H_0 = 1$ T, $\mu_0 H_f = 2$ T, the gap is 0.5 mm (20 mils) wide, the helium pressure is 4 atm, and T_0 is varied from 4.2 to 15 K. The core geometry factors are taken from Section 9.2. The values in this table are per unit volume of the core.

TABLE 9
Entropy Generated by Partially Insulated Void

T_0 (K)	T_a (K)	T_f (K)	ΔS_{gen} (mJ cm^{-3} K^{-1})
4.2	6.41	5.69	5.53
6	8.74	7.14	1.04
10	13.22	12.64	0.29
15	16.93	16.74	0.07

Note that the irreversibility due to partially insulated void is greatest when the segment's temperature is below the helium's critical temperature.

9.7 Relating the various sources of irreversibility to the cycle performance.

A regenerator core can be treated as an entropy pump; the net effect of a refrigeration cycle is to transport entropy from the cold-end to the warm-end of the core. In a perfect device the net entropy flow at any core location is the same, while the net enthalpy flow increases towards the warm-end of the core. The refrigeration goal of our device is to produce ~0.5 W of refrigeration at 4.2 K. This corresponds to a base entropy flow of 120 mW K^{-1} throughout the core. As entropy is generated by various irreversibilities, the excess entropy must also be pumped out of the core's warm-end. Each segment in the core must pump the base entropy, plus all the entropy generated from the cold-end to that segments location. As was seen in Chapter 4, there is a maximum amount of entropy that can be pumped by any segment (that maximum is obtained by an adiabatic percent of ~50). If more entropy is generated than can be pumped by the warm-end of the core, even with use of a perturbation field, the entropy flow is blocked and refrigeration cannot be produced.

In Sections 9.3 to 9.6 various sources of entropy are discussed on a first-order basis. Some of these losses were normalized to appropriate cycle parameters. In order to predict whether the entropy generated in our device is severe enough to block the base entropy flow, and therefore to prevent refrigeration, these losses must be applied to the operation parameters of our device. It should be noted that this analysis can only yield a rough estimate of various irreversibilities on the net cycle performance, and that a higher-order analysis (computer simulation) is necessary for greater accuracy. The main value of this analysis is to roughly compare the severity of each source of irreversibility, and thereby to aid in future core design considerations.

The expected values of pertinent cycle parameters are:

Helium Flow Rate:	$\dot{m} \simeq 0.5$ g/s
Warm Reservoir Temp:	$T_w = 15$ K
Cold Reservoir Temp:	$T_c = 4.2$ K
Flow Channel Perimeter:	$P = 69$ cm
Flow Channel Thickness:	$t = 0.01$ cm
Convective Coefficient:	$\hbar = \frac{7.6\,K_{he}}{t}$

$$\beta \equiv \frac{\hbar P}{\dot{m}\,c_p} = \frac{7.6\,P}{\dot{m}\,t}\,\frac{K_{he}}{c_p} \simeq 1 \times 10^5\,\frac{K_{he}}{c_p} \qquad \text{cm}^{-1}$$

To find the range of values that can be expected for β, we need only to find the maximum and minimum value for K_{he}/c_p. Using helium properties at 3 atm and in the temperature range of 2.5 to 20 K, the maximum is found at 2.5 K and is 9.1×10^{-5} $\mathrm{g\,s^{-1}\,K^{-1}}$, and the minimum is found at 5.6 K and is 7.2×10^{-6} $\mathrm{g\,s^{-1}\,K^{-1}}$. The lower value is characteristic only around the critical point, most of the range has a ratio more similar to the larger value. For this analysis we will assume that $\beta \simeq 5$ $\mathrm{cm^{-1}}$.

The value used for c_p is the average value over the temperature range of interest. $\bar{c}_p = \Delta h/\Delta T \simeq 6$ $\mathrm{J\,g^{-1}\,K^{-1}}$.

$\underline{\beta L < \infty}$: Equation (11) can be solved with $L = 30$ cm, $\beta L = 150$, and $\Delta T_r = (17 - 4.2)/4.2 = 3$ to find a normalized entropy generation of 0.015. Multiplying by $\dot{m}\,c_p$ yields 45 $\mathrm{mW\,K^{-1}}$.

Maladjusted Flow: Equation (12) can be solved for each section of the core, with $L = 7.5$ cm, and $\Delta T_r = 0.75$, 0.43, 0.27, and 0.21 (going from the cold-end to the warm-end). The flow factor is taken to be $f = 0.67$. This value was determined in Section 9.4 to be a reasonable worse case assuming that the slit thickness may vary by up to $\pm10\%$. The normalized entropy generation is $0.011 + 0.0056 + 0.0029 + 0.0019 = 0.021$. Multiplying by $\dot{m}\,c_p$ yields 63 $\mathrm{mW\,K^{-1}}$.

Simple Axial Conduction: The axial conduction losses where estimated in Section 9.5 to be 24 $\mathrm{mW\,K^{-1}}$. This is a predicted value based on initial design calculations and does not take into account the considerably worse case predicted from the experimental data.

Partially insulated void: Section 9.6 predicted a wide range of possible values for $\dot{S}_{gen}$ resulting from partially insulated helium void. The helium void has very little effect for higher temperature ranges where the density of helium is small, but for temperatures less than 6 K, the effect is large. If we use an average value of 1 $\mathrm{mJ\,cm^{-3}\,K^{-1}}$, and multiply by the volume of GGG and helium contained in our core, $\sim$300 $\mathrm{cm^3}$, and divide by 5 seconds time for one flow process, we find $\sim$60 $\mathrm{mW\,K^{-1}}$ of entropy generated.

The table below summarizes the results of this analysis. Note that the entropy flow at the warm-end is predicted to be ~3 times that of the cold-end.

Entropy Source	$\dot{S}$ (mW K^{-1}) at warm-end
Base	120
$\beta L < \infty$	45
$nseg < \infty$	~0
Maladj. Flow	63
Axial Cond.	24
Insulated Void	~60
Total:	312

This implies that a significant deviation from the desired Carnot cycle is required. The cycle efficiency associated with these numbers is:

$$\eta_c = \frac{\frac{15}{4.2} - 1}{\frac{15(312)}{4.2(120)} - 1} = 31\%$$

In Chapter 5 computer simulation are presented. It was found that refrigeration could be achieved with the program if the magnetic field was modeled using the perturbation field. The cycle efficiency of the successful simulation runs was typically around 30%. This implies that it is possible for the device to pump three times the entropy at the warm-end as at the cold-end, and that the irreversibilities predicted by this analysis in this chapter need not "plug" the core.

The conclusions from the irreversibility analysis are:

- Based on the assumptions in this chapter, there are four significant entropy sources in our device.
- These sources need not "plug" the entropy flow in the core if the field-flow phasing is proper.
- Since the total irreversibility predicted by these sources is greater than that used in the computer simulation model, either greater or more complicated field perturbation may be required than originally predicted.
- This analysis did not include the excessive axial conductivity that will be discussed in Chapter 11.

PART 3: PHASE TWO EXPERIMENT AND DISCUSSION

Part 3 returns to the experimental track of this thesis. Chapter 10 contains the Phase Two system modifications which were made to partially correct the improper field-flow phasing in our device. These modifications were based on predictions from the analysis of Part 2. Chapter 11 contains a discussion of all the test data collected from full system operation, and it contains the isolated core tests which were performed afterwards. Chapter 12 is a discussion of the design concerns for the next generation device.

X. PHASE TWO SYSTEM MODIFICATION

10.1 Need for Further Modification

By the Spring of 1988 the core was tested with the Phase One improvements, and had failed to produce steady-state refrigeration over the the temperature range of 4.2 to 15 K. Extensive analysis into the dynamics of active regeneration had also been accomplished by this time. This analysis predicted that even if the core were perfect (no axial conduction, infinite convective heat transfer coefficient, no void) refrigeration could not be achieved by our device with its present field-flow phasing. We found that in order to achieve steady-state refrigeration over large temperature ranges, such as 4.2 to 15 K, it would be necessary to modify the device.

10.2 Design Options:

The analyses in Chapters 4,5 and 8 suggested two experimental modifications that would make a test system workable. One method requires the magnetic field to be functions of both position as well as of time; as a practical solution this requirement can be achieved by dividing the core into two independent fields. The second method is to span the temperature range with a two-stage system. It is difficult to retrofit a complete two-stage system to our present test apparatus, but the individual stages could be tested separately. These two options are discussed in detail in this section.

10.2.1 New Magnetic Field System – 4.2 to 15 K:

It has been shown by computer simulation that our test device could produce refrigeration over the temperature range of 4.2 to 15 K if the core is divided into two sections, each with its own magnetic field control. One possible field-flow phasing (used by the computer simulation program) is shown in Figure 54. Both the warm-end and the cold-end begin the magnetization process at 1 T. At the end of the adiabatic magnetization, the warm-end is at 2 T, while the cold-end is at 1.5 T. By the end of the up-flow process, both the warm and cold-end are at 4 T. During the demagnetization process the warm-end again uses more of the available field swing

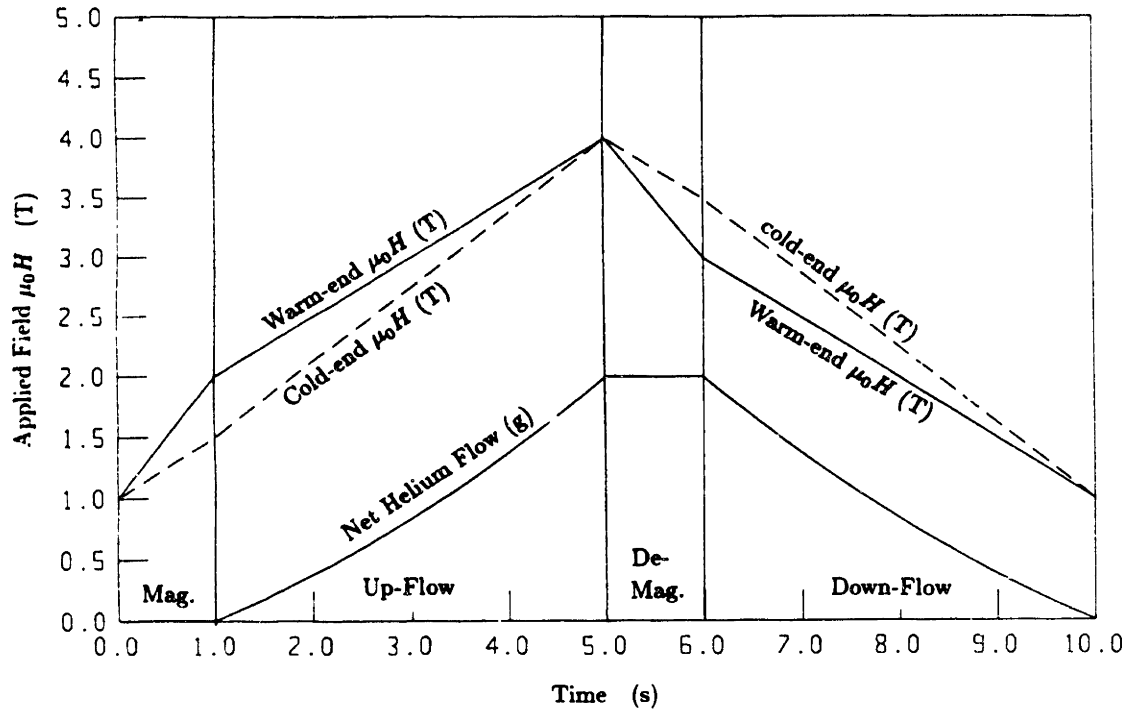

Fig. 54 Cold and Warm-End Field as a Function of Time

for the adiabatic part of the process than the cold-end. This phasing was predicted by the computer simulation program to produce refrigeration over the 4.2 to 15 K range.

Several modifications to our experimental device were considered which would allow for the type of field modification shown in Figure 54. Two potential modifications are discussed in this section. In both of these modifications the old magnetic system is maintained, and a new perturbation field is added to the system. The old system uses a 200-A power supply capable of ramping the current either up or down at a rate of $\sim$20 A s^{-1}. A perturbation field can be driven either by a much smaller current supply, or perhaps even by its own magnetic induction with the larger magnet.

A. Design of an independently controlled Perturbation Field:

This section describes the design that was ultimately chosen for the Phase Two system modification. The purpose of this design was to reproduce the field profiles shown in Figure 54 using a directly controlled perturbation field. A perturbation (secondary) coil was wound over the original coil (primary). A new current supply was purchased, and the computer cycle control programs and the computer interfaces

were modified.

The greatest difference between the cold-end field and the warm-end field in Figure 54 is 0.5 T. The perturbation coil was designed to add 0.25 T to the warm-end and to subtract 0.25 T from the cold-end. It was wound with its warm-end windings in the same direction as the primary coil, and with its cold-end windings in the opposite direction. With this design the net mutual inductance between the primary and secondary coil is close to zero. Control of one coil is not influenced by the other coil. The secondary coil is driven with both positive and negative currents. The purchased current supply provides all combinations of positive and negative current and voltage over the required power range.

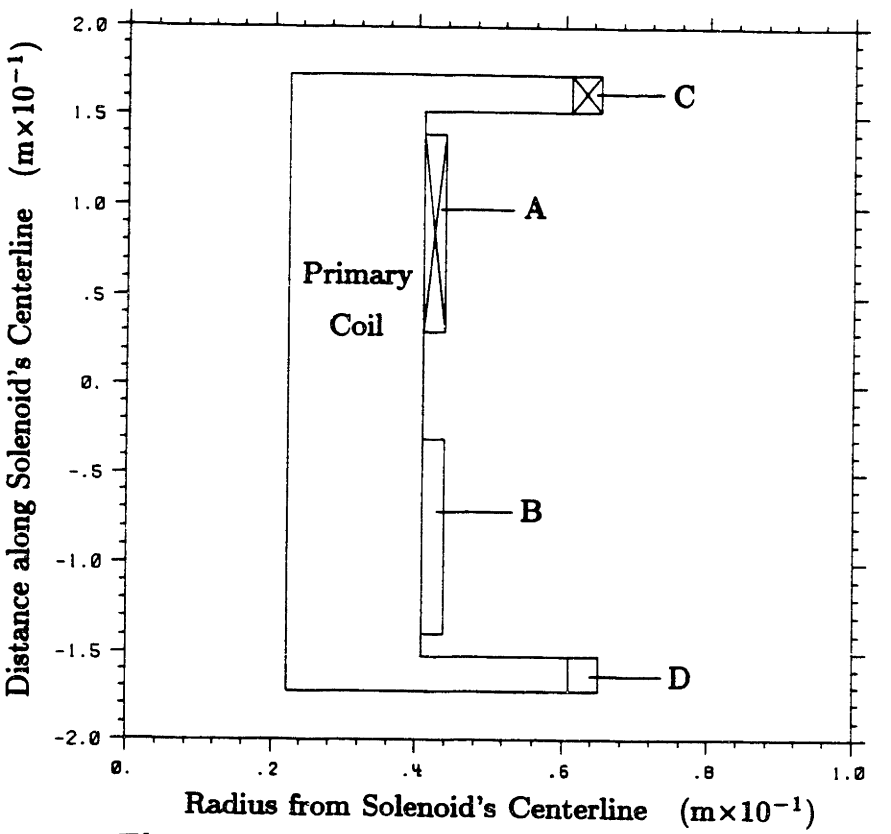

Fig. 55 Location of the secondary windings

The design of the secondary coil was done with use of a solenoid design program. With this program the field profiles were determined, and the net forces generated by the perturbation field were checked. Figure 55 shows the location of one half of the windings of the secondary coil (as well as that of the windings of the primary coil). The secondary coil has four solenoidal sections. The location of these sections was

somewhat predetermined by the dimensions of the primary coil. Sections A and B are each 7 rows deep and 330 turns long; while section C and D are each 15 rows deep and ~60 turns long. The turns are wound side-by-side, while the rows are separated by layers of Mylar tape. The tape is spaced to allow helium between the rows for cooling.

All the field profiles used by computer simulation program had a step change in magnetic field at the center of the core. This was done for ease in analysis. In practice it is neither possible nor desirable to have a step change in magnetic field. The actual field obtained by the secondary coil along the core's center line is shown in Figure 56a with a solid line. The dashed line in this figure is sum of this field plus the primary field operating at 38 A. (Figure 56b shows the magnetic field at the core's center line with the primary coil operating at 100 A and with no current in the secondary.) The perturbation field changes linearly through the center region of the core, and it tails off at each end of the core. It would have been preferable to have the field strength increasing through each end of the core. This could have been accomplished with more windings located at the core's ends. In practice this goal could not be realized because the necessary number of windings could not be fit into the available space. The variation of the magnetic field produced by the secondary coil over the core's cross section is less than 5%.

It was found that the perturbation fields would not significantly alter the stress distribution on the primary coil, and that the total force on the secondary coil in the axial direction will be around 500 N, a manageable size.

B. Design of an inductively coupled perturbation field:

Also considered was the use of a secondary coil driven only by its magnetic coupling with the primary field. If the coupling factor could be made large enough, then a secondary power supply would not be necessary. In this design the secondary coil would be wound around just the cold-end of the primary coil, and shunted across the proper resistance outside of the cryostat. This inductively coupled perturbation coil would act to slow down the field response at the cold-end. This method is wasteful in that magnetic energy is dissipated in the current shunt, but since an extra current supply is not required, it would be more easily implemented.

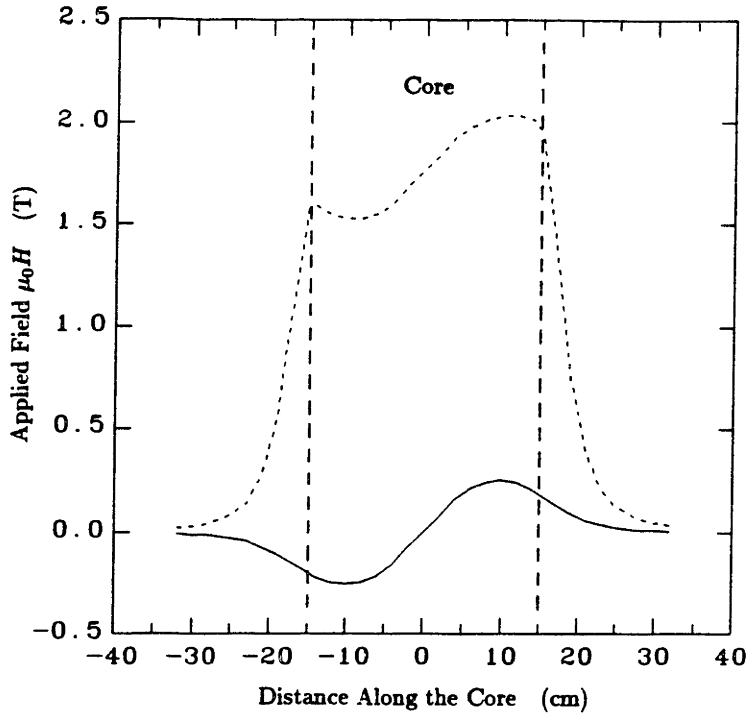

Fig. 56a Actual Perturbation Field, Shown by Itself and Superimposed on Primary Field

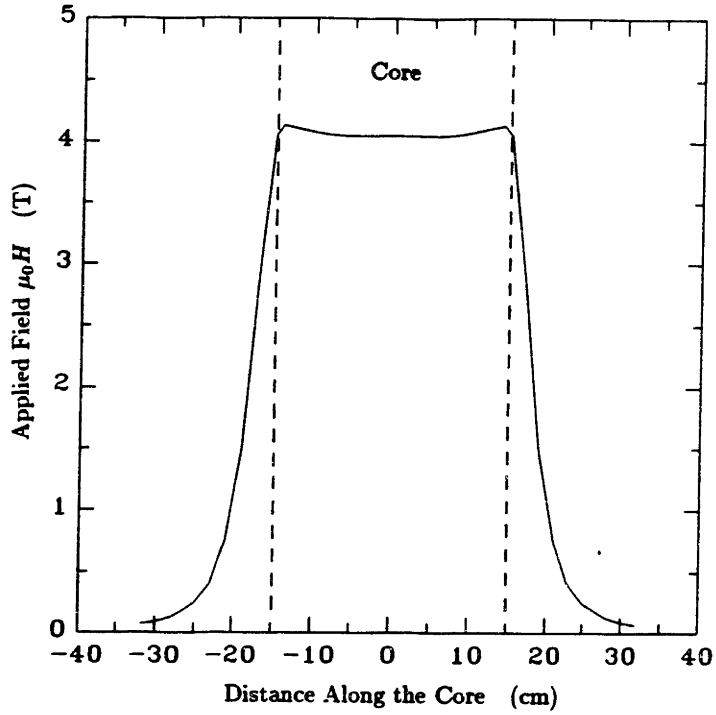

Fig. 56b Actual Primary Field Produced by 100 A

A first-order analysis of this design was performed, and it was found that the inductive coupling between the primary and secondary coils could not be made large enough to satisfy our design goals. For this reason this method was not perused.

10.2.2 New Warm-End Heat Sink – Two-Stage:

The other method of achieving refrigeration over the temperature range of 4.2 to 15 K is to use a two-stage device. In Chapters 4 and 5 two-stage matching was performed. In those analyses it was found that both the average heat load and the average helium flow at the junction of the two stages could be matched. Since the same total helium flow could be used for both stages, a two-stage device would require only one helium displacement system.

The advantage of a two-stage system, when compared with a single-stage system with two independent magnets, is that each stage is within the low-temperature range definition as described in Chapter 8. Proper field-flow phasing is not critical. Refrigeration is likely to be achieved even in the absence of precise cycle control. In addition, should other yet unconsidered factors act to reduce our ability to produce refrigeration, the warm-end temperature of a test device could be varied to find the limit of successful refrigeration.

The disadvantage is that a two-stage system inherently has more irreversibility than a properly controlled single stage system. This results from thermal mixing of the helium at the junction between the two stages.

A two-stage design modification was considered for our present test apparatus. Detail of the design work done for this potential modification is not presented here, since this design was not ultimately chosen, and the detail is lengthy. However, some of the basic design considerations are discussed below.

The heat exchangers in our present apparatus were designed to be operated only at specific temperatures. The cold-end is thermally attached to the helium bath, and therefore must be operated at 4.2 K. The warm-end is designed to be thermally stabilized by a bath of liquid hydrogen, and thus must be operated at a temperature above 14 K.

In order to operate the device over other temperature ranges, it is necessary to modify

the heat exchangers. The cold-end, however, cannot be effectively isolated from the helium bath. This is because there is not room in the cryostat for the necessary additions to the temperature control module. The warm-end can be modified. The proposed warm-end design modification would have entered the hydrogen chamber with a small tube, and have sprayed liquid helium directly onto the warm-end copper block. A heater would have been wrapped around the tube to control the load. Design considerations included: 1) heat transfer between the helium and copper, 2) pressure drop in the tube, 3) control of the primary heater considering response time of the sensors for real-time feedback, and 4) trim of the heat load with a secondary heater already imbedded in the copper block.

With the warm-end modified to allow for colder warm-end temperatures, we would then be able to test the core over the temperature range of 4.2 to 10 K. All previous analysis and experimental results suggest that refrigeration should be obtained over this range with reasonable cycle control and regenerator performance. The other part of the two-stage device, 10 to 15 K, cannot be tested since the cold-reservoir cannot be modified to achieve 10 K. The computer simulation program predicted that this range is more easily operable than the 4.2 to 10 K range. Successful operation over the colder range, and correlation of the test results to the computer simulation results, would ensure refrigeration over the 10 to 15 K range.

10.3 Conclusion

After weighing the advantages and disadvantages of the possible modifications, we decided to proceed with the directly controlled perturbation field. The reasons for this decision are:

- An inductively coupled perturbation field was considered, but a design could not be found which would both produce the necessary magnitude of perturbation, and respond quickly enough for our cycle time of 10 s.
- It is generally more efficient to operate our device in a single stage, since irreversibilities are generated between stages. Since two independent stages require two independent magnet systems anyway, choosing two stages would not allow for a reduction in the number of main components in a complete system. For this reason we decided to modify the magnetic system instead of the reservoirs.

XI. DISCUSSION – ANALYSIS OF EXPERIMENTAL RESULTS

11.1 Introduction

This chapter presents detailed analysis of all test data that have been collected to date. The data from the full system tests are coded by letter and number. The letter indicates the day on which the test took place:

A: September 1987
B: October 1987
C: November 1987
D: January 11, 1988
E: January 29, 1988
F: September 1988
G: October 1988

The number indicates the run number for that day. For example, run D-6 would be the sixth test run performed on January 11, 1988.

This chapter explores all issues that relate to experimental validation of the principles of our device. During the full system tests, it was determined that our core did not behave as well as was expected. The evidence of bad regenerator behavior was in two forms. First, the core seemed to contain more zero-field specific heat than was expected. It was found that if we assumed the helium porosity in the core to be approximately twice the design value, then the test data could be explained (Section 11.2). Later a porosity measurement was performed on the core after it had been removed from the system (Section 11.3). This test confirmed that the porosity was approximately twice as large as expected.

The second, and more serious, problem with the core was evident from warm-end temperature information. The warm-end sensor, W3, indicated that helium leaving the core on an up-flow would often begin the flow process several degrees colder than expected. Section 11.4 uses the irreversibility analysis in Chapter 9 and test data to

explore this problem. This analysis concludes that the most likely explanation of this problem is excessive axial conduction. Unfortunately, the full system experimental apparatus did not allow for temperature measurement of locations within the core. In order to get first hand information to the exact nature of the core's problems, it was necessary to remove the core from the system. An axial conduction test was later performed on the core after it had been removed from the system (Section 11.5). This test confirmed that the axial conduction was approximately 10 times higher than expected.

Another problem found during testing relates to the helium dead space external to the core. Section 11.6 explores the negative effects of helium dead space.

Finally the effect of the perturbation field is discussed in section 11.7. Unfortunately, its effect is masked by the bad core properties.

11.2 Determination of the Actual Helium Void from Full System Test Data

The porosity in our core was calculated to be about 4.4% by volume of GGG.[12] The value used in the computer simulation program has been 5%. Upon analysis of the test data, it was suspected that the effective helium void of the core is actually much higher than this. The evidence supporting this is presented in this section.

11.2.1 The Adiabatic Process

General Description of the Adiabatic Process:

Due to the breathing effect, an adiabatic path cannot be achieved by a core which has any helium void. An adiabatic process in this thesis is defined as one where the helium flow is zero at the cold-end. If the field is increasing, helium is blown out of the warm-end, and if the field is decreasing, helium is sucked into the core through the warm-end.

> *In general, the helium flow is always greater at the warm-end than at the cold-end during a low-flow process.*

The magnitude of helium flow induced by the breathing effect depends on the initial temperature profile of the core and the core's porosity. To analyze an adiabatic process, the computer simulation program described in Chapter 5 is used. Equation

(4) defines the heat balance which is solved by the simulation program.

$$V_g \rho_g T\, dS_g + V_{he} d(\rho u)_{he} = (h_{in} dm_{in} - h_{out} dm_{out})_{he} \qquad (4)$$

h_{out} is taken to be at the temperature of the segment, and h_{in} comes from the segment that is immediately upstream of the segment being analyzed. In general h_{in} and dm_{in} can only be determined by step-wise solution of Equation (4), following the direction of the flow. If a single segment is analyzed with dm_{in} set to zero, then h_{in} need not be considered. In this simplified case (using the same logic as was used in Chapter 6.1) Equation (4) can be rewritten as

$$V_g \rho_g T\, dS_g + V_{he} \rho_{he} c_p dT = 0$$

If the helium porosity of the segment were zero, then an adiabatic process would follow a constant entropy curve of GGG. The extra specific heat of the entrained helium in the segment causes the entropy of the GGG to drop during a magnetization process. Figure 57 shows adiabatic processes for a segment with 5% void plotted on a GGG T-S diagram. Note that the entropy drops most quickly for temperatures near or below 6 K. This is where ρc_p of the helium is greatest.

Our core contains not one but 120 segments. Does the number of individual segments effect the adiabatic process followed by segments at the warm-end, where helium flow is induced by breathing? Actually, if we assume good heat transfer between the helium and GGG, and if we start with a uniform temperature in the core, then a temperature gradient will not be generated during magnetization. The reason for this is that flow coming into a segment from a neighboring segment is always equal to the temperature of that segment. There is never any heating (or cooling) due to this excess flow. We can therefore use the curves plotted in Figure 57 to indicate the temperature of the core during any adiabatic magnetization process, provided that the initial temperature of the core is uniform — $T(x)$ = constant.

The helium rejected at the warm-end is sensed by the temperature sensor W-3. In order for sensor W-3 to accurately reflect the temperature of the core at the end of an adiabatic magnetization, there must be up-flow through the core. The breathing effect will provide a significant amount of up-flow when the core is warmed through the 4 to 8 K temperature range, but will not at higher temperatures. Higher

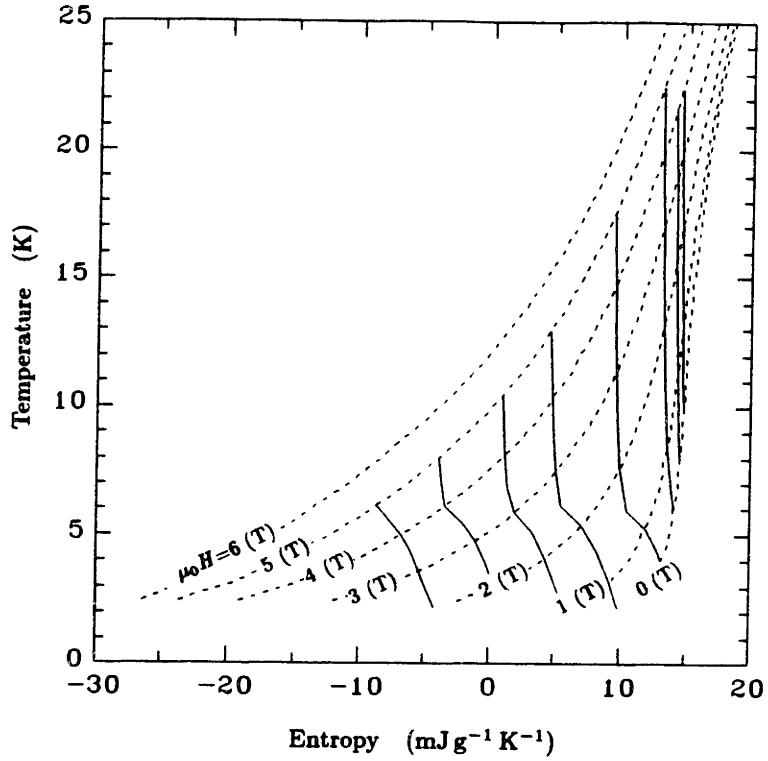

Fig. 57a Adiabatic Magnetization Process for a Single Segment ($P = 3$ atm)

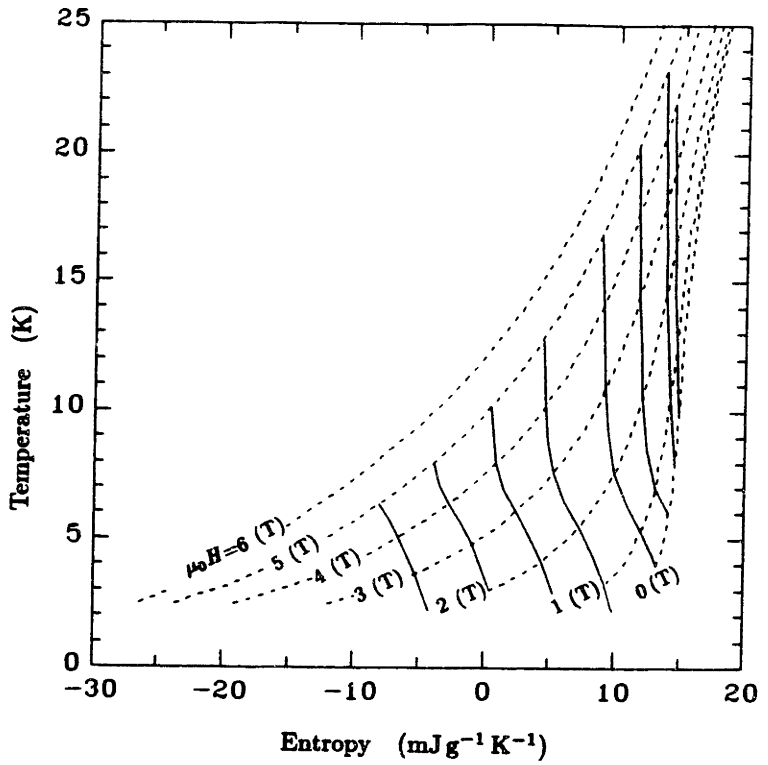

Fig. 57b Adiabatic Magnetization Process for a Single Segment ($P = 5$ atm)

temperature ranges require some amount of forced flow in order to use the test for adiabatic magnetization data.

If the core begins an up-flow magnetization process with a uniform temperature profile, then its profile at the downstream end of the core will remain uniform until the convection wave coming from the cold-end passes (see Chapter 6.6 and Appendix F). In our device, refrigeration-type runs do not have enough helium flow for the convection wave to travel from the cold-end to the warm-end. For this reason it is possible to treat the first magnetization of a refrigeration test as an adiabatic magnetization, before a temperature gradient is generated in the warm-end.

Test Results:

Table 11a and 11b compare the predicted core temperature for simulated adiabatic magnetization with the final temperature recorded at sensor W-3 during actual adiabatic magnetizations. Every test run from September 1987 to October 1988 was scanned to determine whether it could be used in this analysis. All runs which could be used are presented in Table 11a & b. There is a subscript which appears next to the recorded temperature range. This subscript refers to the flow condition which occurs after or during the magnetization. The various conditions are:

n: No forced flow. (breathing only)
c: Small amount of forced up-flow after magnetization.
f: Full displacer motion (up-flow) after magnetization.
r: Up-flow during magnetization, first cycle only.

Any other case was not considered to have produced usable data. The computer simulation runs were performed with one of the following helium porosities.

Gap (mm)	Porosity (%)
0.00	4.4
0.25	7.6
0.51	10.5
0.76	13.4

where the "Gap" is defined in Chapter 9.2 as a possible location for excess entrained helium. The results of this analysis can be summarized as follows: Warm temperature adiabatic magnetizations (the initial temperature beginning at 6.5 K or above)

TABLE 11a
Adiabatic Magnetizations

Run #	Temp Swing (k)	Field Swing (T)	*por* (%)	Pred. Temp (K)	$\frac{\Delta T_{exper.}}{\Delta T_{simul.}}$
A-25,26	$4.2 \rightarrow 7.5_{f,n}$	$0 \rightarrow 3.4$	4.4	12.3	0.41
			10.5	8.7	0.73
			13.4	7.6	0.97
A-27	$4.2 \rightarrow 7.8_{f}$	$0 \rightarrow 3.8$	4.4	13.4	0.39
			10.5	9.6	0.67
			13.4	8.4	0.85
A-28	$4.2 \rightarrow 7.9_{f}$	$0 \rightarrow 3.8$	4.4	13.4	0.40
			10.5	9.6	0.68
			13.4	8.4	0.88
C-8	$7 \rightarrow 14.5_{f}$	$0 \rightarrow 3.8$	4.4	17.4	0.72
			10.5	16.7	0.77
E-6	$6 \rightarrow 15.0_{f}$	$0 \rightarrow 3.7$	4.4	16.3	0.87
			7.6	16.0	0.90
			10.5	15.4	0.96
E-7	$8 \rightarrow 17.5_{f}$	$0 \rightarrow 3.7$	4.4	17.9	0.96
			10.5	17.5	1.00
E-8	$8.5 \rightarrow 13.4_{n}$	$0 \rightarrow 3.7$	4.4	18.0	0.74
			10.5	17.8	0.75
E-15	$6 \rightarrow 11.0_{r}$	$0.8 \rightarrow 3.7$	4.4	13.9	0.63
			10.5	11.5	0.91
E-17,19	$6 \rightarrow 10.3_{r}$	$0.8 \rightarrow 3.7$	4.4	13.9	0.54
			10.5	11.5	0.78
E-21	$4.2 \rightarrow 7.5_{n}$	$0 \rightarrow 3.7$	4.4	12.9	0.38
			10.5	9.3	0.65
E-23	$5 \rightarrow 9.6_{r}$	$0.7 \rightarrow 3.7$	4.4	13.0	0.57
			10.5	9.9	0.82
E-24	$7 \rightarrow 14.0_{r}$	$0.7 \rightarrow 3.7$	4.4	15.7	0.80
			10.5	14.2	0.97
F-7	$11.5 \rightarrow 17.0_{r}$	$0.8 \rightarrow 3.8$	4.4	18.7	0.76
			10.5	18.5	0.79
F-8	$8.5 \rightarrow 15.0_{r}$	$0.8 \rightarrow 3.8$	4.4	17.2	0.75
			10.5	16.4	0.82
F-10	$8.5 \rightarrow 16.0_{f}$	$0 \rightarrow 4.0$	4.4	17.6	0.76
			10.5	17.5	0.83
F-11	$6.0 \rightarrow 13.0_{c}$	$0 \rightarrow 4.0$	4.4	15.9	0.70
			10.5	13.1	0.99
F-12	$5.6 \rightarrow 10_{?}$	$0 \rightarrow 4.0$	4.4	15.2	0.45
			10.5	12.2	0.67
F-13	$8.0 \rightarrow 14.5_{f}$	$0 \rightarrow 4.0$	4.4	18.0	0.65
			10.5	17.0	0.72
			13.4	16.6	0.77
F-14	$6.0 \rightarrow 12.5_{c}$	$0 \rightarrow 4.0$	4.4	15.9	0.66
			10.5	13.0	0.93
F-20	$8.5 \rightarrow 13.4_{c}$	$1 \rightarrow 4.0$	4.4	17.3	0.80
			10.5	16.8	0.84

TABLE 11b
Adiabatic Magnetizations

Run #	Temp Swing (k)	Field Swing (T)	*por* (%)	Pred. Temp (K)	$\frac{\Delta T_{exper.}}{\Delta T_{simul.}}$
F-21	$8.0 \rightarrow 15.0_f$	$0 \rightarrow 4.0$	4.4	18.2	0.69
			10.5	17.6	0.73
F-22,23	$7.0 \rightarrow 14.0_c$	$0 \rightarrow 4.0$	4.4	17.3	0.68
			10.5	16.3	0.75
F-24	$8.5 \rightarrow 16.2_f$	$0 \rightarrow 4.0$	4.4	18.4	0.78
			10.5	18.0	0.81
F-25	$9.0 \rightarrow 16.6_f$	$0 \rightarrow 4.0$	4.4	18.6	0.79
			10.5	17.6	0.82
F-26	$8.0 \rightarrow 15.8_f$	$0 \rightarrow 4.0$	4.4	18.2	0.76
			10.5	17.6	0.81
F-27	$12 \rightarrow 16.6_r$	$0 \rightarrow 3$	4.4	17.8	0.79
			10.5	17.8	0.79
F-29	$9.0 \rightarrow 16.0_f$	$0 \rightarrow 3.7$	4.4	18.0	0.78
			10.5	17.6	0.81
G-2	$7 \rightarrow 12.3_f$	$0 \rightarrow 2.7$	4.4	14.2	0.74
			10.5	13.6	0.80
G-3	$7 \rightarrow 10.5_f$	$0 \rightarrow 1.8$	4.4	11.8	0.73
			10.5	11.0	0.88
G-4	$6.5 \rightarrow 14.5_f$	$0 \rightarrow 3.7$	4.4	16.7	0.78
			10.5	16.0	0.84
G-5	$6.5 \rightarrow 10.5_f$	$0 \rightarrow 1.8$	4.4	11.3	0.83
			10.5	10.6	0.98
G-6	$6.5 \rightarrow 14.7_r$	$0.7 \rightarrow 3.9$	4.4	16.6	0.81
			10.5	15.8	0.88
G-7	$7.5 \rightarrow 13.3_r$	$0.7 \rightarrow 2.9$	4.4	15.0	0.77
			10.5	14.5	0.83
G-8	$8.2 \rightarrow 10.9_r$	$0.7 \rightarrow 1.8$	4.4	12.2	0.68
			10.5	11.7	0.77
G-9	$7 \rightarrow 15.2_r$	$0.8 \rightarrow 3.9$	4.4	16.6	0.85
			10.5	16.1	0.90
G-21	$4.2 \rightarrow 11.8_n$	$0 \rightarrow 4.0$	4.4	15.3	0.68
			10.5	10.5	1.19
G-23	$12 \rightarrow 19.0_r$	$0.7 \rightarrow 3.8$	4.4	19.3	0.96
			10.5	19.6	0.92

achieved ~80 % of the expected temperature swing. Varying the helium porosity for these runs made little difference in the predicted final temperature. The ~20 % loss of temperature swing can be attributed to either:

1. Temperature sensor W-3 reading too low, (Chapter 3.1).
2. Still more core specific heat unaccounted for.
3. Assumed GGG magnetic properties not accurate.

The cold temperature adiabatic magnetizations (the initial temperature beginning at ~4.2 K) were very sensitive to core porosity. When the gap was set to zero, the actual temperature swings reached only ~40 % of the predicted. Increasing the helium gap to 0.51 mm decreased the predicted temperature swing so that the fraction increased to ~70 %. Increasing the the gap further to 0.75 mm can cause even better alignment with the test data, but this is not proper since the warmer adiabatic magnetizations never reached 100%. To achieve 80% agreement (the same as was achieved for the warm tests where porosity is not an issue) it is necessary to have a porosity of more than 10%.

11.2.2 The Isofield Process

General Description of the Isofield Process:

During an isofield path, the magnetic interaction term defined in Chapter 6.2 is zero. All TdS_g acts as specific heat, and can be treated in the same way as the core's zero field specific heat. A good regenerator core acts as a stratified heat storage device; heat transfer occurs primarily between the helium and GGG, and very little heat conducts axially through the core.

If we begin with the core at uniform temperature, and if we assume that there is no dispersion of the convection wave front, then a simple heat balance of the core can be used to calculate the amount of helium flow that is required to push a convection wave through the core. In this limit we can write:

$$\Delta(m\,u)_{he} + \Delta \mathrm{H}_g + \Delta \mathrm{H}_r = [m_{in}\,h_{in} - m_{out}h_{out}]_{he}$$

In this equation H_g is the total magnetic enthalpy of the GGG in the core, and H_r is the total enthalpy of the silicon rubber in the core. Since the helium pressure is constant:

$$\Delta(m\,u) = \Delta(m\,h) = m_2 h_2 - m_1 h_1$$

In this example the following relations hold:

$$h_2 = h_{in}$$

$$h_1 = h_{out}$$

$$m_2 - m_1 = m_{in} - m_{out}$$

After some algebra we can write:

$$m_{in} = \frac{\mathrm{H}_g + \mathrm{H}_r}{h_{in} - h_{out}} + m_2$$

The amount of helium flow into the core which will drive a convection wave through the core is equal to that which is required to change the enthalpy of the GGG and rubber encapsulant, and that which is required to fill the void with helium at the new temperature. We find that the helium flow at the cold-end always exceeds the helium flow at the warm-end by the change in entrained helium in the core. Since in our device the helium flow is controlled from the cold-end, we can rewrite the above equation as:

$$m_c = \frac{\mathrm{H}_g + \mathrm{H}_r}{h_{in} - h_{out}} + m_b \tag{12}$$

where m_c is the total helium flow at the cold-end, and m_b is the component of m_c which is due to the breathing effect. In an up-flow process m_b equals the final entrained helium, and in a down-flow process m_b equals the initial entrained helium.

> *In the isofield example, the breathing effect results in more helium flow at the cold-end than at the warm-end.*

Table 12 shows the total magnetic enthalpy of the core at various temperatures and applied magnetic fields according to the basic property data used in the computer simulation program. A complete graph of the magnetic enthalpy function can be found in Appendix E. Table 14a shows the component of m_c which is due to the magnetic enthalpy of the GGG, Table 14b shows the component of m_c which is due to the rubber encapsulant, and Table 14c shows the component of m_c which is due to the breathing effect. The breathing induced flow is proportional to the helium porosity. At zero Tesla, most of the flow determined from Equation (12) is due to the change in entrained helium. As the field increases, the specific heat of the GGG, c_H, also increases, and more flow is required to change the temperature of the GGG.

Both the computer simulation program and the real device experience dispersion of the convection wave front during the isofield process. With dispersion the front edge of the wave reaches the end of the core sooner than without dispersion, yet it will take much more total helium flow to completely change the temperature of the core to its final value.

An example of an isofield process with dispersion is shown in Figure 58a. This figure was produced with the computer simulation program. In this example the core is heated from 4.2 to 15 K by helium flow entering the core at 15 K. The field is constant at 1 Tesla. The total mass of helium entering the core at 15 K is 2.0 g, while that leaving the core is 3.5 g. The difference, 1.5 g, is the change in the mass of entrained helium in the core. The dispersion effect in this figure results from irreversibilities due to a finite number of segments (31 segments were used in this analysis), and from the variable thermodynamic properties of the helium and GGG. Figure 58b shows the same case only now the field is constant at 4 Tesla. Note that much more helium shuttle mass is necessary for the convection wave to travel the length of the core.

Test Results:

In order to properly analyze the isofield process, it is necessary to find test data where the initial temperature profile in the core is known, and where the convection wave can be seen clearly pushing through the downstream end of the core. Unfortunately, of the many test runs performed there were few which met this criterion. However, there were many test runs where the convection wave would have pushed through the core had the porosity been at the expected value of 4.4%. Table 15 shows several isofield processes which were performed with a known initial temperature profile. m_d is the total forced helium flow of the path as measured by the displacer position, and m_c is the helium flow predicted by adding up all the terms in Equation (12). Irreversibilities lead to dispersion of the convection wave, and dispersion causes the wave to reach the downstream end of the core sooner. Since the amount of dispersion is related to the losses in the core, and these losses are unknown, it is not possible to analyze these data in detail. The value predicted by Equation (12) should be a maximum. One can see from this data that in no case can the isofield process be described by a core with 4.4% void. The overall heat balance of the core can only be satisfied by increasing the void significantly.

	TABLE 12 Core Magnetic Enthalpy, (J) ; with M_g = 1.82 kg				
T (K)	0 T	1 T	2 T	3 T	4 T
2.5	30.8	−29.3	−188.0	−393.1	−613.9
4.2	45.0	−7.1	−148.3	−342.7	−559.8
10.0	62.4	29.7	−64.2	−208.6	−390.2
15.0	81.7	57.9	−11.6	−122.3	−268.1
20.0	125.5	107.4	53.3	−34.6	−152.3

TABLE 13 Helium Properties used in Equation (12)				
	Pres. = 3 atm		Pres. = 5 atm	
Temp. (K)	ρ (g/cc)	h (J/g)	ρ (g/cc)	h (J/g)
2.5	0.151	5.8	0.154	7.0
4.2	0.135	10.2	0.140	11.1
10.0	0.016	61.5	0.028	57.9
15.0	0.010	89.7	0.017	87.7
20.0	0.007	116.8	0.012	115.6

	TABLE 14a $m_c = \Delta H_g/(h_2 - h_1)$ (g)				
ΔT (K)	0 T	1 T	2 T	3 T	4 T
P = 3 atm					
4.2 ↔ 10.	0.34	0.72	1.64	2.61	3.31
4.2 ↔ 15.	0.46	0.82	1.72	2.77	3.67
2.5 ↔ 15.	0.61	1.04	2.10	3.23	4.12
4.2 ↔ 20.	0.76	1.07	1.89	2.89	3.82
P = 5 atm					
4.2 ↔ 10.	0.37	0.79	1.80	2.9	3.6
4.2 ↔ 15.	0.48	0.85	1.78	2.9	3.8
2.5 ↔ 15.	0.63	1.08	2.19	3.4	4.3
4.2 ↔ 20.	0.77	1.10	1.93	2.95	3.90

TABLE 14b
$m_c = \Delta H_r/(h_2 - h_1)$ (g)

ΔT (K)	Pres. = 3 atm		Pres. = 5 atm	
	por=4.4%	*por*=10.5%	*por*=4.4%	*por*=10.5%
4.2 ↔ 10.	0.12	0.10	0.13	0.10
4.2 ↔ 15.	0.35	0.28	0.36	0.29
2.5 ↔ 15.	0.33	0.26	0.35	0.28
4.2 ↔ 20.	0.65	0.52	0.66	0.53

TABLE 14c
m_c entrained (g)

T (K)	Pres. = 3 atm		Pres. = 5 atm	
	por=4.4%	*por*=10.5%	*por*=4.4%	*por*=10.5%
2.5	1.77	4.56	1.81	4.65
4.2	1.59	4.08	1.64	4.23
10.	0.19	0.48	0.33	0.85
15.	0.08	0.21	0.14	0.36

TABLE 15
Isofield Processes

Run #	Temp. Range (K)	Field (T)	m_d (g) Displ.	m_c (g) *por*=4.4%	m_c (g) *por*=10.5%
A-17	4.2→10.	0	3.0	2.2	4.7
B-7	4.2→14.	0	*3.5	2.3	4.7
E-12	2.2→15.	0.7	3.8	3.2	6.1
F-20	15.→5.	4.0	7.0	5.6	7.7
F-21	15.→5.	4.0	7.0	5.6	7.7
F-29	20.→4.2	3.7	8.0	5.8	8.2
G-1a	4.2→15	0	*4.0	2.4	4.8
G-1b	5→15	1.0	*5.6	2.8	5.3

* The convection wave made it through the core

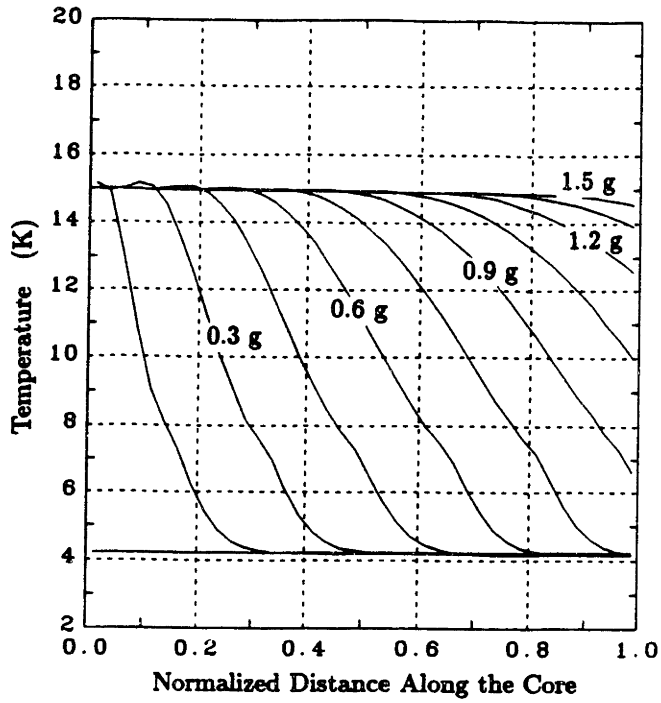

Fig. 58a Computer Simulation of an Isofield Process, 1 Tesla

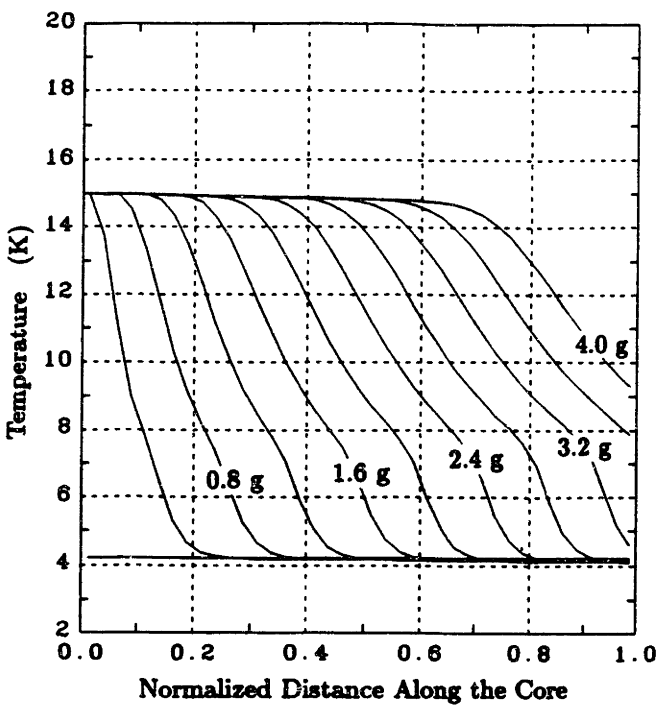

Fig. 58b Computer Simulation of an Isofield Process, 4 Tesla

- The isofield process indicates that the core has an actual helium void much greater than 4.4%, but an exact value cannot be determined because of uncertainties in the degree of convection wave dispersion.

11.3 Direct Measurement of the Core's Helium Porosity

After we had determined that our system could not produce refrigeration with the present core problems, it was decided that the core would be removed from the test apparatus and tested separately. The method of assembly of our apparatus was by stainless to stainless heli-arc welding. To remove the core these welds were cut with a Dremel Tool. The outer vacuum jacket, which separated the core from the superconducting coil, was cut diagonally and peeled off.

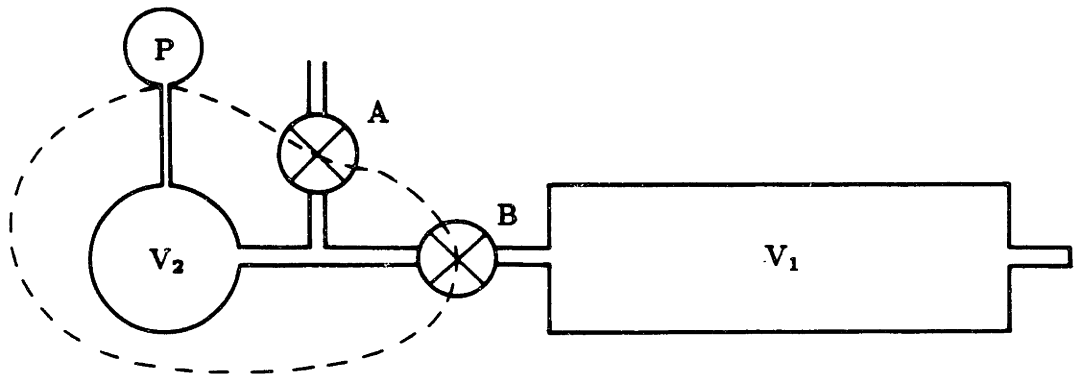

Fig. 59 Schematic of Void Test

Figure 59 shows a schematic of the system which was used to measure the void in our core. Volume V_1 contains the helium void which is to be measured, and volume V_2 is another volume chosen to be of similar size. V_2 is measured by filling it with water. The system is first evacuated through port A, and then V_2 is pressurized with helium gas to pressure P_i, with valve B closed. The pressure in V_2 is measured with a strain-gage type pressure transducer. When valve B is opened the pressure in the two volumes is equalized at P_f. Since helium can be treated as a perfect gas under these conditions, the volume V_1 can be calculated simply from:

$$V_2 P_i = (V_1 + V_2) P_f$$

so long as we wait long enough so that the temperatures are constant. To determine the helium void from V_1, we first need to carefully calculate the volume of all the void in V_1 which is external to the core. The largest external void is contained in the tubes which lead from the GGG segments out through the ends of the core. A filler piece was made to eliminate part of this void. In order to check our data the test was performed with and without the filler piece in place. Many void measurements were made. Below is a list of the volumes which were measured and calculated.:

Volume V_2:	44.1 (cm^3)
Filler Piece:	8.1 (cm^3)
External Void:	26.1±0.5 (cm^3)
Volume V_1:	51.8±1.8 (cm^3)
Helium Void:	25.7±2.3 (cm^3)

In Chapter 9.2 we had an expression which related the total helium void in the core to the porosity. The void determined from this test translates to a helium porosity of 9.2%. This is almost identical to the value of helium porosity which was determined from full system test data (previous section). There are two conclusions that can be deduced from this test.

- The helium porosity is twice as the value which has been assumed since the core was first assembled.
- The computer simulation analysis is accurate.

Where is the extra void?

As was speculated in Chapter 9.2, this void is most likely contained in the gap which separates the silicon rubber from the stainless core jacket. A 0.4-mm radial gap is required to create this extra void.

11.4 Unsatisfactory Regenerator Performance

11.4.1 Description of the Symptoms

A good regenerator acts as a stratified heat storage device, but the warm-end test data indicate that our core is not acting as a good regenerator. The problem can be described by the following examples:

1. During refrigeration type runs, the warm-end is too cold at the beginning of the up-flow process. In some cases the up-flow begins at a temperature below the

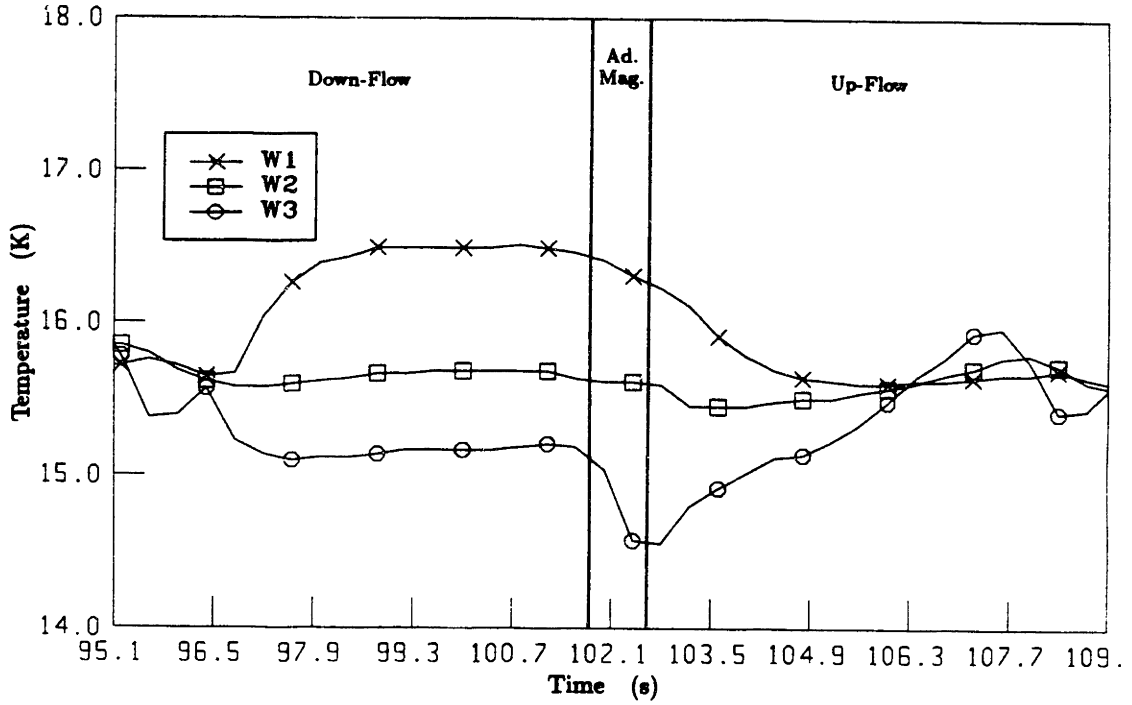

Fig. 60a Unsatisfactory Core Behavior Example 1

warm-reservoir temperature, even though an adiabatic magnetization separates the down-flow from the up-flow. (see Figure 60a)

2. During isofield cycles consisting of a down-flow followed by an up-flow, the up-flow begins at a temperature below the entering down-flow temperature (from the warm-reservoir), and then continues to drop almost linearly as the up-flow continues. (see Figure 60b)
3. When the magnitude of the cycle is reduced by reducing both the field change and the helium shuttle mass proportionally, the situation gets worse. For a small enough field swing, the warm-end temperature never even reached the warm-reservoir temperature. (see Figure 60c)

The cold-end test data are not as clear since the temperature excursions experienced during operation are not as pronounced.

11.4.2 Examination of the Possible Causes

1) Heat leak out of the core: A heat leak from the warm-end of the core to the surrounding helium bath could cause the warm-end to exhibit the behavior listed

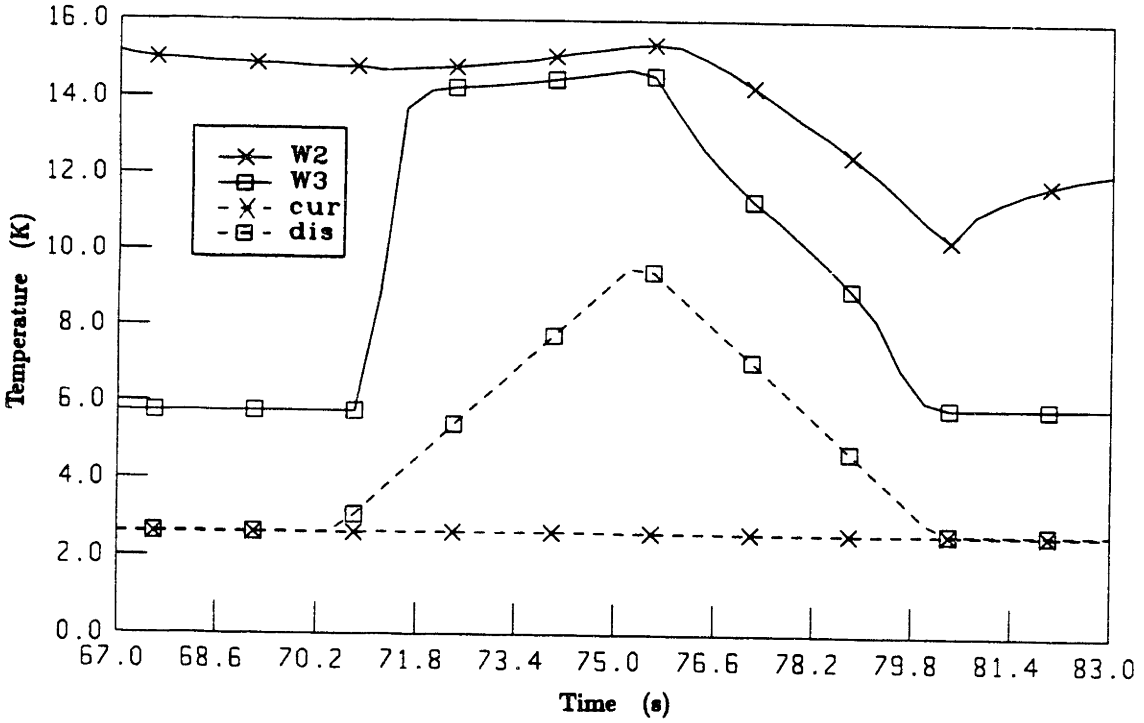

Fig. 60b Unsatisfactory Core Behavior Example 2

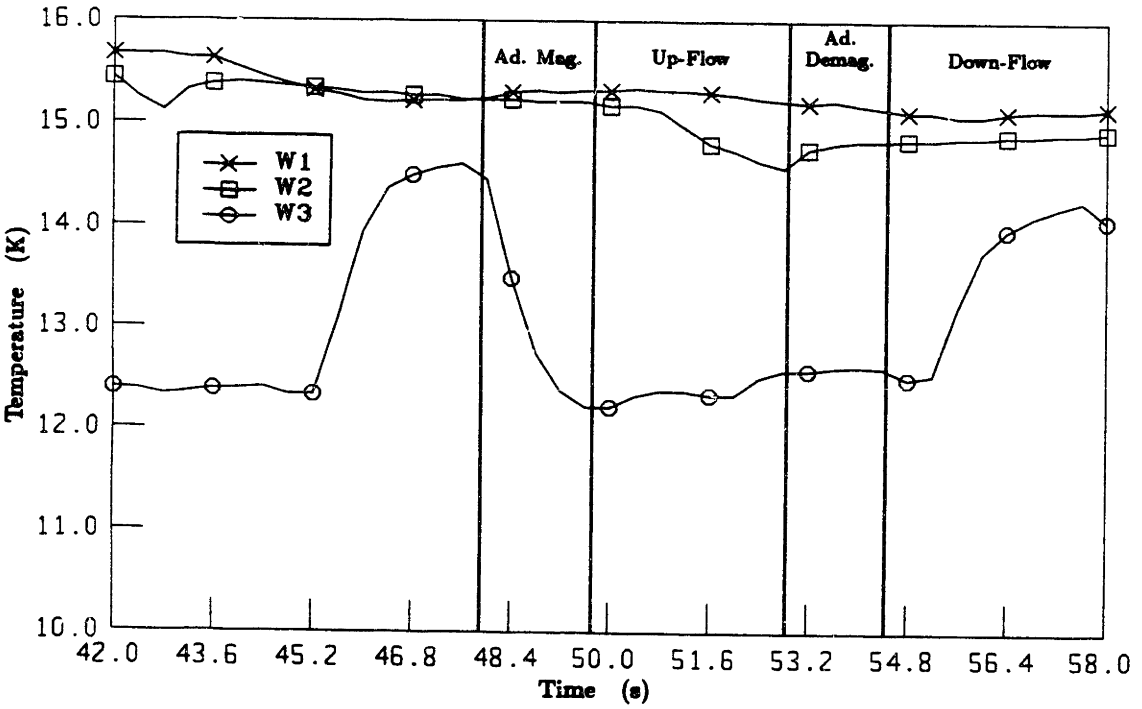

Fig. 60c Unsatisfactory Core Behavior Example 3

above, but there are several other factors that contradict this explanation. When the core is heated by an adiabatic magnetization with a uniform core temperature, the warm-end maintains its heat for a very long time. If there were a heat leak, at least as much heat would leak out of the core from a uniform temperature profile as from a non-uniform temperature profile.

2) Inadequate convective heat transfer: Inadequate convective heat transfer can lead to a large ΔT between the helium and GGG, and can cause some of the symptoms listed above, but there are several other factors that contradict this solution. In an isofield case, the inlet of the core should reach the incoming helium's temperature at a rate determined by the relaxation time of a single core segment. In order to estimate the relaxation time of a single core segment, while allowing for the possibility of a small convective heat transfer coefficient, it is necessary to make some assumptions about the convective model. For this analysis we will assume that the porosity is small enough so that the entrained helium relaxes to its steady-state solution at a much quicker rate than the helium and GGG come to their steady-state solution. This assumption implies that a simple convective model can be used at all times. The steady-state convective model was derived in Chapter 9:

$$T_{out} = T_g - (T_g - T_{in})\, e^{-\beta L}$$

with $\beta \equiv (\hbar\, P/\dot{m}\, c_p)$, L the length of a segment (0.25 cm), T_{in} and T_{out} the helium inlet and outlet temperatures, and T_g the uniform GGG temperature in the segment. The top segment at the inlet to the core receives helium from the warm-reservoir at a constant temperature T_{in}. The transient response of this segment can be studied in the isofield case. (Adding the active term, which results from a changing magnetic field, only causes a slight shift in the steady-state temperature.) The isofield heat balance for the top segment is:

$$\dot{m}\, c_p\, (T_{in} - T_{out}) = C\, L \frac{\partial T_g}{\partial t}$$

Putting the above two equations together we find:

$$\frac{\partial T_g}{\partial t} + \frac{\dot{m}\, c_p}{C\, L}\, (T_g - T_{in})\, (1 - e^{-t/\alpha}) = 0$$

where

$$\alpha \equiv \frac{C\, L}{\dot{m}\, c_p\, (1 - e^{-\beta L})}$$

The relaxation time for a single segment, α, is made longer by a finite convective heat transfer coefficient, β. Remember that this analysis applies only to the first segment in an isofield test.

Using the "typical" values presented in Chapter 9.7, we calculate the expected α, and find that a single segment should relax to the incoming helium temperature within $\sim$0.02 second. In order for the single segment relaxation time to be on the order of the cycle time (as was observed in the isofield test data), β would have to be $\sim$100 times worse than expected. β cannot be that poor, for if it were, we would experience an isothermal ΔT between the helium and GGG of at least 7 K. This was not observed.

There is another major factor which contradicts the assumption that inadequate convective heat transfer could cause the symptoms listed at the beginning of this section. The ΔT which results from convective heat transfer should get smaller as the magnitude of heat transfer per unit time gets smaller. Several tests were run with less field swing and proportionally less helium flow. Just the opposite occurred.

3) Maladjusted flow: Maladjusted flow causes similar problems as does inadequate convective heat transfer; however, there are several differences. With maladjusted flow the problem develops away from the inlet to the core section. At the inlet, maladjusted flow only exaggerates inadequate convective heat transfer slightly. For the same reasons that inadequate convective heat transfer cannot be the solution, neither can maladjusted flow.

4) Partially insulated helium porosity: It is very difficult to analyze the effects of partially insulated helium porosity since its effects vary significantly depending on the degree of insulation. However, it can be predicted that as the core warms up to temperatures above 10 K, the effect of any helium porosity becomes small. Much of the strange "start-up" phenomena that has been observed can be attributed to excess helium void, but steady-state operation of our core has been warm. Since bad warm-end behavior persists even when the core is warm, helium porosity must not be the cause of the problem.

5) Excess axial conduction: This is the one cause that can explain all the symptoms that have been observed. The effects of axial conduction were discussed briefly

in Chapter 9.5. In that discussion it was mentioned that even if the thermal conductance between GGG segments were infinite, heat still would not flow from the warm-reservoir to the cold-reservoir. The reason for this is that there are thermal resistances between each core section (a group 30 segments comprises a core section, the sections are each separated by a helium mixing chamber), and there are very large thermal resistances between the reservoirs and the ends of the core. Large thermal conductivity between the core segments allows each section to reach thermal equilibrium, but does not cause a thermal short between the reservoirs. In the limiting case where the thermal relaxation time of a core section is much faster than the cycle time, the core sections can be treated as a single segment of uniform temperature. This model is described in the next section on a first-order basis, where it is seen that high axial conduction can explain the observed test data.

Another factor which indicates that the main problem with our core is axial conduction is the cycle time dependence of the problem. It was found that if the cycle time was doubled from 10 seconds to 20 seconds, then the warm-end behavior gets worse. Flow related losses such as excess convective heat transfer and maladjusted flow become less with increased cycle time, while non-flow related losses such as axial conduction become worse.

11.4.3 First-Order Analysis of a Core With High Axial Conduction

In this section we analyze a thermally shorted section with a first-order description in order to understand the type of response that can be expected. The results are compared with the test data. One will see from this simple analysis that excess axial conduction at the warm-end can explain the test data that has been observed.

Refrigeration-type run (Figure 60a):

The first-order transient heat balance for a thermally shorted segment with a changing magnetic field is:

$$\dot{m}\, c_p\, (T_{in} - T_{out}) + \dot{Q}_T = C\, L\, \frac{\partial T_g}{\partial t}$$

where L in this case is the length of the shorted section. With reasonable convective heat transfer coefficient, β, the product βL is large enough to assume that the helium leaves the section at the section's temperature, $T_{out} = T_g$. The heat term $\dot{Q}_T$ represents the total heating of this core section due to magnetic interaction. For

the purpose of this first-order discussion we will assume that $\dot{Q}_T$ is constant. The solution to the above equation with constant T_{in} is:

$$T_g = T_{in} + (T_0 - T_{in})\, e^{-t/\alpha} + \frac{\dot{Q}_T}{\dot{m}\, c_p}\,(1 - e^{-t/\alpha}) \tag{13}$$

Where α is just $(C\,L/\dot{m}\,c_p)$, and T_0 is the initial temperature of the section. The steady-state solution for this equation is:

$$T_g = T_{in} + \frac{\dot{Q}_T}{\dot{m}\, c_p}$$

The transient decays to this solution at a rate determined by α. The steady-state solution for a section with an infinite number of segments (negligible axial conductivity) and good convective heat transfer is:

$$T_g = T_{in} + \frac{\dot{Q}_T}{\dot{m}\, c_p}\,\frac{x}{L}$$

Note that T_g at $x = L$ for the infinite segment case is equal to T_g steady-state for the single segment case. During the down-flow process, the thermally shorted warm-end section relaxes towards its steady-state solution. This behavior causes the warm-end to become ~3 K colder than the warm-reservoir by the end of the down-flow process. The adiabatic magnetization process begins with the warm-end up to 3 K colder than it should be. By the end of this process it is still ~3 K too cold. When the up-flow begins, the initial helium temperature out of the warm-end is too cold, but as the flow continues, the warm-end segment warms towards its up-flow steady-state temperature. The actual transient experienced by the warm-end section during the up-flow is not exponential, but is complicated because the incoming helium temperature is not constant. This behavior matches the test runs where the up-flow begins too cold, but then steadily rises towards the expected warm-end temperature.

Isofield Tests (Figure 60b):

The observed data from the isofield cases can also be explained by high axial conduction. The isofield equation for a thermally shorted section is Equation (13) with $\dot{Q} = 0$. If the core begins a down-flow process with a uniform temperature profile colder than the incoming helium temperature, then the warm-end section rises according to Equation (13), while the next section downstream of the warm-end section

receives helium at an exponentially increasing temperature. The dispersion of the convection wave that results from a finite number of segments (Chapter 9.3) occurs over the entire core since in this model it contains only four effective segments.

When the flow reverses for the isofield up-flow, the helium leaving the warm-end section begins at that sections final isofield down-flow temperature, which may be close to its steady-state solution of T_{in}, but then is immediately cooled by helium coming from the inner core sections which are colder than the warm-end. The warm-end temperature continues to drop during the up-flow.

11.5 Direct Measurement of the Core's Axial Conductivity

As was mentioned in Section 11.3, once it was determined that the system could not produce refrigeration with the present core, the core was cut out of the apparatus so it could be tested separately. The axial conductivity of the core was tested in the same temperature range (4 to 15 K) as it was designed to be operated. The core's jacket was thermally isolated, a liquid helium reservoir was attached to the cold-end, and an electric heater was attached to the warm-end. The purpose of this test was to apply heat to the warm-end, and to measure the temperature profile that developed as heat conducted down through the core to the cold-end.

Figure 61 shows a schematic of the test apparatus used to examine the axial conductivity of the core. This test was performed in an evacuated dewar. We were able to obtain a high vacuum of 10^{-7} torr throughout the test. Three stainless tubes entered the vacuum space through the top plate. Through one of these tubes we transferred liquid helium. Two-phase helium entered a copper separator located at the bottom of the dewar. Helium could leave the top of this separator and travel straight up stainless tube #2 and out of the top of the dewar, or it could leave the bottom of the separator and travel through the core before leaving the dewar by stainless tube #3. A thermofoil heater was attached to the tube at the top of the core. The sections of the tubes which connected the warm-end heater and the cold-end separator to the inside of the core were copper. This was necessary since phenolic plugs fill each end of the core jacket. Even with copper leading through the phenolic regions, there is still a large resistance to conduction from the copper to the GGG sections. For this reason the cold-end of the core could not be pinned at 4.2 in the absence of

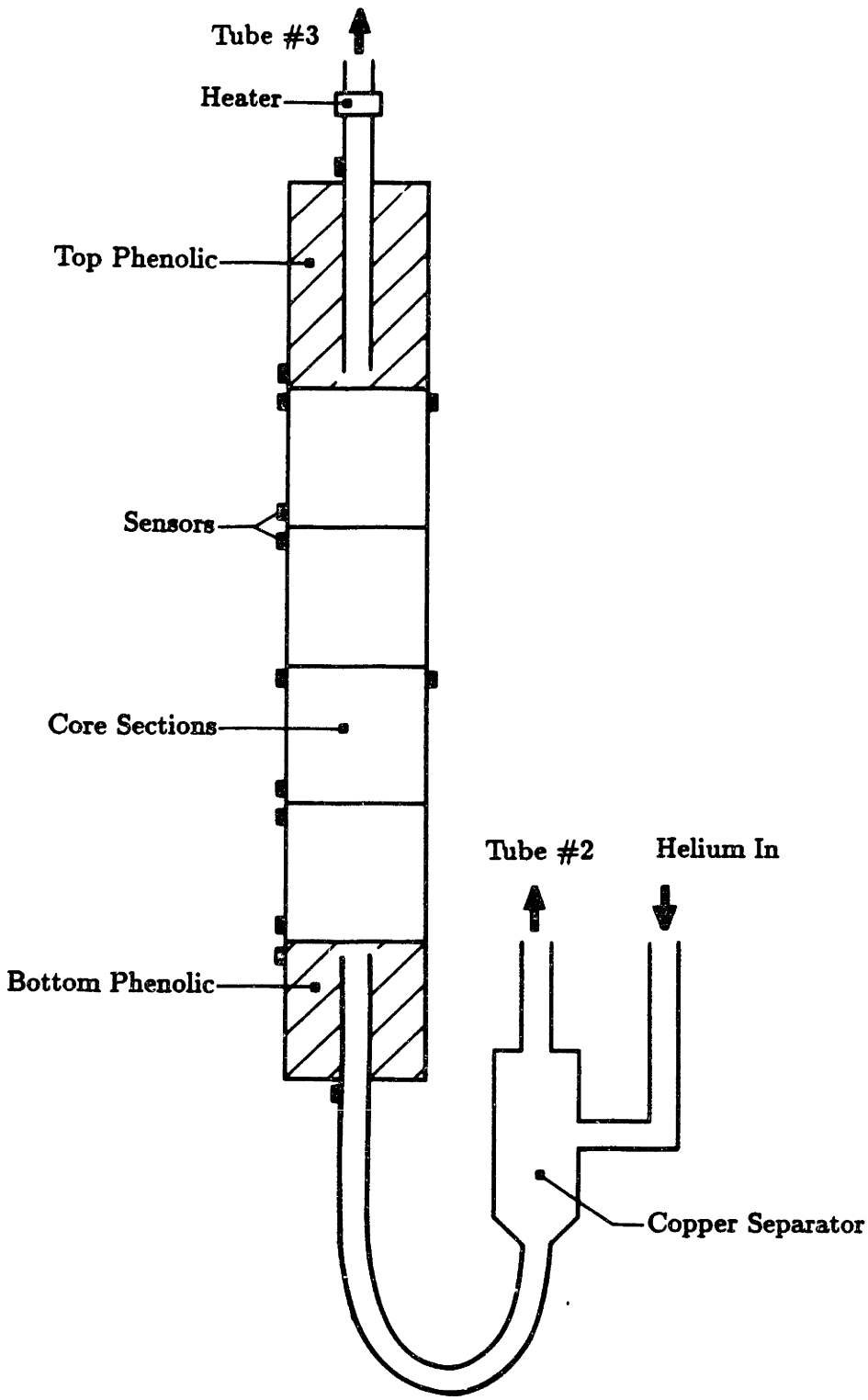

Fig. 61 Schematic of Axial Conduction Test

helium flow. A temperature sensor was located in the copper tube which leads into the cold-end of the core, and one was located in the tube leaving the warm-end of the core. Thirteen sensors were mounted in the vacuum on the outside of the core's jacket. They were attached with copper-powder-filled vacuum grease. These sensors are shown in Figure 61 as solid rectangles. All of the temperature sensor leads which passed through the vacuum space were thermally attached to the copper separator. We also found it necessary to thermally attach certain stainless parts of the core to the copper separator, since they were well isolated from the helium flow and did not cool down in initial experimental attempts. The entire experiment was wrapped in many layers of super-insulation.

As is the case with this type of experiment, any heat that leaks into the dewar eventually makes its way to the experiment. With helium flow though the core, the sensors located on the outside of the stainless core jacket settled out at about 5 K. When flow through the core was stopped, yet allowed to continue through tube #2, the temperature of the core jacket would rise to a steady state profile where the heat leaking in was balanced by the heat conducting out of the cold-end to the copper separator. As the warm-end heater was turned on, a new steady state temperature profile was reached. The steady state temperature drop through the core was recorded with no heater power, with 0.13 W applied, and with 0.29 W applied. Figure 62 shows the steady-state temperature profile with 0.29 W applied. The resulting temperature drop across the core for each case was:

Heat Flow, (W)	Core ΔT, (K)
$\dot{Q}_0$	2.7
$\dot{Q}_0 + 0.13$	4.2
$\dot{Q}_0 + 0.29$	5.7

where $\dot{Q}_0$ is the heat which conducts through the core with no heater power. Assuming that the conductivity is linear in this temperature range, $\dot{Q}_0$ can be calculated from simple ratios of the above data.

$$\frac{\dot{Q}_0}{2.7} = \frac{\dot{Q}_0 + 0.13}{4.2}$$

and

$$\frac{\dot{Q}_0}{2.7} = \frac{\dot{Q}_0 + 0.29}{5.7}$$

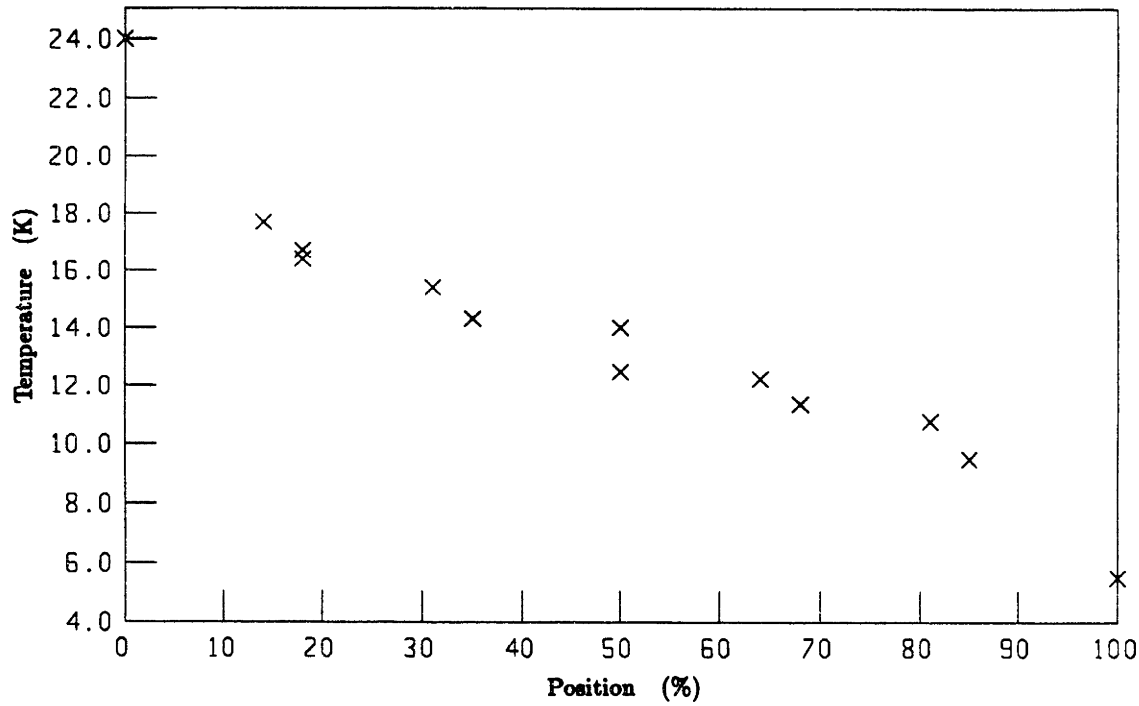

Fig. 62 Temperature Profile During Axial Conduction Test

From the first ratio we find $Q_0 = 0.23$ W, and from the second $Q_0 = 0.26$ W. The two sets of data are consistent, and they indicate an effective axial conductance of $\sim$0.09 $\mathrm{W\,K^{-1}}$. This is $\sim$10 times higher than the assumed value of $\sim$0.01 $\mathrm{W\,K^{-1}}$ (see Chapter 9.5).

In order to have an additional check on this data, the transient response of the core with no applied heat was also analyzed. When the helium flow through the core is stopped, the core heats from $\sim$5 K to its steady state profile, with the warm-end at $\sim$12 K. The sensor traces indicated that the core was heating at a rate of 0.043 $\mathrm{K\,s^{-1}}$ as it passed through 6 K. The zero field specific heat of the core at 6 K, including the rubber and stainless jacket, is $\sim$5 $\mathrm{J\,K^{-1}}$. From this $\dot{Q}_0$ can be calculated:

$$\dot{Q}_0 = (5\,\mathrm{J\,K^{-1}})\,(0.043\,\mathrm{K\,s^{-1}}) = 0.22\,\mathrm{W}$$

This value is the same as was estimated from the steady-state analysis, and it helps confirm our conclusions.

11.6 The Effect of External Helium Dead Volume

The detrimental effect of helium dead volume, which exists between the core and heat exchangers, was first suspected by examination of experimental data; it was then confirmed by computer simulation. Even a minimal amount of helium dead volume can seriously degrade the steady-state performance of the device.

The helium dead-volume includes: the space between the core and the connection tube (~2.7 cm^3); the connection tubes which lead to the heat exchangers (~7.8 cm^3 warm-end, ~1.8 cm^3 cold-end); and the funnel-shaped volume which leads the helium from the connection tube to the copper heat exchanger (~1.6 cm^3). When the copper heat exchangers are not stabilized, the entrained helium within in the copper's slits also acts as another source of dead volume. Table 17 shows the expected dead volumes and the entrained helium mass in each dead volume as a function of temperature with a helium pressure of 4 atm.

TABLE 17
Dead Volumes at P=4 atm

Temp. (K)	ρ ($g\,cm^{-3}$)	c_p ($J\,g^{-1}\,K^{-1}$)	(6.1 cm^3) Cold-End M (g)	(12.1 cm^3) Warm-End M (g)	(10.7 cm^3) Copper M (g)
4	0.141	3.24	0.86	1.70	1.51
5	0.124	5.53	0.76	1.50	1.32
6	0.083	16.89	0.51	1.00	0.89
7	0.043	10.05	0.26	0.52	0.46
8	0.031	7.55	0.19	0.38	0.33
10	0.022	6.25	0.13	0.27	0.24
12	0.017	5.86	0.10	0.21	0.18
15	0.013	5.61	0.08	0.16	0.14

11.6.1 Calculation of Dead Volume from Test Data

The dead space can act in one of two ways. If it stratifies, then helium flow can occur without mixing. The temperature sensor will not reflect the temperature of the oncoming helium until enough helium has flowed to purge the old helium out of

the dead volume. The sensor responds when $m_{in} = \rho V$.

If the dead space mixes, then we can write an energy balance as:

$$\frac{dT}{dm_{in}} = \frac{h_{in} - h}{\rho c_p V}$$

For constant c_p (a good assumption for the warm-end where the temperature is over 15 K, and a reasonable assumption for the cold-end provided that the temperature is between 2.2 and 5 K) $c_p T$ can replace h and the above equation can be rewritten as:

$$\frac{dT}{dm_{in}} = \frac{T_{in} - T}{\rho V}$$

The solution to this equation is:

$$T = T_0 - (T_0 - T_{in})\, e^{-m/\rho V}$$

In this case one constant of decay is reached when $m_{in} = \rho V$. This is the same criteria as is used for the stratified case.

Many test runs were analyzed in order to determine the helium dead space in our device. In this analysis one must first determine whether the conditions are stratified or mixed; and if the conditions are stratified, how much of the void lies between the temperature sensor and the incoming helium. Also, only test cases which stayed clear of the critical point (5.6 K) were considered. This limited the selection of cold-end test cases.

The warm-end dead space was calculated from ~15 test cases. The calculated values ranged from 11.5 cm^3 to 21.5 cm^3. The cold-end dead space was calculated from only 4 test cases. The calculated values ranged from 5 cm^3 to 7 cm^3. The cold-end values were as expected: ~6.1 cm^3. While the warm-end values showed greater scatter and ranged up to almost twice the expected value of 12.1 cm^3. This can be attributed to the greater uncertainty in the warm-end helium flow rate, as well as to the greater effect of parasitic heat loads at higher temperatures.

11.6.2 Computer Simulation with Dead Volume

The original computer simulation program did not include a model for external helium dead space. It has since been modified to include a dead space model. The

basic core model was also modified in order to include the rubber encapsulant in the mathematical expression for the specific heat (Chapter 9.2). In Chapter 5.2.2, Table 7 shows that the computer simulation program predicted that steady-state refrigeration could be achieved with the use of a perturbation field. Table 18 shows the net refrigeration for several different cycle parameters as predicted by the new core model. Though the numbers may differ from Table 18 to Table 7, the basic cycle behavior is the same. The subscript $_v$ refers to helium dead volume present, while the subscript $_n$ refers to no dead volume.

TABLE 18
Computer Simulation, 2 Independent Fields
(10 second cycle time)

T_{R_c} (K)	T_{R_w} (K)	ΔH_{ad} (T)	M_T (g)	$\dot{Q}_c$ (w)	$\dot{Q}_w$ (w)
4.2	15.	A_n	1.6	0.00	2.0
4.2	15.	A_n	1.8	0.01	2.1
4.2	15.	A_v	1.8	−0.32	1.4
4.2	15.	B_n	2.0	0.16	2.5
4.2	15.	B_v	2.0	−0.07	1.7
4.2	15.	C_n	1.75	0.13	2.3
4.2	15.	C_v	1.75	−0.05	1.8

A: Cold-end mag: 0.5, demag: 0.5; Warm-end mag: 1.0, demag: 1.0.
B: Cold-end mag: 0.25, demag: 0.5; Warm-end mag: 1.0, demag: 1.0.
C: Cold-end mag: 0.0, demag: 0.5; Warm-end mag: 1.0, demag: 1.0.

11.6.3 Explanation of Cycle Sensitivity

The detrimental effects of helium dead space are predicted by the basic wave analysis presented in Chapters 6 through 8. The extra enthalpy introduced into the core by external dead volume occurs at the beginning of the down-flow. This warm isothermal imbalance is carried into the center of the core by a convection wave. When the flow reverses for the up-flow path, the warm isothermal imbalance is carried towards the warm-end, but since the convection wave moves farther on the down-flow than on

the up-flow, the warm isothermal imbalance is trapped in the core.

It should be noted that if one were to spread out the extra enthalpy and assume that it enters the core uniformly during the down-flow, then a problem would not arise. Only the enthalpy which enters the core at the beginning of the down-flow is trapped in the core, the rest comes out during the next up-flow process.

- External Dead space at the cold-end will reduce cycle efficiency but should not add to the field-flow imbalances which result in thermal pollution of the cold-end reservoir.

- External Dead space at the warm-end will add to the field-flow imbalances which travel down the core and pollute the cold-end reservoir.

11.7 Refrigeration Runs – The effect of the Perturbation Field

After the Phase One testing program, it was decided that even if the regenerator core worked exceedingly well, the system still could not produce refrigeration with its present field-flow phasing. At that time the Phase Two modifications were suggested, and a perturbation coil was added to the main coil. There were many reasons to suspect that the perturbation field would provide the necessary degree of field-flow control that would enable us to achieve steady-state refrigeration. Unfortunately, the core performance turned out to be poor, and our goal was never achieved.

Many tests were performed with cycle parameters which we hoped would produce steady-state refrigeration. Of these tests, there were several sets of runs where the amount of perturbation field was varied, but all other cycle parameters were held constant. It was expected that the steady-state performance of the device would be better with the perturbation field than without. Comparison of the test results indicated that the perturbation field made little difference to the steady-state performance in that the warm-end and cold-end temperature traces were similar. An indication of how well a cycle is working is the amount of refrigeration (or in our case negative refrigeration) produced by the cycle. The less heat that is dumped into the cold-reservoir, the better the cycle. Since our cold-reservoir was not stabilized to warming, as heat is dumped into it by a bad cycle, its temperature rises. Figure 63a shows both the cold and warm-end temperatures during a refrigeration-type cy-

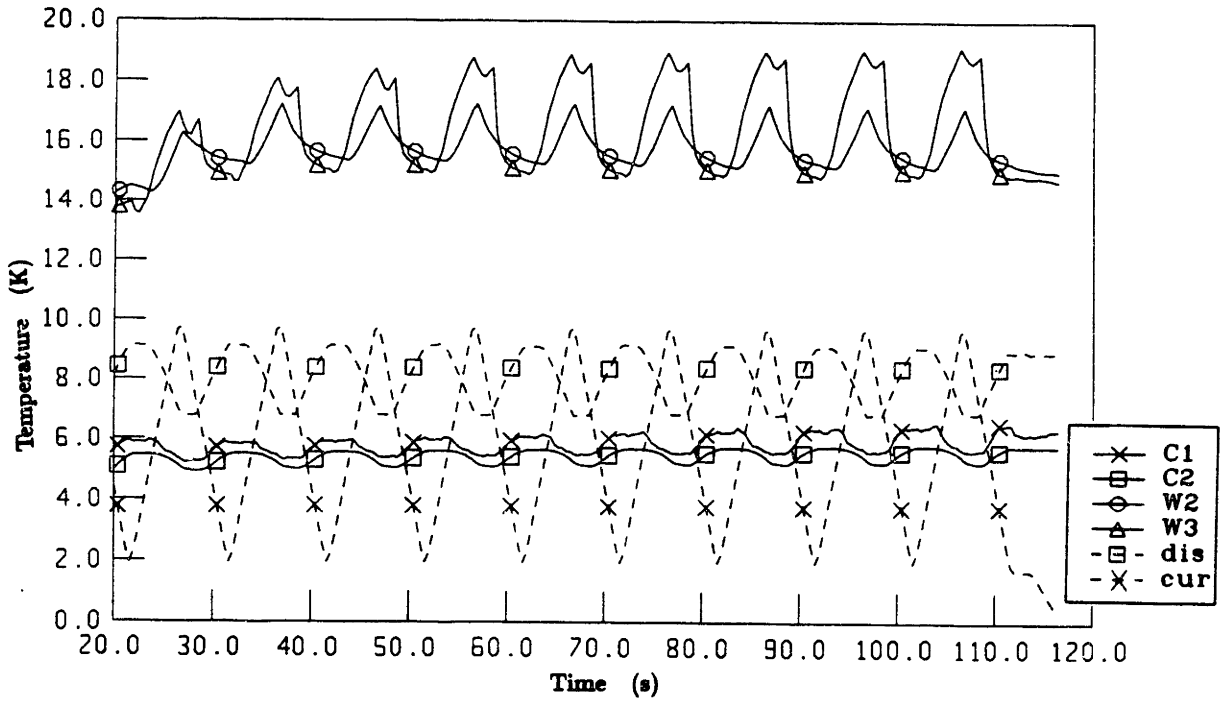

Fig. 63a Refrigeration-Type Run without Perturbation Field

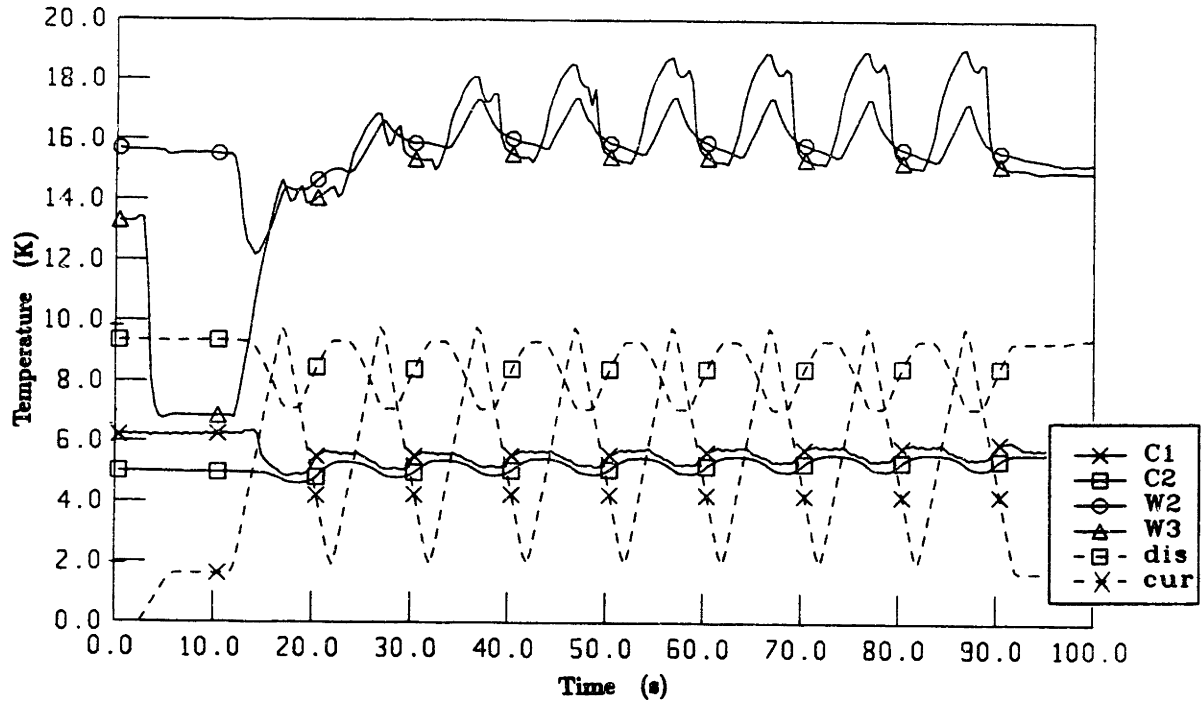

Fig. 63b Refrigeration-Type Run with Perturbation Field

cle without perturbation, and Figure 63b shows the same cycle with perturbation. Careful measurement of the rate of increase of the cycle averaged temperature C2, reveals that the runs with perturbation performed slightly better than without. This was true for all cases tested.

Why not greater effect by perturbation field?

The perturbation field did not have a significant impact on cycle performance. The reason for this has to do with the nature of the core problems discussed earlier in this chapter. The purpose of the perturbation field is to produce a steeper temperature gradient at the warm-end. The axial conductivity problem in the core causes temperature gradients to decay. By steepening the temperature profile, we cause greater losses by axial conduction. The excessive axial conductivity in the core tends to eliminate the benefits of the perturbation field.

XII. DISCUSSION – DESIGN OF THE NEXT GENERATION CORE

12.1 Introduction

In Chapter 4 a cycle design procedure was outlined for the Ideal Carnot system. In that analysis the core was assumed to be ideal in that there were no irreversibilities and no helium entrainment. In addition, the magnetic field was allowed to be an arbitrary function of time (t) and position along the core (x). It was found that Carnot cycles could be followed by every segment in the core with this model. In practice the field function will be much more limited, and the individual segments along the core will not follow Carnot cycles. Much of this thesis has dealt with nonideal behavior of our present GGG cored system.

This chapter discusses briefly some of the issues involved in design of a next generation device. It is clear from previous analysis in this thesis that if we are to refrigerate over large temperature ranges, then proper initial core design is critical. The design issues discussed in this chapter are:

1. the choice of thermodynamic cycle,
2. flow induced irreversibilities in a "perfect" core,
3. selection of paramagnetic materials,
4. the helium porosity,
5. the helium pressure,
6. the magnetic field profile, and
7. the cross sectional area of the core.

Sections 12.2 and 12.3 discuss the design equations pertinent to adiabatic and isothermal path design, and section 12.4 gives a brief outline of one possible design procedure.

12.1.1 What type of Thermodynamic Cycle?

In Chapter 8 we found that the most efficient thermodynamic cycle is the cascaded-Carnot, and that it should be the goal of the designer to approach this cycle. In Chapter 7 it was stated that the adiabatic-isofield cycle could not produce refrigera-

tion over a large temperature range under any circumstance. These statements were based on the use of GGG as the paramagnetic material and may not be true if a paramagnetic material with a Curie temperature higher than the warm-end temperature is used (see below). In any case, we believe that the cycle which poses the greatest potential for cycle efficiency is the cascaded-Carnot cycle in that it minimizes the steepness of the temperature gradient within the core. In the cascaded-Carnot cycle helium flow occurs only during isothermal paths. Most of this chapter deals with parameter selection with this cycle in mind.

12.1.2 Irreversibilities in a "Perfect" Core

It is possible for irreversibilities to be generated in a perfect core (as defined in Chapter 4) when it experiences non-isothermal flow paths. Nonlinear (or thermally dependent) properties of the helium and GGG cause the convection wave to change shape as it progresses through the core. If the upstream end of the convection wave has a higher velocity than the downstream end, then the convection wave will tend to steepen. In a perfect core the wave can reach a step change in temperature, and further helium flow must produce entropy as the wave "crests over" on itself. In a real core the wave will reach a steepness where the dispersion caused by axial conduction, a finite number of segments, and nonperfect heat transfer balances the steepening caused by nonlinear properties.

Since the goal of our design is to have isothermal flow paths, it is not necessary for us to develop a detailed analysis of this type of loss. However, if other types of cycles are attempted, or if it is found that isothermal paths cannot be approximated with an actual system, it would then be necessary to fully understand the implications of this problem.

12.1.3 Selection of Paramagnetic Materials

One of the main parameters available for selection by the design engineer is the paramagnetic salt or salts used. The selection the proper paramagnetic salts will facilitate other design choices. The characteristic temperature of a paramagnetic salt is the Curie temperature. Figure 64 shows a typical paramagnetic's entropy curves as a function of temperature at constant applied field. At temperatures below the Curie temperature, the entropy curves at constant field tend to diverge with

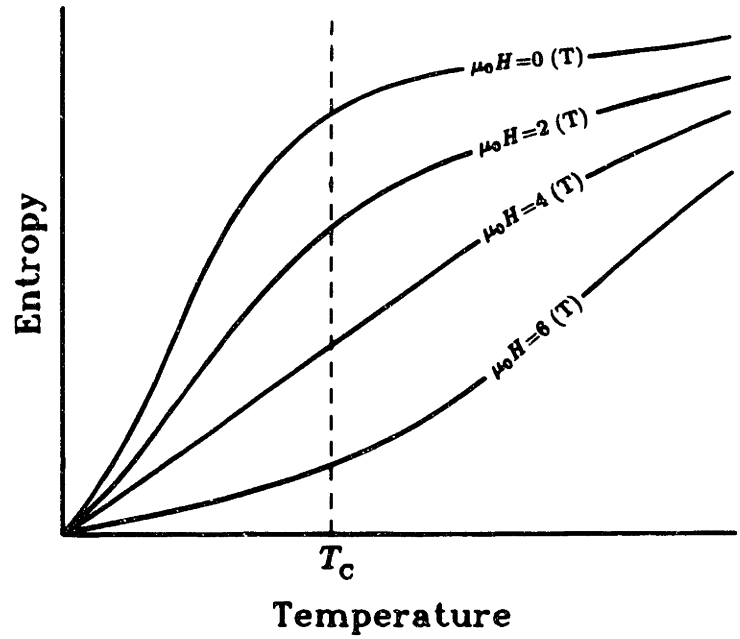

Fig. 64 Entropy Curves for a Typical Paramagnetic Material

increasing temperature. That is, constant field entropy curves increase with temperature more quickly at lower applied fields, or the specific heat at constant field ($c_H = T\,dS_g/dT|_H$) at a given temperature decreases with increasing field. At temperatures above the Curie temperature the trend reverses. The constant field entropy curves increase with temperature more quickly at higher applied fields. When they converge, the specific heat at constant field increases with increasing field. The Curie temperature for GGG is about 0.8 K. When GGG is used for refrigeration over the temperature range of 4.2 to 15 K, the specific heat at constant field increases with magnetic field.

If one uses a paramagnetic material with a Curie temperature higher than the warm-end temperature, then the dependence of specific heat with field is reversed throughout the core. Reversing this dependence reverses the direction of net propagation of isothermal imbalances. The same issues which led to thermal pollution of the cold-end reservoir in Chapters 7 and 8 may not be important when a high Curie temperature paramagnetic salt is used.

The boundary which separates regions of increasing specific heat with applied field from regions of decreasing specific heat with applied field does not occur exactly at the Curie temperature, but instead increases from the Curie temperature with increasing applied fields. Mathematically we can write this boundary as:

$$\frac{\partial}{\partial H}\left(T\frac{\partial S}{\partial T}\Big|_{H}\right)=0$$

Using Maxwell's relations we can translate this to:

$$\frac{\partial^2 S}{\partial H \partial T}=\frac{\partial^2 S}{\partial T \partial H}=\frac{\partial}{\partial T}\frac{\partial S}{\partial H}=\frac{\partial^2 M}{\partial T^2}\Big|_{H}=0$$

We find that the specific heat at constant field increases with field when the curvature of the isofield magnetization curves is positive. The curvature becomes negative when magnetic saturation effects become large.

For design of the cascaded-Carnot cycle other paramagnetic properties are important. For the adiabatic processes the isentropic change in temperature with field is important, and for the isothermal processes $TdS|_T$ is important. The thermodynamic properties of GGG are shown in Appendix E. Even though the isothermal ΔS is maximum around the Curie temperature, the isentropic derivative $\partial T/\partial H$ and the isothermal derivative $T\partial S_g/\partial H$ continue to increase up to ~10 K. Proper field-flow phasing is more easily achieved when a paramagnetic is used at temperatures below its maximum isentropic derivative. In this range simple field modifications can be used to correct improper adiabatic processes. With proper design of the other cycle parameters, GGG is effective up to ~10 K.

Before proceeding with the cycle design, one should assemble thermodynamic information for all paramagnetics which have a Curie temperature around the temperature range of refrigeration.

12.1.4 The Helium Porosity

Helium porosity both adds zero field specific heat to the core and leads to the breathing effect. It is advantageous to minimize the zero-field specific heat in order to increase the temperature swings available and to minimize the percentage of the field swing needed for the adiabatic part of the cycle. It is also advantageous to minimize the breathing effect. The breathing effect produces flow at the wrong cycle time. It

also complicates cycle analysis. For these reasons it is best to choose a core porosity which is as small as is mechanically possible, also considering viscosity induced losses that may result if the helium pressure drop though the core becomes too large. (It was found for our core that the viscosity induced losses were negligible for the smallest flow channel size that was mechanically possible to construct.)

12.1.5 The Helium Pressure

Our experimental device was designed to be operated at supercritical helium pressures. We chose this design before we fully understood the problems involved in cycle control. The logic for this choice was as follows:

> Atmospheric helium will experience a phase change in the cold-end (4.2 k) of our device. If there is liquid helium in the core at the beginning of an adiabatic magnetization, then this helium will evaporate. The cold-end of the core will be thermally anchored by the phase change and a large breathing effect will result. The large breathing effect will overwhelm the warm-end of the core, cooling it even though it is being magnetized. A proper adiabatic magnetization would therefore be impossible.

As we now understand from the wave analysis presented in Chapters 6 through 8, it is not possible to avoid isothermal imbalances during the cycle, and the net result of these imbalances is to warm the cold-end at the end of the down-flow process to a temperature above 4.2 K. All liquid helium should be purged from the core by this action. The decision to use supercritical helium as opposed to atmospheric should be reëxamined. (If, for example, another paramagnetic is used which allows for operation below its Curie temperature, then this purging behavior will not exist. In this case supercritical helium may have to be used.)

As was mentioned in section 12.1.2, non-isothermal process may generate entropy when the thermal properties of the helium and GGG vary with temperature. This type of loss can be minimized by reducing the temperature variation of the helium properties. For this reason operation at a pressure slightly above critical point should be avoided.

The helium pressure influences the breathing effect by dictating the density of the helium entrained in the core. The breathing effect can be minimized for a given

helium porosity by reducing the helium pressure to atmospheric or below. By doing this we could operate from 4.2 to 15 K with only helium vapor in the core.

One disadvantage of lowering the helium pressure is that the losses associated with helium pressure drop become larger. In our device, pressure drop induced losses are never significant.[10] However, in a new design with lower helium pressure, all losses should be reëxamined. Another disadvantage of low helium pressure is that the displacer size must increase correspondingly.

12.1.6 The Magnetic Field Profile

In Chapter 4 we allowed the field to vary as an arbitrary function of time (t), and position along the core (x), $H(x,t)$. In real systems it will be difficult to accomplish this degree of freedom. For an initial design choice the system should be kept as simple as is possible; that is, the magnetic system should consist of a single solenoid and current supply. A single solenoid need not produce a uniform field. The field can be shaped as a function of x by varying the number of turns with x. (The task of finding a practical solenoid design to produce an arbitrary field profile may not be easy.) The functional dependence of the field produced by a single solenoid can be written as:

$$H(x,t) = k(x)\, H_0(t)$$

where the function $k(x)$ shapes the field along the axis of the solenoid, and $H_0(t)$ varies with time according to the applied current. It is important to note that a degree of freedom has been lost by this choice; an arbitrary function of time times an arbitrary function of position cannot in general be made to match an arbitrary function of time and position.

12.1.7 The Cross Sectional Area

It is possible for the cross sectional area of the core to vary with position (x). This option is discussed in section 12.3. The ratio of core length to cross sectional area influences the irreversibilities generated in the core. The axial conduction losses decrease with decreasing cross sectional area, and the flow related losses increase with decreasing cross sectional area. The average value should be chosen to minimize these losses.

12.2 Design Equation for the Adiabatic Processes

In order to design the adiabatic process we first look at equation (8) presented in Chapter 6.5.

$$\frac{dT}{dH} = \frac{(1-por)A\rho_g}{C}\left(-T\frac{\partial S_g}{\partial H}\Big|_T\right) \quad \text{(K/T)} \tag{7}$$

where C is the specific heat of the core per unit length. Substituting the expression for C, we can rewrite the above equation:

$$\frac{dT}{dH} = \frac{(1-por)A\rho_g\left(-T\frac{\partial S_g}{\partial H}\Big|_T\right)}{(por)A\rho_{he}c_p + (1-por)A\rho_g\, c_H}$$

or:

$$dT|_a = \frac{1}{\left(\frac{por\,\rho_{he}\,c_p}{(1-por)\,\rho_g\,c_H}\right)+1}\frac{\partial T}{\partial H}\Big|_{S_g} dH|_x$$

where the relation

$$-\frac{\frac{\partial S_g}{\partial H}\Big|_T}{\frac{\partial S_g}{\partial T}\Big|_H} = \frac{\partial T}{\partial H}\Big|_{S_g}$$

has been used. In writing the adiabatic equation this way we can see more clearly how the helium porosity can effect the adiabatic process. Also note that dH is taken at constant x. Since we may now allow the field to vary with x it is necessary to add this nomenclature. Noting the functional dependence of various terms in the above equation, we can rewrite it as:

$$dT|_a = f_1(T,H)\,dH|_x \tag{15}$$

In this equation f_1 is a function of temperature and field only, it is completely specified by selection of:

1) the porosity of the core,
2) the pressure of the helium,
3) the paramagnetic salt(s) used.

The other part of Equation (15) is $dH|_x$. In general $dH|_x$ may be various functions of time (t) and position along the core (x), but as was mentioned above in Chapter 11.1.6, the single solenoid field is more restricted. With the nomenclature introduced in that section:

$$dH|_x = k(x)\,dH_0$$

The adiabatic path (in the absence of breathing induced flow) is not time dependent. Each segment of the core reacts independently with the applied magnetic field. Given a specified starting condition, the final temperature can be determined by the final field:

$$[T_f(x) - T_i(x)]_a = \int_{H_i(x)}^{H_f(x)} f_1(T,H)\, dH|_x$$

Chosing the magnetic materials

Figure E-5 in Appendix E shows the isentropic temperature change per change in field for GGG. Note that these curves peak at around 10 K. This is significantly above the Curie temperature of 0.8 K. In Chapter 8 it was determined that the temperature profile in the core must be steeper for the up-flow than for the down-flow process. This can be accomplished (neglecting the breathing effect) if the rate of isentropic temperature change increases over the temperature range of operation. It is for this reason that GGG is a good paramagnetic salt for use in a cascaded Carnot system up to a maximum temperature of 10 K. When going above 10 K, a different paramagnetic salt is desirable. One such choice is DAG (Dysprosium Aluminum Garnet). A core could be designed with several paramagnetic salts, each one with increasing $\Delta T|_a$ over the temperature range it is applied.

It is possible to gain greater property variation, and to avoid step transitions, by using more than one paramagnetic salt in a single segment. If for example, GGG is used in the cold-end of the core, and DAG in the warm-end, then the transition segments should consist of a combination of these two salts in thermal contact with each other. The thermodynamic properties of these segments can be determined by accounting properly for the fractional percents of each component.

12.3 Design Equation for the Isothermal Processes

As described in Chapter 6, in order to maintain an isothermal path along the length of the core, the heat associated with magnetic interaction must be balanced by the cooling due to the helium flow. In general, it is not possible to maintain a perfect match between these two interactions, and isothermal imbalances will develop. It is the goal of the designer to minimize the negative effect of isothermal imbalances.

To do this we must first examine the isothermal equation developed in Chapter 6.2.

The equation derived there is:

$$\frac{dT}{dx} = \frac{(1-por)A\rho_g}{c_p}\left(-T\frac{\partial S_g}{\partial H}\Big|_T\right)\frac{\dot{H}}{\dot{m}} \quad \text{(K/cm)} \tag{7}$$

where the time derivatives can be removed by replacing $(\dot{H}/\dot{m})$ with $(dH/dm)|_x$. Equation (7) can be rewritten as:

$$\frac{dT}{dx} = f_2(T,H)\,A\,\frac{dH}{dm}\Big|_x \tag{16}$$

In this equation f_2 is a function of temperature and field only. Just as in the adiabatic case, f_2 is completely specified by the selection of the paramagnetic salt(s), the helium void and the helium pressure. In writing the isothermal equation this way we see that it is simular to the adiabatic equation except that we have two additional independent functions: A and dm.

The isothermal process is time dependent. Each increment of mass flow must satisfy Equation (16), but as was described in Chapter 6, it may not be possible to maintain a true isothermal path throughout the core. To see when isothermal paths can be maintained, we examine the functional dependence of the individual terms found in Equation (16). The isothermal slope is by definition a function of position only. The cross sectional area is a function of position only. The mass flow is an independent function of time only. The material function f_2 is stated to be a function of temperature and field, but since the temperature profile in an isothermal process is by definition a function of position only, the temperature dependence can be replaced by a position dependence. The field dependence is a also a function of time and position; f_2 is therefore a function of time and position only. This allows us to write:

$$T = f(x), \quad H = f(x,t) \quad : \quad f_2(T,H) \Rightarrow f_2(x,t)$$

$$\frac{dT}{dx}(x) = f_2(x,t)\,A(x)\,\frac{dH(x,t)}{dm(t)}\Big|_x$$

In Chapter 4 we were able to obtain isothermal profiles by allowing dH to be an independent function of both time and position. By doing this we were able to cancel the arbitrary time dependence in f_2. If, however, we choose the single solenoid field profile where

$$dH|_x = k(x)\,dH_0(t)$$

we can then combine terms in Equation (16) to get:

$$\frac{dT}{dx}(x) = f_2(x,t)\, Ak(x)\, \frac{dH_0}{dm}(t) \tag{17}$$

The left side of equation (17) is a function of x only. For the right side to be a function of only x, the time dependence which occurs in function f_2 must be cancelled by the time dependence of dH_0/dm. This can only be done if the time-position dependence of f_2 is separable. Actually this result was already presented. Refer to Chapter 6.4 and look at Figure 29, the isothermal slope. In general, this function is an arbitrary function of temperature and field. It was noted that the temperature-field dependence of this function was such that the isothermal profile changes with field (the temperature-field dependence is not separable). However, it was also pointed out that a refrigeration process operating over the temperature range of 10 to 15 K had very little change in isothermal profile with field. If you look at the isothermal slope over this temperature range, you will note that the temperature-field dependence is almost separable in this temperature range. The helium pressure and paramagnetic salts should be chosen when possible to produce a separable isofield slope function.

The area function $A(x)$ can be used to alter the shape of all the isothermal profiles together, but cannot be used to cancel the field dependence. The profiles shown in Figures 30 through 32 (Chapter 6) have been made assuming a constant cross sectional area of the core. If we double the area of the core every where, then profiles become twice as steep. In order to span the same temperature range, the helium flow rate must also be doubled. These two effects cancel and the profiles are unaffected. If we just double A at the cold-end, but not the warm-end, the slope becomes twice as steep at the cold-end only. When the flow rate is subsequently increased to keep the same temperature range, the profiles end up steeper at the cold-end, and less steep at the warm-end.

If we only look at the isothermal paths, then the area function is irrelevant, but when we start to piece the adiabatic paths together with the isothermal paths, we see the importance of $A(x)$. $A(x)$ can be used to alter the shape of the isothermal profiles, and in so doing can be used to change the required adiabatic paths. When one considers varying $A(x)$ he must also consider the effect this would have on the magnet design.

12.4 One Possible Design Procedure

Optimize the Adiabatic Paths:

- Choose the paramagnetic materials such that ΔT_a is increasing throughout the temperature range.
- Choose initial up-flow and down-flow profiles which are consistent for Carnot cycles according to the Second Law (see Chapter 4).
- Determine ΔT_a from the profiles.
- Determine the minimum value of H_0 before adiabatic magnetization, the value of H_0 after magnetization, and the field shape function k(x) which matches the function ΔT_a.
- Do the same for the adiabatic demagnetization path.
- Iterate with all the above until both adiabatic paths use the same field shape function.

Optimize the Isothermal Paths

Once we have selected f_1 from the adiabatic analysis, f_2 is also specified.

- Create isothermal temperature profiles (as in Chapter 6) for the field ranges that are already determined by the adiabatic analysis.
- Compare to the assumed isothermal temperature profiles.

Iterate for best compromise cycle

- Consider varying the initial temperature profiles and the maximum and minimum fields.
- Consider varying the area function to alter the adiabatic analysis
- Consider different paramagnetic salts and helium pressures

Note: Since the worse isothermal imbalances result from improper adiabatic paths (Chapter 8) it is more important to optimize the adiabatic paths than to optimize the isothermal paths.

CONCLUSIONS

This thesis began with the experimental apparatus which was received from Taussig's thesis.[10] A new design goal was decided in that we would build a system which could produce ~0.5 W of refrigeration over the temperature range of 4.2 to 15 K. After examining the old test apparatus it was decided that:

A. The reservoir temperature controls and the fluid displacement systems needed to be replaced.

B. The original core and magnet systems could be reused.

Unfortunately, these decisions where made before we fully understood some of the difficulties involved in cycle control of a magnetic refrigerator based on active regeneration. As our work proceeded, many types of analysis where performed. From these analyses came three primary cycle parameters which influence the overall cycle behavior.

1. Convection Wave Travel Distance: The amount of helium shuttle mass which can best approximate an isothermal path decreases with increasing temperature range. At some temperature range the convection wave (associated with any isothermal imbalances) does not travel the length of the core. When this happens extra heat associated with imperfect field-flow phasings and with irreversibilities accumulate within the core. Small temperature range applications allow for a significant advantage in cycle control; in that, the effects of improper field-flow phasing can be washed out of the core during each isothermal path.
2. The Curie Temperature: The Curie temperature of a paramagnetic is approximately where the curvature of the isofield magnetization curves go from negative to positive. Positive curvature implies that the core's specific heat increases with temperature, negative curvature implies that the core's specific heat decreases with temperature. Over a single cycle isothermal imbalances may accumulate in the core (item 1. above). Over many cycles these imbalances have been shown to move towards the Curie temperature. Since the Curie temperature of GGG is ~1 K, isothermal imbalances move towards the cold-end of our core.
3. Maximum Isentropic ΔT: Cascaded Carnot cycles can be approximated in a regenerator with a fairly uniform magnetic field profile if the maximum temper-

ature of operation is below the temperature where $\Delta T|_s$ is maximum. Since GGG peaks around 10 K, it is best to use another paramagnetic above this temperature, although GGG can be used to higher temperatures with greater field perturbation.

We chose a design goal which was inherently difficult to achieve as our system attempted to operate on the wrong side of all the above parameters. We used a single paramagnetic, GGG with Curie temperature of $\sim$ 1 K, to refrigerate over the temperature range of 4.2 to 15 K. In order for a regenerative device to refrigerate successfully under these conditions, the field-flow phasing must be "proper," and the regenerator must produce minimal irreversibilities. Either improper field-flow phasing or poor regenerator performance can lead to large isothermal imbalances superimposed on the attempted Carnot cycles. As described in item 1 above, these imbalances end up trapped in our core, and as described in item 2 above, they eventually make their way down to the cold-end, reducing or even eliminating all net refrigeration.

- Field-Flow Phasing: We found that the original field design did not allow for "proper" field-flow phasing. To help correct this problem we added a perturbation coil to the main coil.
- Regenerator Performance: The regenerator did not perform as expected.

Irreversibilities in the Regenerator Core:

In order to successfully operate a regenerative magnetic refrigerator over a large temperature range, the field-flow phasing must provide a workable thermodynamic cycle, and the regenerator must produce minimal irreversibilities. Irreversibilities may be generated in the core by the following sources:

1. Finite convective heat transfer between the helium and GGG,
2. Finite number of segments in the core,
3. Maladjusted flow,
4. Partially insulated helium void and parasitic heat loads,
5. Axial conductivity,
6. Helium pressure drop.

Even if the helium void is in full thermal-contact with the GGG, the breathing effect may produce excess helium flow which may in turn damage the field-flow phasing. Bad field-flow phasing may exaggerate the above irreversibility sources.

Our core failed on two of the above design considerations.

- The helium porosity was found to be twice the design value,
- The axial conductivity was found to be about 10 times greater than the design value.

The next generation core:

Successful correlation of the computer simulation output with both test data and first-order logic presented throughout the thesis indicates that the dynamics of active regeneration are now understood. It was found that proper initial selection of the core parameters facilitates other design considerations; the most critical design step involves selection of the paramagnetic salts. Field modification can then be used to fix minor cycle imperfections. A design procedure for the next generation device is outlined in Chapter 12.

Glossary of Terms

This is a partial list of terms which are either specific to this thesis or are used in a specific way in this thesis.

Thermodynamic Cycle: A thermodynamic cycle is defined by completely specifying the applied magnetic field as a function of both time and space, and the forced helium mass flow as a function of time (see the definition of *Forced Helium Flow* below). It should be noted that the independent variable time loses its significance in the absence of irreversibilities such as axial conduction, peripheral heat loss, and finite convective heat transfer between the GGG and helium. In this case the thermodynamic cycle can be completely defined by specifying the forced helium flow as a function of the applied magnetic field.

Cycle Efficiency: The cycle efficiency used in this paper compares the actual work per refrigeration with that of the Carnot:

$$\eta = \frac{\frac{\dot{W}}{\dot{Q}_c}\Big|_{Carnot}}{\frac{\dot{W}}{\dot{Q}_c}\Big|_{actual}} = \frac{\frac{T_w}{T_c} - 1}{\frac{\dot{Q}_w}{\dot{Q}_c} - 1}$$

In this equation T_c and T_w are the cold and warm reservoir temperatures, $\dot{Q}_c$ is the refrigeration, and $\dot{Q}_w$ is the heat of rejection.

Cycle Processes: A complete cycle can be broken into a set of processes. For example, a Carnot cycle consists of an adiabatic magnetization, an isothermal magnetization, an adiabatic demagnetization, and an isothermal demagnetization. Our cycle processes are more generic and are defined as either magnetization or demagnetization with some amount of forced helium flow (zero being an allowable amount). The up-flow, in which helium is forced to flow through the core from the cold reservoir to the warm reservoir, occurs during the magnetization processes, and the down-flow, with opposite flow from the up-flow, occurs during the demagnetization processes.

Low-Flow-Rate and High-Flow-Rate Processes: In general, each segment of the core is subject to two energy interactions: that due to convection of helium through the

core and that due to magnetization of the GGG. In a "Low-Flow-Rate" process the magnetization effects dominate, and in a "High-Flow-Rate" process the convection effects dominate. In an isothermal process the two effects are equal and cancel. It is possible (or even likely) that the core will be "Low-Flow-Rate" at one end and "High-Flow-Rate" at the other end during the same process.

The Breathing Effect: When the core changes temperature due to magnetic field interaction, the helium entrained within the core also changes temperature. If the pressure of the helium is kept constant, then the density of the helium must be allowed to vary. As the core is heated, entrained helium expands and flows out from the ends of the core; as the core is cooled, helium is pulled back into the core. This field induced flow is referred to as the breathing effect.

Forced Helium Flow: Due to the Breathing Effect, the helium flow at the cold-end of the core may not equal the helium flow at the warm-end. The simulation program assumes that the flow is determined at the cold-end. This assumption corresponds to our real system since the helium is driven by a displacer located in the cold end. The forced helium flow is that which enters (positive) or leaves (negative) the cold end of the core.

Adiabatic Process: The breathing effect makes it impossible to run an adiabatic path throughout our core. The best we can do is approach an adiabatic path. For the purpose of this project, an adiabatic process is one which has zero forced helium flow. In this case the cold-end will be adiabatic, but the warm-end will have helium flow which is induced by breathing from various locations along the core.

Cyclic Steady-State: The temperature profile of the core changes in a complicated way as the thermodynamic cycle proceeds. It is for the most part warmer during the up-flow and colder during the down-flow, but there is at no time an isothermal path. A cyclic steady state is reached when the core has the same temperature profile at any given cycle time. We can define the cycle to begin as the field starts to increase from its minimum value. This is at the end of the down-flow. When a steady state is reached, the beginning temperature profiles are identical from cycle to cycle.

Thermal Pollution of the Reservoirs: The goal of our system is to transport heat out of the cold-end reservoir and deposit heat into the warm-end reservoir. We use

helium as the heat transport medium. When helium is forced into the cold-end reservoir on a down-flow, it should enter at a temperature below 4.2 K; and when helium is forced into the warm-end reservoir on the up-flow, it should enter at a temperature above 15 K. Thermal pollution is defined as when the temperature of the helium entering a reservoir transports heat in the wrong direction.

Units used for the Magnetic Field: In SI units the magnet field is measured in A/m. The relationship between magnetic induction and magnetic field is:

$$B = \mu_0(H + M)$$

where B is the magnetic induction, H is the applied magnetic field, and M is the magnetization of the medium. All the GGG property data used in this report is expressed as a function of $\mu_0 H$, not just H. (This is a carry over from the original source of the GGG data.) For this reason the magnetic field is expressed in units of tesla. This is not the magnetic induction B, but is simply the applied magnetic field multiplied by the permeability of free space μ_0, $4\pi \times 10^{-7}$ H m^{-1}.

APPENDIX A

Heat Transfer Analysis of the Copper Block Heat Exchangers

The copper block heat exchangers are described briefly in Chapter 2. Figure 8 shows a schematic of the design chosen. This appendix presents the heat transfer analysis which was used to design these heat exchangers. From this analysis the length, the number of radial slits and the depth of the radial slits was selected.

Preliminary Analysis:

The goal of this analysis is to determine if the copper block heat exchanger will be of uniform temperature, and if there is enough surface area for the helium to reach thermal equilibrium with the copper.

Model the copper as having axial conduction, convective boundaries, and uniform heat generation from the electric heaters:

$$KA\frac{\partial^2 T_{Cu}}{\partial x^2} - \hbar P\left(T_{Cu} - T_{he}\right) + \frac{\dot{Q}}{L} = 0 \tag{18}$$

Model helium as having mass flow and convective boundaries:

$$\dot{m}c_p\frac{\partial T_{he}}{\partial x} + \hbar P\left(T_{he} - T_{Cu}\right) = 0 \tag{19}$$

These equations are coupled and cannot be easily solved in closed form.

Define $\beta \equiv \hbar P/\dot{m}c_p$, and $\alpha \equiv \hbar P/KA$. Solve Equation (19) for $T_{he}(x)$ by first assuming that T_{Cu} is essentially constant. Then substitute this T_{Cu} into Equation (18), and solve for the actual temperature profile, thus checking the accuracy of the original assumption.

Solving Equation (19) with constant T_{Cu}:

$$T_{he} = T_{Cu} - \left(T_{Cu} - T_{in}\right)e^{-\beta x}$$

Where T_{in} is the boundary condition for the incoming helium. We can now solve for the heat transfer between the helium and copper:

$$q(x) = \hbar P\left(T_{cu} - T_{he}\right) = \hbar P\left(T_{Cu} - T_{in}\right)e^{-\beta x}$$

and the total heat transfer is:

$$\dot{Q} = \int_0^L q(x)\,dx = \dot{m}c_p\,(T_{Cu} - T_{in})(1 - e^{-\beta L})$$

After defining $(T_{Cu} - T_{in})$ as ΔT_0, we can rewrite Equation (18) as:

$$\frac{\partial^2 T_{Cu}}{\partial x^2} = -\alpha\,\Delta T_0\,e^{-\beta x} - \frac{\alpha}{\beta L}\,\Delta T_0\,(1 - e^{-\beta L})$$

Integrating once with respect to x:

$$\frac{\partial T_{Cu}}{\partial x} = -\frac{\alpha}{\beta}\,\Delta T_0\,e^{-\beta x} - \frac{\alpha}{\beta}\,\Delta T_0\,(1 - e^{-\beta L})\,\frac{x}{L} + C_0$$

which rearranges to:

$$\frac{\partial T_{Cu}}{\partial x} = -\Delta T_0\,\frac{\alpha}{\beta}\left[e^{-\beta x} + (1 - e^{-\beta L})\frac{x}{L}\right] + C_0$$

The constant of integration can be determined by forcing the heat flow to be zero at one of the ends (it will also be zero at the other end):

$$C_0 = \Delta T_0\,\frac{\alpha}{\beta}$$

So:

$$\frac{\partial T_{Cu}}{\partial x} = -\Delta T_0\,\frac{\alpha}{\beta}\left[(1 - e^{-\beta x}) + (1 - e^{-\beta L})\frac{x}{L}\right]$$

Integrating once again with respect to x:

$$T_{Cu} = \Delta T_0\,\frac{\alpha}{\beta}\left[x + \frac{e^{-\beta x}}{\beta} - (1 - e^{-\beta L})\,\frac{x^2}{2L}\right] + C_1$$

We are interested in finding the difference between the temperature of the copper block at the inlet, $x = 0$, and the outlet, $x = L$. Normalizing this difference to ΔT_0, we can write:

$$\frac{\alpha}{\beta}\left[L + \frac{e^{-\beta L}}{\beta} - (1 - e^{-\beta L})\,\frac{L}{2} - \frac{1}{\beta}\right]$$

or finally:

$$\frac{\alpha L}{\beta}\left[1 - \left(\frac{1}{\beta L} + \frac{1}{2}\right)(1 - e^{-\beta L})\right]$$

This expression will be checked to see if the uniform copper block temperature assumption is valid.

The other design parameter is choosing a value for βL. For the helium to leave the heat exchanger at essentially the copper's temperature, we should have a βL of at least 2, probably closer to 4. The design parameters for our two heat exchangers appear on the next page.

Design parameters of the copper heat exchangers

Warm-End:

$L = 5 \quad \text{cm}$

$P = 2(33)(2.54) = 168 \quad \text{cm}$

$A = (\pi 1^2 - (.010)(35))2.54^2 = 18.0 \quad \text{cm}^2$

$t = 0.010(2.54) = 0.0254 \quad \text{cm}$

$K_{he}(16\ \text{K}) = .24 \quad \text{mW}\,\text{cm}^{-1}\,\text{K}^{-1}$

$c_{p_{cu}}(16\ \text{K}) = 5.6 \quad \text{J}\,\text{g}^{-1}\,\text{K}^{-1}$

$K_{cu}(16\ \text{K}) = 8 \quad \text{W}\,\text{cm}^{-1}\,\text{K}^{-1}$

$\hbar = 3.8\,K_{he}/t = 0.036 \quad \text{W}\,\text{cm}^{-2}\,\text{K}^{-1}$

$\beta = \hbar P/\dot{m}\,c_p = 1.08 \quad \text{cm}^{-1}$

$\beta L = 5.4$

$\alpha = hP/K_{cu}\,A = 0.042 \quad \text{cm}^{-2}$

$\frac{\alpha L}{\beta} = 0.19$

$\left[1 - \left(\frac{1}{\beta L} + \frac{1}{2}\right)(1 - e^{-\beta L})\right] = 0.32$

$0.19(0.32) = 6\%$ temperature variation

Cold-End:

$L = 5 \quad \text{cm}$

$P = 2(33)(2.54) = 168 \quad \text{cm}$

$A = (\pi 1^2 - (.010)(35))2.54^2 = 18.0 \quad \text{cm}^2$

$t = 0.010(2.54) = 0.0254 \quad \text{cm}$

$K_{he}(4\ \text{K}) = 0.21 \quad \text{mW}\,\text{cm}^{-1}\,\text{K}^{-1}$

$c_{p_{cu}}(4\ \text{K}) = 3.5 \quad \text{J}\,\text{g}^{-1}\,\text{K}^{-1}$

$K_{cu}(4\ \text{K}) = 2.5 \quad \text{W}\,\text{cm}^{-1}\,\text{K}^{-1}$

$\hbar = 3.8\,K_{he}/t = 0.032 \quad \text{W}\,\text{cm}^{-2}\,\text{K}^{-1}$

$\beta = \hbar P/\dot{m}\,c_p = 1.54 \quad \text{cm}^{-1}$

$\beta L = 7.7$

$\alpha = hP/K_{cu}\,A = 0.119 \quad \text{cm}^{-2}$

$\frac{\alpha L}{\beta} = 0.39$

$\left[1 - \left(\frac{1}{\beta L} + \frac{1}{2}\right)(1 - e^{-\beta L})\right] = 0.37$

$0.39(0.37) = 14\%$ temperature variation

APPENDIX B

Helium Dead Space and Parasitic Heat Loads

Helium dead space is contained in the piping between the heat exchangers and the core. When we redesigned the temperature control modules, one goal was to minimize this dead space. There is a trade off however with dead space and pressure drop. The smaller the connection tube, the less the dead space, but the greater the pressure drop. There is additional dead space located at the ends of the core which we could not affect.

Cold-end connection tube pressure drop:

Assume 1 g/s of helium flow, with average properties at 4 K and 3 atm.

$\mu = 38 \times 10^{-6}$ g cm^{-1} s^{-1}
$c_p = 3.415$ J g^{-1} K^{-1}
$K = 0.21 \times 10^{-3}$ W cm^{-1} K^{-1}
$\rho = 0.138$ g cm^{-3}

The length of the tube is:

$L = 13$ cm

Using a Moody-Diagram to determine the friction factor, f, as a function of the Reynolds Number, Re, we can calculate the pressure drop per unit length:

$$\frac{\Delta P}{L} = \frac{f}{2}\rho V^2 \pi D = \frac{8 f \dot{m}^2}{\pi \rho D^3}$$

For D = 1/8 in - 0.020 in = 0.105 in = 0.267 cm
Re = 9.9×10^4, f = 0.0047, $\Delta P/L$ = 0.0081 atm cm^{-1}
ΔP = 0.11 atm

For D = 5/32 in - 0.020 in = 0.136 in = 0.346 cm
Re = 7.6×10^4, f = 0.0053, $\Delta P/L$ = 0.0025 atm cm^{-1}
ΔP = 0.033 atm

For D = 3/16 in - 0.020 in = 0.168 in = 0.425 cm
Re = 6.2×10^4, f = 0.0056, $\Delta P/L$ = 0.00095 atm cm^{-1}

$\Delta P = 0.012$ atm

The final design used a 4 mm (5/32 inch) OD tube.

Cold-end connection tube dead space:

volume $= \pi(0.346/2)^2\,(13) = 1.2 \quad \mathrm{cm}^3$

Entrained helium $= 1.2\,(0.138) = 0.17 \quad \mathrm{g}$

Warm-end connection tube pressure drop:

Assume 1 g/s of helium flow, with average properties at 15 K and 3 atm.

$\mu = 30.8 \times 10^{-6} \quad \mathrm{g\,cm^{-1}\,s^{-1}}$

$c_p = 5.50 \quad \mathrm{J\,g^{-1}\,K^{-1}}$

$K = 0.232 \times 10^{-3} \quad \mathrm{W\,cm^{-1}\,K^{-1}}$

$\rho = 0.010 \quad \mathrm{g\,cm^{-3}}$

The length of the tube is:

$L = 18 \quad \mathrm{cm}$

Using a Moody-Diagram to determine the pressure drop we find:

For $D = 3/8$ in - 0.020 in = 0.355 in = 0.902 cm

Re = 3.6×10^4, $f = 0.0063$, $\Delta P/L = 0.00034 \quad \mathrm{atm\,cm^{-1}}$

$\Delta P = 0.0061 \quad \mathrm{atm}$

For $D = 1/4$ in - 0.020 in = 0.300 in = 0.584 cm

Re = 5.6×10^4, $f = 0.0056$, $\Delta P/L = 0.0027 \quad \mathrm{atm\,cm^{-1}}$

$\Delta P = 0.049 \quad \mathrm{atm}$

For $D = 5/16$ in - 0.020 in = 0.293 in = 0.743 cm

Re = 4.4×10^4, $f = 0.0060$, $\Delta P/L = 0.00086 \quad \mathrm{atm\,cm^{-1}}$

$\Delta P = 0.015 \quad \mathrm{atm}$

The final design used a 8.5 mm (5/15) inch OD tube.

Warm-end connection tube dead space:

volume $= \pi(0.743/2)^2\,(18) = 7.8 \quad \mathrm{cm}^3$

entrained helium $= 7.8\,(0.010) = 0.08 \quad \mathrm{g}$

The effect of the Phenolic which surrounds the connection tubes

The helium is in contact with the phenolic only in the space at the end of the core. The design of the connection tubes insulates the rest of the flow passage from the phenolic. For cyclic conditions, the thermal boundary layer will penetrate into the phenolic as $\delta \sim \sqrt{\alpha t}$. where α is the thermal diffusion, and t is time. On a first-order analysis the heat transferred from the phenolic is:

$$q = \Delta U = \rho\, c_p\, (vol)\, \Delta T$$

where in this analysis the volume can be expressed as:

$$\delta\, A = \sqrt{\alpha t}\, A = \sqrt{\frac{Kt}{\rho c_p}}\, A$$

so:

$$q = \sqrt{K \rho c_p\, t}\, A\, \Delta T$$

To analyze this equation for the warm-end, we use the thermo-physical properties of Teflon at 15 K:

$c_p = 0.05 \quad \mathrm{J\,g^{-1}\,K^{-1}}$
$K = 0.001 \quad \mathrm{W\,cm^{-1}\,K^{-1}}$
$\rho = 1 \quad \mathrm{g\,cm^{-3}}$

And the cycle parameters are:

$A = \frac{\pi}{4}(1.5^2 - .5^2)(2.54^2) = 10 \quad \mathrm{cm^2}$
$\Delta T = 3 \quad \mathrm{K}$
$t = 5 \quad \mathrm{s}$

From this we find that $q = 0.2$ J; less than 1% of the expected heat of rejection.

The full heat capacity of the phenolic as $t \rightarrow \infty$ is:

$$Q = \rho\, c_p\, A\, L\, \Delta T$$

so Q= (1)(0.05)(10)(10)(3) = 15 J; this is ~50% of the total heat of rejection.

For the cold-end, we use the thermo-physical properties of Teflon at 4 K:

$c_p = 0.001 \quad \mathrm{J\,g^{-1}\,K^{-1}}$

$K = 0.0001 \quad \mathrm{W\,cm^{-1}\,K^{-1}}$

$\rho = 1 \quad \mathrm{g\,cm^{-3}}$

And the cycle parameters are:

$A = 10 \quad \mathrm{cm^2}$

$\Delta T = 1 \quad \mathrm{K}$

$t = 5 \quad \mathrm{s}$

From this we find that $q = 0.01$ J; again this is less than 1% of the expected refrigeration per 10 s cycle.

The full heat capacity of the phenolic as $t \rightarrow \infty$: is $Q = (1)(0.001)(10)(10)(1) = 0.1$ J; this is ~2% of the total refrigeration per 10 s cycle.

These calculations show that there should be no appreciable effect of the phenolic on the helium during steady-state operation of the device. However, transient operation will be influenced by the large total heat capacity of the phenolic at 15 K.

APPENDIX C

AC losses in the Copper Heat Exchangers and Stainless Structure

The Copper Block Heat Exchangers:

The copper block heat exchangers were designed to minimize the losses due to eddy current heating. These losses are generated whenever the magnetic flux through them changes with time. One factor that keeps the losses small is that the copper blocks are located well beyond the main magnetic field. This can be seen by looking at Figure 56 in Chapter 10. The other factor that minimizes AC losses is that the helium flow channels where all cut in the radial direction. This creates a long path with an increased effective electrical resistance, and it minimizes the flux area enclosed by the path. Figure 8 in Chapter 2 shows the design of the helium flow channels. The following analysis estimates the AC losses generated in the copper block heat exchangers.

Following the slits in the heat exchangers

Here we look at the total flux captured by the copper block, and assume that the current must follow the helium channels.

The perimeter of the block following the slits is: $L = 168$ cm. This comes from Appendix A.

The maximum thickness of the wedges is: $t = \pi(2)(2.54)/48 = 0.33$ cm. This is the maximum circumference divided by the total number of slits.

The area for current flow is: $A_c = (t/2)\,(2)(2.54) = 0.84\ \text{cm}^2$

The electrical resistivity of copper at 4.2 K is: $\rho_c \sim 10^{-8}\ \ \Omega\text{-cm}$

The resistance of the current path is: $R = \frac{L\,\rho_c}{A_c} = \frac{(168)\,10^{-8}}{.84} = 2 \times 10^{-6}\ \ \Omega$

The maximum field at the copper block is about 0.1 T.

Total Flux area: $A_f = \pi\,(1)(2.54)^2 = 20\ \text{cm}^2 = 0.002\ \text{m}^2$

The rate of change of magnetic flux is: $\frac{dB}{dt} = \frac{.1-.025}{5} = 0.015\ \text{T s}^{-1}$

The voltage generated is: $V = \frac{dB}{dt}\,A_f = .015(.002) = 3 \times 10^{-5}\ \text{V}$

The loss generated is: $P_d = V^2/R = 9 \times 10^{-10}/2 \times 10^{-6} = 0.45$ mW

This loss is negligible compared to the expected refrigeration of 500 mW.

The solid center of the heat exchanger

Next we will look at just the solid center of the heat exchanger.

A conservative estimate for the current flow area is: $A_c = .25\ (2.54)(2)(2.54) = 3.2$ cm^2

The length for the current path is: $L = \pi\,(.5)(2.54) = 4$ cm

The area which captures the flux is: $A_f = \pi\,(.25)^2(2.54)^2 = 1.3\text{cm}^2 = 1.3 \times 10^{-4}$ m^2

The voltage generated is: $V = .015(1.3 \times 10^{-4}) = 2 \times 10^{-6}$

The loss generated is: $P_d = 4 \times 10^{-12}/1 \times 10^{-8} = 0.4$ mW

Again this is negligible.

The Stainless Core Jacket

The stainless steel tube which contains the core receives a large value of magnetic flux and will generate AC losses. Since the tube is in thermal contact with the contents of the core, this heat will end up in the core effecting the process.

The resistivity of stainless at 4.2 is: $\rho_{ss} = 60 \times 10^{-6}$ Ω-cm

The area for current flow is: $A_c = .035(2.54)40 = 3.6$ cm^2

The length of the current path is: $L = \pi(1.5)(2.54) = 12$ cm

The resistance of the current path is: $R = \frac{60\times10^{-6}(12)}{3.6} = 2 \times 10^{-4}$ Ω

The area which captures the magnetic flux is: $A_f = \pi(.75)^2(2.54)^2 = 11.4\text{cm}^2 = .00114$ m^2

The rate of change of magnetic flux is: $\frac{dB}{dt} = \frac{4-1}{5} = 0.6$ T s^{-1}

The voltage generated is: $V = .6(.00114) = 6.8 \times 10^{-4}$ V

The loss generated is loss: $P_d = V^2/R = (6.8 \times 10^{-4})^2/2 \times 10^{-4} = 2$ mW

Again, this loss is negligible when compared with the convective heat fluxes experienced by the core during operation.

APPENDIX D

Temperature Sensor Locations

The temperture sensor locations are shown in Figure 14 in Chapter 3. The cold-end sensors, C-1 through C-5, are all nominal 47-ohm 1/4-W Allen Bradley carbon resistors. They have been calibrated in the temperature range from 1.5 to 4.2 K. Readings much above 4.2 K are therefore out of the calibrated range and should be taken as approximate. The warm-end sensors, W-1 through W-5 are all nominal 220-ohm Allen Bradley carbon resistors. These sensors have been calibrated over the larger temperature range of 4.2 to 20 K. Readings much above 20 K should be taken as approximate.

The method of mounting and the purpose of each sensor is described below:

[C-1] This sensor is located in the helium flow path right below the core. Its purpose is to measure the temperature of the helium entering and leaving the core's cold-end. It is attached to a stainless wire which is glued to the end of the evacuated tube which connects the cold-end heat exchanger to the core.

[C-2] This sensor is mounted inside the cold-end copper block heat exchanger. It is mounted in a hole drilled into the end of the copper block that faces the core, and is held in place with copper-filled vacuum grease.

[C-3] This sensor is located in the exit port leaving the cold-end heat exchanger. It is mounted on a stainless stud attached to the copper block. Its purpose is to measure the temperature of the helium entering and leaving the heat exchanger to and from the cold-end displacer. It should always register 4.2 K.

[C-4] This sensor was located in the manifold at the bottom of the cold-end reservoir tubes. During one of the tests a leak developed at this sensor's wire feed-through. Analysis of previous data indicated that no new information was derived from this sensor. The sensor was removed and its leak plugged.

[C-5] This sensor is located in the manifold at the top of the cold-end reservoir

tubes. It measures the temperature of the helium entering and leaving the cold-end displacer. It is important that the helium at this location stay at 4.2 K if we are to use piston's displacement as a measure of helium flow.

[W-1] This sensor is located directly above the warm-end copper block heat exchanger. Its purpose is to measure the temperature of the helium entering and leaving the copper block to and from the warm-end displacer. It is mounted on a stainless wire which in turn is attached to the large stainless piece which separates the helium space from the hydrogen space.

[W-2] This sensor is located inside the warm-end copper block. Since the hydrogen boiling tube takes up most of the center of this heat exchanger, there was not enough room to mount this sensor deep inside the copper. A horizontal hole was cut in the bottom end of the copper below the boiling tube. The sensor is held in place with copper filled vacuum grease.

[W-3] This sensor is located in the helium flow path right above the core. Its purpose is the measure the temperature of the helium entering and leaving the warm-end of the core. It is attached to a stainless wire which is glued to the end of the of the evacuated tube which leads from the warm-end heat exchanger to the core.

[W-4] This sensor is located in the guard bath. It hangs loose right above the copper screen, and is held in place by a weight. Its purpose is to measure the temperature of the guard bath.

[W-5] This sensor (added after the preliminary tests) is attached to the top plate of the warm-end heat exchanger. It was found that this plate could cool below 14 K and that the hydrogen would freeze onto it, thus removing liquid hydrogen from the boiling tube. This sensor is used to control a heater which prevents this from happening.

APPENDIX E

Thermo-Properties of GGG

This appendix presents various thermodynamic properties of GGG, the paramagnetic salt used in our device. Some of these properties were presented in the main body of the thesis, and some are presented for the first time here. The graphs included are:

E-1: GGG Entropy as a Function of Temperature at Constant Applied Field

E-2: Magnetic Enthalpy as a Function of Temperature at Constant Applied Field

E-3: Isothermal Magnetic Interaction

E-4: Isofield Magnetic Interaction – Specific Heat

E-5: Isentropic Temperature Change with Field

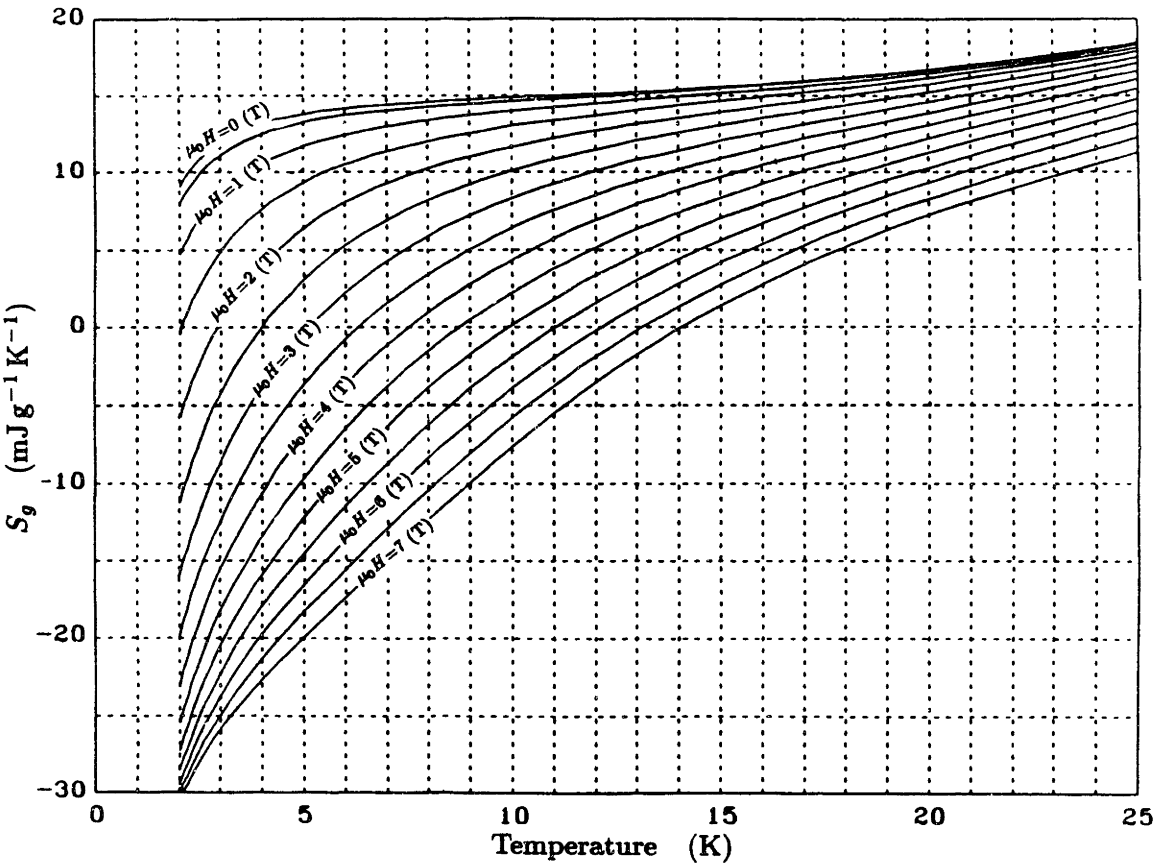

Fig. E-1 GGG Entropy as a Function of Temperature at Constant Applied Field

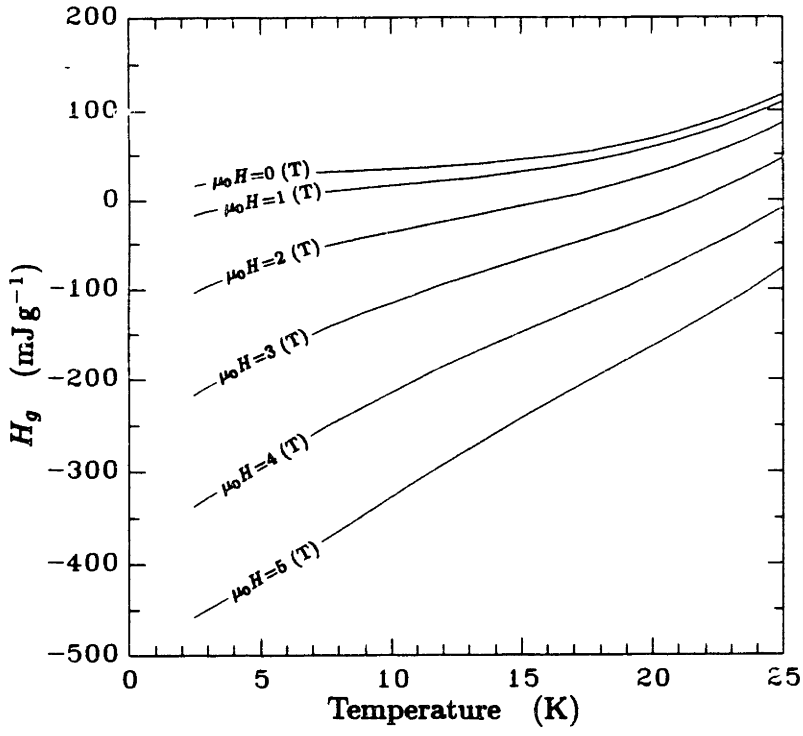

Fig. E-2 Magnetic Enthalpy as a Function of Temperature at Constant Applied Field

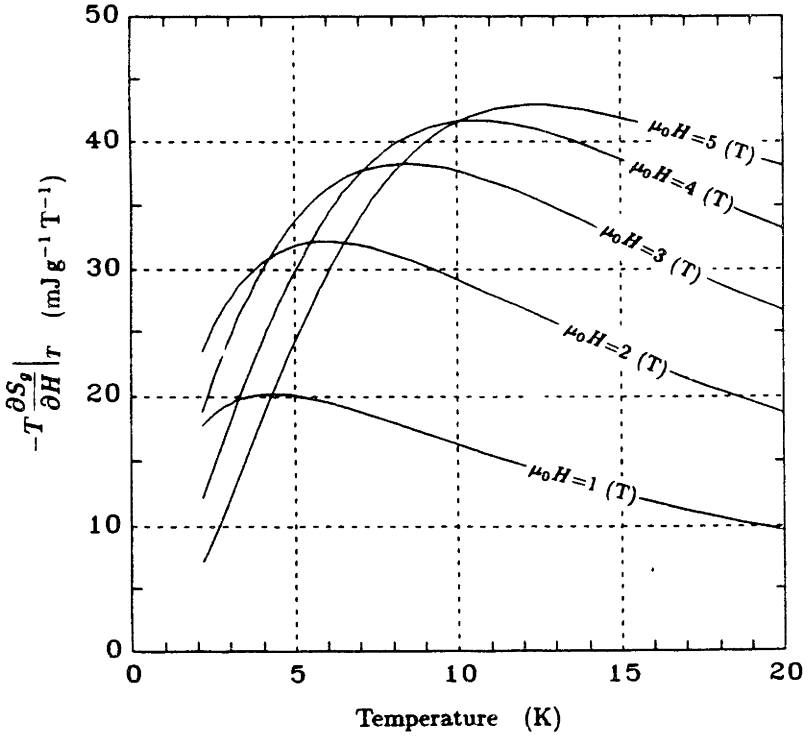

Fig. E-3 Isothermal Magnetic Interaction

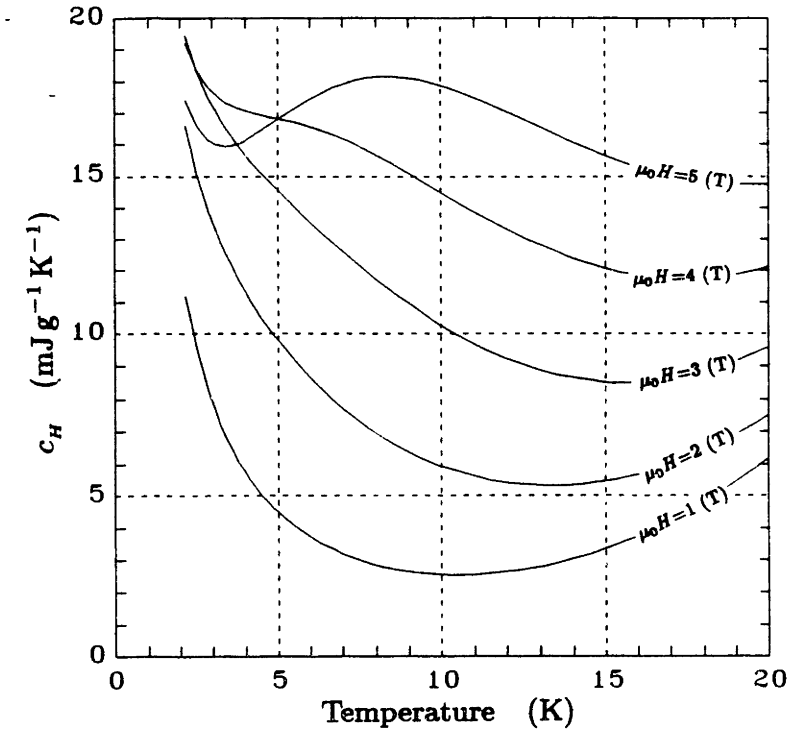

Fig. E-4 Isofield Magnetic Interaction – Specific Heat

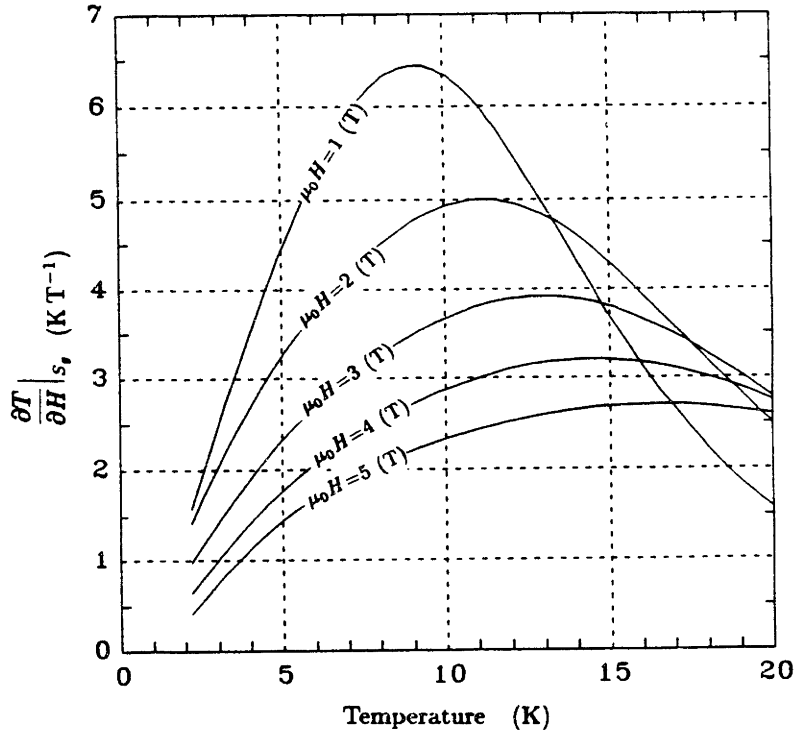

Fig. E-5 Isentropic Temperature Change with Field

APPENDIX F

Graphical Solutions to an Active Core
With Step-Wise Constant Parameters

This appendix shows graphical solutions to the equation:

$$\frac{dT}{dt} + v\frac{dT}{dx} = q$$

where v is the convection wave velocity, and q is a uniform heat input over the core, divided by the core's specific heat. For the first examples both q and v are constant during the flow process. Disturbances are produced by either starting with an initial profile which is not the proper steady-state profile, or by allowing the upstream boundary condition to vary.

Ex. 1) B.C: at $x = 0$, $T = 0$; I.C: at $t = 0$, $T = 0$: (figure F-1)

Note that without the active term, q, the temperature would just remain at zero for ever. The active term causes the temperature to rise uniformly until it reaches its steady state profile, $T = (q/v)\,x$. The steady state profile is reached at any give location when the convection wave reaches that location. The right end of the core takes the longest time to reach the steady state temperature, $t = L/v$.

Ex. 2) B.C: at $x = 0$, $T = 0$; I.C: $T = (q_0/v)\,x$; $q = 1.5\,q_0$: (figure F-2)

Here we generalize the above example by starting with a steady state profile derived by one q, and then switch to a different q at $t = 0$. We find that

$$T = (q - q_0)t + \frac{q_0}{v}x \quad \text{, for} \quad (x > vt)$$

Note that the rate of temperature change is given by $(q - q_0)$, and is independent of position. The length of time for which the temperature changes is equal to x/v, and is not dependent on how great the difference between q and q_0.

Ex. 3) B.C: at $x = 0$, $T = \frac{1}{2}(q_0/v)\,L$; I.C: $T = (q_0/v)\,x$; $q = q_0$: (figure F-3)

This example shows the response when q is constant but there is a step change in temperature at the inlet to the core. The response is identical to that of a nonactive core except that it is shifted by the initial steady state solution. Note that the right end of the core doesn't know of the disturbance until the wave propagates the length of the core.

Ex. 4) B.C: at $x = 0$, $T = Ct$; I.C: $T = (q_0/v)\,x$; $q = q_0$: (figure F-4)

This time we show a ramp change in the boundary condition. For this particular example the boundary temperature is rising such that $C = q$. This produces a region in the core where the temperature is constant with x. Note that as in the previous example, changes in the boundary condition are not known downstream until the new convection wave can propagate there. In general we find that:

$$T = \frac{q - C}{v}x + Ct \quad \text{, for} \quad (x < vt)$$

Ex. 5) See description below: (figure F-5)

This example combines two of the previous examples. The entire core starts with a steady state profile developed by $q = q_0$. At $t = 0$ the left half of the core experiences a step change in q to $2q_0$, while in the right half q remains at q_0. This example shows that even though the disturbance, a flow imbalance, occurs in the left half of the core, the right or down-stream half will experience the greater temperature excursion.

Ex. 6) Computer simulation: (figure F-6)

This example was produced using the computer simulation program developed in Chapter 6. It uses real properties for both the GGG and the helium, so the parameters v and q vary considerably. It is testing the same situation as is described in example 1 (figure F-1). Note that the temperature response here strongly resembles the response in example 1. This indicates that the properties of an active regenerator described in examples 1 through 5 can be used to describe our real core even though the parameters are variable.

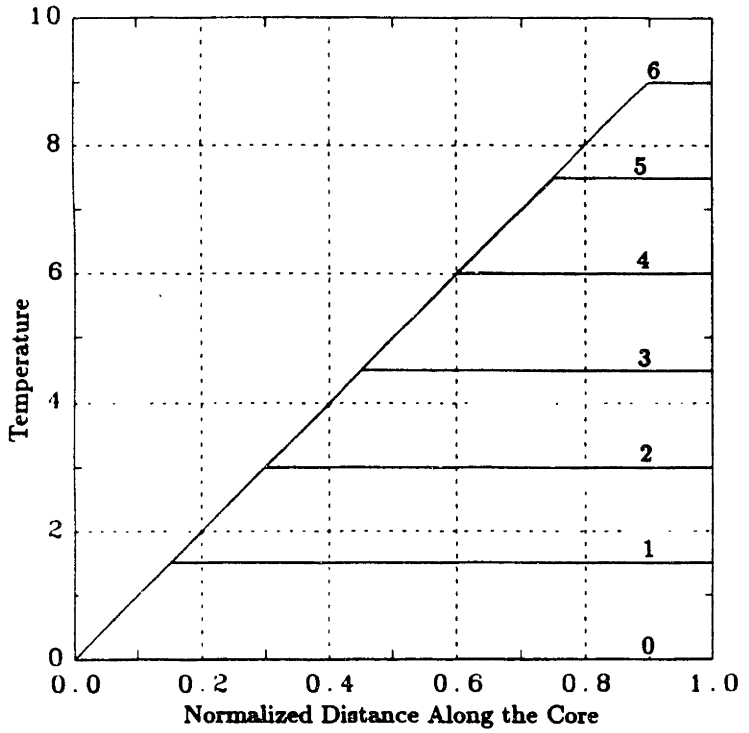

Fig. F-1 Transient from $T = 0$

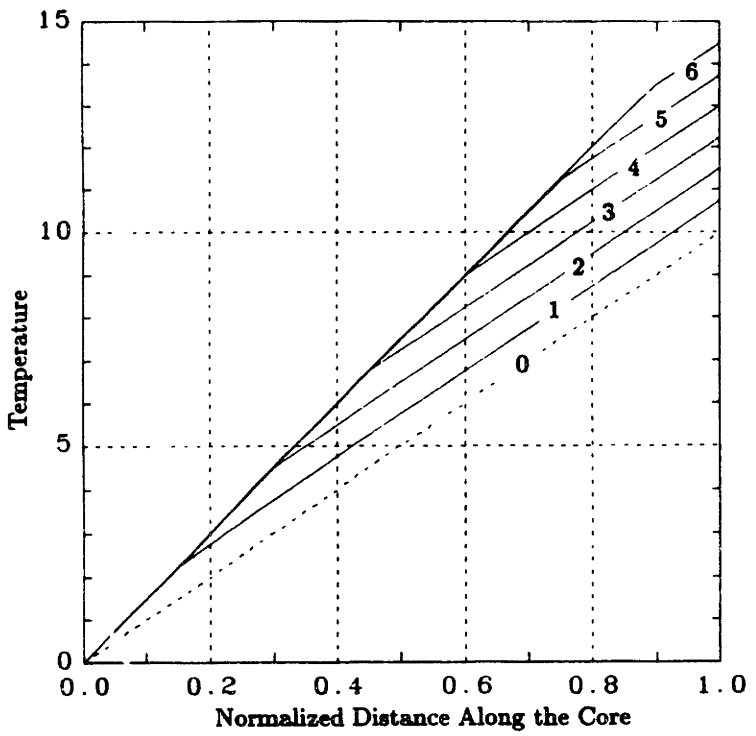

Fig. F-2 Transient from $T = (q_0/v)\,x$

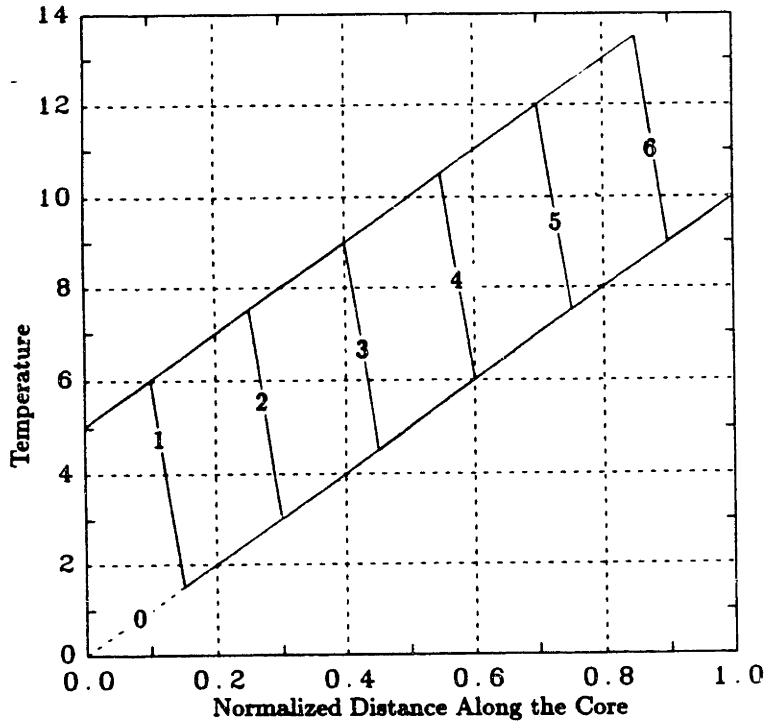

Fig. F-3 Step Change in $T(x = 0)$

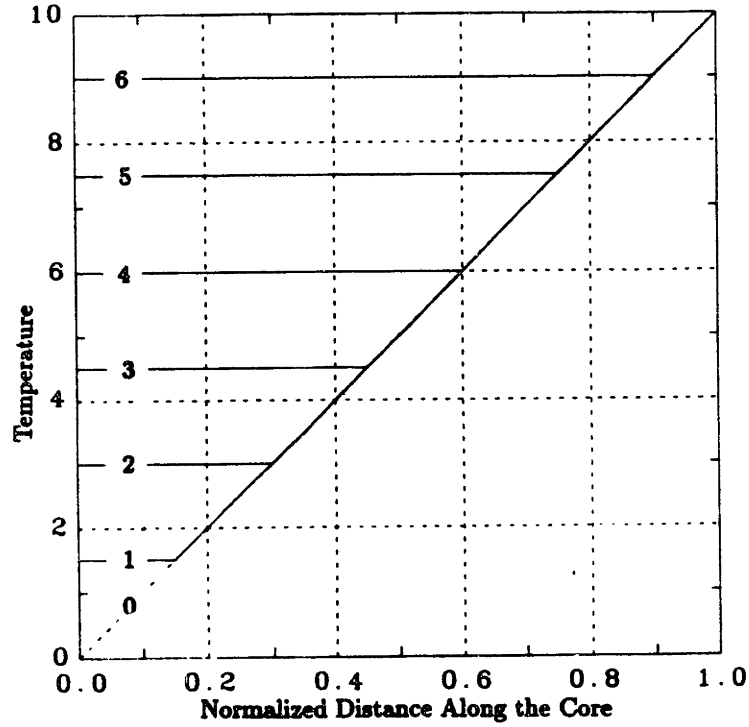

Fig. F-4 Ramp Change in $T(x = 0)$

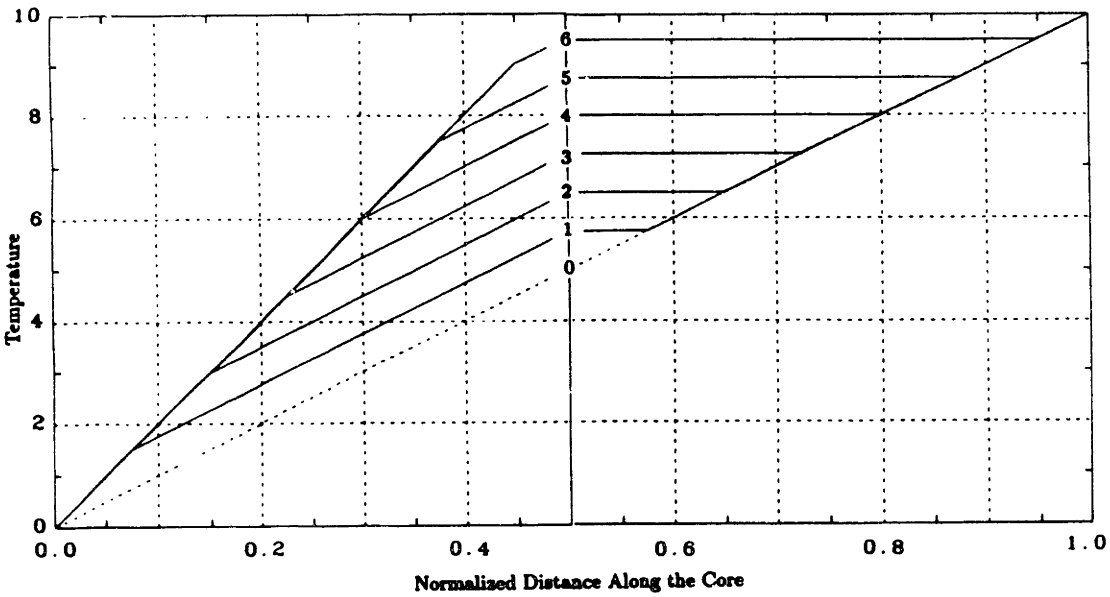

Fig. F-5 Combined Response

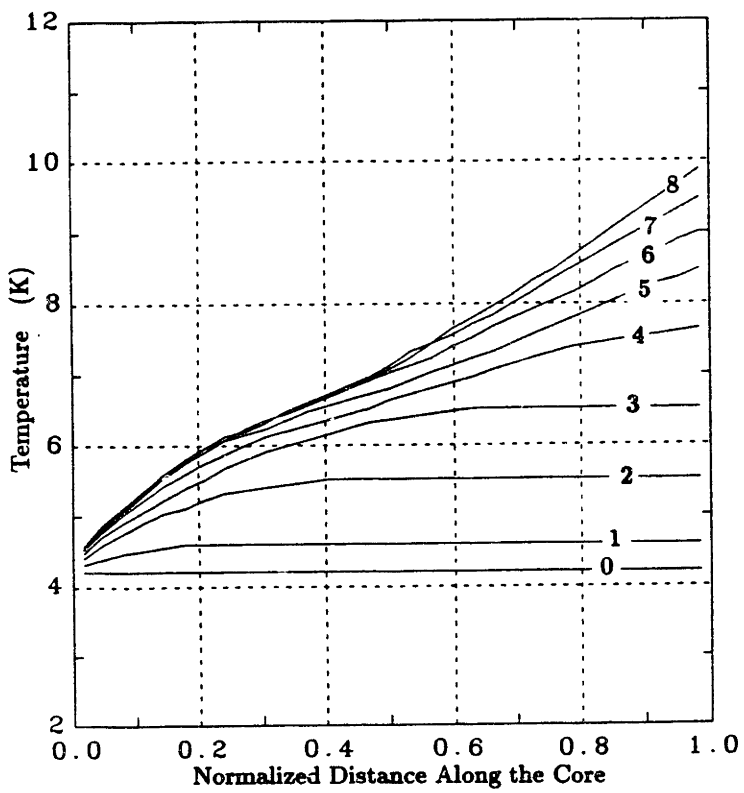

Fig. F-6 Computer Simulation

Conclusions from the first 6 examples:

1. A disturbance in boundary condition propagates downstream at velocity v. The perturbation moves in the same way as in a nonactive core, superimposed on the active core's steady state temperature profile.

2. A change in heat input into a core section causes that section to change temperature immediately at a rate proportional to the change. The core reaches its new steady state temperature profile from left to right at velocity v.

3. The real core responds in a similar way to this simplified model, even though its real parameters v and q vary considerably.

4. The generalized relationships developed here are:

$$T_{new} = \frac{q - C}{v} x + C\,t, \quad \text{for} \quad (x < v\,t)$$

$$T_{old} = \frac{q_0}{v} x + (q - q_0)t, \quad \text{for} \quad (x > v\,t)$$

where T_{old} is the section of the core not yet corrected by the convection wave coming from the inlet, and T_{new} is the section of the core which has been passed by the convection wave.

Varying q during the flow process

Fine field-flow phasing in an active regenerator is accomplished by varying the parameter $\dot{H}/\dot{m}$. In the limit of many steps, we can simulate fine field-flow phasing by varying the parameter $\Delta H/\Delta M$ for each step. For these examples with stepwise constant parameters we can make the following relations:

$$q \propto \Delta H$$

$$v \propto \Delta M$$

over the time step. The fact that the core's specific heat may vary does not effect this substitution, since both q and v are inversely proportional to the core's specific heat.

Figure F-2 showed an example where $\Delta H/\Delta M$ is constant during the flow process. The following examples have the same total ΔH, the same total ΔM, and the same intial temperature profile, but the ΔH per time step varies. There are six time steps.

Ex. 7) Variable q/v: (figure F-7)

This example shows the response of the core with the ratio $\Delta H/\Delta M$ increasing with each step. This is equivalent to a path where the flow starts out fast and then decreases.

Ex. 8) Variable q/v: (figure F-8)

For this example the ratio $\Delta H/\Delta M$ decreases with each step. This is equivalent to a path where the flow starts out slow then increases.

Conclusions from the last two examples

1. When $\Delta H/\Delta M$ increases during the path, more heat is rejected out the warm-end, and the profile averages a lower temperature by the end of the process.

2. The temperature of the wave front at the end of the process is independent of the field-flow phasing. Note that for each of the examples (2, 6, & 7), the temperature at 90% of the core is 9 .

3. The average gradient within the core is therefore independent of field-flow phasing.

But what if we doubled the total amount of helium flow M_T, and doubled the total heat input during the process? The equivalent to this is to half the length of the core. Look again at figures F-2, F-7 and F-8, but now pretend that the core ends at 50%. The wave front passes all the way through the core. All information to the right of 50% is lost as it mixes in the warm-end. When the flow is reversed, the average gradient is determined from the new end of the core. This temperature varies considerable (5 to 7.3 to 2.8) depending on the previous field-flow phasing.

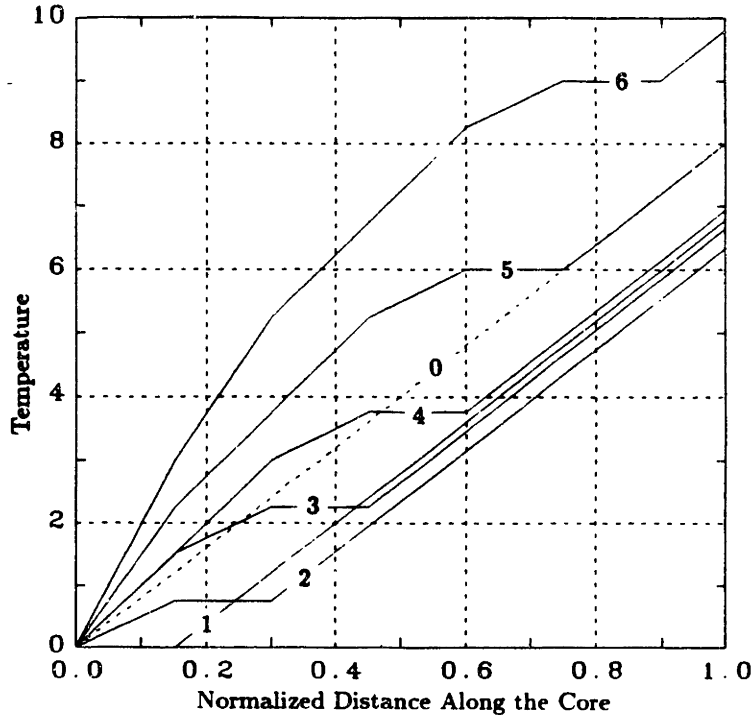

Fig. F-7 Increasing $\Delta H/\Delta M$

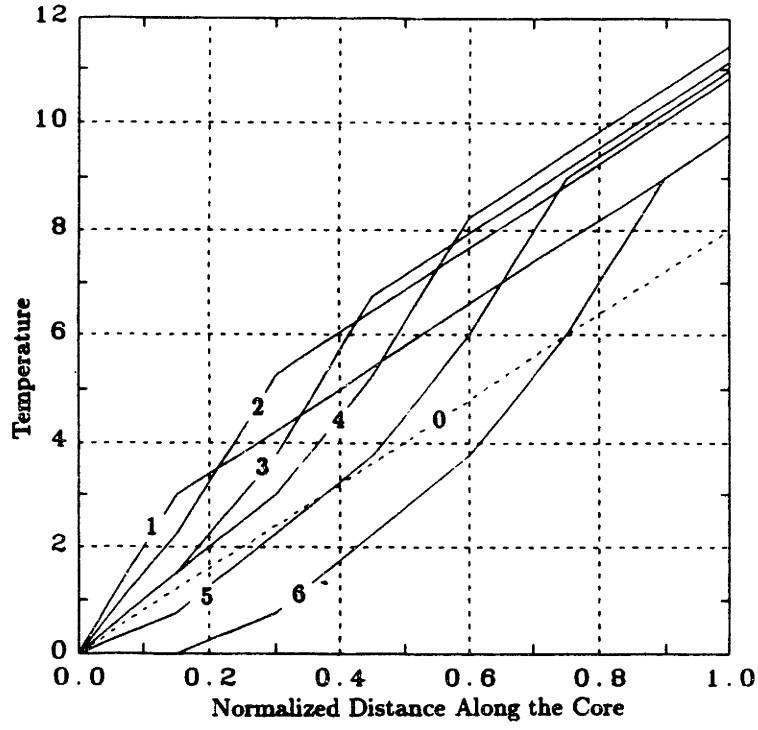

Fig. F-8 Decreasing $\Delta H/\Delta M$

APPENDIX G

A Criterion for High-Shuttle-Mass Flow Process

Chapter 8 ended with a qualitative statement about the difference between low and high-shuttle-mass refrigeration. It was found that a cycle could always be controlled if the convection wave could travel the length of the core during a single flow-path; thus purging all old temperature information from the core. This criterion can be expressed mathematically as:

$$\int_0^{t_f} v\,dt > L$$

where this integral must follow the wave front at convection wave velocity v. If for simplicity we assume that helium porosity is zero then v can be written as:

$$v = \frac{\dot{m}\,c_p}{\rho_g\,A\,c_H} = \frac{\dot{m}\,c_p}{\rho_g\,A\,T\frac{\partial S_g}{\partial T}\Big|_H}$$

The convection wave velocity is proportional to the helium flow rate $\dot{m}$. We found in Chapter 8 that the desirable helium flow rate is given by the isothermal limit:

$$\dot{m}\,c_p = \frac{\rho_g\,A(-T\frac{\partial S_g}{\partial H}\Big|_T)}{\frac{dT}{dx}}\dot{H}$$

Combining the above two equations and then using Maxwell's cyclic equality:

$$v = \frac{\rho_g A(-T\frac{\partial S_g}{\partial H})\,\dot{H}}{\rho_g A(T\frac{\partial S_g}{\partial T})\,\frac{dT}{dx}} = \frac{\partial T}{\partial H}\Big|_S \left(\frac{\frac{dH}{dt}}{\frac{dT}{dx}}\right)$$

Putting this value into the integral:

$$\int v\,dt = \int \frac{\partial T}{\partial H}\Big|_S \frac{dx}{dT}\,dH > L$$

At this point we assume that dT/dx is fairly constant, and make the substitution:

$$\frac{dT}{dx} = \frac{\Delta T_0}{L}$$

where the temperature range ΔT_0 is that which must be obtained during the flow process. It is greater than the temperature range between the reservoirs. To the

extent that this substitution is inaccurate, this analysis is in error. Yet with this substitution we are able to develop a simple criteria for high-shuttle-mass refrigeration:

$$\int \frac{\partial T}{\partial H}\Big|_s dH > \Delta T_0$$

or

$$\Delta T_a > \Delta T_0$$

This condition states that the temperature range obtainable by an "adiabatic" magnetization (including helium porosity) must be greater than the temperature range attempted by the process in order to have high-shuttle-mass refrigeration.

APPENDIX H

Computer Programs

This appendix contains only the major computer programs developed for this project. It is not a complete list of all the programs, and program variations, employed during the course of this thesis. The programs contained in this appendix are:

1. PROFILE.FOR: (page 204 to 211) Used for the Ideal Carnot Analysis presented in Chapter 2.
2. SIMULATE.FOR: (page 212 to 218) The main version of the computer simulation program which is described in Chapter 6.
3. SIMFUNCT.FOR: (page 219 to 220) The functions used with SIMULATE.FOR
4. VOID.FOR: (page 221) The program used to model partially insulated void which is described in Chapter 10.6.

These programs are not "user-friendly." It is not recommended that anyone use these programs without first fully understanding every line of code.

```
      program profile
      Real x(361),temp1(361),temp2(361)
      character*20 file1
      real w(361),deltcool(361)
      real factor(361),T(5,5),S(5,5)
      integer cycle(5)
      real Splot(120),factplot(361,5)
      real TGGG(50,7),SGGG(50,7)
      real field(51,5),xtime(51)
      real mdot
c ***************************************************************************
c  Greg's helium stuff...
      COMMON HETEMP(594),HEDENS(594),CURVDENS(594),HEENTH(594),
     1 CURVENTH(594),HEENTR(594),CURVENTR(594),HECP(594),CURVCP(594),
     2 HECOND(594),CURVCOND(594)
      data num/360/
      OPEN(UNIT=3,FILE='[cogswell.heprop]HEPROP.DAT',TYPE='OLD')
      OPEN(UNIT=4,FILE='[cogswell.heprop]HECURV.DAT',TYPE='OLD')
      DO I=1,394
        HETEMP(I)=2.12+I*0.02
        READ(3,*) HEDENS(I),HEENTH(I),HEENTR(I),HECP(I),HECOND(I)
        READ(4,*) CURVDENS(I),CURVENTH(I),CURVENTR(I),CURVCP(I),
     1   CURVCOND(I)
      END DO
      DO I=395,594
        HETEMP(I)=10.+(I-394)*0.05
        READ(3,*) HEDENS(I),HEENTH(I),HEENTR(I),HECP(I),HECOND(I)
        READ(4,*) CURVDENS(I),CURVENTH(I),CURVENTR(I),CURVCP(I),
     1   CURVCOND(I)
      END DO
c ***************************************************************************
c
10    type*,' '
      type*,'This program does massive amounts of iteration in order '
      type*,'to get each segment to span the total field differential.'
      type*,'Enter Tout on the cold blow'
      accept*,tout
      type*,'Enter Tin on the cold blow'
      accept*,tin
      type*,'Enter Tin on the warm blow'
      accept*,tinh
      type*,'Enter high field,low field in tesla'
      accept*,Hhigh,Hlow
      if (Hlow .eq. 0.) Hlow = .01
      type*,'Enter title for graph'
      accept*,file1
      type*,'Enter 1 for initial profile constant delta-h,'
      type*,'      0 for constant delta-T'
      accept*,icp
      k = 0
      adj = .1

      hin = He_HT(tin)
      hout = He_HT(tout)
      if (icp .eq. 1) then
           const = (hin - hout)/float(num)
      end if
      type*,'const',const
      do i=1,num
           deltcool(i) = const
      end do

100   type*,'Enter 1 for graph of temp profile, 2 for work profile,
     & 3 for both graphs, and 0 for no graphs'
```

```
      accept*,iflag

c  Create temperature array for cold blow profile.
      if (icp .eq. 1) then
        temp1(1) = tout
        temp1(2) = deltcool(1)/cpf(temp1(1),1) + temp1(1)
        do i=3,(num+1)
           x(i) = (i-1.)/float(num)
           temp1(i) = 2.*deltcool(i-1)/cpf(temp1(i-1),1) + temp1(i-2)
        end do
      else
        do i = 1,num+1
           x(i) = (i-1.)/float(num)
           temp1(i) = tout + (i-1.)*(tin-tout)/float(num)
        enddo
      endif
c  Smooth the profile with subroutine filter.
      call filter(temp1,361,2)
      type*,temp1(1),temp1(num+1)

c  Create temperature array for warm blow profile using second law.
      temp2(1) = tinh
      temp2(2) = tinh* ( temp1(2)/temp1(1) )**
     &         (cpf(temp1(1),1) / cpf(temp2(1),1) )

      do i=3,num+1
           value = (1.+ (temp1(i)-temp1(i-2))/(2*temp1(i-1)) )**
     &             (cpf(temp1(i-1),1) / cpf(temp2(i-1),1) )
           temp2(i) = 2*temp2(i-1)*(value-1.) + temp2(i-2)
      end do
      type*,temp2(1),temp2(num+1)
      avgden1 = density(temp1,num)
      avgden2 = density(temp2,num)
      type*,'avgden1',avgden1,'  avgden2',avgden2
      type*,'delta S stream 1 =',(He_ST(temp1(1))-He_ST(temp1(361)))
      type*,'delta S stream 2 =',(He_ST(temp2(361))-He_ST(temp2(1)))

      if (iflag .eq. 2 .or. iflag .eq. 0) goto 200
      CALL SET_TRACE_MG(' ',0,' ',1.)
      CALL TRACE_MG(x(1),temp1(1),num+1)

      CALL SET_TRACE_MG(' ',0,' ',1.)
      CALL TRACE_MG(x(1),temp2(1),num+1)

      scale = 10.
      if(temp2(num+1) .gt. 10.) scale = 15.
      if(temp2(num+1) .gt. 15.) scale = 20.
      call scale_MG('y',0.,scale,2.)
      call title_MG(file1)
       call ylabel_MG('Temperature',0.8,'v','TR')
       call xlabel_MG('Distance along core',0.8,'h','TR')
      call fancy_MG
       call graph_MG
       call stop_mg
c
c  Determine work per segment per mass of helium.
200   wtot = 0.
      do i=2,num
           w(i) = .5*(  cpf(temp2(i),1)*( temp2(i+1)-temp2(i-1) )
     &                - cpf(temp1(i),1)*( temp1(i+1)-temp1(i-1) )  )
           wtot = wtot + w(i)
      end do
      w(1) = w(2)
      w(num+1) = w(num)
```

```
      wtot = wtot + w(1)

      if (iflag .eq. 1 .or. iflag .eq. 0) goto 300
c     call scale_MG('y',0.,.05,.01)
      CALL SET_TRACE_MG(' ',0,' ',1.)
      CALL TRACE_MG(x(1),w(1),num)
      call title_MG(file1)
       call ylabel_MG('dWork / total mass of he',0.8,'v','TR')
       call xlabel_MG('Distance along core',0.8,'h','TR')
      call fancy_MG
       call graph_MG
       call stop_mg

c  Find the factor for each segment which will cause it to span
c  from Hhigh to Hlow.
300   do i=1,num
          tlow = temp1(i)
          thigh = temp2(i)
          factor(i) = w(i)/(thigh-tlow) / (sht(Hlow,tlow)-sht(Hhigh,thigh))
      end do
      call filter(factor,361,2)
      factavg = 0.
      do i=1,num
          factavg = factavg + factor(i)
      end do
      factavg = factavg/num

c  Find the lowest and highest values for factor,
c  and their corresponding segment numbers.
      factlow = 9999.
      facthigh = 0.
      do i=1,num
          if(factor(i) .lt. factlow) then
              factlow = factor(i)
              ilow = i
          end if
          if(factor(i) .gt. facthigh) then
             facthigh = factor(i)
              ihigh = i
          end if
      end do

c  Output to terminal...
      type*,' '
      type*,'work per total shuttle mass of helium=',wtot
      type*,'factlow, facthigh ',factlow,facthigh
      type*,'limiting segment numbers; low,high',ilow,ihigh
      work = wtot/facthigh/num*1000.
      type*,'Work per kg of GGG ',work
      refrig = ((He_HT(tinh)-He_HT(tout))/facthigh)/num*1000.
      type*,'Refrig. per kg of GGG ',refrig
      type*,'Carnot Efficiency ',(tin/tinh -1.)/work*refrig
      type*,' '

      type*,'Enter 1 to save this factor profile for plotting, 0 for no'
      accept*,i
      if (i .eq. 1  .and.  k .lt. 5) then
          k = k + 1
          do i=1,num
              factplot(i,k) = factor(i)/factavg
          end do
      end if

      type*,'Enter 1 to continue, 0 to go back and recalculate temps'
```

```
      accept*,j
      if (j .eq. 0) then
        hold = 0.
        do i=1,num
           deltcool(i) = deltcool(i) * (facthigh - adj*factor(i)
     &                 - (1.-adj)*factavg ) / (facthigh - factavg)
           hold = hold + deltcool(i)
        end do

        hold = hold/num
        do i=1,num
           deltcool(i) = deltcool(i)*const/hold
        end do
        type*,'adj =',adj,'Enter new value:'
        accept*,adj
      end if
      if (j .eq. 0) goto 100

c  End of temperature profile iteration.
ccc
c  Output to disk file...
      write(7,15) file1
      write(7,20)
      write(7,25) temp1(1),temp1(num+1),temp2(1),temp2(num+1)
      write(7,30) Hhigh,Hlow
      write(7,35) facthigh
      write(7,45) work
      write(7,50) refrig
      write(7,55) (tin/tinh -1.)/work*refrig
15    format(20a)
20    format(' ')
25    format(' Tout cold=',f5.2,'  Tin cold=',f5.2,'  Tin hot=',f5.2,
     &'  Tout hot=',f5.2)
30    format(' high field=',f4.2,'  low field=',f4.2)
35    format(' Mass of GGG per element / shuttle mass of He ',f8.5)
40    format(' Cycles which where ploted ',5i5)
45    format(' Total work per cycle per kg of GGG ',f7.3)
50    format(' Refrigeration per cycle per kg of GGG ',f7.3)
55    format(' Carnot efficiency (not a function of optimizatoin)',f3.2)

c  Plot all factor distributions which were saved.
      if (k .gt. 0) then
           do i=1,k
                call set_trace_mg(' ',0,' ',1.)
                call trace_mg(x(1),factplot(1,i),num)
           end do

           call title_MG(file1)
            call ylabel_MG('Segment Factors',0.8,'v','TR')
            call xlabel_MG('Distance along core',0.8,'h','TR')
           call fancy_MG
            call graph_MG
            call stop_mg
      end if

      type*,'Enter 1 for plot of first order irreversibilities, 0 for no'
      accept*,i
      if (i .eq. 1) then
           type*,'Enter value for helium flow rate in g/s'
           accept*,mdot
           j = 0
           stot = 0.
           do i=1,(num-2),3
                j = j+1
```

```
            A = (temp1(i)-temp1(i+2)) / temp1(i+2)
            call heprop(temp1(i+1),dens,enth,ent,cp,cond)
            bl = 17100.*cond/cp /mdot
           type*,bl
            Splot(j) = cpf(temp1(i+1),1)*S_irr(A,bl)
            A = (temp2(i+2)-temp2(i)) / temp2(i+2)
            call heprop(temp2(i+1),dens,enth,ent,cp,cond)
            bl = 17100.*cond/cp /mdot
           type*,bl
            Splot(j) = Splot(j) + cpf(temp2(i+1),1)*S_irr(A,bl)

            stot = stot + splot(j)
            Splot(j) = Splot(j) / (w(i)+w(i+1)+w(i+2))
     &                    * (temp2(i+1) - temp1(i+1))
            x(j) = (j-1)/120.
         end do
         type*,'Stot=',stot

         call set_trace_mg(' ',0,' ',1.)
         call trace_mg(x(1),Splot(1),120)

         call title_MG(file1)
          call ylabel_MG('(S_i_r_r / ~DS) per seg',0.8,'v','TR')
          call xlabel_MG('Distance along core',0.8,'h','TR')
         call fancy_MG
          call graph_MG
          call stop_mg
      end if

      type*,'Enter 1 to plot selected cycles on T-S diagram, and then have'
      type*,'the option to plot field as a percent of Isothermal path for'
      type*,'these same cycles, or enter 0 for no plots'
      accept*,iflag
      if (iflag .eq. 0) goto 500

      cycle(1) = ihigh
      type*,'The limiting segment number ',ihigh,' will be plotted'
350   type*,'Enter segment numbers for the 4 other cycles to be plotted'
      read(5,*) (cycle(i),i=2,5)
c  Sort the cycle numbers from lowest to highest.
      i = 2
400   if (cycle(i) .ge. cycle(i-1)) then
           i = i + 1
      else
           ihold = cycle(i)
           cycle(i) = cycle(i-1)
           cycle(i-1) = ihold
           if (i .eq. 2) then
                i = i + 1
           else
                i = i - 1
           end if
      end if
      if (i .lt. 6) goto 400
      if (cycle(5) .gt. num) then
           type*,'maximum cycle number is:',num
           goto 350
      end if
      write(7,40) (cycle(i),i=1,5)

      do i=1,5
           tlow = temp1(cycle(i))
           thigh = temp2(cycle(i))
           shigh = sht(Hlow,tlow)
```

```
            slow = shigh - w(cycle(i)) / (thigh-tlow) / facthigh
            T(1,I) = Tlow
            T(2,I) = Thigh
            T(3,I) = Thigh
            T(4,I) = Tlow
            T(5,I) = Tlow
            S(1,I) = slow
            S(2,I) = slow
            S(3,I) = shigh
            S(4,I) = shigh
            S(5,I) = slow
      end do

      do i=1,5
            CALL SET_TRACE_MG(' ',0,' ',1.)
            CALL TRACE_MG(S(1,i),T(1,i),5)
      end do

c Determine and plot GGG properties.
      itmax = temp2(num+1) + 1
      do j=1,7
            H = j-1.
            if(H .eq. 0.) H=.01
            do i=1,50
                  TGGG(i,j) = 2. + i*(itmax - 2)/50.
                  SGGG(i,j) = sht(H,TGGG(i,j))
            end do
      end do

      do i=1,7
            CALL SET_TRACE_MG(' ',0,' ',1.)
            CALL TRACE_MG(SGGG(1,i),TGGG(1,i),50)
      end do

      call title_MG(file1)
       call ylabel_MG('Temperature',0.8,'v','TR')
       call xlabel_MG('Entropy',0.8,'h','TR')
      call fancy_MG
       call graph_MG
       call stop_mg
c
      type*,'Enter 1 to plot field as a funct. of percent iso-path'
      accept*,iflag
      if (iflag .ne. 1) goto 500
c Determine field as a function of distance along isthermal path and plot.
      do i=1,5
            do j=1,21
                  ent = s(3,i) - (j-1.)/20.*( s(3,i) - s(1,i))
                  field(j,i) = hst(ent,t(2,i))
                  field(43-j,i) = hst(ent,t(1,i))
            end do
            field(43,i) = field(1,i)
      end do
      do i=1,21
            xtime(i) = (i-1.)/20.
            xtime(43-i) = xtime(i)
      end do
      xtime(43) = 0

      CALL SCALE_MG('x',-.1,1.1,.2)
      CALL GRID_MG

      type*,'Enter 1 for field profile of first cycle, 0 for none'
      accept*,i
```

```
      if (i .eq. 1) then
           CALL SET_TRACE_MG('1',0,'Open Circle',1.)
           CALL TRACE_MG(xtime(1),field(1,1),43)
      end if

      type*,'Enter 1 for field profile of second cycle, 0 for none'
      accept*,i
      if (i .eq. 1) then
           CALL SET_TRACE_MG('2',0,'Solid Circle',1.)
           CALL TRACE_MG(xtime(1),field(1,2),43)
      end if

      type*,'Enter 1 for field profile of third cycle, 0 for none'
      accept*,i
      if (i .eq. 1) then
           CALL SET_TRACE_MG('3',0,'Open Square',1.)
           CALL TRACE_MG(xtime(1),field(1,3),43)
      end if

      type*,'Enter 1 for field profile of fourth cycle, 0 for none'
      accept*,i
      if (i .eq. 1) then
           CALL SET_TRACE_MG('4',0,'Solid Square',1.)
           CALL TRACE_MG(xtime(1),field(1,4),43)
      end if

      type*,'Enter 1 for field profile of fifth cycle, 0 for none'
      accept*,i
      if (i .eq. 1) then
           CALL SET_TRACE_MG('5',0,'Cross',1.)
           CALL TRACE_MG(xtime(1),field(1,5),43)
      end if

      call title_MG(file1)
       call ylabel_MG('Field',0.8,'v','TR')
       call xlabel_MG('Percent of isothermal path',0.8,'h','TR')
      call legend_MG(,80.,25.,0.7,,'ICI')
      call fancy_MG
       call graph_MG
       call stop_mg

500   type*,'Enter 1 to plot field as a function of position for'
      type*,'0, 20, 40, 60, 80, and 100% of the isothermal paths.'
      accept*,iflag
      if (iflag .eq. 0) goto 999

c  Determine field as a function of distance along the core for
c  0%,20%,40%,60%,80%,100% of the isothermal warm blow path.
      do i=1,51
           x(i) = (i-1.)/50.
      end do

      do i=1,51
           tlow = temp1((i-1)*num/50 + 1)
           thigh = temp2((i-1)*num/50 + 1)
           shigh = sht(Hlow,tlow)
           slow = shigh - w((i-1)*num/50 + 1) / (thigh-tlow) / facthigh
           do j=1,6
                ent = shigh - (j-1)/5.*(shigh - slow)
                field(i,j) = hst(ent,thigh)
           end do
      end do

      CALL SCALE_MG('y',0.,hhigh,1.)
```

```
      do j=1,6
           CALL SET_TRACE_MG(' ',0,'Open Circle',1.)
           CALL TRACE_MG(x(1),field(1,j),51)
      end do

      CALL GRID_MG
      call title_MG(file1)
       call ylabel_MG('Field at 20% int., incr.',0.8,'v','TR')
       call xlabel_MG('Distance Along the Core',0.8,'h','TR')
      call fancy_MG
       call graph_MG
       call stop_mg

c  Determine field as a function of distance along the core for
c  0%,20%,40%,60%,80%,100% of the isothermal cold blow path.
      do i=1,51
           tlow = temp1((i-1)*num/50 + 1)
           thigh = temp2((i-1)*num/50 + 1)
           shigh = sht(Hlow,tlow)
           slow = shigh - w((i-1)*num/50 + 1) / (thigh-tlow) / facthigh
           do j=6,1,-1
                ent = slow + (6-j)/5.*(shigh - slow)
                field(i,j) = hst(ent,tlow)
           end do
      end do

      CALL SCALE_MG('y',0.,hhigh,1.)
      do j=1,6
           CALL SET_TRACE_MG(' ',0,'Open Circle',1.)
           CALL TRACE_MG(x(1),field(1,j),51)
      end do

      CALL GRID_MG
      call title_MG(file1)
       call ylabel_MG('Field at 20% int., decr.',0.8,'v','TR')
       call xlabel_MG('Distance Along the Core',0.8,'h','TR')
      call fancy_MG
       call graph_MG
       call stop_mg

999   stop
       end

c     type*,'Enter X**2 term for parabola'
c     accept*,ecc
c     A = tout
c     B = tin - tout - ecc
c     C = ecc
c     do i=1,(num+1)
c          x(i) = (i-1.)/float(num)
c          temp1(i) = A + B*x + c*x**2
```

```
      program SIMULATE.FOR
      real m0,mout          !  (g / segment volume)
      real T1(50,50),T2(50),x(50),x1(20)
      real hout_c(20),hout_w(20),tout_c(20),tout_w(20)
      real m_var(50),m_error,tot_mass,tot_des   T  (g)
      real vol  ! (cc) for entire core
      real volseg          ! (cc) per segment
      real flow(0:50),s_flow(0:50),m_flow(0:50),h_flow(0:50)
      real T_c(0:30,0:20),S_c(0:30,0:20)  ! (i,seg)
      real x2(0:50),error
      real Tin_c,Tin_w

      common pres
      COMMON hedens(58,5),heenth(58,5),hecp(58,5),other(58,5)
      common s_array(58)
      OPEN(UNIT=3,FILE='[cogswell.heprop]NEWPROP.DAT',TYPE='OLD')
      do j=1,5
        do i=1,58
          READ(3,*) hedens(i,j),heenth(i,j),hecp(i,j),other(i,j)
        enddo
      enddo

      vol = 356.

      type*,'Enter 1 for external dead space, else enter 0'
      accept*,flag
      if (flag .eq. 1) then
        type*,'Enter decay factor'
        accept*, fact
      endif
      type*,'Enter number for temperature input from file'
      type*,'  enter 0 for input from screen'
      accept*,idat
      if (idat .eq. 0) then
        write(6,*) 'Enter initial temps, before magnetization,'
        write(6,*) ' For a linear profile: Tcold_end, Twarm_end'
        accept*,Tcold_end, Twarm_end
        write(6,*) 'Enter number of segments in core (less than 51)'
        accept*,nseg
c     Initialize temperature arrays.
          do j=1,nseg
            x(j) = (j - .5) / float(nseg)
            T1(j,1) = Tcold_end + (Twarm_end - Tcold_end) * x(j)
            T2(j) = T1(j,1)
          enddo
      else
          read(idat,*) nseg
          read(idat,15) (T2(j),j=1,nseg)
          do j=1,nseg
            x(j) = (j - .5) / float(nseg)
            T1(j,1) = T2(j)
          enddo
      endif
      volseg = vol/nseg
      write(6,*) 'Enter the frequency of segments to be plotted'
      accept*,jstep
      if (jstep .le. 0) jstep = nseg - 1
        write(10,*) ((nseg-1)/jstep + 1)

      write(6,*) 'Enter the operating pressure between 2.5 and 10'
      accept*,pres
      write(6,*) 'Enter the temperature of the warm reservoir'
      accept*,Twarm
      if (Twarm .gt. 10.  .or. Twarm_end .gt. 10.) then
```

```
         ymax = 20.
      else
         ymax = 12.
      endif
      write(6,*) 'Enter the temperature of the cold reservoir'
      accept*,Tcold
      write(6,*) 'Enter Helium Gap on outside edge of core, (mils)'
      accept*,del
      del = del*2.54/1000.
      por = (1.53*2.54 - del/2.) * 3.1415 * del / 11.86
c   Create entropy function for helium.
      s_array(1) = 0.
      call heprop2(2.2,dens,enth,cp,cond)
      hold = cp/2.2
      do i=2,39
         temp = 2.1 + i/10.
         call heprop2(temp,dens,enth,cp,cond)
         s_array(i) = s_array(i-1) + (hold + cp/temp) * 0.1/2.
         hold = cp/temp
      enddo
      do i=40,58
         temp = 6. + float(i-39)
         call heprop2(temp,dens,enth,cp,cond)
         s_array(i) = s_array(i-1) + (hold + cp/temp) * 1./2.
         hold = cp/temp
      enddo
      write(6,*) 'Enter segment number for field divide'
      accept*,ndivide
      write(6,*) 'Enter initial field for the cold and warm ends'
      accept*,Hint_c,Hint_w
      if (flag .eq. 1) then
        write(6,*) 'Enter Tin_c and Tin_w for dead volumes'
        accept*, Tin_c,Tin_w
      else
        Tin_c = Tcold
        Tin_w = Twarm
      endif

10    write(6,*) 'Enter final field for the cold and warm ends'
      accept*,Hfin_c,Hfin_w
      write(6,*) 'Enter number of steps in H (less than 51)'
      accept*,num
      H_c = Hint_c
      delt_H_c = (Hfin_c - Hint_c)/num
      H_w = Hint_w
      delt_H_w = (Hfin_w - Hint_w)/num
      write(6,*) 'Enter the frequency of plotting, 1 = every time step'
      write(6,*) '    2 = every other time step, ... ; 0 = never'
      accept*,istep
         if (istep .le. 0) istep = 100
         if (num/istep .gt. 20) istep = num/20 + 1
         write(10,*) (num/istep + 1)
      write(6,*) 'Enter 1 for variable flow'
      accept*,idat
      if (idat .eq. 1) then
         write(6,*) 'Enter flow in (g) for each time step'
         accept*,(m_var(i),i=1,num)
      else
         write(6,*) 'Enter total forced helium flow during process'
         accept*,hold
         do i=1,num
           m_var(i) = hold/num
         enddo
      endif
```

```
      IF (Hfin_c .ge. Hint_c) then

c     MAGNETIZING
      write(6,*) ' '
      error = 0.
      tot_mass = 0.

c     Iterate over time with i.
      do i=1,num

         flow(0) = m_var(i)
         h0 = He_HT(Tin_c)
         m0 = flow(0)/volseg
         m_flow(0) = m_flow(0) + flow(0)
         h_flow(0) = h_flow(0) + h0*flow(0)
         s_flow(0) = s_flow(0) + HeST(Tcold)*flow(0)
c       Iterate over the segments with j.
         do j=1,nseg
            if (j .gt. ndivide) then
               H1 = H_w
               H2 = H_w + delt_H_w
            else
               H1 = H_c
               H2 = H_c + delt_H_c
            endif
            f = -.1
            del_T = 1.
            dowhile (abs(del_T) .gt. .005)
               dowhile (del_T*f .lt. 0)
                 T2(j) = T2(j) + del_T
                 f = trans(T2(j),T1(j,i),H2,H1,por,m0,h0,havg,mout)
               enddo
               del_T = -.2*del_T
            enddo
            flow(j) = mout*volseg
            m_flow(j) = m_flow(j) + flow(j)
            tavg = (T2(j) + T1(j,i)) / 2.
            h_flow(j) = h_flow(j) +  havg * flow(j)
            s_flow(j) = s_flow(j) + HeST(tavg) * flow(j)
            m0 = mout
            h0 = havg
            error = error + f
         enddo

         i_c = i_c + 1
         T_c(i_c,0) = Tcold
         S_c(i_c,0) = s_flow(0)
         j_c = 1
         do j=jstep,nseg,jstep
            T_c(i_c,j_c) = ( T2(j) + T1(j,i) ) / 2.
            S_c(i_c,j_c) = s_flow(j)
            j_c = j_c + 1
         enddo

         tot_mass = tot_mass + flow(nseg)
         tout_w(i) = 1.5 *T2(nseg) - .5 *T2(nseg-1)
         hout_w(i) = ( He_HT(tout_w(i)) - He_HT(twarm) )*flow(nseg)

         write(6,23) flow(nseg),T2(1),T2(nseg-1),T2(nseg)
23       format(f9.2, f6.2, f6.2, f6.2 )
         H_c = H_c + delt_H_c
         H_w = H_w + delt_H_w
         do j=1,nseg
```

```
            T1(j,i+1) = T2(j)
          enddo
          if (flag .eq. 1) then
            if(m_var(i) .gt. .06) Tin_c = fact*Tin_c + (1-fact)*Tcold
            Tin_w = tout_w(i)
          endif

        enddo     ! end of time step (i)

        Else

c DEMAGNETIZING: solve from right to left.
c m0 is guessed at right side and then is checked at left side.
c The entire proces is repeted at each time step to get m0 on the
c left end to equal zero.
        m_error = 0.
        tot_mass = 0.
        tot_des = 0.
        error = 0.

c     Iterate over time with i.
        do i=1,num
          flow(nseg) = m_var(i) - m_error * (.1/(.1+por))

          icount = 0
100       m0 = flow(nseg) / volseg
          h0 = He_HT(Tin_w)
          do j=1,nseg
            T2(j) = T1(j,i)
          enddo
c       Iterate over the segments with j.
          do j=nseg,1,-1
            if (j .gt. ndivide) then
              H1 = H_w
              H2 = H_w + delt_H_w
            else
              H1 = H_c
              H2 = H_c + delt_H_c
            endif
            f = .1
            del_T = -1.
            dowhile (abs(del_T) .gt. .005)
              dowhile (del_T*f .lt. 0)
                T2(j) = T2(j) + del_T
                f = trans(T2(j),T1(j,i),H2,H1,por,m0,h0,havg,mout)
                if ( mout .lt. 0.) then
                  flow(nseg) = flow(nseg) - 5.* mout * volseg
                  goto 100
                endif
              enddo
              del_T = -.2*del_T
            enddo
            flow(j-1) = mout*volseg
            m0 = mout
            h0 = havg
            error = error + f
          enddo

c  Decide whether to send back and recalculate with new m right.
          if (icount .eq. 0) tot_des = tot_des + m_var(i)
          m_error =  tot_mass + flow(0) - tot_des
          type*,'flow(n),flow(0),m_error ',flow(nseg),flow(0),m_error
          if (i .eq. num  .and. m_var(i) .gt. .1) then
            factor = .4
```

```
            if ( abs(m_error) .gt. .02  .and. icount .lt. 6) then
               flow(nseg) = flow(nseg) - factor*m_error
               icount = icount + 1
               goto 100
            endif
         endif

         do j =0,nseg-1
            m_flow(j) = m_flow(j) - flow(j)
            tavg = (T2(j+1) + T1(j+1,i)) / 2.
            h_flow(j) = h_flow(j) - He_HT( tavg ) * flow(j)
            s_flow(j) = s_flow(j) - HeST( tavg ) * flow(j)
         enddo
         m_flow(nseg) = m_flow(nseg) - flow(nseg)
         h_flow(nseg) = h_flow(nseg) - He_HT(Twarm )*flow(nseg)
         s_flow(nseg) = s_flow(nseg) - HeST(Twarm)*flow(nseg)

         i_c = i_c + 1
         j_c = 0
         do j=0,nseg,jstep
            T_c(i_c,j_c) = (T2(j+1) + T1(j+1,i)) /2.
            s_c(i_c,j_c) = s_flow(j)
            j_c = j_c + 1
         enddo

         tot_mass = tot_mass + flow(0)
         tout_c(i) = 1.5 *T2(1) - .5 *T2(2)
         hout_c(i) = ( He_HT(tout_c(i)) - He_HT(tcold) ) * flow(0)

         write(6,23) flow(0),T2(1),T2(nseg-1),T2(nseg)
         H_c = H_c + delt_H_c
         H_w = H_w + delt_H_w
         do j=1,nseg
            T1(j,i+1) = T2(j)
         enddo
         if (flag .eq. 1) then
           if(m_var(i) .gt. .06) Tin_w = fact*Tin_w + (1-fact)*Twarm
           Tin_c = tout_c(i)
         endif

      enddo     ! End of time steps (i)

      endif     ! End of warm vrs. cold

      write(6,25) tot_mass
25    format(' tot_mass = ',f6.3)
      write(11,*) ' s_flow'
      write(11,30) (s_flow(j),j=0,nseg)
      write(11,*) ' m_flow'
      write(11,30) (m_flow(j),j=0,nseg)
      write(11,*) ' h_flow'
      write(11,35) (h_flow(j),j=0,nseg)
      write(11,*) ' Enthalpy error=', error*volseg
      write(11,*) ' ---- '
30    format(10f8.3)
35    format(10f8.2)

c     PLOT: temperature array when required, and save info. for 'cycle'
      do i=1,num+1,istep
         call set_trace_mg(' ',0,' ',1.)
         call trace_mg(x(1),T1(1,i),nseg)
         H_c = Hint_c + (i-1.)*delt_H_c
         H_w = Hint_w + (i-1.)*delt_H_w
         write(10,*) H_c,H_w
```

```
         write(10,15) (T1(j,i),j=1,nseg,jstep)
       enddo

       call xlabel_mg('Distance Along Core',0.8,'h','TR')
       call scale_mg('Y',2.,ymax,2.)
       call fancy_mg
       call grid_mg
       call graph_mg
       call stop_mg

c      SAVE: Saves last temperature profile in FOR(idat).dat.
       type*,'Enter number to save final temperature array'
       accept*,idat
       if (idat .ne. 0) then
          write(idat,*) nseg
          write(idat,15) (T2(j),j=1,nseg)
15        format(10f6.2)
       endif

c      PLOT: Optional temperature and enthalpy graphs.
       type*,'Enter 1 to plot refrigeration graphs'
       accept*,idat
       if (idat .eq. 1) then
           do i=1,num
              x1(i) = i-.5
           enddo
c      PLOT: Temperature graphs.
           if (Hfin_c .ge. Hint_c) then
              ! graph warm-blow outlet temps
              call set_trace_mg(' ',0,' ',1.)
              call trace_mg(x1(1),tout_w(1),num)
           else
              ! graph cold-blow outlet temps
              call set_trace_mg(' ',0,' ',1.)
              call trace_mg(x1(1),tout_c(1),num)
           endif
           call ylabel_mg('Temperature',0.8,'v','TR')
           call xlabel_mg('time steps',0.8,'h','TR')
           call fancy_mg
           call grid_mg
           call graph_mg
           call stop_mg
c      PLOT: Enthalpy graphs.
           if (Hfin_c .ge. Hint_c) then
              ! graph heat of rejection
              call set_trace_mg(' ',0,' ',1.)
              call trace_mg(x1(1),hout_w(1),num)
           else
              ! graph refrigeration
              call set_trace_mg(' ',0,' ',1.)
              call trace_mg(x1(1),hout_c(1),num)
           endif
           call ylabel_mg('Enthalpy difference',0.8,'v','TR')
           call xlabel_mg('time steps',0.8,'h','TR')
           call fancy_mg
           call grid_mg
           call graph_mg
           call stop_mg
       endif

c      PLOT: Optional entropy and enthalpy flows
       type*,'Enter 1 to plot s_flow and h_flow'
       accept*,idat
       if (idat .eq. 1) then
```

```
            do i=0,nseg
               x2(i) = float(i)/float(nseg)
            enddo
            call set_trace_mg(' ',0,' ',1.)
            call trace_mg(x2(0),h_flow(0),nseg+1)
            call ylabel_mg('Enthalpy Flow (J)',0.8,'v','TR')
            call xlabel_mg('Distance along core',0.8,'h','TR')
            call fancy_mg
            call grid_mg
            call graph_mg
            call stop_mg
            call set_trace_mg(' ',0,' ',1.)
            call trace_mg(x2(0),s_flow(0),nseg+1)
            call ylabel_mg('Entropy Flow (J/K)',0.8,'v','TR')
            call xlabel_mg('Distance along core',0.8,'h','TR')
            call fancy_mg
            call grid_mg
            call graph_mg
            call stop_mg
         endif

c PLOT: Optional S_c plots
         type*,'Enter 1 to plot S_c at selected segments'
         accept*,idat
         if (idat .eq. 1) then
            do j=0,j_c-1
               T_c(0,j) = T_c(i_c,j)
               call set_trace_mg(' ',0,' ',1.)
               call trace_mg( S_c(0,j), T_c(0,j), i_c+1)
            enddo
            call ylabel_mg('Temperature',0.8,'v','TR')
            call xlabel_mg('Entropy Flow',0.8,'h','TR')
            call fancy_mg
            call grid_mg
            call graph_mg
            call stop_mg
         endif

         Hint_c = Hfin_c
         Hint_w = Hfin_w
         do j=1,nseg
            T1(j,1) = T2(j)
         enddo
         goto 10

         end
```

```
c  SIMFUNCT.FOR:  Functions used with SIMULATE.FOR.

      FUNCTION TRANS(T2,T1,H2,H1,por,m0,h0,enthavg,mout) ! (j/g)
      real T2,T1,H2,H1,por,m0,h0
      real enthavg,mout
        x_g = .714
        x_r = .253 - por
        x_he = .033 + por
        rho_g = 7.14                ! (g/cc)
        rho_r = 1.                  ! (g/cc)
        Tavg = (T2+T1)/2. ! (K)
        enthavg = He_HT(tavg) ! (j/g)
        Havg = (H2 + H1)/2.         ! (T)
        mout = m0 + x_he*( He_rho(T1) - He_rho(T2) ) ! (g/cc)
        call GGGPROP(Tavg,Havg,dSdH,S,dSdT)
        x1 = x_g*rho_g*Tavg *( dSdT*(T2-T1) + dSdH*(H2-H1) )
        x2 = x_r*rho_r*( Rub_HT(T2) - Rub_HT(T1) )
        x3 = x_he*( rhoHe_H(T2) - rhoHe_H(T1) )
        x4 = -h0*m0 + enthavg * mout
        trans = x1 + x2 + x3 + x4
        if (mout .lt. 0.) then
           write(5,*) 'Flow reversal!'
        endif
      return
      end

      FUNCTION Rub_HT(temp)         ! (J/g-K)
      real temp
           if (temp .lt. 7.045) then
             Rub_HT = 0.
           else
             Rub_HT = (4.4*temp**2 - 62*temp + 250) / 1000.
           endif
      return
      end

      FUNCTION He_rho(Temp)  ! (g/cc)
      real temp
           CALL HEPROP2(temp,dens,enth,CP,COND)
           He_rho = dens
      return
      end

      FUNCTION rhoHe_H(temp)  ! (j/cc)
      real temp
           CALL HEPROP2(temp,dens,enth,CP,COND)
           rhoHe_H = dens * enth    ! (j/cc)
      return
      end

      FUNCTION He_HT(temp)  ! (j/g)
      real temp
           CALL HEPROP2(temp,dens,enth,CP,COND)
           He_HT = enth
      return
      end

      subroutine HEPROP2(temp,dens,enth,cp,cond)
      real temp,dens,enth,cp,cond
      real array(5)
      common pres
      common hedens(58,5),heenth(58,5),hecp(58,5),other(58,5)
      common s_array(58)
      data array/2.5,3.,4.,5.,10./
```

```
      if (pres .lt. 2.5) then
          type*,'Pressure less than 2.5 Atm.'
          return
      endif
      if (pres .gt. 10.) then
          type*,'Pressure greater than 10 Atm.'
          return
      endif
      j = 1
      dowhile ( pres .gt. array(j+1) )
          j = j+1
      enddo
      pfactor = (pres - array(j)) / (array(j+1) - array(j))

      if (temp .lt. 2.2) then
          type*,'Helium temp less than 2.2'
          dens = ( hedens(1,j) + pfactor * ( hedens(1,j+1) -
     &             hedens(1,j)) ) / 1000.
          cp = hecp(1,j) + pfactor * ( hecp(1,j+1) - hecp(1,j) )
          enth =  heenth(1,j) + pfactor * ( heenth(1,j+1) -
     &             heenth(1,j)) - (2.2 - temp) * cp
          cond = ( other(1,j) + pfactor * ( other(1,j+1) -
     &            other(1,j)) )/1000.
          return
      elseif (temp .gt. 25.) then
          type*,'Helium temp greater than 25'
          i = 58
      else
         if (temp .gt. 6.) then
             i = temp
             tfactor = (temp - float(i))
             i = i + 39 - 6
         else
             i = 10.*temp
             tfactor = (10.*temp - float(i))
             i = i - 21
         endif
      endif

      hold1 = hedens(i,j) + tfactor*(hedens(i+1,j)-hedens(i,j))
      hold2 = hedens(i,j+1)+tfactor*(hedens(i+1,j+1)-hedens(i,j+1))
      dens = ( hold1 + pfactor*(hold2 - hold1) ) / 1000.
      hold1 = heenth(i,j) + tfactor*(heenth(i+1,j)-heenth(i,j))
      hold2 = heenth(i,j+1)+tfactor*(heenth(i+1,j+1)-heenth(i,j+1))
      enth = hold1 + pfactor*(hold2 - hold1)
      hold1 = hecp(i,j) + tfactor*(hecp(i+1,j)-hecp(i,j))
      hold2 = hecp(i,j+1)+tfactor*(hecp(i+1,j+1)-hecp(i,j+1))
      cp = hold1 + pfactor*(hold2 - hold1)
c     hold1 = other(i,j) + tfactor*(other(i+1,j)-other(i,j))
c     hold2 = other(i,j+1)+tfactor*(other(i+1,j+1)-other(i,j+1))
c     cond = (hold1 + pfactor*(hold2 - hold1))/1000.

      return
      end
```

```
      program void

      COMMON pres
      COMMON hedens(58,5),heenth(58,5),hecp(58,5),hecond(58,5)
      OPEN(UNIT=3,FILE='[cogswell.heprop]NEWPROP.DAT',TYPE='OLD')

      do j=1,5
        do i=1,58
          READ(3,*) hedens(i,j),heenth(i,j),hecp(i,j),hecond(i,j)
        enddo
      enddo

      type*,'Enter x_1, x_2'
      accept*,x_1,x_2
      x_g = 1. - x_1 - x_2
      type*,'Enter T_0, and T_a'
      accept*,T_0,T_a
      H = 2.
      pres = 4.
      rho_g = 7.14

      call GGGPROP(T_a,H,d1,S,d3)
      S_g = x_g*rho_g*S
      write(1,*) T_a, S_g
      write(1,*) ' '

      Tnew = T_0
      dowhile(T_a .gt. T_0)
      type*,'enter q'
      accept*,q

20    call HEPROP2(T_0,rho_1,enth_1,d1,d2)
      call HEPROP2(Tnew,rho_2,enth_2,d1,d2)
      error = Q - x_1 * (rho_2 + rho_1)/2. * (enth_2 - enth_1)
      type*,error
      if (abs(error) .gt. 5e-5) then
         Tnew = Tnew + 10.*error
         goto 20
      endif
      dm_1 = - x_1 * (rho_2 - rho_1)
      T_0 = Tnew
      type*,'T_0=',T_0
      havg_1 = (enth_2+enth_1)/2.

      Tnew = T_a
30    call HEPROP2(T_a,rho_1,enth_1,d1,d2)
      call HEPROP2(Tnew,rho_2,enth_2,d1,d2)
      Tavg = (T_a + Tnew)/2.
      havg_2 = (enth_2 + enth_1)/2.
       call GGGPROP(Tavg,H,d1,d2,d3)
      c_h = Tavg*d3
      error = x_g*rho_g*c_h*(Tnew-T_a) + x_2*(rho_2+rho_1)/2.*
     &        (enth_2-enth_1) + Q + dm_1*(havg_2-havg_1)
      type*,error
      if (abs(error) .gt. 5e-5) then
         Tnew = Tnew - 4.*error
         goto 30
      endif
      dm_2 = dm_1 - x_2 * (rho_2 - rho_1)
      write(1,*) dm_2, T_a, Tnew
      T_a = Tnew
      type*,'T_a=',T_a

      enddo

      call GGGPROP(T_a,H,d1,S,d3)
      S_g = x_g*rho_g*S
      write(1,*) ' '
      write(1,*) T_a, S_g

      end
```

REFERENCES

1. J.R. Van Geuns, "A Study of a New Magnetic Refrigerating Cycle," *Philips Res. Rept. Suppl.* **6**, (1966).

2. C. Delpeuch, R. Béranger, G. Bon Mardion, G. Claudet, and A.A. Lacaze, "Double acting reciprocating magnetic refrigerator: first experiments," *Cryogenics*, **21**:579–584, (1981).

3. A.F. Lacaze, R. Béranger, G. Bon Mardion, G. Claudet, and A.A. Lacaze, "Efficiency improvements of a double acting reciprocating magnetic refrigerator," *Cryogenics*, **23**:427–436, (1983).

4. J.A. Barclay, W.F. Stewart, W.C. Overton, R.J. Candler, and O.D. Harkleroad, "Experimental results on a low-temperature magnetic refrigerator," *Advances in Cryogenic Engineering*, **31**:743–752, (1985).

5. Y. Hakuraku and H. Ogata,"Thermodynamic analysis of a magnetic refrigerator with static heat switches," *Cryogenics*, **26**, (1986).

6. H. Nakagome, T. Kuriyama, H. Ogiwara, T. Fujita, T. Yazawa, and T. Hashimoto, "Reciprocating magnetic refrigerator for helium liquefaction," *Advances in Cryogenic Engineering*, **31**:753–762, (1985).

7. P. Seyfert, P. Brédy, G. Claudet, "Construction and testing of a magnetic refrigeration device for the temperature range of 5 to 15 K," *Presented at ICEC12*, South Hampton, July 12-15, (1988).

8. "Super Coolers May Chill Space Sensors," *Defense Electronics*, May, (1987), pp. 57.

9. C.P. Taussig, G.R. Gallagher, J.L. Smith, Jr., and Y. Iwasa, "Magnetic Refrigeration Based on Magnetically Active Regeneration," *Proc. of the Fourth International Cryocoolers Conference,"* 79–88, (1986).

10. Carl P. Taussig, "Magnetically Active Regeneration," MIT Ph.D. Thesis, 1986.

11. R. F. Barron, *Cryogenic Systems*, 2nd ed., pp. 244-276. Oxford University Press, New York, 1985.

12. Gregory R. Gallagher, "Analysis of a Magnetically Active Regenerator,"MIT M.S. Thesis, 1986.

13. R. J. Corruccini, and J. J. Gniewek, "Specific Heats and Enthalpies of Technical Solids at Low Temperatures," A Compilation From the Literature, *NBS Monograph 21*, 1960.

14. J. A. Barclay, W. A. Steyert, "Materials for magnetic refrigeraiton between 2 and 20 K," *Cryogenics*, Vol. 22, (1982), pp. 73-79.

Other Reference Sources:

1. G. E. Childs, L. J. Ericks, and R. L. Powell, "Thermal Conductivity of Solids at Room Temperature and Below, A Review and Compilation of the Literature," *NBS Monograph 131*, (1973).

2. R. D. McCarty, "Thermophysical Properties of Helium-4 from 2 to 1500 K with Pressures to 1000 Atmospheres," *NBS Technical Note*, (1972).